A RESORPTION COGENERATION CYCLE FOR POWER AND REFRIGERATION

Thesis by

Yiji Lu

In Partial Fulfilment of the Requirements

For the Degree of

Doctor of Philosophy

Sir Joseph Swan Centre for Energy Research

School of Mechanical and Systems Engineering

Newcastle University

Newcastle upon Tyne

United Kingdom

June 2016

Abstract

Heat-driven energy system attracts ever increasing attentions to improve the efficiency of overall energy utilisation by recovering the heat energy such as solar thermal energy, wasted heat from industry and geothermal energy. Adsorption technology is recognised as one of the promising solutions to convert low-grade heat to refrigeration or be used as heat pump. Based on the working principle of this technology, it can promisingly be developed into combined refrigeration and power generation system by integrating an expander in to the system. However, due to the limited research efforts on the system investigation, refrigeration generation by adsorption technology is still immature. The investigation on the working conditions of the system, the selection of proper expansion machine for power generation part of the cogeneration and overall system evaluation are important to be conducted.

This study aims to explore the feasibility of integration the adsorption technology with expansion machine for refrigeration and power generation. The proposed cogeneration combines resorption system, which has potentially twice of the cooling capacity compared with conventional adsorption system, integrated with expansion machine to continuously produce refrigeration and power. The design and optimisation methods of the proposed system were studied in order to select the proper resorption working pairs under different heat source conditions. Furthermore, the system performance with and without the optimisation methods were evaluated by the first and second law analysis. Results indicated attractive performance and $MnCl_2$-$SrCl_2$ was stood out as the optimal resorption working pair for the purpose of high refrigeration generation under low grade heat source, when ammonia is the working fluid in the system.

An adsorption performance test rig was designed, constructed and used to test the dynamic kinetic performance of the candidate adsorbents pointed out from the evaluation results. The study and development of composite chemisorption adsorbent were conducted. The manufacture processes of expanded graphite to be used as the matrix in the composite adsorbent to improve heat/mass transfer and manufacture of the composite chemisorption adsorbents were reported. Furthermore, an adsorption simulation model using the physical parameters of the designed tube type adsorbent bed was introduced to explore the variation performance of the resorption cogeneration with the time.

Scroll expander was selected as the expander to be explored in this study because of its highest average isentropic efficiency, low cost, low vibration noise, high availability and easy modification from compressor to expander for our special application demand. A lab scale scroll expander test rig was designed, constructed and tested to obtain the performance such as isentropic efficiency and electrical efficiency of a selected scroll machine under various working conditions.

An assessment of a case study of the resorption cogeneration system was conducted to evaluate the variation of the power and refrigeration performance with the time. Results indicated that a resorption cogeneration with 25.2 kg $MnCl_2$ and 18.9 kg $SrCl_2$ could potentially produce 1 kW power and 2.5 kW cooling capacity when the cycle time is around 25 minutes.

Acknowledgements

I would like to express my deepest gratitude to my supervisors Professor Tony Roskilly and Dr Yaodong Wang for their support, guidance, understanding and encouragement throughout my PhD studies.

Besides my supervisors, I would like to thank our technicians Mr Ian Douglass and Mr Stephen Crosby for their continuous help in the lab. Colleagues and other staff who deserve thanks include Dr Huashan Bao, Dr Guohong Tian, Dr Dawei Wu, Dr Zhiwei Ma, Mr Jonathan Heslop, Mr John Richardson, Mrs Jan Fairless and Mr Leigh Ingle for their kindly support.

I also would like to thank for the encourage and recognition on this study from China Scholarship Council for the '2015 Chinese Government Award for Outstanding Self-financed Students Abroad'. Special thanks to the Engineering and Physical Sciences Research Council for the supports through the grants Impact Acceleration Account (EP/K503885/1) -Wasted heat recovery project, LH Cogen (EP/I027904/1) and Global SECURE (EP/K004689/1). The financial support from the Henry Lester trust to support this study is also acknowledged.

My sincere thanks also go to Professor Ruzhu Wang in Shanghai Jiao Tong University, who introduced me to join SWAN Centre on 2011 as an exchange student for my final year project. I am also grateful to Professor Liwei Wang for her guidance and patient instruction on the resorption cogeneration project.

Last but not least, I would like to thank my family members especially my wife Chenxuan Dong for their unconditional love and support during my PhD studies.

List of Papers

I. **Lu Y***, Wang Y, Dong C, Wang L, Roskilly AP. Design and assessment on a novel integrated system for power and refrigeration using waste heat from diesel engine. Applied Thermal Engineering. 2015;91:591-9.

II. **Lu Y***, Wang Y, Bao H, Yuan Y, Wang L, Roskilly AP. Analysis of an optimal resorption cogeneration using mass and heat recovery processes. Applied Energy. 2015;160:892-901.

III. **Lu Y***, Wang Y, Wang L, Yuan Y, Zhen L, Roskilly AP. Experimental Investigation of a Scroll Expander for Power Generation Part of a Resorption Cogeneration. Energy Procedia. 2015;75:1027-32.

IV. **Lu Y***, Bao H, Yuan Y, Wang Y, Wang L, Roskilly AP. Optimisation of a Novel Resorption Cogeneration Using Mass and Heat Recovery. Energy Procedia. 2014;61:1103-6.

V. **Lu Y***, Wang L, Tian G, Roskilly AP. Study on A Small Scale Solar Powered Organic Rankine Cycle Utilizing Scroll Expander. International Conference on Applied Energy. Suzhou, China, July 5-8, 2012.

VI. Yuan Y*, **Lu Y**, Bao H, Wang Y, Wang W, Roskilly AP. Investigation of a Heat Pipe Heat Exchanger Integrated with a Water Spray for the Heat Recovery from Boil Exhaust Gas. Energy Procedia. 2014;61:2141-4.

VII. Tian G*, **Lu Y**, Zhang Y. A review of IC engine waste heat recovery by Rankine cycle technologies. Hydromechatronics Engineering. 2012;40:1-9.

VIII. Liu Z, Tian G*, Wei M, Song P, **Lu Y**, Ashby G, et al. Modelling and Optimisation on scroll expander for Waste Heat Rocovery Organic Rankine Cycle. International Conference on Applied Energy. Abu Dhabi, United Arab Emirates, March 28 - 31, 2015.

Contents

Abstract I

Acknowledgements III

List of Papers IV

Nomenclature XIII

Index of Figures XVII

Index of Tables XIV

Chapter 1. Introduction 1

1.1 Background 1

1.1.1. Challenges 1

1.1.2. Energy policy of the United Kingdom 3

1.2 Project description 4

1.3 Contribution to existing research 6

1.4 Structure of the thesis 7

Chapter 2. Critical analysis of the research in the field 10

2.1 Introduction 10

2.2 Review on system level of adsorption technology and Rankine-based power generation cycles 11

2.2.1. Review of adsorption systems 11

2.2.2. Rankine-based power generation systems 22

2.3 Current status of adsorption technology 29

2.3.1. Selection of refrigerants 29

2.3.2. Working pairs 32

2.3.3. Methods of the adsorption performance measurement 42

2.4 Review of expansion machines for power generation part of the resorption cogeneration 47

2.4.1. Turbines 48

2.4.2. Positive displacement expanders 51

2.4.3. Selection of the expansion machine for the cogeneration 58

2.5 Summary 59

Chapter 3. Design and assessment of a resorption cogeneration 62

3.1 Introduction 62

3.2 Principle of a resorption cogeneration 62

3.3 Analysis of the resorption cogeneration 65

3.3.1. Selection of resorption working pairs 65

3.3.2. Heat recovery process 68

3.3.3. Mass recovery process 69

3.4 Results and Discussions 74

3.4.1. Selection of the resorption working pair 74

3.4.2. Heat and mass recovery 80

3.4.3. Second law analysis 82

3.5 Summary 85

Chapter 4. Experimental investigation of chemical composite adsorbents 87

4.1 Introduction 87

4.2 Design and construction of an adsorption performance test bench 88

4.2.1. System design 88

4.2.2. System components 89

4.3 Preparations 98

4.3.1. Manufacture processes of porous matrix using natural expandable graphite 98

4.3.2. Making composite adsorbents 101

4.3.3. Test plan and procedure 102

4.4 Experimental investigate of the high temperature composite salt - $MnCl_2$ 104

4.4.1. Heat transfer performance of the composite HTS 104

4.4.2. Reaction kinetics of the composite HTS 108

4.4.3. Isobaric sorption performance of the composite HTS 111

4.4.4. SCP of the composite HTS 115

4.5 Experimental investigation of the low temperature composite salt - $SrCl_2$ 117

4.5.1. Heat transfer performance of the composite LTS 117

4.5.2. Reaction kinetics of the composite LTS 121

4.5.3. Isobaric sorption performance of the composite LTS 123

4.5.4. SCP of the composite LTS 126

4.6 Summary 128

Chapter 5. Investigation of scroll expander 130

5.1 Introduction 130

5.2 Design and construction of a scroll expander test bench 130

5.2.1. System design 130

5.2.2. System components 132

5.3 Geometric study and measurement of the scroll unit 139
5.3.1. Geometric study of the scroll unit 139
5.3.2. Measurement of the scroll unit 141
5.4 Experimental test of the scroll expander 146
5.4.1. Test plan 147
5.4.2. Description of the test procedure 149
5.5 Results and discussion of the experimental tests 149
5.5.1. Identification of real volumetric expansion ratio 149
5.5.2. Electrical generation and friction losses 152
5.5.3. Performance under different inlet temperature and pressure 154
5.6 Summary 160
Chapter 6. Assessment of the resorption cogeneration based on the experimental results 163
6.1. Introduction 163
6.2. Mathematical model of an adsorption unit 163
6.2.1. Adsorption kinetic 163
6.2.2. Physical model of one adsorption unit 165
6.2.3. Heat transfer equations 167
6.2.4. Energy balance equations 169
6.3. Simulation model of scroll expander 172
6.3.1. Description of the scroll expander model 172
6.3.2. Determination of the parameters of the simulation model 178
6.4. Performance evaluation of the cogeneration 181

6.5.1. Evaluation methods 182
6.5.2. Performance of power generation 184
6.5.3. Performance of refrigeration 188
6.5.4. Performance of the full cycle 190
6.5. Summary 191
Chapter 7. Conclusions and Recommendations 193
7.1. Summary of main conclusions 193
7.2. Recommendations for future work 195
References 197
Appendices 206

Nomenclature

Symbols	Definition
A_c	Internal area of the Condenser & Evaporator, m^2
Ar	Arrhenius factor
C_p	Heat capacity at constant pressure,
D_{in}	Diameter of the inlet port as expander, mm
D_{inner}	Diameter of the inlet port of the stationary scroll, mm
D_{out}	Diameter of the outlet port as expander, mm
E	Exergy, J
H_s	Height of the scroll, mm
h	specific enthalpy, kJ/kg
i	Number of the expansion chambers in scroll machine
L_{am}	latent heat of ammonia, kJ/kg
$\dot{m}$	mass flow rate, kg/s
N_s	Scroll turns
P_s	Pitch of the scroll blade, mm
P_c	System restricted pressure, kPa
Q	Heat, J
r_s	Radius of basic circle of scroll unit, mm
R_{gy}	Radius of gyration of the orbiting scroll, mm

s	Specific entropy, kJ/(kg. K)
T	Temperature, K or ^{o}C
t_s	Thickness of the scroll, mm
V_{SV}	Swept volume of the scroll machine, cm^3
$V_{exhaust}$	Geometric exhaust volume of the scroll machine, cm^3
$V_{suction}$	Geometric suction volume of the scroll machine, cm^3
$\dot{V}$	Volumetric flow rate, m^3/s
W	Work, J

Greek Letters

α	Start angle of the involute of scroll unit
λ_{ad}	Thermal conductivity of composite adsorbent, W/(m.K)
λ_w	Thermal conductivity of wall, W/(m.K)
γ_{v_in}	Internal volumetric expansion ratio of the expander
γ_{v_real}	Real volumetric expansion ratio of the expander
ρ	Density, Kg/m^3
ϕ	Involute angle of scroll unit
θ	Crank angle between the stationary and orbiting scrolls
η	Efficiency
δ_{ad}	Thickness of adsorbent, mm
δ_w	Thickness of wall, mm
Δh	Specific enthalpy , kJ/kg

ΔH	Molar reaction enthalpy , J/mol
Δp	Pressure difference, kPa
ΔS	Molar reaction entropy , J/(mol · K)
Δx	Conversion ratio, kg/kg
Δu	Specific internal energy, kJ/kg

Subscripts

ad	Adsorbent bed
ads	Adsorption
am	ammonia
con	Condenser
des	Desorption
ele	Electricity
f	Thermal fluid
hr	Heat recovery
in	Inlet
int	Internal
$isen$	Isentropic
mr	Mass recovery
out	Outlet
rec	Received
ref	Refrigeration
0	Environmental condition
eq	Equilibrium point

Acronym

AC	Activated carbon
COP	Coefficient of performance
$CFCs$	Chlorofluorocarbons
CHP	Combined heat and power
CV	Check valve
EG	Expanded graphite
GWP	Global warming potential
$HCFCs$	Hydrochlorofluorocarbons
HTS	Gigh temperature salt
$HVAC$	Heating ventilation air conditioning
LTS	Low temperature salt
$LMTD$	Log mean temperature difference, K
ODP	Ozone depletion potential
ORC	Organic Rankine cycle
SCP	Specific cooling power

Index of Figures

Figure 1-1 World energy consumption[1] 2
Figure 1-2 Global Land-Ocean Temperature Index[3] 3
Figure 2-1 The composition of adsorption cycles 13
Figure 2-2 Principle of adsorption cycle 14
Figure 2-3 Principle of resorption cycle 19
Figure 2-4 Principle of steam Rankine cycle 22
Figure 2-5 Three types of ORC working fluids: dry, isentropic and wet 24
Figure 2-6 Schematic diagram of Kalina cycle 26
Figure 2-7 Schematic diagram of the Goswami cycle [60] 28
Figure 2-8 Schematic diagram of an adsorption 44
Figure 2-9, The adsorption performance test bench using volumetric method-constant volume [101] 45
Figure 2-10,The adsorption performance test bench using volumetric method-constant pressure [83] 46
Figure 2-11 Working principle of flow 48
Figure 2-12 Detailed drawing of the radial flow turbine used in an ORC system using R245fa as working fluid[110] 49
Figure 2-13 Working principle of reciprocating piston expander 52
Figure 2-14 Working principle of screw expander[117] 53
Figure 2-15 Basic structures of the two different types of scrolls [123] 54
Figure 2-16 Working principle of scroll expander[126] 55
Figure 2-17 Working principle of vane-type expander [121] 57
Figure 3-1 Principle of the resorption cogeneration 63
Figure 3-2 Clausius-Clapeyron diagram of the resorption cogeneration 65

Figure 3-3 P-T diagram for the heat recovery process between HTS_1 and HTS_2 (a) after Step2 before Step1 (b) After Step 2 before Step 1 68
Figure 3-4 P-T diagram of the mass recovery process between the HTS_1 and the LTS_2 69
Figure 3-5 Schematic diagram of a resorption cogeneration applying heat recovery process (a) Step 1, HTS_1 & LTS_1 power generation, HTS_2 & LTS_2 refrigeration generation; (b) Step 2 HTS_1 & LTS_1 refrigeration generation, HTS_2 & LTS_2 power generation 70
Figure 3-6 Equilibrium lines of selected salts and ammonia in P-T diagram 75
Figure 3-7 Relationship between the COP and heat source temperature of the resorption cogeneration at 10 ^{o}C refrigeration temperature 77
Figure 3-8 Relationship between the energy efficiency of the electricity production and heat source temperature 79
Figure 3-9 COP of the resorption with working pair (a) $BaCl_2$-$MnCl_2$; (b) $SrCl_2$-$MnCl_2$; (c) $BaCl_2$-$NiCl_2$; (d) $SrCl_2$-$NiCl_2$ 80
Figure 3-10 Electrical energy efficiency of the resorption working pair 81
Figure 3-11 Exergy flow chart of the resorption cogeneration applying mass and heat recovery 82
Figure 3-12 Second law efficiency of the resorption cogeneration using 84
Figure 4-1, Adsorption performance test bench 88
Figure 4-2, Structure of the adsorbent bed 89
Figure 4-3 Picture of the oil bath for the adsorbent bed 90
Figure 4-4, Design of the condenser/evaporator 93
Figure 4-5 Picture of the cryostat for condenser/evaporator 94
Figure 4-6 Picture of the differential pressure transmitter 95
Figure 4-7 Electron microscope image of expandable and expanded graphite [145] (a) Expandable graphite, 200μm, (b) Expanded graphite, 200μm 98
Figure 4-8 Photo of oven 99
Figure 4-9 Photo of electronic balance 99
Figure 4-10 Photo of expandable graphite and expanded graphite 100

Figure 4-11 Detailed information about the adsorbent and adsorbent bed 101
Figure 4-12 Temperature evolution of the composite HTS under the heat source temperature at (a) 150 ^{o}C, (b) 160 ^{o}C, (c) 170 ^{o}C, (d) 180 ^{o}C; condensing temperature 20 ^{o}C 107
Figure 4-13 Adsorbent temperature under different heating source temperatures 108
Figure 4-14 The global conversion ratio of the composite HTS during 109
Figure 4-15 Temperature evolution on the top of the Evaporator/condenser during desorption process under different heating source temperatures 110
Figure 4-16 The global conversion ratio of the composite HTS during 111
Figure 4-17 Isobaric sorption performance of the composite HTS..... 113
Figure 4-18 Relationship between global conversion ratio and adsorbent temperature of the composite HTS 114
Figure 4-19 SCP evolution of the HTS composite adsorbent at different refrigeration temperature 115
Figure 4-20 Average SCP of the HTS composite adsorbent at different refrigeration temperature 116
Figure 4-21 Temperature evolution of the LTS composite adsorbent under the heat source temperature at (a) 90 ^{o}C, (b) 95 ^{o}C, (c) 100 ^{o}C, (d) 105 ^{o}C 119
Figure 4-22 Adsorbent temperature under different heating source temperatures 120
Figure 4-23 The global conversion ratio of the LTS during desorption process under different heating temperature 121
Figure 4-24 The global conversion ratio of the LTS during adsorption process under different refrigeration temperature 122
Figure 4-25 Isobaric sorption performance of the composite LTS 124
Figure 4-26 Relationship between global conversion ratio and adsorbent temperature of the composite LTS 125
Figure 4-27 SCP evolution of the composite LTS at different refrigeration temperature 127

Figure 4-28 Average SCP of the composite LTS at different refrigeration temperature 128
Figure 5-1 Schematic diagram of the scroll expander test bench 131
Figure 5-2 Flow meter to measure the inlet flow rate 132
Figure 5-3 Flow meter to measure the outlet flow rate of the expander 133
Figure 5-4 Electrical generator (a) front view ; (b) side view 134
Figure 5-5 Photo of the electrical heat unit 135
Figure 5-6 Picture of the Sanden TRSA09 Scroll Compressor 136
Figure 5-7 Removal process of the check valve from the stationary scroll 137
Figure 5-8 The internal and external involute lines of scroll unit 139
Figure 5-9 Picture of the dissembled scroll expander 141
Figure 5-10 Comparison of the geometric scroll blade and real scroll unit 143
Figure 5-11 Schematic diagram of the expansion process 144
Figure 5-12 Photo of the scroll expander test rig 146
Figure 5-13 Relationship between inlet pressure and volume flow rate at the inlet and outlet of the expander 150
Figure 5-14 Relationship between inlet pressure and 151
Figure 5-15 Relationship between inlet pressure 152
Figure 5-16 Relationship between inlet pressure 153
Figure 5-17 Relationship between the inlet temperature and achieved electricity 155
Figure 5-18 Relationship between isentropic efficiency of the scroll expander and the inlet temperature 157
Figure 5-19 Relationship between electrical efficiency and inlet temperature . 159
Figure 6-1 Schematic diagram of the physical model 166
Figure 6-2 One-dimensional heat flow through 168
Figure 6-3 Schematic diagram of the parameters 172
Figure 6-4 Schematic diagram of the scroll expander model 174
Figure 6-5 Relationship between friction losses and rotational speed 179
Figure 6-6 Relationship between leakage area and rotational speed 180

Figure 6-7 Relationship between electrical work and time under the heat source temperature at 180 ^{o}C and heat sink temperature at 20 ^{o}C 184
Figure 6-8 Relationship between the electrical power and time under the heat source temperature at 180 ^{o}C and heat sink temperature at 20 ^{o}C 185
Figure 6-9 Relationship between the electrical work and time under different heat source temperature 186
Figure 6-10 Relationship between the electrical power and time under different heat source temperature 187
Figure 6-11 Relationship between cooling work and time under refrigeration temperature at 10 ^{o}C and heat sink temperature at 20 ^{o}C 188
Figure 6-12 Relationship between the cooling capacity and time under refrigeration temperature at 10 ^{o}C and heat sink temperature at 20 ^{o}C 189
Figure 6-13 Performance of two sets of resorption system under the heat source temperature at 180 ^{o}C and refrigeration temperature at 10 ^{o}C 190

Index of Tables

Table 2-1 Physical properties of the most common refrigeration in adsorption system 29
Table 2-2 Comparison of the common refrigerants in adsorption system 31
Table 3-1 Thermodynamic parameters for the chosen salts and ammonia[7] ... 67
Table 3-2 Equilibrium pressure of the HTS under different heating temperatures 76
Table 3-3 Equilibrium pressure of the LTS at environmental temperature and refrigeration temperature 77
Table 3-4 Exergy destruction comparison between two cases 83
Table 4-1 Recorded data of the data acquisition system 97
Table 5-1 Recorded data of the data acquisition system 138
Table 5-2 Physical parameters of the Sanden TRSA 09..... 142
Table 5-3 Working conditions of the resorption cogeneration under the heat source temperature from 70 to 125 ^{o}C 148
Table 6-1 Physical dimensions of the one tube adsorption unit 167
Table 6-2 Parameters of the adsorption tube unit model [151] 171
Table 6-3 Sum of the parameters of the scroll expander model..... 181
Table 6-4 Parameters of the evaluated cogeneration 182

Chapter 1. Introduction

1.1 Background

Ever-increasing demand of energy over the last 200 years forces Human beings to improve the overall efficiency of existing energy systems. Attentions are focusing on utilising renewable energy resources such as solar thermal energy, tide energy, wind power and geothermal energy.

This research project is proposed to use low grade heat such as industrial waste heat, solar energy and geothermal heat. And convert the heat to refrigeration and power under the circumstance of ever increasingly demand of energy and environmental problems such as global warming and depletion of the ozone layer.

1.1.1. Challenges

Oil, natural gas and coal have become three main energy resources for both commercial and residential applications since 1960s [1]. However, with the growing consumption of these three natural resources, human beings are facing a severe problem of running out of these energy resources as suggested by the world energy consumption from 1960 to presents shown in Figure 1-1.

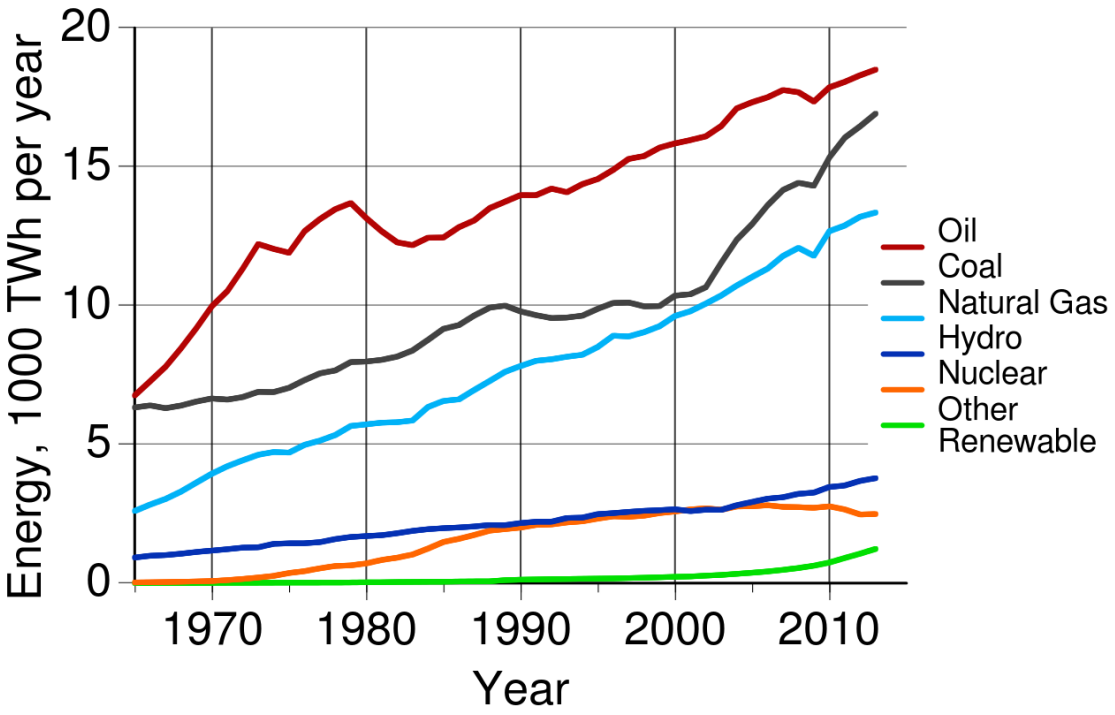

Figure 1-1 World energy consumption[1]

The extensive use of these resources generates large amount of carbon dioxide (CO_2) and other harmful substances such as nitrogen oxides (NO_x) and sulphur dioxide (SO_2). Carbon dioxide is widely recognized by the scientists as one of the main greenhouse gases and scientists believe the increasing concentrations of greenhouse gases will potentially cause the global warming problem[2]. Figure 1-2 shows the temperature rise of the Earth's climate system and indicates that the dramatically increase starts from 1950s [3]. Chlorofluorocarbon (CFC) and hydro fluorocarbons (HFCs) are also recognized as a type of greenhouse gases and one of the main reasons for the depletion of ozone layer, which have been widely applied in conventional refrigeration system as the main refrigerant. Therefore alternative refrigeration technology attracts increasing attentions since 1990s [4].

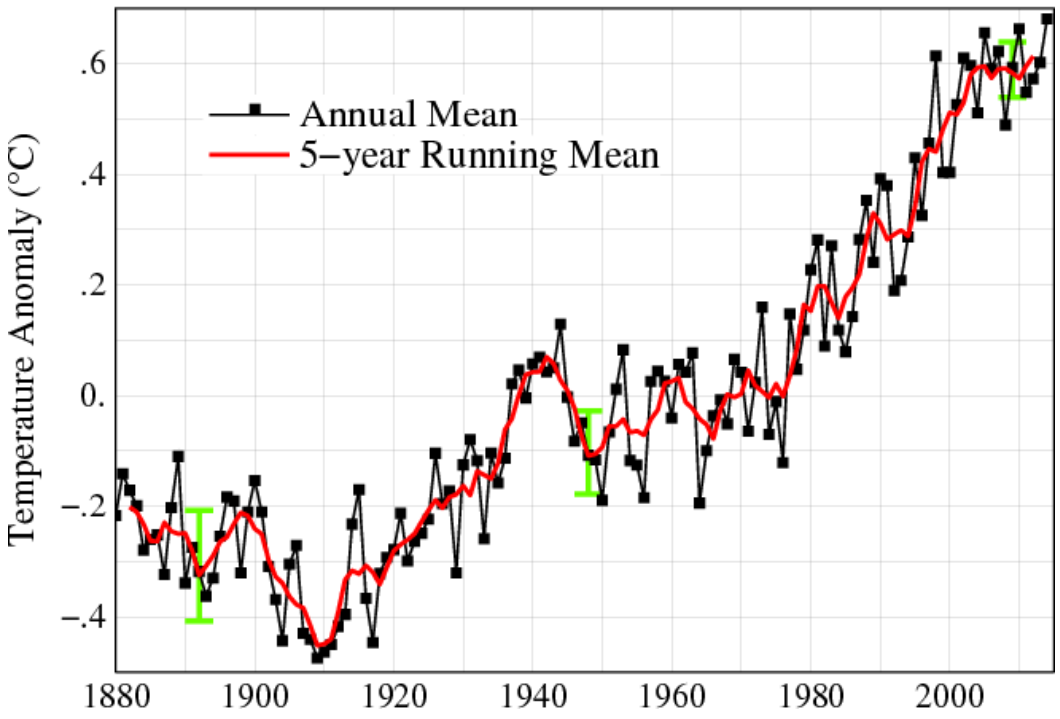

Figure 1-2 Global Land-Ocean Temperature Index[3]

1.1.2. Energy policy of the United Kingdom

According to the 2012 IEA review of the United Kingdom's energy policies, the United Kingdom has set a target to reduce the green gas emission by 50% from 1990 to 2027 and cut the emission by 80% by 2050 [5]. To achieve this long term objective, the UK is going to deliver 15% of the energy demand from renewable sources by 2020 and UK had already demonstrated in 2012 when renewable sources contributed more than 4.1% of the UK's overall energy [6]. The UK's currently approaches towards renewable sources are mainly from installing more offshore/onshore wind station, improving sustainability of biomass, applying solar PV, using tidal power and working on renewable heat sources.

1.2 Project description

Adsorption technology starts to attract attentions because of the oil crisis in the 1970s. And increasingly focuses on this technology is started in the 1990s due to the ecological problems caused by the use of CFCs and HCFCs in conventional refrigeration system [4].

Adsorption refrigeration technology is a type of technology converting heat into refrigeration and normally applies environmentally friendly working fluid as the refrigerant such as water, ammonia and methanol. And most of the refrigerants of the adsorption refrigeration system are so called green refrigerants having zero ODP (Ozone depletion potential) and zero GWP (Global-warming potential). Adsorption refrigeration system has a wide selection of adsorbents including physical and chemical adsorbents for the application of different heat source temperature from 50 ^{o}C to 400 ^{o}C [7].

Resorption is an advanced adsorption cycle first adopted into thermochemical system since 1993 [8]. Resorption system contains two adsorbent beds filled with two different adsorbents. This advanced adsorption system applies the reaction heat of the sorbent to yield cooling effect, while the conventional adsorption utilise the latten heat of refrigerant. The reaction heat of the sorbent is normally larger than the latten heat of refrigerant, which means the theoretical cooling capacity from resorption system, is larger than that of conventional adsorption system. Compared with conventional adsorption system, the resorption has a relatively lower working pressure and simpler system construction. Moreover, there is no liquid phase state existing in resorption system, which means the system is more durable under vibration conditions such as vehicle, fish boats, space cooling and marine application.

A concept design of a novel resorption cogeneration was first proposed by Wang et al in 2011 [9]. This cogeneration system combines the adsorption technology with turbine to produce refrigeration and electricity in a loop. The resorption cogeneration inherits all the advantages of resorption refrigeration system and uses the pressure difference between two adsorbents to generate extra power from an expansion machine.

The main attractions of resorption cogeneration can be summarised as

1) dual energy production including power and refrigeration
2) energy saving (no electrical consumption such as compressor, pump, etc)
3) environmental friendly system (no ODP and GWP working fluid)
4) simple construction, no liquid phase existing in the system (suitable to be used under vibration environment)
5) high coefficient of performance (twice of the conventional adsorption system)
6) wide selection of adsorbents for different temperature range's application

However, due to the limited research efforts on the system investigation, refrigeration generation by adsorption technology is still immature. The investigation on the working conditions of the system, the selection of proper expansion machine for power generation part of the cogeneration and overall system evaluation are important to be conducted.

This study aims to investigate the feasibility of integration the adsorption system with expansion machine for refrigeration and power generation. Resorption

technology was selected as the base of the system due to the mentioned advantages of resorption technology. The first task of this work is to conduct the system design and explore the optimisation methods such as heat/mass recovery processes of the resorption cogeneration system by selecting the optimal resorption working pair and analysing the performance. The second task of this study is to experimentally investigate components performance includes studying the kinetic performance of the identified adsorbents under various working conditions and experimentally testing on a selected expansion machine. The final task is to predict and evaluate the variation performance of a small scale resorption cogeneration system and provide necessary parameters about the designed system such as the weight/size, ranges of power and refrigeration production.

1.3 Contribution to existing research

Many scientists and research groups have analysed, investigated and reported the adsorption technology for refrigeration generation since 1970s [4, 8, 10-14]. However, only few of them have study the combination of adsorption technology with expansion machine and detailed studies on resorption cogeneration have been hardly reported[9, 15-18]. And we found the resorption cogeneration is worth to be investigated because of the previously mentioned advantages.

In this thesis, the existing adsorption technology and the adsorption working pairs have been reviewed to design the cogeneration system. Ammonia-salts were selected as the working pair because of its quick reaction time, high COP, etc. A novel resorption cogeneration has then been designed, proposed and investigated with different resorption working pairs under the driven temperature from 100 ^{o}C to 300 ^{o}C. Results from thermodynamic analysis indicated the

$MnCl_2$-$SrCl_2$ is the optimal resorption working pair to be used of the resorption cogeneration system for the main purpose of refrigeration generation to recovery low grade heat source. Advanced optimisation methods have been introduced and studied, which indicates overall system performance can potentially improve by 35% under the optimal working conditions[16]. An adsorption/desorption performance test bench was designed, constructed and tested in the lab to investigate the reaction speed, working conditions, manufacture processes of adsorbents. The review of existing expansion machines pointed out that scroll expander is one of the promising expansion machine for the integration with adsorption technology. A scroll expander test rig has been design, built and tested in the lab to investigate the performance of this type of expansion machine under similar working conditions of resorption cogeneration [18]. Both of the experimental results obtained from two rigs are used to predict and evaluate the variation performance of a small scale resorption cogeneration system under different working conditions.

1.4 Structure of the thesis

This thesis is organised as follows,

Chapter 2 presents a detailed review of existing low grade heat driven system in order to understand the design and problems of energy system. A detailed study of adsorption technology has been conducted including different types of adsorption working pairs, methods of adsorption performance measurement and optimisation methods for adsorption technology. Moreover, the review of existing expansion machines has been conducted to find out the optimal expander to be integrated with adsorption technology.

Chapter 3 conducted the design and detailed thermodynamic analysis of a resorption cogeneration based on the knowledge gained from chapter 2. Optimal resorption working pair for the cogeneration system has been identified and the performance of twelve resorption working pairs has been evaluated. Heat and mass recovery technology has been introduced and analysed to further improve the performance of the original resorption cogeneration.

Chapter 4 presents the experimental investigation on two optimal adsorbents selected by the analysis in chapter 3. The manufacture process of composite adsorbent using expanded graphite as the matrix of chemical adsorbent has been developed. An adsorption performance test rig using volumetric measurement method has been developed and constructed in the lab to test the adsorption/desorption performance of the composite adsorbent under the similar working conditions of the resorption cogeneration.

Chapter 5 describes the design, construction and experimental tests on a scroll expander test rig. The modification process of the scroll machine from compressor to expander has been reported. A detailed geometric study on the scroll machine has also been conducted to obtain the important parameters of the tested unit. The scroll expander was tested under the similar working conditions of the resorption cogeneration to evaluate the power generation performance of this type machine.

Chapter 6 analysed and predicted the dynamic performance of a small scale resorption cogeneration using the parameters obtained from Chapter 4 and Chapter 5. The evaluation results can be used to predict the refrigeration and power scale from a specific designed system.

Finally, Chapter 7 provides suggestions and recommendations to conduct further work on the resorption cogeneration.

Chapter 2. Critical analysis of the research in the field

2.1 Introduction

Heat driven cycles are widely accepted as promising methods to convert the wasted energy into useful power and can potentially be integrated with existing system to improve the overall system efficiency.

As a types of heat driven technology, adsorption was originally introduced as a concept heat pump and refrigeration system[19]. Extensively attentions have been paid on using sorption technology since the 1970s[7] as a result of ever increasing cost of burning fossil fuels to produce energy, global concerns on the global warming problem.

Chapter 2.2.1 focused on the system level of adsorption technology through conducting a detailed review of existing and developed adsorption systems in order to understand the principle and obtain up to date knowledge of this technology.

The study on the combination of adsorption technology with expander for power generation is still immature. The review on conventional power generation technology is therefore essential in this study, which can be found in Chapter 2.2.2.

Detailed compound level review on the existing adsorption technology and expansion machines have been completed in Chapter 2.3 and Chapter 2.4

to identify the suitable adsorption technology and expansion machine in a combined cogeneration producing power and refrigeration.

2.2 Review on system level of adsorption technology and Rankine-based power generation cycles

Low grade heat is commonly defined as the temperature lower than 250 ^{o}C and huge amount of low heat are available from solar energy, geothermal energy, biomass products and the waste heat from industry[20, 21]. The effective utilisation of low grade heat into useful energy not only can decrease our dependence on limited reserves of conventional energy resources but also help reduce the carbon dioxide emissions produced from conventional energy systems. This chapter focus on the system level review of adsorption cycles and Rankine-based systems to provide detailed information and knowledge about the existing adsorption and power generation systems.

2.2.1. Review of adsorption systems

An interesting approach of using low grade heat is converting it into refrigeration by using adsorption technology. The historical track of the scientific work on adsorption can be traced from 1773, by Scheele and Fontana. However until 1848, this type of technology was first used for cooling, when Michael Faraday built a system using ammonia and silver chloride as adsorption working pair[22]. After the short appearing of this technology for refrigeration production, it disappeared for almost 60 years because the intensively attentions have been paid on using vapour-compression refrigeration for cooling production.

With the growing concerns over the oil crisis, and the ozone layer depletion due to the utilisation of CFCs and HCFCs as refrigerants in conventional vapour-compression refrigeration system, the interests on adsorption systems has increased since 1970s. Adsorption technology is one of the alternative options to recover the low grade heat such as waste heat or solar energy into cooling power. Moreover, adsorption technology can employ environmental friendly refrigerants such as ammonia in the system, which has zero ODP and GWP, as working fluid [23-25]. Wang et al. [4] pointed out the sorption system is one of the most promising technologies to recovery low grade heat into refrigeration

In comparison with vapour compression refrigeration system, the COP of adsorption system is quite low. The COP of a simple adsorption cycle is normally lower than 0.4 and when the required refrigeration drops, the COP of a simple adsorption refrigeration system can be as low as 0.1 or even lower. The intermittent production of refrigeration power from single adsorption cycle is another obstacle of this technology. Therefore the development of innovative and advanced adsorption cycles to improve the cooling performance and produce continuous refrigeration are extremely necessary for the application of this technology. A summary of existing adsorption cycles proposed and studied by previous researchers can be found in Figure 2-1. Further explanations and comparisons of different adsorption cycles will be given later in this Chapter.

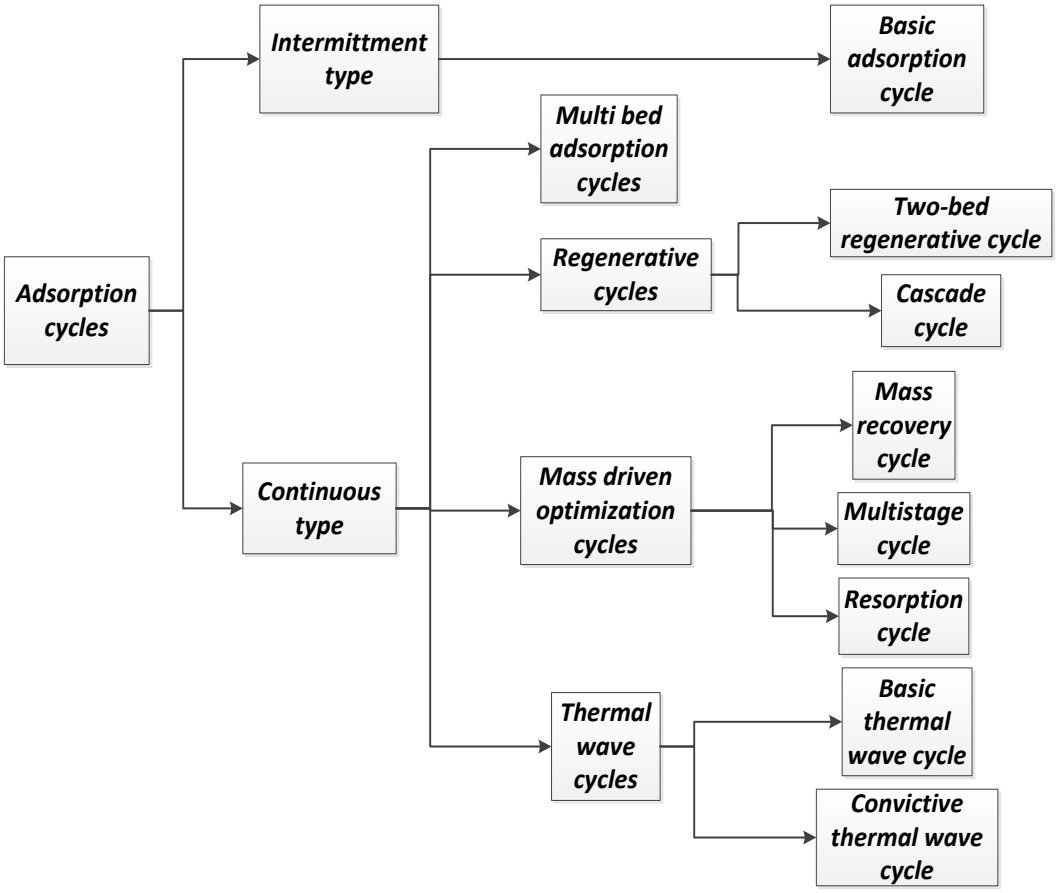

Figure 2-1 The composition of adsorption cycles

Basic Adsorption cycle

In a basic adsorption system, a full cycle includes two processes, adsorption process and desorption process as indicated in Figure 2-2 (a) and Figure 2-2 (b), respectively. In adsorption mode, the liquid phase refrigerant evaporates from evaporator and absorbs by the adsorbent, while the sensible heat and adsorption heat of the adsorbent bed are consumed or removed by heat transfer media such as water or air. The rejected energy is dumped to environment. The cooling power can be obtained from the evaporator, when the refrigeration consumes heat by means of cooling production Q_{cool} from environmental temperature for the

evaporation process inside the evaporator. Desorption mode is running like a reverse way of adsorption mode. In desorption mode, the adsorbent bed is heated by the heating sources when the refrigerant released from the adsorbent bed and flows to the condenser. The liquid refrigerant is normally stored into a liquid tank.

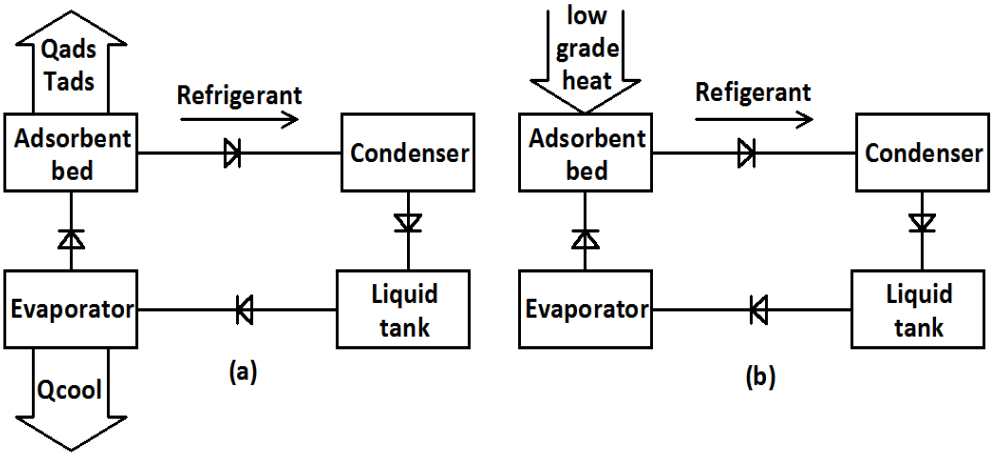

Figure 2-2 Principle of adsorption cycle
(a) adsorption phase, (b) desorption phase

The adsorption system possesses several advantages such as simple control, no need of pump equipment, relatively low operation costs, no vibration and applying environmental friendly working fluid compared with conventional vapour-compression refrigeration system. When compares with another popular refrigeration technology- absorption system, the adsorption refrigeration technology still has several advantages which can be summarised as follows[26],

1) Large range of heat sources: With the proper selection of adsorption working pair, adsorption system can be powered by the temperature ranged from 50 ^{o}C to 600 ^{o}C, which will normally be provided by solar energy and waste heat. The driven temperature for absorption

system is narrow than that for adsorption system and the absorption technology requires the minimum driven temperature at 80 ^{o}C[26].

2) Large range of application: Adsorption system is insensitive towards vibration, therefore it is suitable for operating in serious condition, such as train, bus, boat and spacecraft [27-30]. On the contrary, since the working mediums of absorption system are in liquid phase and flow inside the system randomly, vibration or shock could cause the system working abnormally and reduce the system efficiency.

3) Simple construction: The adsorption system does not require splitter and rectifier, which are necessities in absorption refrigeration system.

4) No Corrosion: The working pair normally used in adsorption system has not got corrosion problem. However, absorption system suffers from corrosion issue as long as the operation temperature is higher than 200 ^{o}C.

Regenerative cycles

In a basic adsorption cycle, huge of heat is consumed by the adsorbent bed to start the desorption process and in order to produce refrigeration, the adsorbent will normally be cooled down by media such as air or water. The concept of regenerative adsorption system was proposed to recover the sensible heat of metallic components of the adsorbent bed and the sensible heat of the adsorbent during adsorption process. The recovered heat will normally be stored in heat transfer oil and be used to serve as the

preheated heat to heat the other adsorbent bed. The overall system efficiency of multi-bed adsorption cycle can be effectively improved by using regenerative method[31]. The regenerative cycles can be further classified as two-bed/multi-bed regenerative adsorption cycle, cascade adsorption cycle, cascading cycle, thermal wave cycle [32] and desiccant adsorption cycle [33, 34].

Saha et al. studied on a dual-mode regenerative adsorption refrigeration system using silica gel and water as adsorption working pair [35, 36]. Theoretical analysis indicated that this advanced refrigeration system can effectively recovery the waste heat energy with the temperature ranging from 40 to 90 ^{o}C [35]. Further experimental exploration on this regenerative adsorption system has been conducted, the average COP achieved from this advanced system in single-stage mode and three-stage mode is 0.45 and 0.2, respectively[36]. A multi-bed adsorption regenerative cycle was proposed by Chua et al. to extract the most enthalpy from the low grade heat source and minimise the fluctuation of the chilled water temperature[37]. The simulation results indicated that a four-bed adsorption regenerative system could potentially produce 70% more cooling capacity compared with a typical two bed system and a six-bed adsorption system can even improve 40 % cooling production[37].

The regenerative heat from one adsorbent bed to the other adsorbent bed was also been employed in cascading refrigeration cycles such as the reported experimental approach conducted by Douss and Meunier [38]. The cascading adsorption refrigeration system consists of two working pairs, zeolite-water as high temperature stage and active carbon-methanol as low temperature stage[38]. Results indicated COP of the system can be as high as 1.06, which is higher than that of a two-bed adsorption refrigeration cycle (≈0.75) and much higher than that of an intermittent cycle (≈0.5) under the same working conditions[38].

The concept of using the regeneration between several adsorbent beds has also been employed in thermal wave adsorption cycles, which was studied by Critoph with the COP from 0.3 to 1.3 under various working conditions[39]. A detailed simulation on thermal wave adsorption heat pump was conducted by Sward et al. [40]. Results shown the COP of thermal wave adsorption refrigeration cycle under 393 K heat source temperature could be higher than 1.2. However, the study on thermal wave concept is still stagnated in theoretical calculation and simulation stage because of the difficulty of controlling flow rate of this technology to be used in the real adsorption refrigeration system[41].

Mass driven optimized cycles

Unlike regenerative cycles, mass driven optimisation cycles utilise the different working conditions of refrigerant between the adsorbent beds to optimise the performance of adsorption and desorption processes. The mass driven optimisation cycles include mass recovery cycle, multistage cycle and resorption cycle. All of the mass driven optimisation cycles require to be started between two or more than two adsorbent beds.

In mass recovery adsorption cycle, the first adsorbent bed who has just ended the desorption process at high pressure condition will be bypassed to the second adsorbent bed who has just ended the adsorption process at low pressure condition. In this instance, the decomposition rate in the first adsorbent bed is sharply increased with the aid of huge pressure difference between the two adsorbent beds. As a result the cyclic adsorption quantity is enhanced with the mass recovery technology. Akahira et al. [42, 43] investigated a silica gel-water adsorption cycle by utilising mass recovery technology. Results showed the SCP of the mass recovery cycle was higher than that of common adsorption cycle and the mass recovery cycle was more suitable with low temperature source. An experimental comparison between a double stage mass recovery cycle, a single stage

mass recovery cycle and a conventional adsorption cycle was presented by Oliveira et al. [44]. The double-stage mass recovery cycle generated 42% more refrigerant mass than the common cycle at 85 ^{o}C, while the single stage mass recovery cycle could generate 37% more refrigerant mass than the latter. L.W. Wang et al. [45]compared the performance of a $CaCl_2$-AC adsorption cycle with and without mass recovery. The COP and SCP of the system were improved by 48.6% and 54.5%, respectively, when the mass recovery was applied. Moreover the mass recovery technology could also be employed with heat recovery adsorption cycle. The experimental results proved that the COP of a heat recovery adsorption cycle could be increased with the mass recovery technology [46].

Resorption cycle is a type of mass driven optimisation adsorption refrigeration cycles and this advanced adsorption system was first proposed adopted by thermochemical system since 1993 [8]. Resorption system mainly contains two adsorbent beds who individually filled with two different salts. Under the same working pressure, the equilibrium temperatures of the two adsorbents are different. The salt who reacts at lower temperature is called low temperature salt (LTS), and the other is named high temperature salt (HTS). The principle of resorption cycle is shown in Figure 2-3. The working processes of resorption cycle are as follows:

(a) Heating process: The HTS is heated by low grade heat in this process, when the LTS adsorbed the ammonia gas escaping from the HTS. The LTS is cooled down at ambient temperature to release the synthesis heat.

(b) Refrigeration process: The HTS exothermally reacts with ammonia desorbed from LTS due to the pressure difference between HTS and LTS. Meanwhile, decomposition of LTS ammoniate extracts the heat from surrounding resulting in the cooling production.

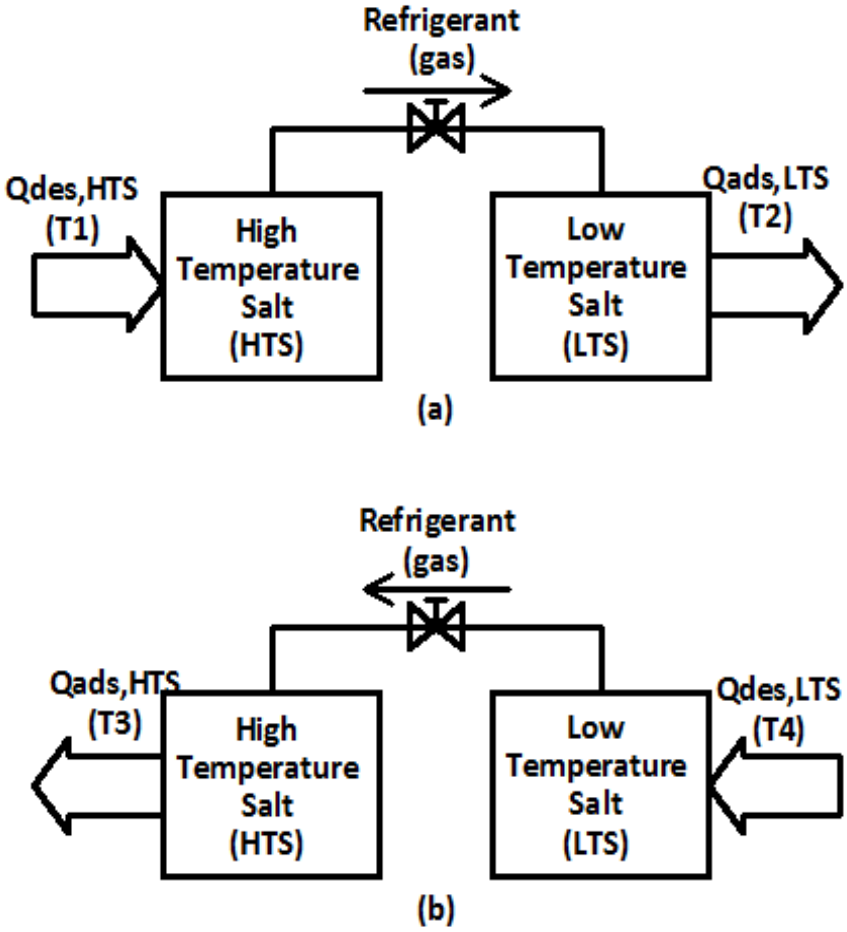

Figure 2-3 Principle of resorption cycle

(a) heating phase, (b) refrigeration phase

In resorption cycle, the adsorbent bed with low temperature salt is dual-purpose serving as both condenser and evaporator. The application of resorption cycle can be utilised for refrigeration, heat pump and the purpose of increasing temperature. Spinner[8] proposed a heat recovery resorption cycle, which recovered the adsorption heat to reduce system heat consumption. An innovative multimode, multi-salt and multi-effect solid-gas chemisorption refrigeration system was first presented by T.X. Li et al. [47]. The evaporation in adsorption process and the decomposition of

LTS in resorption process both contributed to the cooling production. The synthesis heat of HTS was recovered for the generation process within the middle temperature salt (MTS). The theoretical analysis shown the COP of this system could be achieved from 0.91 to 1.80. Several modes about conventional adsorption cycle, resorption cycle and combined adsorption and resorption cycle were investigated by Oliveira et al. [48].

In order to obtain a more comprehensive understanding of resorption cycle, the comparison of resorption cycle and normal adsorption cycle has been conducted and summarised [49]:

(1) Resorption cycle is more suitable for vibrating circumstances than adsorption cycle. Because second adsorbent bed (LTS) of resorption cycle replaces the evaporator and condenser normally used in adsorption cycle, which causes no liquid phase refrigerant in the whole cycle.

(2) Resorption cycle is safer than adsorption cycle, as the working pressure of resorption cycle is relatively lower than that of traditional adsorption cycle.

(3) The cooling capacity of resorption cycle is theoretically larger than that of normal adsorption cycle. Because the resorption employs desorption heat to yield cooling production and the desorption heat is almost twice of the vaporisation enthalpy of ammonia, which is used to produced refrigeration in conventional adsorption refrigeration cycle.

In summary, this chapter has introduced and summarised the existing adsorption refrigeration cycles. The comparison of adsorption refrigeration and absorption refrigeration system has been included in order to obtain the necessary knowledge of

adsorption refrigeration system. The regenerative method and mass driven optimisation method have high potential to improve the overall refrigeration system performance as reported by previous researchers. As an advanced adsorption refrigeration technology, resorption system can theoretically achieve twice of the cooling capacity compared with that of conventional adsorption cycle under the same working conditions. Moreover, no liquid phase of fluid exists in the system, which means this technology is more suitable to be used under vibration conditions. Because both experimental and theoretical study on combining adsorption technology with expansion machine for combined refrigeration and power generation is still immature in the early stage. As the most popular and must mature power generation systems, Rankine-based cycles have been widely applied for domestic and industrial application since it was developed. The review of existing Rnakine-Based system should be conducted to obtain the knowledge for the system level design of power generation system for the design of combined refrigeration and power cogeneration system using adsorption technology and expansion machine. The detailed review of Rankine-based power generation systems will be covered in the following chapter.

2.2.2. Rankine-based power generation systems

Rankine cycle

Steam Rankine cycle has been widely employed in large scale power plants in industry. This technology has been recognised as the most popular energy conversion systems, which mainly consists of four components, a pump, an evaporator, a turbine and a condenser shown in Figure 2-4.

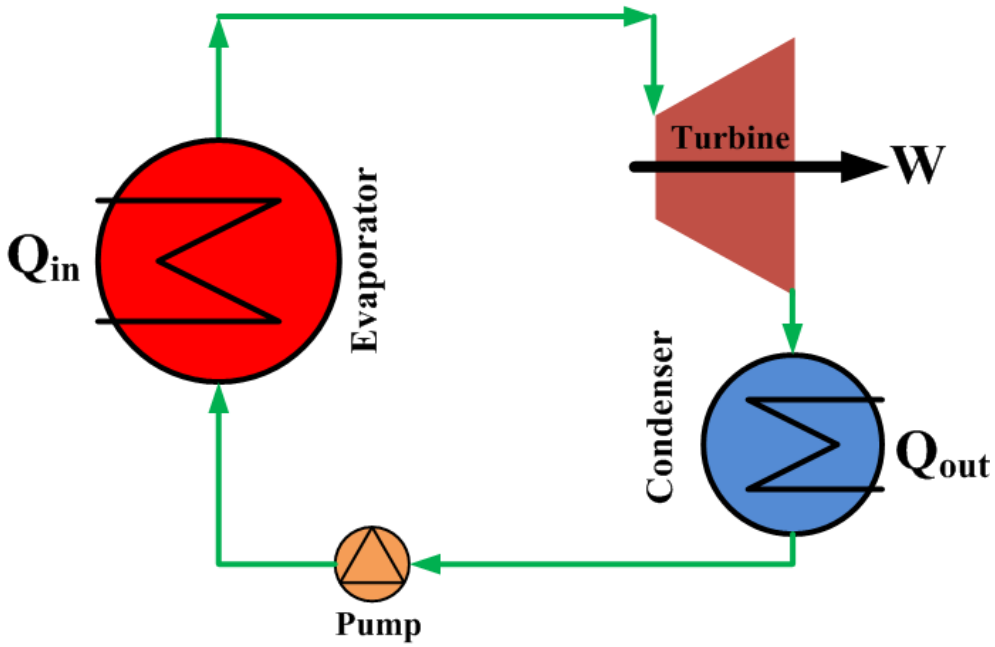

Figure 2-4 Principle of steam Rankine cycle

The working principle of steam Rankine cycle can be described as follows. The liquid-phase water is first compressed to high pressure state and flows into the evaporator, where the heat is provided from the heat sources to change the water from liquid phase into gas phase. The high temperature and high pressure steam is then flowing through an expansion machine where the power can be retrieved or converted into electricity. In the final

step, the condenser removes the heat from the expander steam and condenses the steam into liquid phase.

Rankine cycle applies water as the working fluid, which has the advantages of high specific heat capacity, broad ranges of working conditions, non-toxic, safe to use and environmentally friendly. However, steam Rankine system requires very high driven temperature in order to keep the steam in gas phase at the exit of the expander. Because the exiting of liquid phase of fluid requires to be prevented otherwise the blades of turbine will be gradually damaged resulting to the reduce of lifetime and decrease of the turbine efficiency [50]. In conclusion, the steam Rankine cycle is not recommended to be used to recover low grade heat.

Organic Rankine cycle

As mentioned before, steam Rankine cycle requires very high heat source temperature. The Organic Rankine cycles have been widely investigated since the 1880s. Instead of using water in Rankine cycle, the Organic Rankine cycles employ organic working fluids such as refrigerants and hydrocarbons to recover the low grade heat from biomass power plant, geothermal power and solar ponds[51].

The working fluids used in Organic Rankine cycle can be classified as wet, dry and isentropic types, who have different slopes of the vapour saturation curves in T-s diagram as indicated in Figure 2-5. The wet fluids such as R717 have negative slope of the vapour saturation curve, on the other hand the dry fluids have a positive slope. The isentropic fluids have a vertical slope on the vapour saturation curve such as R134a.

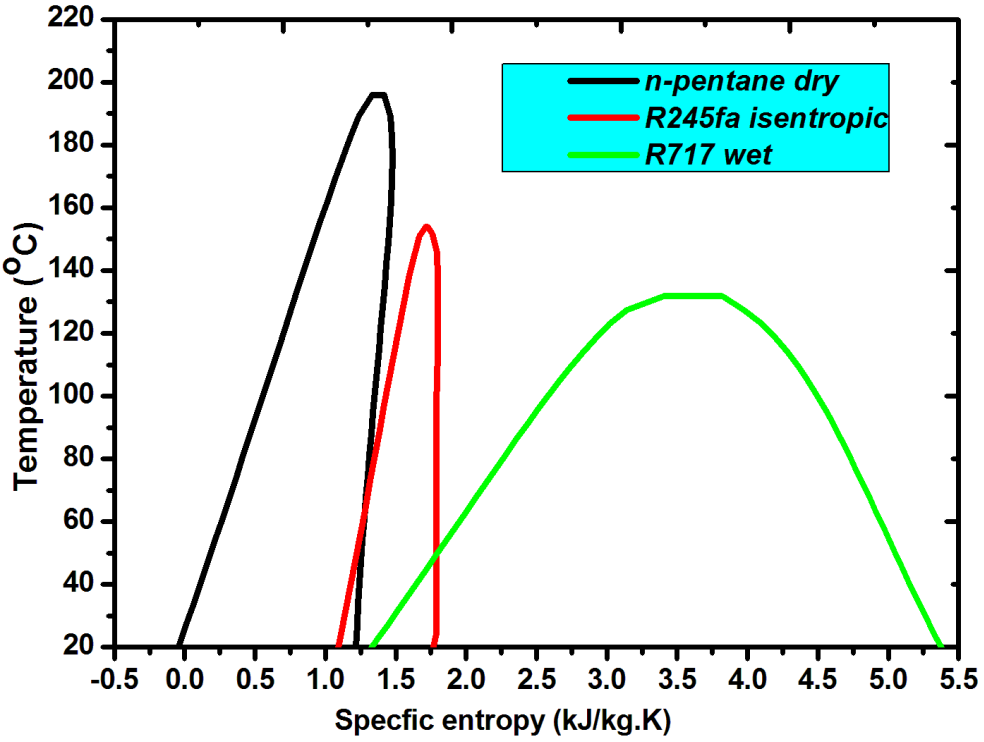

Figure 2-5 Three types of ORC working fluids: dry, isentropic and wet

Several researchers pointed out a wrong choice of working fluid could lead to a low efficient and expensive plant of ORC system. Tchanche et al. [52] assessed the thermodynamic and environmental properties of 20 different fluids for solar Organic Rankine Cycle by comparing the system efficiency, irreversibility, flow rate, pressure ratio, toxicity, flammability, ozone depletion potential (ODP) and global warming potential (GWP). The influence of fluid properties on an ORC and a supercritical Rankine cycle with 35 different working fluids were assessed by Chen et al. [53] considering the latent heat, density, specific heat and the effectiveness of superheating. An exergy based study of fluid selection for geothermal generated ORC system was conducted by Heberle et al. [54]. The exergy analysis indicated in series circuit, working fluids with high critical temperatures such as isopentane are more favourable to be used. The working fluids with low critical temperatures, such as R227ea, are favoured in parallel circuits and power generation under the heat source temperature

below 450K. The author investigated a small scale solar powered regenerative ORC system using 6 different refrigerants. The first and second law analysis suggested that R600 and R600a have the best performance under the temperature ranges from 70 ^{o}C to 120 ^{o}C [50].

In conclusion, Organic Rankien cycle is one of the promising technologies to recovery low grade energy into power. The working fluid selection for Organic Rankine cycle plays a very critical role to utilise this technology. The working fluids used in ORC system will normally has a lower critical point than water, which has the benefit of being able to be driven by low grade heat such as solar energy and waste heat from industry. Dry and isentropic types of working fluid are suggested to be used in ORC system to prevent the damage of the expansion machine. For the purpose of power generation, the expansion machine is the most important component in any power generation plants and the detailed study of different types of expansion machines will be covered in Chapter 2.4.

Kalina cycle

As a transformation ORC system, Kalina cycle was proposed by Kalina in 1984[55], using ammonia-water mixture as the working fluid, which enable a better thermal march under various heat source temperature compared with conventional pure working fluid ORC system [56]. The Kalina cycle requires addition equipment-a separator compared with ORC system and the schematic diagram of Kaline cycle was show in Figure 2-6

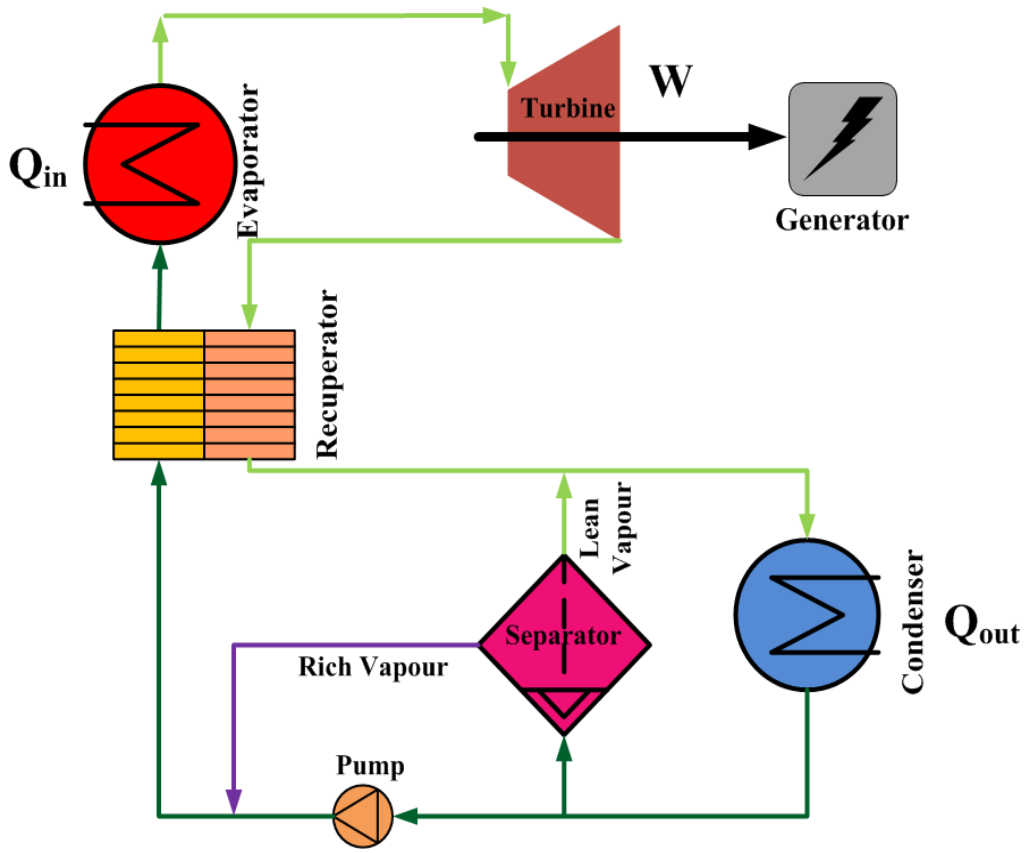

Figure 2-6 Schematic diagram of Kalina cycle

Theoretical analysis indicated that under the heat source temperature at 532 ^{o}C, the first law and second law efficiency of the Kalina cycle are 32.86 % and 70.03 %, which is around 20 to 50 % higher than that of the Rankine cycle[55],. The first commercial Kalina cycle was constructed in Husavik, Iceland in 1999 using geothermal energy [57], which was designed to generate 2 MW power under the heat source temperature at 124 ^{o}C. The remaining energy of the geothermal water at 80 ^{o}C was utilised for district heating supply. Bombarda et al. [58] recently presented a thermodynamic comparison between Kalina cycle and ORC system to recovery the waste heat from two diesel engines. The results indicated the Kalina cycle requires higher maximum pressure compared with ORC system to generate the same power output and the ORC system shows a better performance for the heat recovery process under medium temperature ranges. An integrated Kalina and Rankine cycle was proposed

by Zhang et al. [59] to generate power/heat in winter and power in the other seasons. The thermal efficiency and power recovery efficiency of the integrated system are reduced by 18.0 % and 24.7 %, respectively compared with that of the system running in the other seasons.

Both the theoretical and experimental investigation of Kalina cycle has indicated this advanced power generation system can be used to effectively recovery low grade heat energy into useful power and can potentially recovery wider heat source temperature by changing the concentration of the working fluid. However, this Kalina cycle requires more components and precise controlling strategies than conventional ORC system, which will result to a more expensive and complex system.

Goswami cycle

Goswami cycle was proposed to produce power and refrigeration within on loop by adding a heat exchanger at the outlet the expansion machine to obtain the cooling effect. The theoretical overall energy efficiency of Goswami cycle can be higher than that of Kalina cycle because of the cooling production. The schematic diagram of Goswami system can be illustrated as Figure 2-7 [61]. The Goswami cycle is a combination of Rankine technology and absorption refrigeration system, which can continuously generate power and refrigeration in a loop [62-66]. Hasan et al. [66] found the absorber has the highest exergy destruction under the heat source temperature from 47 ^{o}C to 187 ^{o}C while the rectifier occupies the highest exergy loss when the temperature is higher than 187 ^{o}C. The maximum second law efficiency was achieved at 65.8% under the heat source temperature of 420K reported by Hasan et al. [63]. However, the Goswami cycle suffers from its system design to produce refrigeration whose energy efficiency of refrigeration is only about 1.2 % [60].

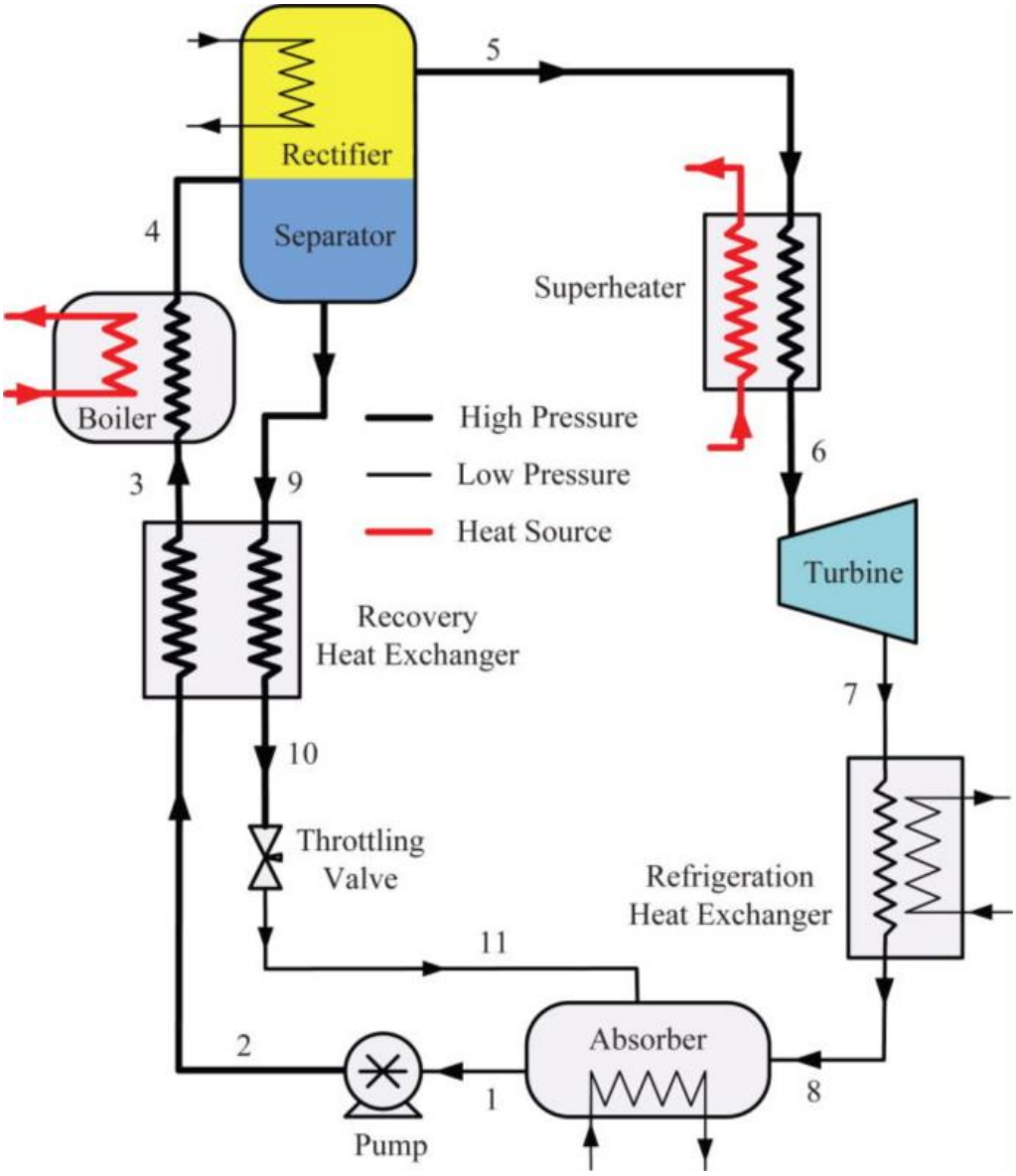

Figure 2-7 Schematic diagram of the Goswami cycle [60]

In summary, although the Goswami cycle can potentially produce combined power and refrigeration, the low performance for refrigeration generation this system restricts the application of this technology for the place requiring dual-energy sources such as supermarket and commercial buildings.

2.3 Current status of adsorption technology

In this chapter, a comprehensive component level review of adsorption technology has been conducted in order to obtain the necessary knowledge of adsorption technology to be upgraded in to system level of study. The common refrigerants used in adsorption system, conventional adsorption working pair, and different measurement methods of adsorption quantity and potential component level optimisation methods have been covered in this chapter.

2.3.1. Selection of refrigerants

Common refrigerants

Table 2-1 Physical properties of the most common refrigeration in adsorption system

Refrigerant	Chemical formula	Boiling point (℃)	Relative molecular weight (g/mol)	Latent heat of vaporization L (kJ/kg)	Standard density (kg/m^3)	ρL (MJ/m^3)
Water	H_2O	100	18	2258	958	2163
Ammonia	NH_3	-33.3	17	1368	681	932
Methanol	CH_3OH	64.7	32	1102	791	872

The selection of refrigerants depends on the different application, for instance temperature range, application places (commercial, industrial and residential application) and power output. In adsorption system, the most

generally considered refrigerants are ammonia, methanol and water. The physical properties of these three refrigerants are listed in Table 2-1.

1) Water

Water is considered as an ideal refrigerant in many respects, possessing the highest latent heat and no-toxic. Water is commonly paired with zeolite and silica gel as adsorption working pair. Nevertheless, there are mainly two problems, when the water is utilised in adsorption system. When the working temperature is below 0 ^{o}C, the water will become into ice, which will damage the system components and therefore the system cannot be applied as freezer. Moreover, the low evaporating pressure limits the mass transfer and leads to a slow reaction speed and small specific cool power (SCP) output.

2) Ammonia

The latent heat of ammonia is almost half of water. However, due to the high evaporating pressure of ammonia (about 8 bars at 30 ^{o}C), the adsorption process is faster than water and methanol systems. The ammonia boils at -33.3 ^{o}C and solidifies at -77.7 ^{o}C under one atmosphere[67]. Although ammonia is an environmentally friendly refrigerant, the irritating ammonia gas could be dangerous with high concentration when it is exposed at ambient. Therefore the ammonia system requires secure gas tightness.

3) Methanol

Methanol has higher evaporating pressure than water, which leads it can be used into ice making machine. It is instable at temperature higher than 120 ^{o}C, and reacts with copper under high temperature. Methanol is one of the smallest and simplest organic molecules, which is a good property for

physical adsorption. Under condition of one atmosphere, the boiling point and solid point of methanol is 64.7 ^{o}C and -97 ^{o}C, respectively [67].

Table 2-2 Comparison of the common refrigerants in adsorption system

	Water	Ammonia	Methanol
Advantages	Safe and no-toxic; Non-pollution; Compatible with copper; Highest latent heat	Natural refrigerant; Non-pollution; High evaporating pressure; High latent heat; Good heat stability	Low refrigeration temperature (ice-making)
Disadvantages	Not suitable for the temperature lower than 0 ^{o}C; Low evaporating pressure	Incompatible with copper; Flammable in a specific concentration; Toxicity; Blasting danger in air	Toxic; Inflammable; Low evaporating temperature (lower than 1atm); Incompatible with copper under high temperature; Instable at temperature higher than 120 ^{o}C; Low evaporating pressure
Common adsorbents	Zeolite Silica gel	Activated carbon Metal chlorides	Activated carbon Zeolite

The selection of refrigerant in refrigeration system commonly consider the following parameters: large specific latent evaporating heat, high thermal stability, environmental friendly, non-flammable and low operational pressure during operational conditions. It is quite hard to find a refrigerant, which can meet all the requirements as listed. In adsorption refrigeration system, water, ammonia and methanol are the most popular used refrigerant. The comparisons considering about the preferred selection methods of refrigerant of these three refrigerants are listed in Table 2-2.

2.3.2. Working pairs

Likewise the working fluids in ORC system, the adsorption working pairs in adsorption system determine the optimal working conditions of the system and decide the required designed parameters. The adsorption working pairs can be classified into two groups by means of physical and chemical adsorption working pairs.

Physical adsorption is mainly caused by Van der Waals force between the adsorbent and refrigerant. The fully adsorbed physical adsorbent can still continually adsorbs more molecules through the monolayer adsorbed gas molecules using the intermolecular force between each other. In theory, the physical adsorption process happens on the surface of solid sorbent, which has no selectivity to adsorb gas molecules. After specific treatments on the physical adsorbent, more paired refrigerant can be adsorbed on the adsorbent [68-70], which means special treatments on the physical adsorbent can potentially improve the adsorption performance of physical adsorbent.

Chemical adsorption is caused by the reaction effect between adsorbed molecules and the surface molecules of adsorbents, such as electron transfer, atom rearrangement and fraction or formation of chemical bonds, etc. The adsorbed molecule will not keep its original state in chemical adsorption process, for example coordination reaction. More detailed explanations on the principle of chemisorption will be provided in the following chapter.

Physical working pairs

The most commonly used physical adsorbents include activated carbon (AC), zeolite and silica gel.

Activated carbon based working pair

Activated carbon is made from high-carbon materials, such as wood, peat, coal, fossil oil, chark, bone and so on. Activated carbon can be paired with methanol or ammonia as adsorption working pair.

Activated carbon – Methanoal ($AC-CH_3OH$): This working pair is widely use in adsorption system, which has the advantages, such as large adsorption/desorption capacity, low driven temperature (lower than 120 ℃), high latent heat, etc. Moreover, this working pair is suitable to use solar energy as heat source, because of its low desorption temperature, which is around 100 ℃. In 1999, Sumathy[71] presented a solar-powered ice maker, which achieved refrigeration COP about 0.1-0.2. Later, Shanghai Jiaotong University proposed a hybrid system of solar-powered water heater and adsorption ice maker. This hybrid system can heat 60kg water to 90℃ or produce 10kg ice per day [72].

Activated carbon – Ammonia ($AC-NH_3$): This working pair has the similar adsorption process as $AC-CH_3OH$. Compared with $AC-CH_3OH$, this working pair has higher working pressure under the same driven heat source temperature, which can help to increase the mass transfer performance, and reduce the cycle time [73].

Zeolite based working pair

Zeolite is a type of alumina silicate crystal, which can accommodate with metallic cations such as Na^+, K^+, Ca^{+2} and Mg^{+2}. Chabazite, sodium chabazite, cowlesite and faujasite are four most commonly used zeolite types of physical adsorbents in adsorption technology.

Zeolite – Water: The most common utilization of this working pair is in dehumidification cooling system and adsorption refrigeration system. The adsorption heat of this pair is from 3300 to 4200kJ/kg. Because the intermolecular forces between Zeolite-water is so high that the desorption heat is as high as 250-300℃. Poyelle et al. [74] built an adsorption air conditioning unit, in which they achieved the 0.68 of COP and the 135 W/kg of SCP. Later, Lai et al. [75] presented a periodic reversal forced convective cycle with zeolite 13X-water pair. The results of calculation showed that the heat pump COP and refrigeration COP can achieve 0.17 and 0.9, respectively. An adsorption cold storage system with zeolite water pair was proposed by Lu, YZ. et al. [10], which achieved 4.1kw in the whole cycle.

In adsorption refrigeration system, Zeolite-water has been widely applied for open dehumidification system and close adsorption system. This working pair is suitable to be used under the heat source temperature around 200 ^oC, because of its large intermolecular forces and high chemical stability. This adsorption working pair cannot produce the

refrigeration temperature lower than 0 ^{o}C, which means it is not suitable to be used as an ice maker. Moreover, the mass transfer of this working pair is quite poor, which is a result of negative system pressure.

Silica gel based working pair

Silica gel is a type of amorphous synthetic silica. In industry, the silica gel is made from Sodium silicate solution and inorganic acid (HCl or H_2SO_4). The ionic reaction of the manufacture process can be displayed as $SiO_3^{-2} + 2H^+ + nH_2O \rightarrow SiO_2 \cdot nH_2O + H_2O$. The silica gel, which is type of white polymer, is presented as $SiO_2 \cdot nH_2O$ in the equation. In adsorption refrigeration, the silica gel is normally worked with water.

Silica gel – Water ($SiO_2 \cdot nH_2O - H_2O$): In this working pair, the hydrogen bond is the main adsorption force, which causes desorption temperature can be very low. Soha et al. [69, 76, 77] developed a three stage adsorption system, which can be driven by the temperature about 50℃. W.D. Wang et al. [78, 79] in Shanghai Jiao Tong University developed a silica gel adsorption chiller, which can be powered by temperature of 55℃. Nevertheless, the adsorption quantity of this pair is just 0.2kg/kg and this working pair cannot produce evaporating temperature below 0℃.

In conclusion, this physical working pair has the advantages such as relatively low driven temperature for regeneration process, which can be as low as 55 ^{o}C [78, 79], safe and environmental friendly refrigerant. However, similar as Zeolite-water, silica gel-water cannot be used to produce cooling effect when the required temperature is lower than 0 ^{o}C. The cyclic adsorption/desorption performance of this working pair is not very high, which will results to relatively large size of the whole system.

Chemical working pairs

The reaction between chemical working pairs is commonly driven by the internal force of the adsorbent and refrigerant, which mainly includes functions of complication, coordination, hydrogenation and oxidisation [7]. The most used chemical working pairs include Metal chlorides-ammonia and Metal hydrides-hydrogen[80].

Metal chlorides – Ammonia $(M_aCl_b - NH_3)$

In chemisorption refrigeration system, Metal chlorides-Ammonia is the most commonly selected and used working pair and $CaCl_2$, $SrCl_2$, $MnCl_2$ and $BaCl_2$ are four usually used Metal chlorides in adsorption refrigeration system to meet different requirements[80]. In general, the Metal chlorides will first complex with ammonia into a complex compound $M_aCl_b(NH_3)_c$, which can still start complex reaction with ammonia and convert into $M_aCl_b(NH_3)_d$ as indicated in Equation 2-1. The molar enthalpy for the chemical reaction between the Metal chlorides and ammonia is displayed as ΔH_r , which is the required heat to decomposition the chemical complex compound.

$$M_aCl_b(NH_3)_c + (d-c)NH_3 \rightleftarrows M_aCl_b(NH_3)_d + (d-c)\Delta H_r \qquad \text{Equation 2-1}$$

In convention adsorption refrigeration system, the cooling effect can be obtained from the condenser/evaporator when the ammonia evaporating and adsorbs by the adsorbent. The evaporating process will obtain heat

from the environment and the latent heat of the ammonia will be used to produce refrigeration. The Metal chlorides have large adsorption capacity and because of the process of adsorption is chemical reaction the reaction speed is quite quick at the start of adsorption and desorption process. However, the most commonly problem of Metal chlorides are the swelling and agglomeration phenomenon, which will reduce the performance of adsorption system after several operating cycles of adsorption/desorption process. The development of new composite adsorbent using porous matric to enhance the heat and mass transfer inside the adsorbent is one of the solutions to overcome the swelling and agglomeration phenomenon, which will be introduced and discussed later of this chapter.

Metal hydrides – Hydrogen $(MH_n - H_2)$

The working principle of this working pair for the refrigeration generation is differently from that of Metal chlorides-Ammonia. Instead of using the latent heat of the ammonia during evaporating process for cooling production, the Metal hydrides-Hydrogen uses the endothermic reaction heat required during the decomposition process of the complex compound $MH_n \cdot mH_2$. The synthesis of Metal hydride requires to be started under very high temperature, when the chemical reaction starts from the left side to the right side of the Equation 2-2.

$$M + \frac{n}{2} H_2 \xrightleftharpoons{High\_temperature} MH_n \qquad \text{Equation 2-2}$$

However, the hydrogen is a flammable and combustible refrigerant. And the manufacture cost of Metal Hydrides is quite high, this chemical adsorption working pair is mainly used for cryogenic or high temperature heat pump applications[81]. Because the Metal hydrides have extensively ability adsorption capacity to adsorb hydrogen and the density of the

adsorbed hydrogen is even higher than that of liquid hydrogen, this adsorption working pair is also used for hydrogen storage.

Composite working pairs

The emergence of composite working pairs is to solve two problems in physical and chemical adsorbents. The swelling and agglomeration problem commonly exist in chemisorption, which will reduce the mass and heat transfer of the refrigerant into the adsorbent and therefore reduce the overall performance of the adsorption system.

The other problem is that the adsorption capacity of physical adsorbents is relatively small. Compounding some chemical adsorbents with physical adsorbents can increase the adsorption performance of the original physical adsorbent and enhance the mass and heat transfer to solve the common problems in chemical adsorbents.

Mixture, impregnation and consolidation are three main procedures of making composite adsorbents. Vasiliev et al. [82] mixed activated carbon fibres with metal chlorides, by which significantly improved the performance of the system. By the methods of simple mixture, impregnation and intercalation, three composite adsorbents manufacturing by different methods of processes made from carbon fibres and $MnCl_2$ was investigated. Results showed that the composite made by the combination of impregnation and intercalation methods had the best performance [83, 84]. Adsorption performance of three types of adsorbents are tested by L.W. Wang et al. [85], and results proved the composite adsorbent made by $CaCl_2$ and activated carbon improved the mass transfer and effectively enhanced adsorption quantity. K. Wang [30] and Oliveira RG [86] investigated on the composite adsorbents made from $CaCl_2$ and expanded graphite. The coefficient of heat conductivity and coefficient of heat transfer are both substantially raised.

In conclusion, the working pairs usually used for adsorption technology can be divided into two groups, physical adsorption working pairs and chemical adsorption working pairs. For the purpose of refrigeration generation, these two types of working pairs can both be selected but this study is going to explore the feasibility of combining adsorption technology with expansion machine for dual energy production. In order to drive the expansion machine, the relatively high mass flow rate and pressure difference are required. The chemical adsorption working pairs are selected to meet these purposes. The most popularly used and extensively studied adsorption working pair to be driven by low grade heat for refrigeration production is Metal Chlorides-Ammonia as introduced in Chapter 2.3.2. The problems of Metal chlorides-Ammonia are the swelling and agglomeration phenomenon, which will commonly happen in chemical adsorbents and can be effectively overcome by using porous material as the matrix to improve the heat and mass transfer performance.

Therefore, in this study the manufacture and experimental investigation of composite adsorbents using expandable graphite as the matrix added into Metal chlorides based chemical adsorbents will be investigated in order to obtain the reaction relationships between composite adsorbent and ammonia. The detailed manufacture processes, testing processes and experimental results of the chemical composite adsorbents will be introduced and reported in Chapter 4.

Resorption working pairs

As summarised in Chapter 2.2.1, the resorption technology can potentially produce twice of the refrigeration capacity of conventional adsorption system under the same working conditions. And the resorption system has no liquid ammonia existing in the system, which means this technology can be used under vibration condition such as vehicle application. In order to

use resorption technology to be integrated with expander for power and refrigeration production, which will be introduced in Chapter 3, the review of the study on potential resorption working pairs is necessary for this study.

The working principle of resorption technology can be found in Chapter 2.21. At present, the applications of this technology are mainly on refrigeration [87, 88], heat pump [89], temperature increase and combined heat and power (CHP).

Since the beginning of 1990s, the concept of resorption technology had been introduced in adsorption technology[90]. This concept was first utilised into refrigeration system by Goetz al et. [90]. They tested a solid-gas thermochemical cooling system using $NiCl_2$ and $BaCl_2$, and simulated the influence of external temperature for resorption reaction speed and working pressure[90]. At the same time, a chart to reveal the relationship between the output power per unit volume with external temperature for both adsorbents has been reported[90].

Oliveira al et. [91] first pointed out to use NaBr and expanded graphite (EG) in chemisorption refrigeration system. The NaBr-EG was used as low temperature adsorbent in a resorption refrigeration system when the high temperature adsorbent is $MnCl_2$ [91]. An experimental investigation on a prototype resorption system using $MnCl_2$-NaBr as the resorption working pair has been conducted[91]. Results show that the specific cooling power (SCP) and coefficient of performance (COP) of the tested system under the refrigeration temperature at 15 ^oC can be as high as 129W/kg and 0.46, respectively. Xu J. al et. [92] latterly reported a study of a resorption system for simultaneous cold and heat production using $MnCl_2$ and NH_4CL as the resorption working pair. The experimental study on a prototype resorption rig reports the COP can be as high as 0.35 and the SCP is 1.12 MJ/kg per day. The other widely studied and used high temperature adsorbent in resorption system is $NiCl_2$, which has a higher desorption temperature

around 250 ^{o}C compared with that of $MnCl_2$ while ammonia is the fluid in the system[8, 89, 90, 93, 94].

Advanced transformation of resorption refrigeration system has also attracted the attentions and been explored by several researchers. A combined double-way chemisorption refrigeration system using adsorption and resorption processes was proposed and investigated by T.X. Li al et. [95]. This innovative system applies $MnCl_2$ and $BaCl_2$ as the resorption working pair, while ammonia is selected as the refrigerant in the system [95]. The theoretical results obtained from this study indicated that the double-way chemisorption refrigeration system has potential to improve the COP by 167% and 60% compared with conventional adsorption and resorption cycle under the same working conditions[95]. Moreover, a simple test unit was set up and used in order to study the feasibility of this proposed cycle and the ideal COP of the proposed cycle can reach as high as 1.24 as reported by T.X. Li al et. [95]. A further experimental investigation on this novel chemisorption refrigeration system was conducted by L. Xu et al. [96] and the results obtained from the system show that the COP and SCP is 0.703 and 225 W/kg, respectively.

Experimental investigation and comparison on three different chemisorption resorption working pairs using ammonia as the refrigerant was conducted by Bao HS et al. [97]. The results indicated when the required cooling temperature is below 0 ^{o}C, the SCP of $MnCl_2$-NH_4Cl was 5% higher than that of $MnCl_2$-NaBr and $MnCl_2$-$BaCl_2$ is not suitable to be used to meet this desirable cooling temperature.

In summary, the review of working pairs in adsorption refrigeration system indicated that chemical working pairs are more suitable to be integrated with expansion machine. Because chemical working pairs have large adsorption/desorption capacity and higher power density of the system compared with that of a system using physical adsorption working pairs. The most commonly used chemisorption working pairs include Metal

chlorides-Ammonia and Metal hydrides-Hydrogen. Due to the high manufacture cost of Metal hydrides, the availability of this material is so low that this material is commonly used for cryogenic application.

Metal chlorides-Ammonia is therefore selected to be used and studied in this PhD project. The chemisorption adsorbents suffer from the swelling and agglomeration phenomenon, which will reduce the heat and mass transfer performance of the materials and reduce the overall performance of the system. The exploration and development of composite chemisorption adsorbents have been proven as an effectively solution to overcome the problems. Therefore, in this PhD study, the development of composite chemisorption adsorbents using Metal-Chlorides and expanded graphite will be conducted, which will be introduced in Chapter 4. More extensively comparison and investigation on different types of resorption working pair to meet different refrigeration demands and working conditions should be conducted and explored. Thermodynamic analysis and comparisons of twelve different resorption working pairs used in a combined refrigeration and power generation system to meet various requirements will be introduced in Chapter 3.

2.3.3. Methods of the adsorption performance measurement

The adsorption performance is mainly determined by two aspects – the equilibrium state and the adsorption ratio of the adsorbent. The adsorbent parameters need to be clarified before the design of any adsorption related system. The measurements of adsorption performance can be mainly classified into three types: calorimetric, gravimetric, and volumetric methods [80].

Calorimetric method

The calorimetric method measures the adsorption capacity and kinetic parameters by calculating the energy balance[13]. This measurement method was first proposed by Ruthven [98], which has been proven as an effective method and is a quite useful to measure the liquid adsorption performance test. This measurement method can measure the interaction between the refrigerant and adsorbent relationship and the interaction between the adsorbent molecules. This measurement method highly relies on the sensitivity of the detector. Therefore the application of this method to measure adsorption performance is quite limited.

Gravimetric method

The other approach of measuring the adsorption performance by calculating the mass changes of the adsorbent is called gravimetric method [99, 100]. A schematic diagram of an adsorption performance test bench using gravimetric method is shown in Figure 2-8.

This type of method has the advantages of simple device, easy operation and high sensitivity. One of the drawbacks of using this measurement method is the potential existing of capillary condensation phenomenon when the pressure increases dramatically with the increase of temperature of adsorbents, which will results the system pressure higher than the saturation pressure.

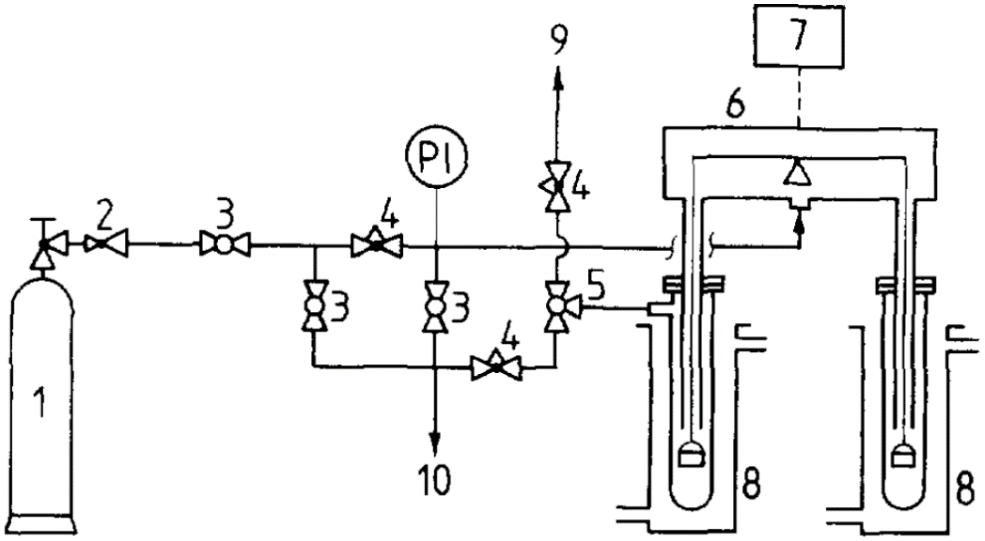

Figure 2-8 Schematic diagram of an adsorption performance test bench using gravimetric method

1. Cylinder; 2. Pressure reduction valve; 3. Ball valve; 4. Needle valve; 5. Three directions ball valve; 6. High pressure microbalance; 7. Electronic balance unit; 8. Water bath; 9. Vent point; 10. Vacuum point; PI. Electronic pressure transducer. [99]

Volumetric method

The volumetric method can be divided into two types – constant volume method and constant pressure method. In constant volume method, the variation of the mass transfer of the ammonia is measured by the variation of the pressure inside the vessel with constant volume. The principle of constant volume volumetric method is shown in Figure 2-9.

The working fluid is storage inside the vapour vessel and the temperature of the vapour vessel is controlled the water circulator while the temperature of the adsorbent is controlled by the oil circulator. This measuring method need to know the dead volume of the system before the testing, which is defined as the whole volume of the adsorbent bed minus the adsorbent volume. The adsorption ratio can be calculated by the variation of the P_1 and P_2. In order to achieve precise results, type of test bench needs to be

designed as small as possible. For example, an adsorption performance test rig reported by Dawoud et al. [101] only uses the tested sample at 3 gram.

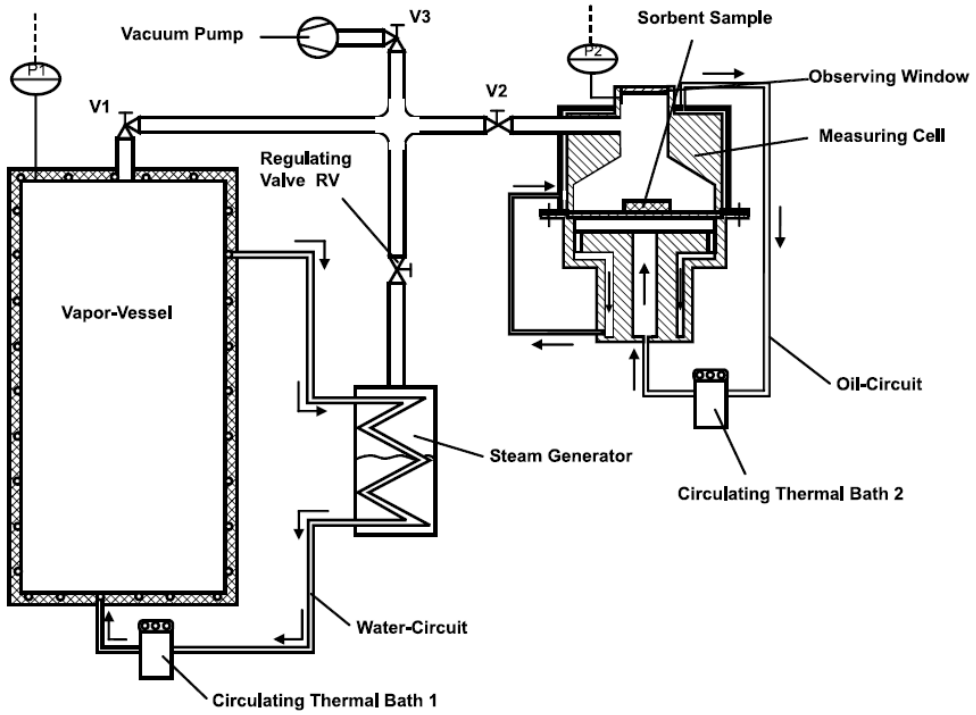

Figure 2-9, The adsorption performance test bench using volumetric method-constant volume [101]

Adsorption performance can also be measured by volumetric measurement method using constant pressure type. This method normally requires a vessel connected with adsorbent bed and calculate the adsorption capacity under different working conditions by measuring the changes of liquid level of the refrigerant inside the vessel. A conversion equation will be used to calculate the adsorption/desorption quantity with provided working conditions of the refrigerant and detailed design of the vessel. A schematic diagram of a test rig using this method is illustrated in Figure 2-10 [83]. This measurement method highly depends on the accuracy and sensibility of the liquid level gage and proper testing procedures should be developed in order to test the sorption performance of different adsorbents.

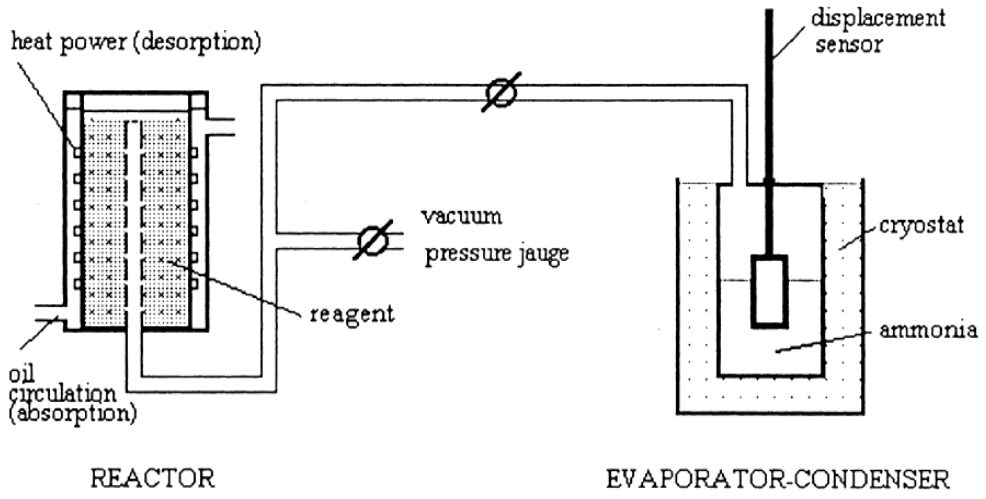

Figure 2-10,The adsorption performance test bench using volumetric method-constant pressure [83]

In summary, three different types of adsorption performance measurement methods have been introduced in this Chapter. The calorimetric method highly depends on the sensibility of detector and conductivity of the testing sample, which is not desirable to be used for chemisorption performance test. The gravimetric method and constant volume volumetric method are effective measurement methods for adsorption performance. However, these two methods can only test the adsorption performance under steady state conditions, which means in order to reveal the adsorption performance the results require to be linked point by point. The duration of the tests conducted by these two methods are quite longer compared with that of constant pressure type volumetric method. A proper designed adsorption performance test rig using constant pressure type volumetric method is a promising method to obtain the dynamic adsorption/desorption performance. Therefore, an adsorption performance test rig will be designed and constructed to test the performance of candidate chemisorption adsorbents in this PhD study. The detailed design, construction and experimental testing procedures of an adsorption performance test rig using constant pressure type volumetric method will be introduced in Chapter 4.

2.4 Review of expansion machines for power generation part of the resorption cogeneration

The idea of using the huge pressure difference occurring inside the adsorption technology during desorption and adsorption process for power generation was first proposed within our research group by the researcher L.W Wang in 2011 [9]. The proposed cogeneration combines chemisorption technology with a candidate expansion machine to produce electricity and refrigeration. Preliminary study on the resorption cogeneration shows the resorption cogeneration has promising performance with the maximum exergy efficiency of 0.69 for power generation and 0.29 for refrigeration [102]. However, the study and selection of expansion machine to be integrated with adsorption system in order to meet the special working conditions of adsorption technology are still blank. Therefor the extensively review of existing expansion machines and comparisons of different types of expander to be integrate with adsorption technology is critical and necessary to be conducted.

The expander is a critical component in order to design and construct a cost effectively and relatively efficiency power generation system. The expansion machines can generally been divided into two types turbine machine using the kinetic energy of the working fluid to drive the expander and positive displace expander producing power by changing the volume of working chamber. The detailed discussions and comparisons on different types of expansion machine will be provided within Chapter 2.4.

2.4.1. Turbines

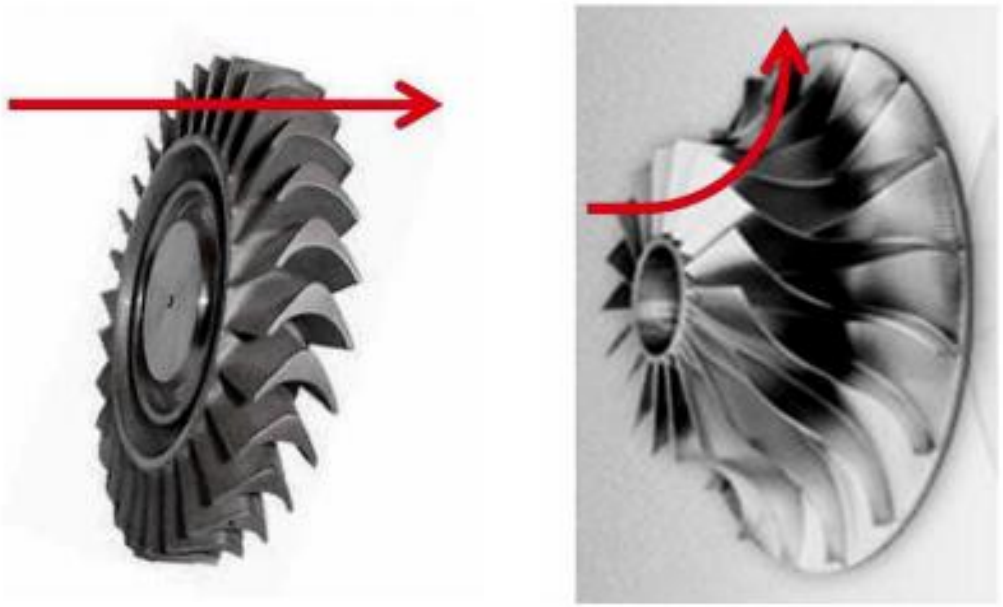

(a) (b)

Figure 2-11 Working principle of flow

(a) axial flow turbine, (b) radial flow turbine [103]

Turbines consumes the internal energy of vapour into kinetic energy, which results the velocity of the flow are relatively high but the pressure and forces between the supply and exhaust point are rather small[104]. The mechanical power is then been obtained from the shaft of the turbine by turning the rotor blades, when the high velocity fluid pass through the turbine. Currently, there are mainly two types of turbines: axial flow turbines and radial flow turbines[105]. The axial flow turbines are driven by the flow in parallel direction to the shaft, while the radial flow turbines are rotated by the flow travelling through the hub to the tipoff the turbine as indicated in Figure 2-11.

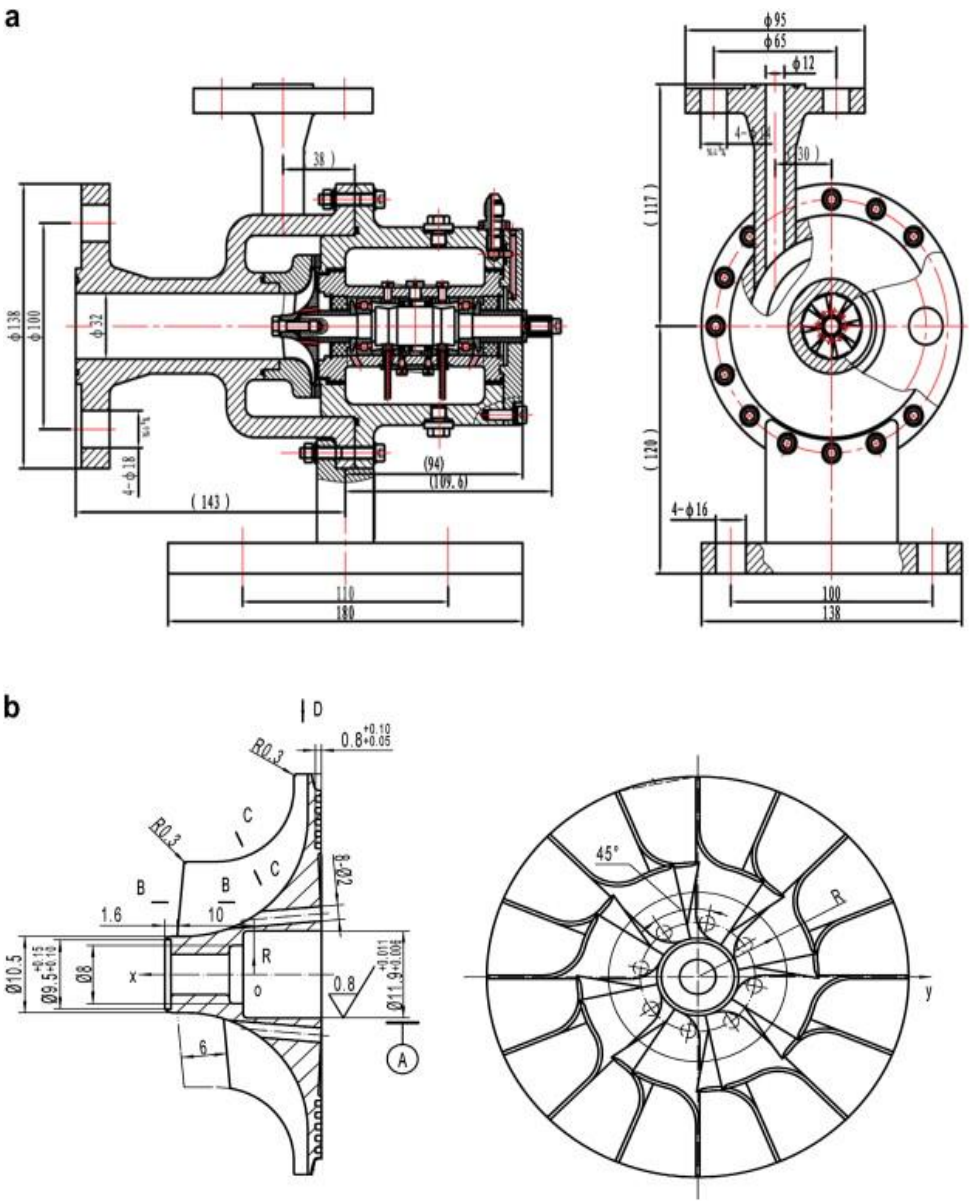

Figure 2-12 Detailed drawing of the radial flow turbine used in an ORC system using R245fa as working fluid[110]

Compared with positive displacement expander, turbines are easier to be designed with relatively less required parts. A single stage turbine only requires two bearings to be mounted to the generator on the shaft. Furthermore, there is no contact seal existing in the turbines, which means no lubrication oil is necessary to be adapted in the system. The rotational speed of conventional turbines ranges from 10,000 rpm to 100, 000 rpm because of the physical design of this type of expansion machine, which

results to a limited or hard sourcing of proper generator for electricity production. One of the solutions to adapt the turbine machine directly with generator is to use high-speed generator, which will leads to high initial cost and increase the overall cost of electricity generation system. The other method to obtain the mechanical work from the turbine and convert it into electricity is by using gear. This method can effectively solve the high initial cost of the system but will require larger space for the turbine unit and reduce the efficiency of the turbine machine by means of mechanical losses in the gear.

Turbines have been widely applied as the expansion machine to replace the piston type of expander in steam Rankine cycle since 19th and have been acknowledged as the optimal expander for large scale power plants. However, the application of turbines for small scale power generation system has not been widely accepted as the best expansion machine especially in the power plants lower than 100 kW. Radial flow turbines are one of the exceptions, which have been recently used for small scale application in Organic Rankine cycle (ORC)[106-111]. Kang reports the design and experimental investigation of an ORC using R245fa as the working fluid and radial flow turbine as the expansion machine [106]. The radial turbine was directly connected to a high speed generator to produce electricity and results indicated the maximum cycle efficiency, the isentropic turbine efficiency and electricity power obtained from the testing rig is 5.22%, 78.7% and 32.7 kW, respectively[106]. Pei et al. [111, 112] carried out experimental investigation on an 1 to 2 kW ORC system using a special designed and constructed radial flow turbine as shown in Figure 2-12. The reported study achieves the isentropic efficiency of the radial flow turbine at 65% to 68% with the rotational speed around 20,000 to 40,000 using R123 as the organic working fluid in the ORC system [110, 111].

However, the application of turbine for small scale application is still not successful because the turbine is designed under rather low expansion ratios and high volume flows. Therefore turbines require to be coupled with high rotation speed generator, which will result to high initial cost of the system. Furthermore, the availability of small scale turbine machine is still limited. The currently used radial flow turbines in small scale power generation system are either from special designed by the researcher or modified from a conventional turbine from automotive turbocharger. The comparisons and selections of the expansion machine to be integrated with sorption technology system will be summarised in Chapter 2.4.3.

2.4.2. Positive displacement expanders

Differently from the working principle turbine machines, positive displacement expanders use the expansion power by changing the volume inside the expansion chambers, which can also been named volumetric expanders. The most commonly used positive displacement expanders include piston type expander, screw expander, scroll expander and vane expander, which will be introduced in the following chapter. Furthermore, the positive displacement expanders can be classified into two types- reciprocating piston expanders and rotary expanders. Screw expander, scroll expander and vane expander are three main types of rotary expanders.

Piston expander

The piston type of machine attracts extensive intentions since it was invented and has been widely applied in different areas to meat various requirements such as the most commonly using in internal combustion engine. In the past 30 years, piston expander has been adopted and

developed as the expander into steam Rankine system integrating with the internal combustion engine to recover the exhaust energy[113].

The piston type of expander can be designed and constructed with one valve version and two valve version in order to allow the expansion process starting and ending inside the piston volume chamber. The working principle of these two versions of reciprocating piston expander can be illustrated in Figure 2-13.

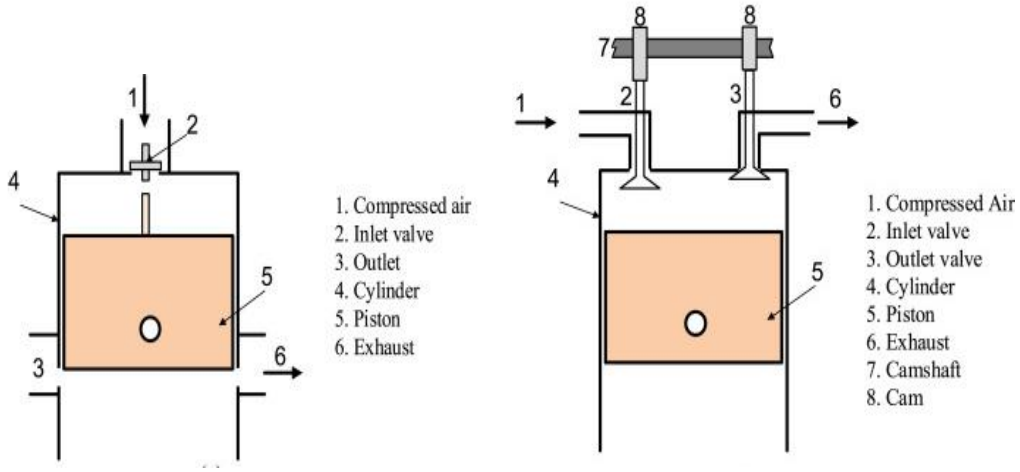

(a) (b)

Figure 2-13 Working principle of reciprocating piston expander

(a) Single valve piston expander; (b) two valve piston expander[114]

However, piston type of expansion machine requires precisely controlled methods for the intake and exhaust valves, which will result to the requirement of a complex control system although this type of expander can potentially reach very high expansion efficiency [115]. Moreover, piston expander requires a lot of bearings, a great number of moving parts and balancing setting up, which results a relatively complex and costly system.

Screw expander

Screw expander is composed of two meshing helical rotors-a male and a female rotor, which requires at least four bearings for the two rotors. This type of expansion machine has been widely applied in steam Rankine cycle plants for geothermal waste heat recovery system[116].

Lubrication oil is commonly used in the screw machine to seal the expanded working fluid inside the expansion chamber which can effectively reduce the internal leakage losses during the expansion process. Screw expander has a relatively high rotational speed in positive displacement expanders and the rotation speed of this machine can reach as high as 6000 rpm[116]. The electricity production from screw expander therefore requires a special designed high speed generator or adding a gear box to convert the mechanical power from the screw machine into electricity.

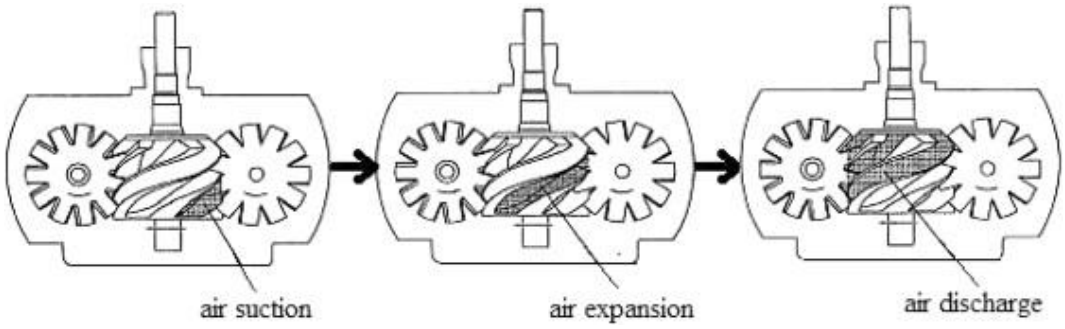

Figure 2-14 Working principle of screw expander[117]

This type of expansion devices has the advantages such as medium internal frictions, medium leakage losses, low vibration noise, wide ranges of power output and long life time. The power produced from this expansion machine as reported by previous researchers ranging from 1.5kW to 1MW with the expansion ratio of 2 to 8[118]. The Figure 2-14 shows the working principle of this expansion device. Leibowitz et al.

developed an ORC power generation system using screw expander in a demonstration unit to cost effectively recover the waste heat into power. Results indicated that screw expander is a good candidate expansion machine for the ORC system with the power output at 20kW with installation cost in the range of $1,500 to $2,000/kWe [119]. However, there is no commercial available product under the power output lower than 10 kW from the market as reported by Ian et al[120]. Because small size of screw expander needs extremely precise machining requirements to make the rotors and internal leakages of small size screw expander are relatively higher than that of large scale device [117, 121]

Scroll expander

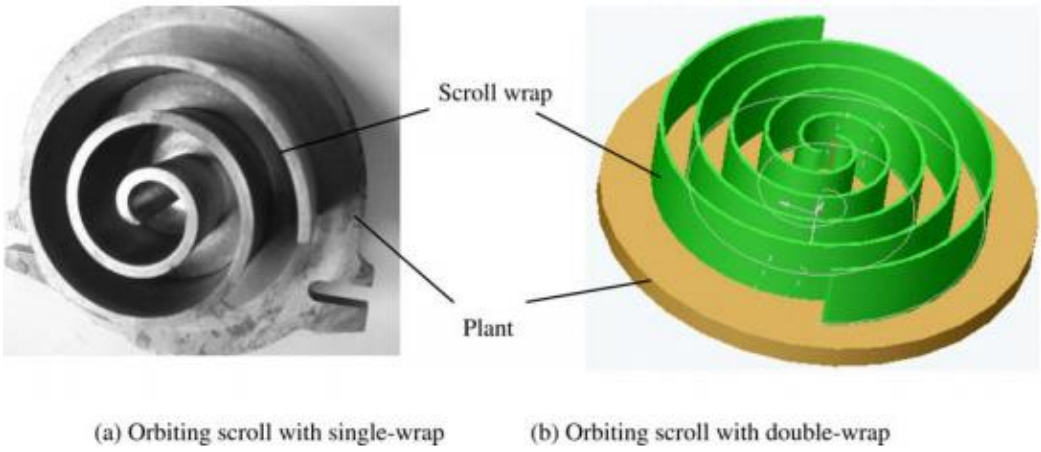

Figure 2-15 Basic structures of the two different types of scrolls [123]

Scroll type of machine was first developed by a French inventor in 1905 and then the scroll machine starts to attract attentions to be applied in Air condition system as a compressor to produce refrigeration since the mid of 1980s[122]. The most of the available scroll expanders from the market are modified from scroll compressor by swapping the inlet and outlet positions to change the device working mode from compressor to expander. Scroll device is relatively simple equipment, which mainly includes two scrolls.

The scroll wraps can be divided in to two types, single wrap and double wrap as shown in Figure 2-15.

Because of the mature development of scroll device for small scale air condition system, scroll device can be easily adapted and modified into power generation system as an expander. The scroll expander has the advantages of little vibration, low noise, limited number of moving parts, broad availability, high reliability and low initial cost [124, 125]. Scroll device has two scrolls and one of the scrolls is fixed on the shell, which is called situational scroll, while the other scroll orbiting eccentrically without rotating is named orbiting scroll. During the expansion process, high pressure vapour enters and expands centrally of two scrolls pushing the orbiting scroll to start orbit as indicated in Figure 2-16. The mechanical work can be continually obtained from the orbiting scroll through the shaft.

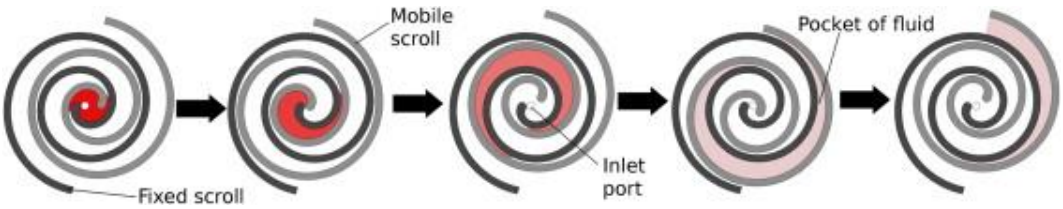

Figure 2-16 Working principle of scroll expander[126]

Likewise the other positive displacement expanders, scroll expander has a fixed built in expansion ratio. The optimal performance of scroll expander can be obtained when the specific volume ratio of the designed system equal to the built in expansion ratio. Quoilin et al. pointed out the losses appearing when scroll type of expansion machine is working under and over expansion processes[126].

The application of scroll expander for small scale power plants has extensively increased and attracts ever increasing attentions to use this

type of expansion machine in small size power generation system in the last 20 years [18, 127-137]. Saitoh et al. [138] reported on the experimental results of the scroll expander unit and the practical operation of the Solar Organic Rankine Cycle using R113 as the working fluid. The results showed that expander isentropic efficiency reached 63%, while the total thermal efficiency of the system attained 7%. A prototype of ORC system using an open-drive oil-free scroll expander with R123 as the working fluid was experimentally investigated by Lemort et al. [139]. Results indicated the maximum isentropic efficiency of the scroll expander could be as high as 68% [139].

However, most of the existing scroll expanders from the market are modified from scroll compressors, which are not designed to be used for expansion applications. And most of the scroll expanders require lubrication system for the contact seals of two scrolls to reduce the radial leakage. The other function of the oil is to seal the working fluid inside the expansion chambers during the expansion process to prevent and reduce the flank leakage of the scroll type machine.

Vane expander

Vane expanders have the advantages of simple construction, easy manufacture, low cost, self-start under load and smooth torque production [140, 141]. The working principle of vane expander is shown in Figure 2-17. The expansion process happens between the cylinder wall and the sliding vanes. When the high pressure working fluid flows into the inlet port and fills chamber A, the spinning power from the rotor can be gathered. The pressure differences among the chambers resulted by expansion process driver the rotor. G.Q. Qiu et al.[121, 142] investigated a vane expander in a biomass-fire CHP system with ORC and achieved the isentropic efficiency of 54.5% at the speed of 824 RPM (mechanical work of 1.552 kW). The

electricity generated by the vane expander was 792 W, which lighted seventeen 50 W bulbs. The efficiencies of several vane expanders using different working fluids at different working temperatures and pressures were summarised by Aoun[143]. Results showed that the maximum efficiency of 80% was achieved by a vane expander using R-11 at 800 RPM.

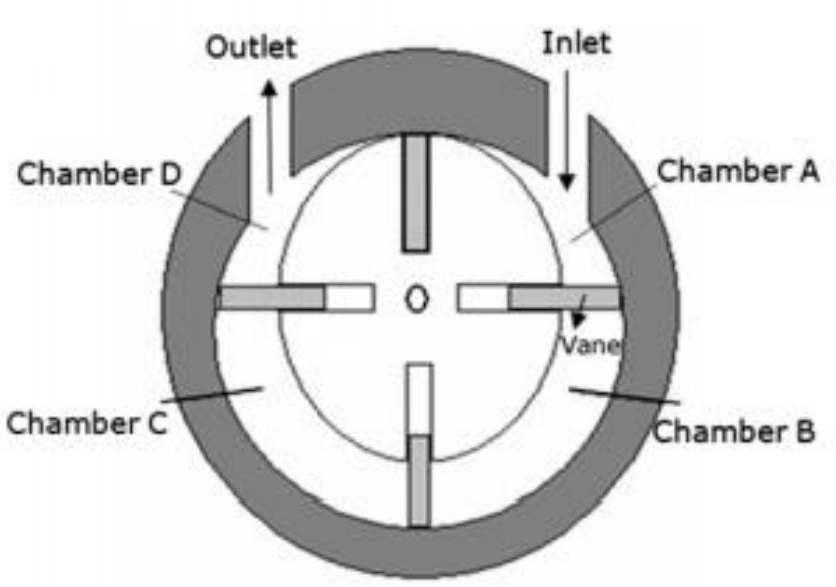

Figure 2-17 Working principle of vane-type expander [121]

The rotational speed of vane type of expanders are relatively lower than other expansion machines with commonly from 1500 to 3000rpm, which can be directly installed to generator without requiring of gear box[140]. However, the average isentropic efficiency of vane expanders is with the range of 15% to 55%, which is not that competitive compared with other volumetric expansion machines, as reported by Muhammad et al. [118]. Moreover, this type of expander requires a lubrication system to lubricate the contact surface of the rotor and vane. The existing of lubricate oil will contaminate the working fluid and flow back to the system.

2.4.3. Selection of the expansion machine for the cogeneration

Due to the application of expansion machine for this study is to be integrating with a cogeneration system using sorption technology. Lubrication oil should first be avoided in the sorption technology because of the contamination issue, which will contaminate the adsorbent and affect the adsorption/desorption performance of the overall system. Moreover, the unstable and intermittent properties of sorption technology will results to an unstable power output from the expansion machine. The mass flow rate of the sorption system will continuous changes all over the duration of adsorption and desorption process. A proper selection of expansion machine is quite critical for this study and the performance of expander to be integrated with sorption technology should mainly focus on the low mass flow rate rather than large scale application.

Therefore, the candidates to be used into sorption technology include radial flow turbines and positive displacement expanders. Although the radial turbines have very attractive performance, the initial cost to use this equipment is quite high because of the necessity of high-speed generator. Moreover, the reaction inside sorption performance is not stable, which cannot always produce high velocity flow into the turbine. Screw expander is commonly not suggested to be used in a power generation system under 10 kW as pointed out by previous researchers. Scroll expander has stood out to be the optimal expansion machine to meet the design purpose of the cogeneration system.

2.5 Summary

This chapter reviews the system level and component level development of adsorption technology and power generation technology. The review of existing adsorption system introduces different working principles and optimised design methods to improve the system performance of sorption technology. As an advanced adsorption refrigeration cycle, resorption technology can potentially produce twice of cooling capacity compared with conventional adsorption refrigeration system under the same working conditions. And resorption technology has the advantages of no existing of liquid refrigerant inside the system, which is desirable to be used under vibration condition such as integrated with vehicle for air-condition application. Moreover, the system pressure of resorption system is relatively lower than that of adsorption refrigeration system, which will be safer to be used and easier to be constructed, when compared with conventional adsorption system. Therefore this PhD study will develop a cogeneration system based on resorption technology because of previous reasons.

Due to the purpose of this PhD study is to develop and investigate the feasibility of a combined refrigeration and power generation system using sorption technology, which has hardly been reported and studied by previous researchers. In order to obtain required knowledge for the system design of power generation part of the resorption cogeneration proposed in Chapter 3, Rankine-based power generation systems have been reviewed.. As an advanced transformation Rankine based system, Kalina cycle use the mixture working fluid ammonia and water. The ratio of the mixture working fluid by a separator in order to meet various heat source temperature, which means Kalina cycle has better thermal match than pure working fluid Organic Rankine cycle. By adding an extra heat exchange at

the exit of the expansion machine, Kalina cycle can generate cooling effect and the modified Kalina cycle is also called Goswai cycle. However, design of the Goswami system limits the refrigeration production of this system.

A detailed component level review of the current status of adsorption technology, which can be found in Chapter 2.3, pointed out the potential refrigerant and working pair to be used in the sorption part of the cogeneration system. Considering about the high mass flow rate of the fluid and high pressure difference are required to run expansion machine for the power generation purpose, chemical working pairs stand out to be the optimal working pair to meet the requirement. Moreover, the development and manufacture of composite chemisorption adsorbent is quite important and necessary in order to overcome the commonly existing swelling and agglomeration problems in chemical sorbents. In order to obtain required data for the design purpose of the cogeneration system using chemisorption technology, an adsorption performance test rig is required to conduct this study. A review of adsorption performance testing methods for adsorbents pointed out the constant pressure volumetric measurement method is a promising method to test the dynamic adsorption performance of adsorbents, which is selected as the testing method in this PhD project. The manufacture/development of composite chemisorption adsorbents, design/construction of an adsorption performance test rig and experimental investigation on the candidate composite adsorbents using the test rig will be introduced in Chapter 4.

The selection of proper expansion machine is quite critical for the power generation part of any power generation system. The review of existing expansion machines have been conducted, which includes turbines, piston type expander, screw expander, scroll expander and vane expander, which can be found in Chapter 2.4. To be integrated with adsorption system for power generation purpose, the commonly used lubricated oil should first be

forbidden to be added in the system, which will contaminate the adsorbent and reduce the overall system performance. The working principle of adsorption technology results to unstable and intermittent mass flow rate of the system. The selected expansion machine should be suitable to be used under various working conditions, especially the good performance when the mass flow rate of the system is quite low. Radial flow turbines have very attractive performance. However this type of expansion machine requires to be integrated with special made high-speed generator, which will leads to a very expansive electricity generation system. Moreover, the radial flow turbines are designed to be used under low pressure difference conditions in vehicle exhaust system, which is also not desirable in sorption system. Although the piston-type of expanders are mature technology, this expansion machine needs precisely controlling methods on the valves to achieve optimal performance. Considering about the isentropic efficiency of expansion machine, cost of the electricity generation system, availability and vibration of the expanders, scroll type of expander is the most suitable expansion machine to meet our special requirements. The detailed study scroll expander and experimental investigation of it can be found in Chapter 5.

Chapter 3. Design and assessment of a resorption cogeneration

3.1 Introduction

This chapter describes the design and thermodynamic analysis of a resorption cogeneration. The resorption cogeneration combines ammonia-resorption technology and expansion machine into one loop, which is able to generate refrigeration and power from low grade heat sources such as solar energy and industrial waste heat, etc. Two sets of resorption cycle are designed to overcome the intermittent performance of the chemisorption in order to produce continuous/simultaneous refrigeration and power. Twelve resorption working pair of salt complex candidates are analysed by first law analysis. Optimal candidates under the driven temperature from 100 ^{o}C to 300 ^{o}C are identified. Mass and heat recovery methods were introduced and analysed in this chapter to further improve the performance of the cogeneration.

3.2 Principle of a resorption cogeneration

The resorption cogeneration includes two high temperature salts (HTS), two low temperature salts (LTS), an expander and some accessories. This system is able to provide continuous power and refrigeration by switching it between Step 1 and Step 2, which is shown in Figure 3-1.

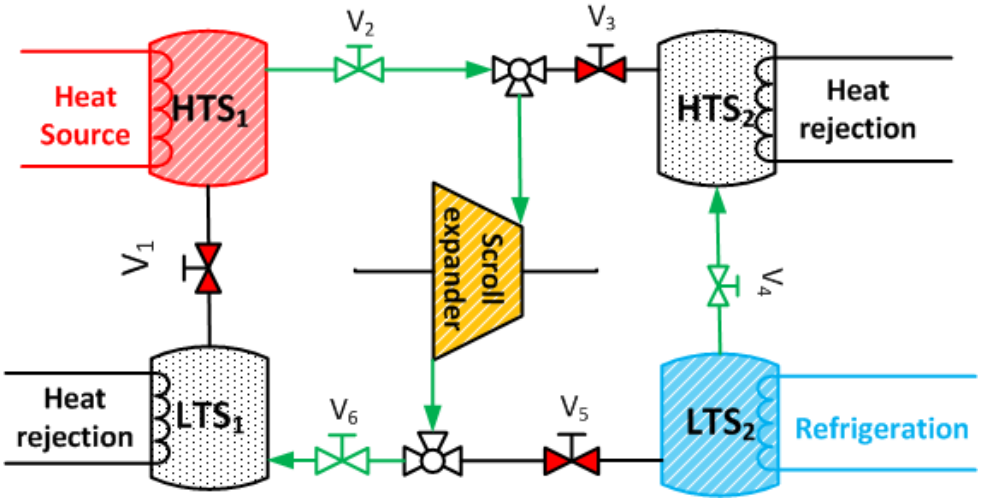

(a)

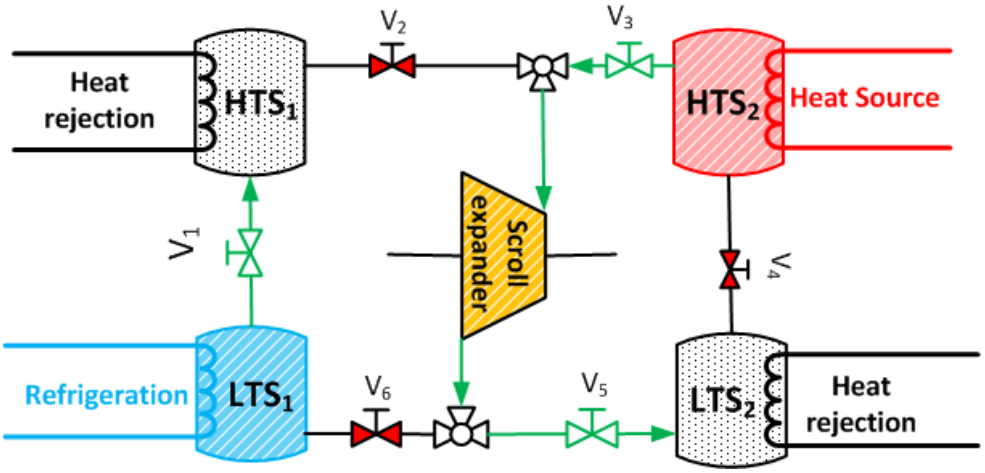

(b)

Figure 3-1 Principle of the resorption cogeneration

(a) Step1, HTS_1 and LTS_2-desorption process, LTS_1 and HTS_2-adsorption process; (b) Step2, HTS_1 and LTS_2-adsorption process, LTS_1 and HTS_2-desorption process

In step 1, V_1, V_3, V_5, V_{m1}, V_{m2} are closed; V_2, V_4, V_6 are opened.

The HTS_1 is heated by the heat source and ammonia vapour flows to the expander. The high pressure ammonia drives the expander to produce

electricity while the LTS_1 adsorbs ammonia and rejects the adsorption heat to the environment such as a cooling tower. On the other side of this system, the HTS_2 adsorbs the ammonia from LTS_2 where the refrigeration can be obtained. Step 2 is working as the mirror mode of step 1, where the HTS_2 is heated by the heat source and the LTS_1 generates refrigeration. The V_1, V_3, V_5 are opened and V_2, V_4, V_6, V_{m1}, V_{m2} are closed in step 2, which is illustrated in Figure 3-1 (b).

Three HTS ($NiCl_2$, $FeCl_3$, $MnCl_2$) and four LTS ($BaCl_2$, $PbCl_3$, $CaCl_2$, $SrCl_2$) are chosen to be analysed in the resorption cogeneration. Their reaction equations are list as follows,

$$NiCl_2 \cdot 2NH_3 + 4NH_3 \Leftrightarrow NiCl_2 \cdot 6NH_3 + 4\Delta H_{NiCl_2} \quad \text{Equation 3-1}$$

$$FeCl_3 \cdot 2NH_3 + 4NH_3 \Leftrightarrow FeCl_3 \cdot 6NH_3 + 4\Delta H_{FeCl_3} \quad \text{Equation 3-2}$$

$$MnCl_2 \cdot 2NH_3 + 4NH_3 \Leftrightarrow MnCl_2 \cdot 6NH_3 + 4\Delta H_{MnCl_2} \quad \text{Equation 3-3}$$

$$SrCl_2 \cdot NH_3 + 7NH_3 \Leftrightarrow SrCl_2 \cdot 8NH_3 + 7\Delta H_{SrCl_2} \quad \text{Equation 3-4}$$

$$CaCl_2 \cdot 4NH_3 + 4NH_3 \Leftrightarrow CaCl_2 \cdot 8NH_3 + 4\Delta H_{CaCl_2} \quad \text{Equation 3-5}$$

$$BaCl_2 + 8NH_3 \Leftrightarrow BaCl_2 \cdot 8NH_3 + 8\Delta H_{BaCl_2} \quad \text{Equation 3-6}$$

$$PbCl_2 \cdot 3.25NH_3 + 4.75NH_3 \Leftrightarrow PbCl_2 \cdot 8NH_3 + 4.75\Delta H_{PbCl_2} \quad \text{Equation 3-7}$$

The equilibrium reaction lines and thermodynamic features of the resorption cogeneration are shown in Figure 3-2. Line A-B is the heating process of the ammonia inside the HTS, where Point B and Point A are on the equilibrium reaction line of the HTS. The isentropic expansion process is represented by line B-C. The refrigeration generation is achieved from Line D-A and the refrigeration temperature of the system is T_D. In this study the environmental temperature is set at 20 ^oC.

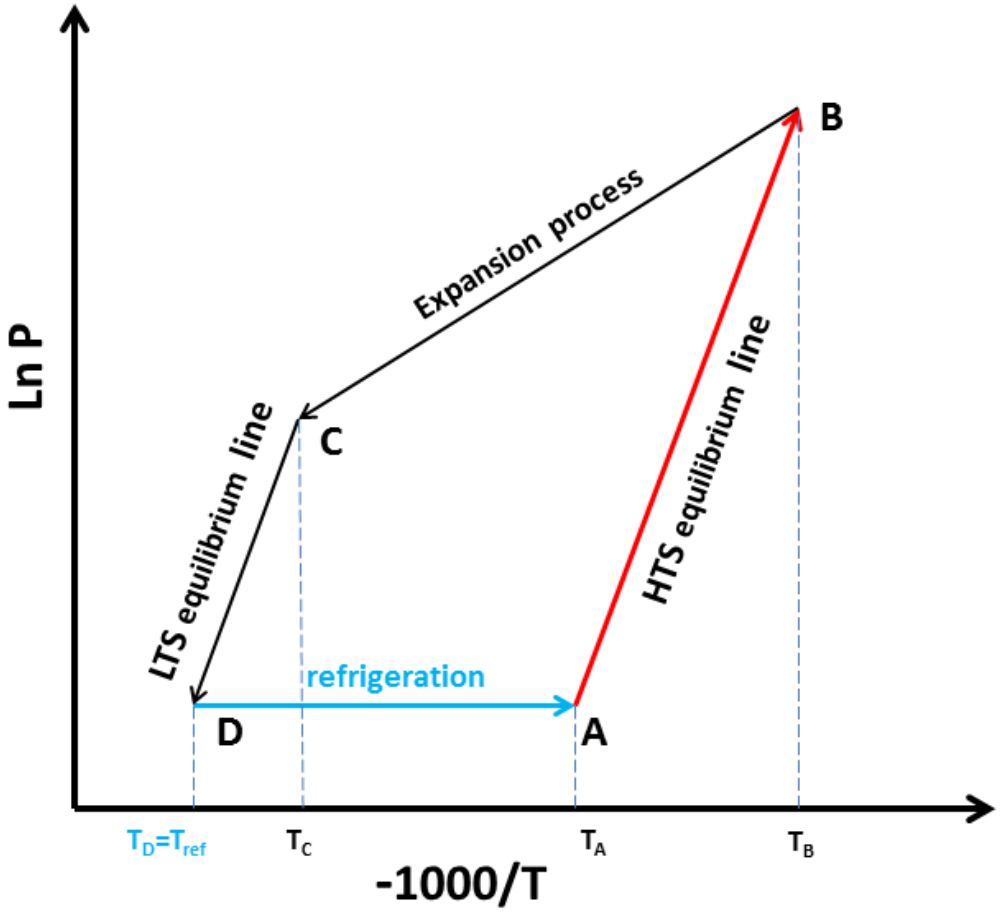

Figure 3-2 Clausius-Clapeyron diagram of the resorption cogeneration

3.3 Analysis of the resorption cogeneration

3.3.1. Selection of resorption working pairs

The total heat input includes the reaction heat and the sensible heat of the adsorbent, which is described by Equation 3-8. m_{am} is the total mass of the adsorption/desorption ammonia between the HTS and the LTS.

$$\begin{aligned} Q_h &= m_{am} \times \Delta x \times \Delta h_{HTS} + m_{am} \times \Delta u_{HTS} \\ &= m_{am} \times \Delta x \times \Delta h_{HTS} + m_{HTS} \times c_{pHTS} \times (T_h - T_0) + m_{am} \times c_{pam} \times (T_h - T_0) \end{aligned}$$ Equation 3-8

The refrigeration generation includes the sensible heat for LTS to cool down at refrigeration temperature and the chemical reaction heat producing cooling.

$$Q_{ref} = m_{am} \times \Delta x \times \Delta h_{LTS} + m_{am} \times \Delta u_{LTS}$$
$$= m_{am} \times \Delta x \times \Delta h_{LTS} - m_{LTS} \times c_{pLTS} \times (T_0 - T_{ref}) - m_{am} \times c_{pam} \times (T_0 - T_{ref})$$

Equation 3-9

The isentropic expansion process inside the expander is calculated by the enthalpy difference between Point B and Point C.

$$W = m_{am} \times \Delta x \times (h_B - h_C)$$

Equation 3-10

The coefficient of performance (COP) of the resorption system without mass and heat recovery is

$$COP = Q_{ref} \div Q_h$$

Equation 3-11

The power generation performance with and without heat recovery process are calculated by

$$\eta_{I\_ele} = W \div Q_h$$

Equation 3-12

The equilibrium state of the salt is calculated by the Clausius-Clapeyron equation (Equation 3-13) and the thermodynamic parameters to use this equation are listed in Table 3-1.

$$\ln p_{NH_3} = \frac{\Delta H^0}{RT} - \frac{\Delta S^0}{R} \qquad \text{Equation 3-13}$$

Table 3-1 Thermodynamic parameters for the chosen salts and ammonia[7]

Molecular formula	ΔH $J \cdot mol^{-1}$	ΔS $J \cdot mol^{-1} \cdot K^{-1}$	C_{p_mol} $J \cdot mol^{-1} \cdot K^{-1}$	M_{r_mol} $g \cdot mol^{-1}$	Reaction salt with per mol ammonia g
NH_3	22839	191.39	80.27 (liquid)	17.03	
$PbCl_2$ (8-3.25)	34317	223.76	70.05	278.1	57.34
$BaCl_2$ (8-0)	37665	227.25	75.1	208.23	26.03
$CaCl_2$ (8-4)	41013	230.3	72.52	110.98	27.74
$SrCl_2$ (8-1)	41431	228.8	75.53	158.53	22.65
$MnCl_2$ (6-2)	47416	228.07	72.86	125.84	31.46
$FeCl_3$ (6-2)	51266	227.99	76.57	162.2	40.55
$NiCl_2$ (6-2)	59217	227.75	71.6	129.6	32.40

3.3.2. *Heat recovery process*

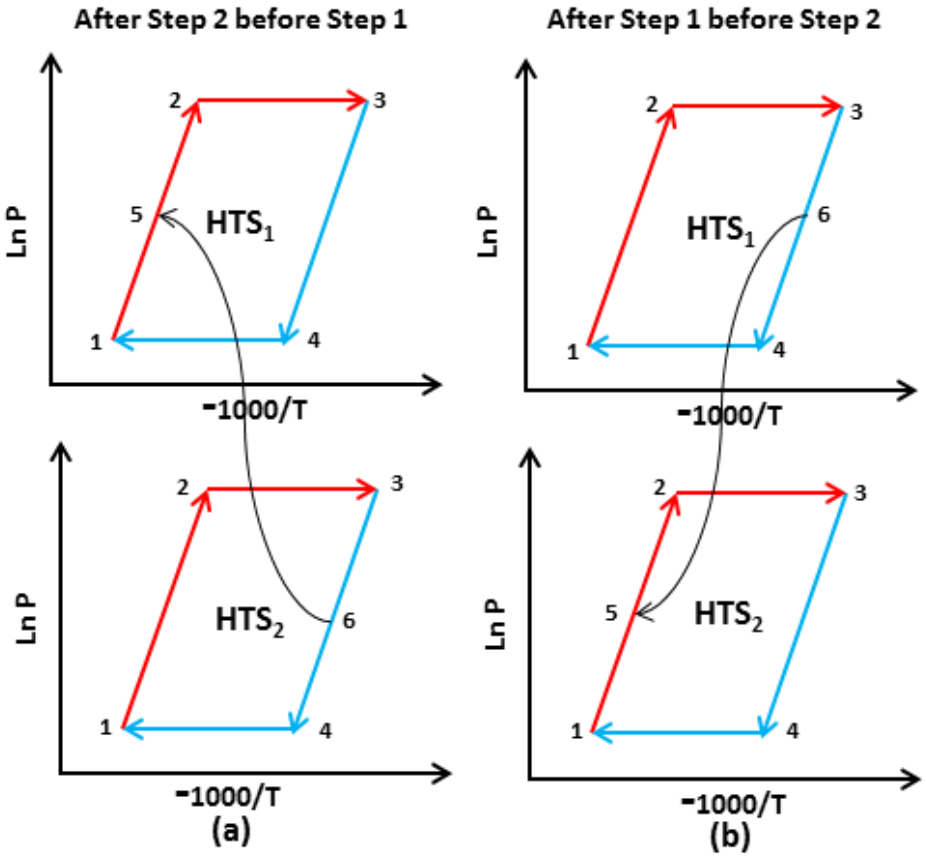

Figure 3-3 P-T diagram for the heat recovery process between HTS_1 and HTS_2 (a) after Step2 before Step1 (b) After Step 2 before Step 1

To regenerate the sensible heat from HTS after the heating process, a separate circulator is added between the HTS_1 and the HTS_2. The heat recovery process applies between the Step 1 and the Step 2 during the switch time. Figure 3-3 (a) illustrates the principle of the heat recovery process, when the system switches from Step 2 to Step 1. Line 3-6 is the heat removed from one of the HTS to preheat the other HTS from Point 1 to Point 5. In ideal heat recovery process, the temperature of Point 5 is the

same as the temperature of Point 6 (T_5=T_6=T_{hr}). The P-T diagrams of the heat recovery process between two HTS are shown in Figure 3-3.

3.3.3. Mass recovery process

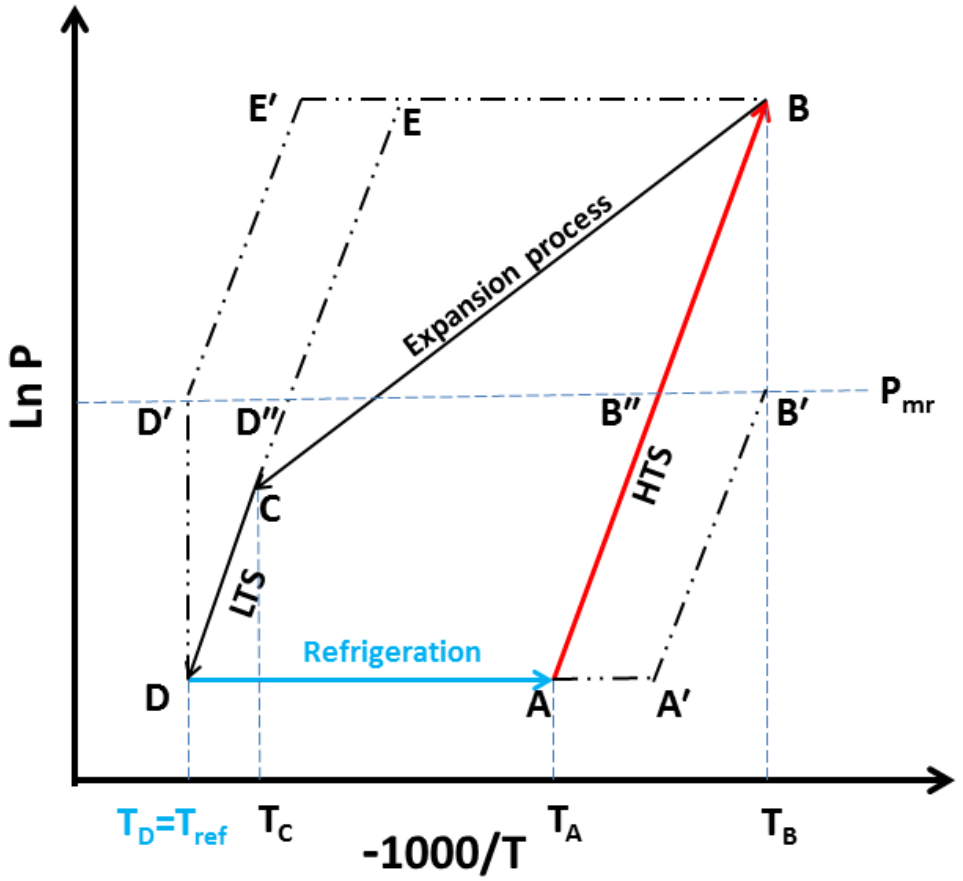

Figure 3-4 P-T diagram of the mass recovery process between the HTS_1 and the LTS_2

To further improve the refrigeration generation, mass recovery process is introduced here to equalise the pressures of the four adsorbent beds. In the end of step 1, the pressure of the HTS_1 is higher than the saturated pressure under heat source temperature. Meanwhile the pressure of the LTS_2 is lower than the saturated pressure under refrigeration temperature. During the mass recovery process, all valves need to be switched off except V_{mr1}. The V_{mr1} only needs to be switched on for 10 seconds to let

ammonia evaporating from the HTS_1 into the LTS_2. The further obtained ammonia into the LTS_2 can be represented as line E-E′ in Figure 3-4.

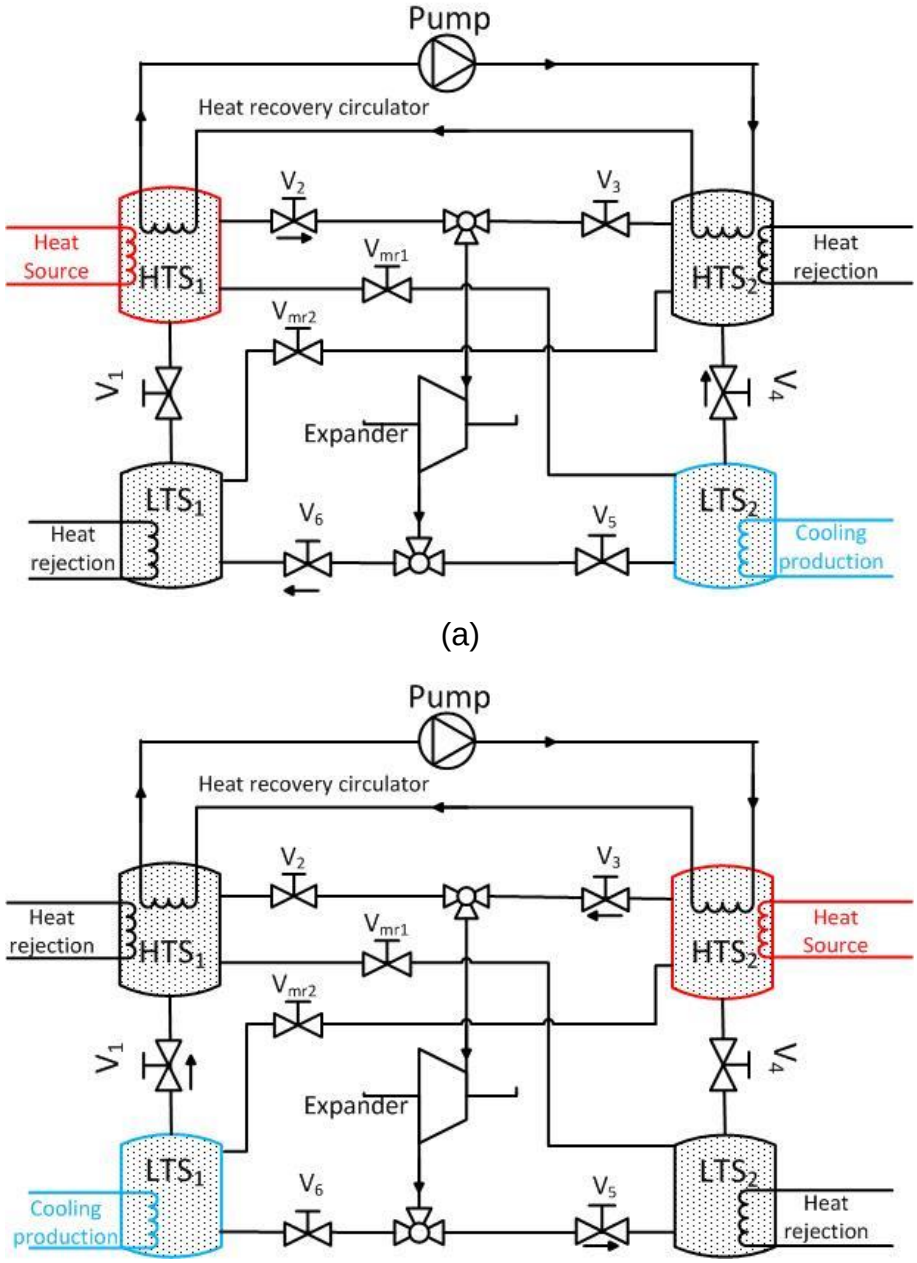

Figure 3-5 Schematic diagram of a resorption cogeneration applying heat recovery process (a) Step 1, HTS_1 & LTS_1 power generation, HTS_2 & LTS_2 refrigeration generation; (b) Step 2 HTS_1 & LTS_1 refrigeration generation, HTS_2 & LTS_2 power generation

This equalisation process not only can speed up these two beds reaching their saturation state but also increase the total mass flows into the system. In the end of this equalisation process, the mass recovery valve V_{mr1} needs to be switched off. The further achieved refrigeration is obtained from the LTS_2 by switching on the V_4, when the ammonia desorbs from the LTS_2 and adsorbed by the HTS_1. The dash dot lines present the mass recovery process as shown in Figure 3-4. The operational processes of the heat and mass recovery methods are illustrated as Figure 3-5.

Several assumptions are applied here for the analysis of the mass recovery process.

1. The processes B-B′ and D-D′ are recognised as isothermal processes. ($T_B=T_{B'}$, $T_D=T_{D'}$)
2. The further desorbed ammonia from the HTS_1 is fully adsorbed by the LTS_2. ($\Delta x_{D-D'}=\Delta x_{B-B'}$)
3. By using mass recovery process, the final pressure state of the HTS_1 is equivalent to that of the LTS_2. ($P_{B'}=P_{D'}=P_{mr}$)
4. Point B" and Point D" are on the equilibrium lines of HTS and LTS. The temperature difference between Point B′ and Point B" is the same as that between Point D′ and Point D". ($T_{B'}-T_{B"}=T_{D"}-T_{D'}$)
5. The extra adsorption heat, which is caused by the mass recovery process, needs to be rejected to the environment is shown as Line A-A′ in Figure 3-4. The temperature increase of the HTS_2 equal to the temperature difference between Point B′ and Point B". ($T_A-T_{A'}=T_{B'}-T_{B"}$)
6. The chemical reaction can be 100% completed without considering the reaction time.

The heat recovered by the heat recovery process can be calculated as

$$Q_{hr} = (Q_{hr\_HTS1} + Q_{hr\_HTS2}) \div 2$$
$$= [m_{HTS} \times c_{pHTS} \times (T_B - T_{hr}) + m_{am} \times c_{pam} \times (T_B - T_{hr}) \times (1 - \Delta x) \quad \text{Equation 3-14}$$
$$+ m_{HTS} \times c_{pLTS} \times (T_{hr} - T_0) + m_{am} \times c_{pam} \times (T_{hr} - T_0) \times \Delta x] \div 2$$

The extra cooling production caused by the mass recovery process is described as

$$Q_{ref\_mr} = m_{am} \times (1 - \Delta x) \times \Delta h_{LTS} + m_{am} \times \Delta u'_{LTS}$$
$$= m_{am} \times (1 - \Delta x) \times \Delta h_{LTS} - m_{LTS} \times c_{pLTS} \times (T_{D'} - T_{ref}) \quad \text{Equation 3-15}$$
$$- m_{am} \times c_{pam} \times (T_{D'} - T_{ref})$$

With mass recovery process only

$$COP_{mr} = (Q_{ref} + Q_{ref\_mr}) \div Q_h \quad \text{Equation 3-16}$$

With heat recovery process only

$$COP_{hr} = Q_{ref} \div (Q_h - Q_{hr}) \quad \text{Equation 3-17}$$

With mass and heat recovery

$$COP_{mr\&hr} = (Q_{ref} + Q_{ref\_mr}) \div (Q_h - Q_{hr}) \quad \text{Equation 3-18}$$

The power generation performance applying heat recovery process is calculated by

$$\eta_{I\_ele\_hr} = W \div (Q_h - Q_{hr}) \quad \text{Equation 3-19}$$

The second law analysis is applied in this study to evaluate the utilization of useful work from this resorption cogeneration. The exergy from the heat source of the resorption cogeneration applying mass and heat recovery is defined as

$$\begin{aligned} E_{h\_mr\&hr} &= E_h - E_{h\_hr} \\ &= m_{am} \times [(h_B - h_0) - T_0 \times (s_B - s_0)] - m_{am} \times [(h_{hr} - h_0) - T_0 \times (s_{hr} - s_0)] \end{aligned} \quad \text{Equation 3-20}$$

Due to the chemical reaction process for refrigeration generation, the refrigeration exergy is calculated by

$$E_{ref\_mr\&hr} = E_{ref} + E_{ref\_mr} = (Q_{ref} + Q_{ref\_mr}) \times (T_0 / T_{ref} - 1) \quad \text{Equation 3-21}$$

The second law efficiency of the electricity generation part from this system is

$$\eta_{II\_ele} = W \div E_{h\_mr\&hr} \quad \text{Equation 3-22}$$

The second law efficiency for refrigeration process is

$$\eta_{II\_ref} = E_{ref\_mr\&hr} \div E_{h\_mr\&hr} \quad \text{Equation 3-23}$$

The overall system evaluation by the second law analysis is defined as

$$\eta_{II\_total} = \eta_{II\_ele} + \eta_{II\_ref} \quad \text{Equation 3-24}$$

3.4 Results and Discussions

3.4.1. Selection of the resorption working pair

For chemisorption adsorption, the final state of the salt will reach the point on the equilibrium lines, which is shown in Figure 3-6. In this study, the temperature of the heat source is chosen from 100 ^{o}C to 300 ^{o}C and the refrigeration temperatures are set at 10 ^{o}C. The promising LTS and HTS for the resorption cogeneration are $PbCl_2$, $BaCl_2$, $CaCl_2$, $SrCl_2$ as LTS and $MnCl_2$, $FeCl_3$, $NiCl_2$ as HTS. To simplify the system design and reduce the

construction cost, the highest system pressure is set at 40 bar. The pressures of the three HTS candidates under 40 bar are listed in Table 3-2.

A minimum start pressure (the pressure difference between the HTS and the LTS) is set at 100 kPa to ensure the electrical generation from the scroll expander. In another word, the pressure difference between the HTS (in desorption process under heat source temperature) and the LTS during (in adsorption process cooled down to the environmental temperature) needs to be higher than 100kPa. The pressures of the LTS under the refrigeration temperature (10 ^{o}C) and environmental temperature (20 ^{o}C) are listed in Table 3-3.

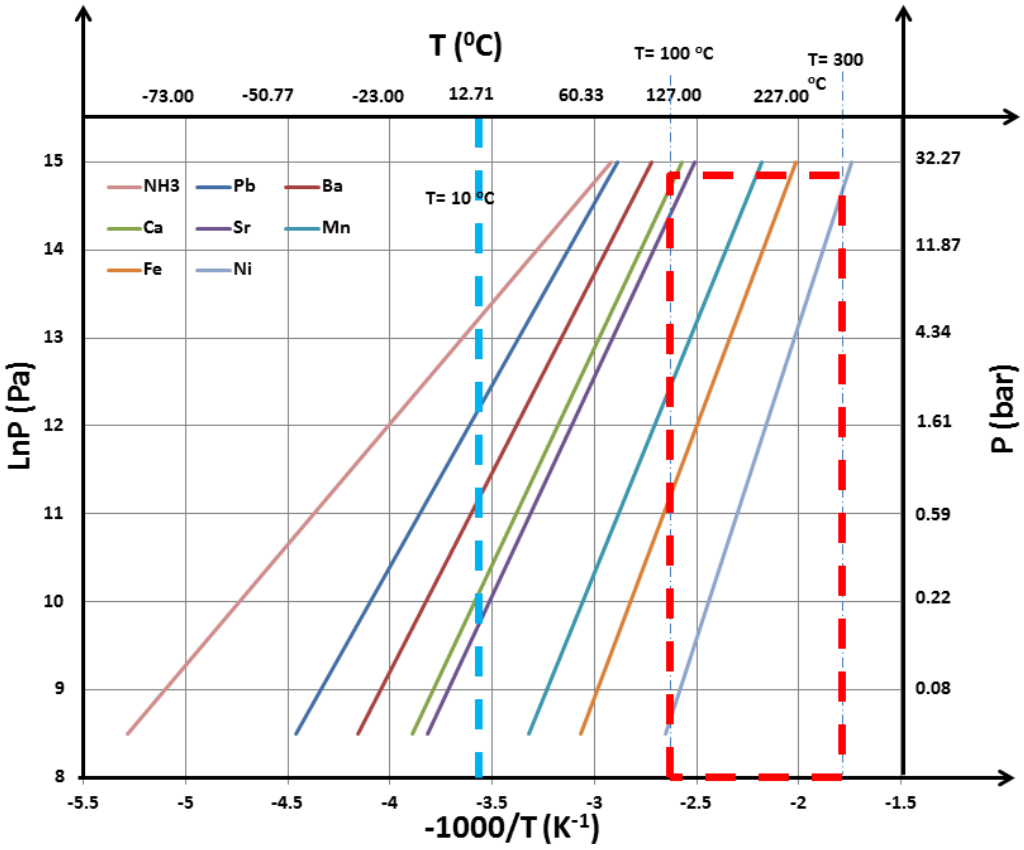

Figure 3-6 Equilibrium lines of selected salts and ammonia in P-T diagram

Table 3-2 Equilibrium pressure of the HTS under different heating temperatures

Heat source temperature(^{o}C)	P_{MnCl2} (kPa)	P_{FeCl3} (kPa)	P_{NiCl2} (kPa)
100	188.70	53.97	
110	281.35	83.12	
120	411.03	125.23	
130	589.30	184.88	
140	830.28	267.83	
150	1150.99	381.26	38.58
160	1571.68	533.95	56.92
170	2116.17	736.51	82.53
180	2812.12	1001.58	117.72
190	3691.33	1344.09	165.35
200		1781.43	228.94
210		2333.69	312.74
220		3023.85	421.84
230		3877.96	562.28
240			741.12
250			966.57
260			1248.12
270			1596.56
280			2024.18
290			2544.79
300			3173.84

Table 3-3 Equilibrium pressure of the LTS at environmental temperature and refrigeration temperature

T (^{o}C)	P_{PbCl2} (kPa)	P_{BaCl2} (kPa)	P_{CaCl2} (kPa)	P_{SrCl2} (kPa)
20	374.14	143.96	52.54	36.94
10	227.38	83.34	28.97	20.25

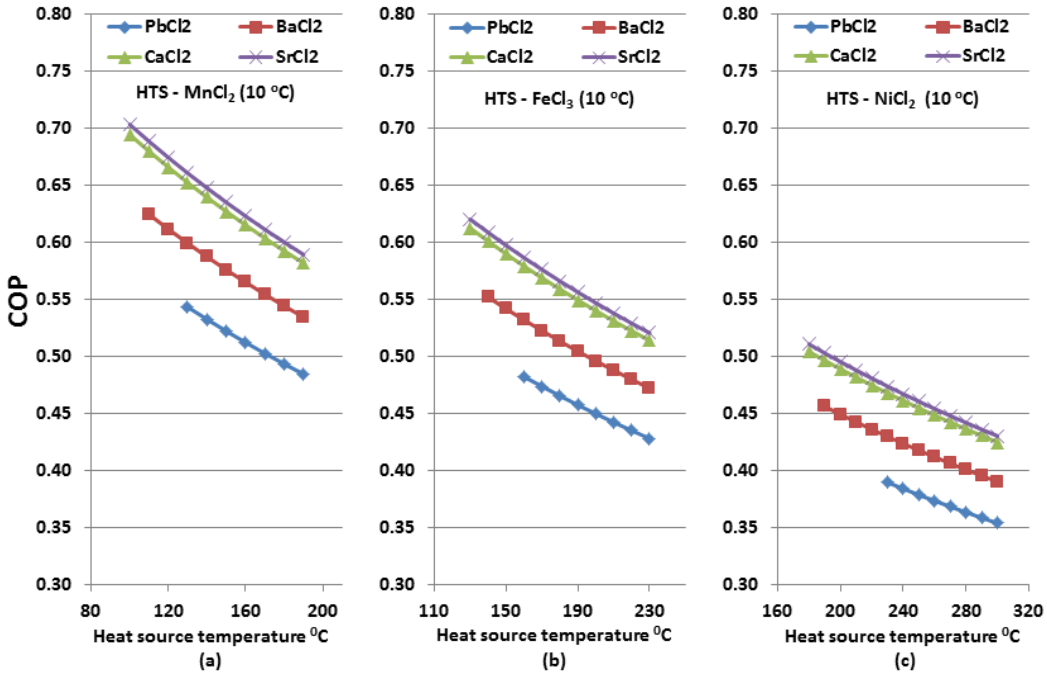

Figure 3-7 Relationship between the COP and heat source temperature of the resorption cogeneration at 10 ^{o}C refrigeration temperature
(a) HTS - $MnCl_2$; (b) HTS - $FeCl_3$; (c) HTS - $NiCl_2$

In this study, the sorption quantity (Δx) is assumed at 80%. The refrigeration performance at 10 ^{o}C of this resorption cogeneration is calculated by Equation 3-11, and the results are shown in Figure 3-7. Among the twelve resorption pairs, the COP of this system declines with the increase of the heat source temperature. The highest heating temperature of the chosen high temperature salts is 190 ^{o}C for $MnCl_2$, 240 ^{o}C for $FeCl_3$ and 300 ^{o}C for $NiCl_2$. The pressure of $PbCl_2$ at 20 ^{o}C is as high

as 374.14 kPa, which is the highest among the four LTS candidate. Therefore $PbCl_2$ requires relatively high supply pressure from the HTS, which will limit the system flexibility. The highest COP is achieved at 0.70 by the $SrCl_2$-$MnCl_2$ working pair with the heating temperature at 100 ^oC.

The energy efficiency of the electricity generation with the increase of the heat source temperature is shown in Figure 3-8. The ammonia enthalpy at the inlet and the outlet of the expander determines the power generation performance, which is calculated by Equation 3-10. Among the four LTS candidates, the $PbCl_2$ shows a competitive performance during the power generation part. The electrical energy efficiency of the resorption working pair $PbCl_2$-$MnCl_2$, $BaCl_2$-$MnCl_2$, $CaCl_2$-$MnCl_2$ and $SrCl_2$-$MnCl_2$ is around 8.2%, 6.5%, 5.0% and 4.5%, respectively. Under the same working conditions, the electrical energy efficiency of the resorption cogeneration using HTS-$FeCl_3$ is higher than that using HTS-$MnCl_2$. The $PbCl_2$-$NiCl_2$ achieves the highest electrical energy efficiency at 12.49% under the heat source temperature at 300 ^oC. However, the weight of reaction adsorbents also needs to be considered to simplify the system design and reduce the construction cost. Based on the adsorption reaction equations, the reaction weight of salts with per mol ammonia is listed in Table 3-1

In summary, this resorption cogeneration can be used under the heat source temperature from 100 ^oC to 300 ^oC using different HTS ($MnCl_2$, $FeCl_3$ or $NiCl_2$). The $FeCl_3$ has the highest reaction weight with 1 mol ammonia among the three HTS, which is not preferred in the system. Therefore the $MnCl_2$ and $NiCl_2$ are chosen as the optimal HTS for further analysis. For the selection of LTS, the performance of power and refrigeration generation of the cogeneration using $SrCl_2$ and $CaCl_2$ are quite close, which are shown in Figure 3-7 and Figure 3-8. The $SrCl_2$ who has a lower reaction weight with per mol ammonia can be selected as a representative for $CaCl_2$. The $PbCl_2$, who needs higher supply pressure

and higher reaction weight with one mol ammonia compared with the other LTS candidates, is not suggested to be used as the LTS in this system.

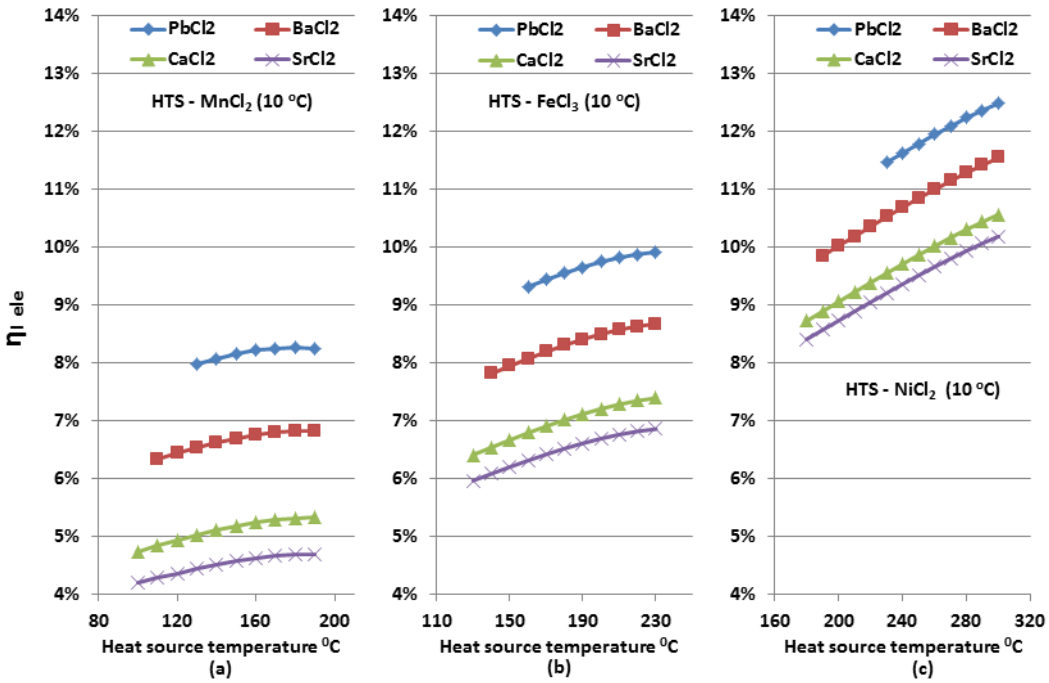

Figure 3-8 Relationship between the energy efficiency of the electricity production and heat source temperature

(a) HTS - $MnCl_2$; (b) HTS – $FeCl_3$; (c) HTS – $NiCl_2$

To investigate the effect of mass and heat recovery processes for this resorption cogeneration, the COP and electrical energy efficiency of this resorption system using four optimised working pairs are conducted and discussed in the next section.

3.4.2. Heat and mass recovery

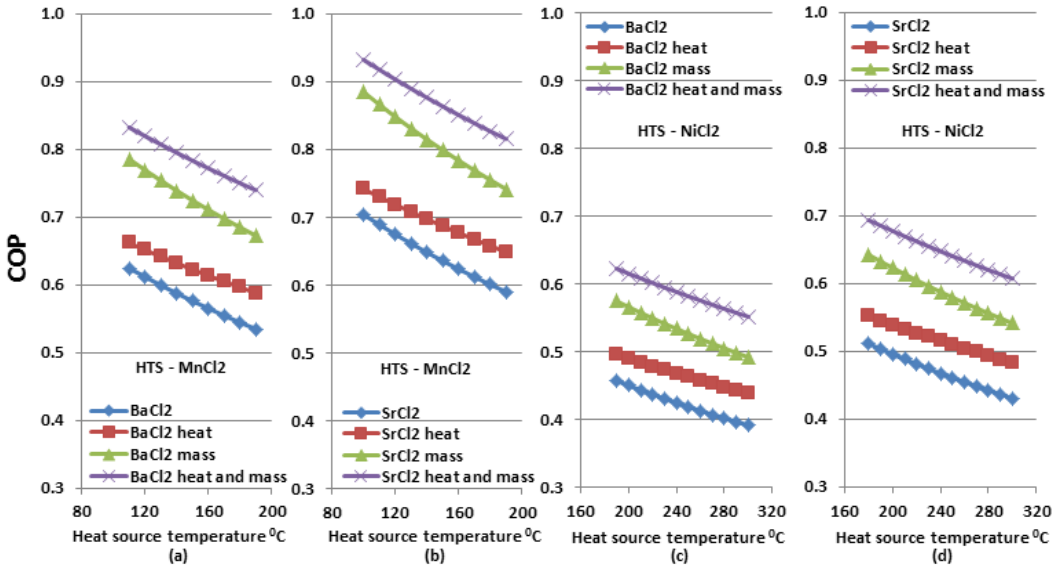

Figure 3-9 COP of the resorption with working pair (a) $BaCl_2$-$MnCl_2$; (b) $SrCl_2$-$MnCl_2$; (c) $BaCl_2$-$NiCl_2$; (d) $SrCl_2$-$NiCl_2$

To further improve the system performance, heat recovery and mass recovery process are introduced here. Figure 3-9 shows the COP improvement of the system applying heat recovery, mass recovery and heat/mass recovery. Results suggest that all of these three methods can effectively improve the refrigeration performance. The COP entrancement with mass recovery is higher than that with heat recovery, which means the mass recovery has a more important role than the heat recovery for refrigeration generation in this system. For the working pairs $BaCl_2$ – $MnCl_2$ and $SrCl_2$ – $MnCl_2$, their COP are both improved by 35% with the help of heat/mass recovery. Under the heat source temperature from 110 ^oC to 190 ^oC, the COP of the system with $SrCl_2$ – $MnCl_2$ as working pair is around 0.85 which is higher than that of the system with $BaCl_2$-$MnCl_2$ working pair. The COP enhancement of the other two resorption working pairs $BaCl_2$-$NiCl_2$ and $SrCl_2$-$NiCl_2$ also show effectively improved by 38% after applying heat/mass recovery.

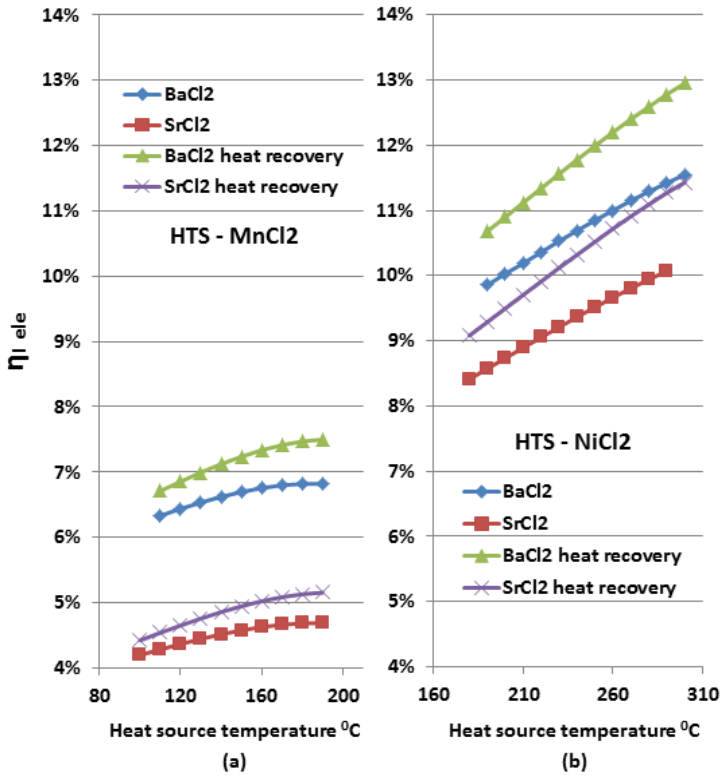

Figure 3-10 Electrical energy efficiency of the resorption working pair (a) $BaCl_2$-$MnCl_2$ and $SrCl_2$-$MnCl_2$; (b) $BaCl_2$-$NiCl_2$ and $SrCl_2$-$NiCl_2$

The heat recovery also improves the system performance for electricity generation, which is shown in Figure 3-10. It can be seen that heat recovery can effectively increase the electrical energy efficiency of this resorption cogeneration. With increasing heat source temperature, the contribution rate from the recovered heat is higher than that from the electricity generation. Therefore the slope of the electrical energy efficiency line using heat recovery is greater than that of original system. Although heat recovery cannot increase the power produced from this system, the electrical energy efficiency of this system using $MnCl_2$ and $NiCl_2$ as HTS is improved by 3% and 1.5%, respectively. To further evaluate the performance of the resorption cogeneration, second law analysis is applied in the following section.

3.4.3. Second law analysis

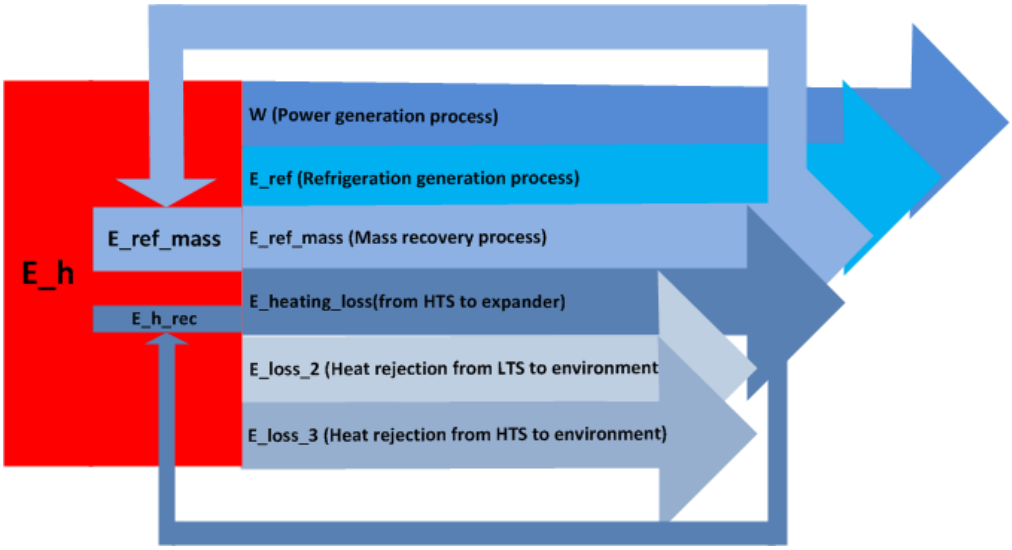

Figure 3-11 Exergy flow chart of the resorption cogeneration applying mass and heat recovery

To have a better understanding of the exergy utilisation of this novel resorption cogeneration, the exergy flow chart is shown in Figure 3-11. The total exergy input is coming from the heating process of the HTS. The exergy destructions include the exery losses during the heating process from HTS to the inlet of the expander, adsorption heat rejection from the LTS to the environment and adsorption heat rejection from the HTS to the environment. The heat recovered from HTS_1 to HTS_2 and the refrigeration recovered from the mass recovery process can be seen from Figure 3-11.

Table 3-4 Exergy destruction comparison between two cases

	Case 1 $BaCl_2$-$MnCl_2$ at 150 ^oC		Case 2 $BaCl_2$-$NiCl_2$ at 250 ^oC	
	Exergy (J/kg)	Ratio of Exergy to Total Exergy (%)	Exergy (J/kg)	Ratio of Exergy to Total Exergy (%)
Total Exergy				
Heat input (E_h)	15593	100%	30763	100%
Exergy Destruction				
Heating loss (E_{hl})	3439	22.06%	8133	26.44%
Heat rejection ($E_{hl\_LTS}+E_{hl\_HTS}$)	7716	49.49%	14004.3	45.50%
Exergy Output				
Power (W)	3397	21.79%	7587	24.66%
Refrigeration (E_{ref})	1033	6.62%	1033	3.36%
Exergy Recovery				
Heat recovery (E_{hr})	688.6	4.42%	1181	6.12%
Mass recovery (E_{ref_mr})	266.1	1.17%	266.1	0.86%

Two cases are studied to investigate the key processes of this system. Results are listed in Table 3-4. The majority of exergy destructions are coming from the adsorption processes of the LTS and HTS, where the adsorption heat is released to the environment. There is 49.49% of the exergy released of $BaCl_2$-$MnCl_2$ working pair and 45.50% of the exergy released of $BaCl_2$-$NiCl_2$. The heat loss from the heating process of the HTS is around 22% and 26% in case 1 and case 2, respectively. Results also show the heat recovery can recover around 20% of the heat loss during the heating process to regenerate the heat. The effect of the mass recovery for exergy utilisation is 1.17% and 0.86 in case 1 and case 2, respectively.

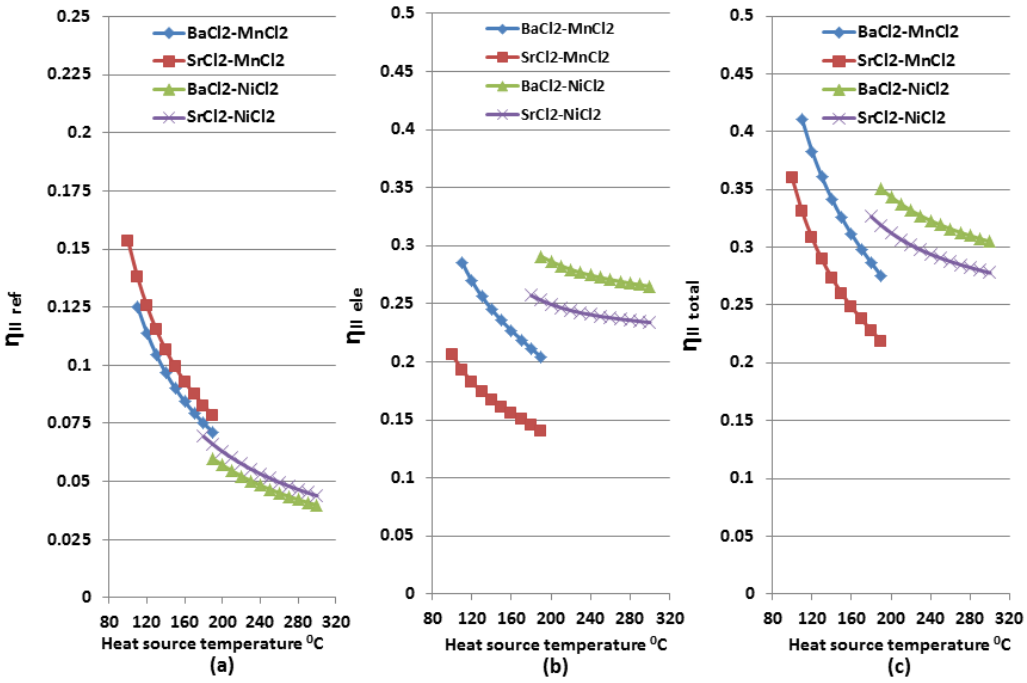

Figure 3-12 Second law efficiency of the resorption cogeneration using HTS-$MnCl_2$, $NiCl_2$ and LTS-$BaCl_2$,$SrCl_2$

(a) refrigeration generation; (b) electricity generation;

(c) refrigeration and electricity generation

The second law efficiency of refrigeration generation, electricity generation and the combined generation is plotted in Figure 3-12. In this study, the refrigeration generation is only determined by the conversion rate of

ammonia without considering the cycle time. Therefore the second law efficiency for refrigeration generation decreases with the increase of heat source temperature. When the resorption working pair is $BaCl_2$- $MnCl_2$, the second law efficiency for electricity generation can reach as high as 0.28. The second law efficiency for electricity generation decreases with the increase of heat source temperature, which can be seen from the Figure 3-12(b).

Compared with the refrigeration generation, the electricity generation consumes more useful work in the system, which can be observed from the tendency of the second law efficiency in Figure 3-12 (b) and Figure 3-12 (c). The highest second law efficiency obtained by the cogeneration is as high as 0.41 by the resorption working pair ($BaCl_2$-$MnCl_2$) at 110 ^oC heat source temperature. Although the $SrCl_2$-$MnCl_2$ shows better performance than the $BaCl_2$-$MnCl_2$ in refrigeration part, the second law efficiency for power generation achieved by the working pair $BaCl_2$-$MnCl_2$ is around 46% higher than that of the $SrCl_2$-$MnCl_2$. The overall exergy efficiency of this optimal resorption cogeneration is around 0.30 under the heat source temperature from 100 ^oC to 300 ^oC.

3.5 Summary

- Analysis of this resorption cogeneration shows attractive performance for refrigeration and electricity generation under the heat source temperature ranging from 100 ^oC to 300 ^oC. First law analysis is applied to choose the optimal resorption working pairs from twelve candidates. Considering about the start pressure for the expansion machine, three HTS candidates are analysed to fit different heat source temperature application. Under the heat source temperature at 110 ^oC, the system without using mass and

heat recovery can achieve its highest COP at 0.70 using $MnCl_2$-$SrCl_2$ as working pair. The highest electrical energy efficiency is achieved at 12.49% by the working pair $PbCl_2$-$NiCl_2$ under 300 ^oC heat source temperature.

- Four resorption working pairs are selected to be further calculated and compared with applying mass and heat recovery after considering the results from the first law analysis and reaction weight of the salts with per mol ammonia. Results show the mass recovery has a more critical effect on the refrigeration generation than the heat recovery. The exergy destruction analysis indicates that the majority of exergy losses are coming from the adsorption processes of the HTS and LTS, when the adsorption heat is rejected to the environment. The combined heat and mass recovery improves the COP by 35% for the HTS-$MnCl_2$ and by 38% for the HTS-$NiCl_2$. Furthermore, the percent increase of electrical energy efficiency of the system using $MnCl_2$ and $NiCl_2$ as the HTS is by 3% and 1.5%, respectively, when the heat recovery is applied. The highest overall system law efficiency is achieved at 0.41 by the resorption working pair ($BaCl_2$-$MnCl_2$) with 110 ^oC heat source temperature. This cogeneration shows a potential application to recovery low grade heat such as solar energy and industry waste heat into refrigeration and electricity. This system can be applied for either small-scale or large-scale application with the advantages of simple construction, dual energy generation, high COP, wide flexibility for different heat source temperature, etc.

Chapter 4. Experimental investigation of chemical composite adsorbents

4.1 Introduction

The overall performance of the resorption cogeneration cycle is mainly determined by two components, expansion process in the expander and the reaction in the chemisorption process. An adsorption performance test bench using volumetric method is designed and constructed in the lab to experimentally investigate the adsorption/desorption performance of the selected chemical adsorbents. $MnCl_2$-$SrCl_2$ has been theoretically proven to be one of the optimal working pair of the resorption cogeneration. These two salts are selected and tested.

In order to overcome the swelling and agglomeration problems of chemical adsorbents, composite adsorbents were selected to be investigated in this study, which is a mixture of chemical adsorbent and porous media. The composite adsorbent has all the advantages of chemical adsorbents such as high adsorption and desorption performance. Activated carbon, expandable graphite, carbon fibre and silica gel are four most commonly used porous media. Natural expandable graphite was selected as the matrix of the composite adsorbent because of its relatively high electrical/thermal conductivity, good heat/mass transfer characteristics, strong chemical stability, wide operating temperature, relatively low thermal expansion, non-hazardous and non-toxic, etc

4.2 Design and construction of an adsorption performance test bench

4.2.1. System design

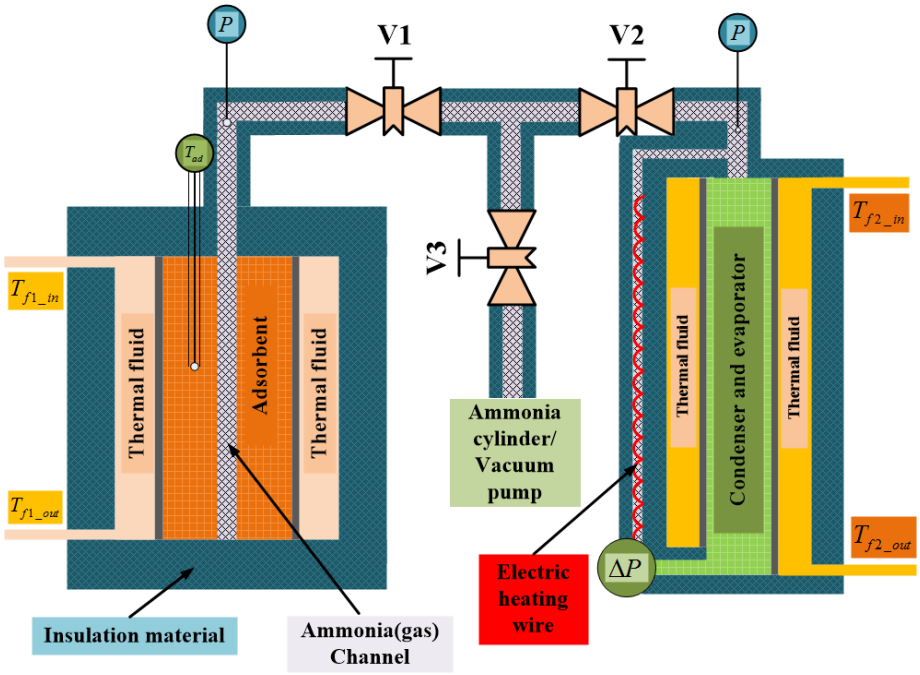

Figure 4-1, Adsorption performance test bench

The schematic diagram of the adsorption performance test bench is shown in Figure 4-1. This test bench contains an adsorbent bed, condenser/evaporator, differential pressure sensor, high temp pressure sensors, temperature sensors, oil bath, cryostat, high temp control valves, etc. The adsorbent bed and condenser/evaporator are designed as double tube construction. The heating and heat rejection of the adsorbent bed is controlled by the oil bath. The cryostat is filled with Thermal G bath fluid (Temperature range from -30 to +80), which is used to control the restricted temperature of the condenser/evaporator. The differential pressure sensor is designed to measure the pressure difference between the two sides of the condenser/evaporator. The data collected by the differential pressure senor can be converted to calculate the quantity of ammonia adsorbed and desorbed by the tested adsorbent. Two rope heaters are encircled on the

other side of the differential pressure pipe to prevent the vapour phase ammonia condensing inside the pipe, which will affect the measurement from the different pressure sensor.

4.2.2. System components

Adsorbent bed

The adsorbent bed was designed to be used for all metal chlorides. Therefore the designed working conditions of the adsorbent were set at 300^{o}C and 30bar based on the Clausius-Clapeyron reaction diagram of the Metal chlorides. Figure 4-2 shows the structure of the adsorbent bed. The height of and the diameter of the inner tube are 300 mm and 52.48mm respectively.

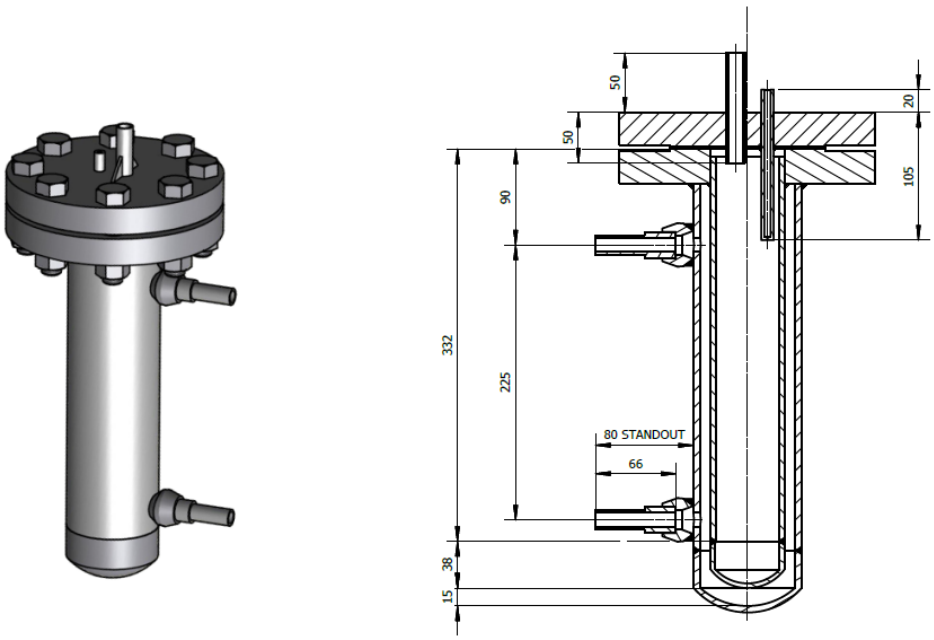

Figure 4-2, Structure of the adsorbent bed

The lid of the adsorbent bed was designed as flange type using eight ¾ inch bolts, which enables easily change of adsorbent. A 4-wire RTD

temperature sensor was selected and inserted into the centre of the adsorbent to accurately measure the adsorbent temperature. The inner tube of the adsorbent bed was designed for placing the adsorbent. We selected 120 stainless steel mesh and inserted it into the centre of the adsorbent to leave a mass channel and prevent the collapsing problem. The volume of the designed adsorbent is 612.88 cm^3.

Oil bath

Figure 4-3 Picture of the oil bath for the adsorbent bed

The oil bath integrated with the adsorbent bed was manufactured by Julabo with the model of SE-6, which is shown in Figure 4-3. The working temperature of this oil bath is from 20 ^oC to 300 ^oC and the maximum heat capacity is 3 kW. The heating oil is used to simulate the heat source when

desorption heat is required during the desorption process of adsorbent. On the other hand, the heat transfer fluid removes the adsorption heat from the adsorbent bed, when the test rig is running as adsorption test mode.

Condenser/Evaporator

In desorption process, this component works as a condenser to condense the vapour phase ammonia into liquid phase. In adsorption process, the component serves as an evaporator and the ammonia flows through the pipe line into the adsorbent bed.

The condenser/evaporator is designed as double tube structure. The ID of the inner tube is 24mm. The designed volume for liquid phase ammonia at environmental temperature is 45.238cm^3. The most conventional metal chlorides are $CaCl_2$, $SrCl_2$, $MgCl_2$, $BaCl_2$, etc. $CaCl_2$ has the smallest relative molecular mass among these metal chlorides and 1mol $CaCl_2$ can adsorb 8mol NH_3. Therefore, $CaCl_2$ has the highest adsorption quantity, which has been used to calculate the quantity of ammonia inside the condenser/evaporator.
During the experiment on composite adsorbent, the mixture ratio of metal chloride and expanded graphite will normally be set at 65:35. There will be 1.44mol $CaCl_2$ inside the adsorbent bed. The theoretically adsorption ratio of $CaCl_2$ and NH_3 is 1:8. Therefore the highest adsorption quantity of ammonia is 11.48mol (NH_3). The highest height can be obtained in the condenser/evaporator is 734.3mm. In order to prevent the overflow of liquid ammonia, the designed height of the inner tube of the condenser/evaporator was set at 1000.00mm.

In the beginning of the experiment, the temperature of condenser/evaporator will be controlled at -25 ^{o}C $(\rho = 671.140\mathrm{kg}/m^3)$, which attracts the largest amount of liquid ammonia $(\mathrm{g} = 303.62\mathrm{g}, \mathrm{n} =$

17.86mol) inside the condenser/evaporator. The real adsorption ratio for $CaCl_2$ is 6mol/mol, therefore the amount of ammonia which reacts with $CaCl_2$ will be 8.64mol. According to all the previously given information, the rangeability of the liquid ammonia inside the condenser/evaporator is 48.376%.

The pipe on the top of the condenser/evaporator was designed as spiral shape, which has been indicated in Figure 4-4 (b). With the application of this design, the condensed ammonia will not easily flow to the pipe line of the condenser/evaporator, which will affect the results achieved from the differential pressure sensor.

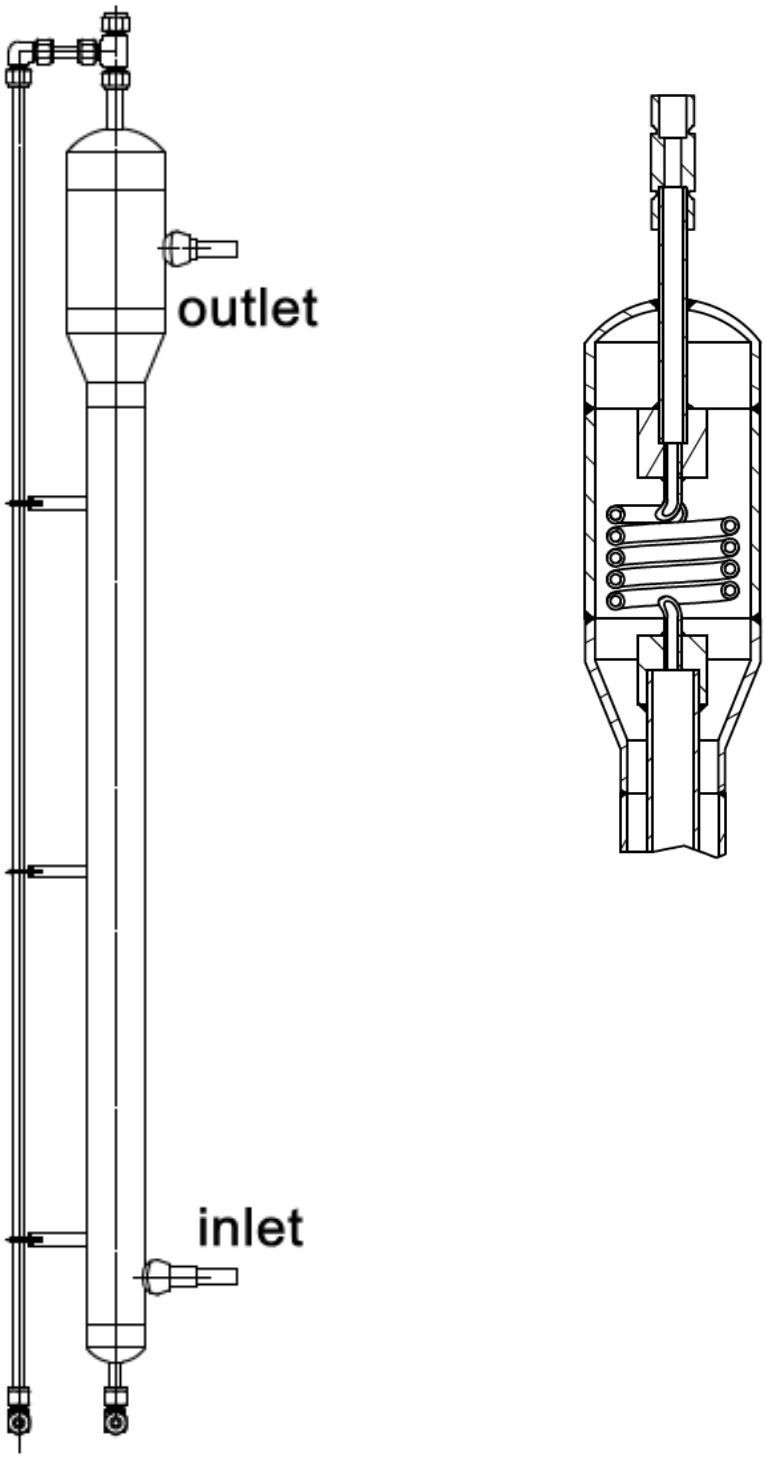

(a) Structure of the condenser/evaporator

(b) inner design of the condenser/evaporator

Figure 4-4, Design of the condenser/evaporator

Cryostat

The temperature of the condenser/evaporator is controlled by a cryostat filled with thermal G bath fluid, which is shown in Figure 4-5. The cryostat has the working temperature range from -40 to 200 ^{o}C. When the test rig is operating as desorption process, the cryostat maintains the temperature at 20 ^{o}C to simulate the environmental condition. During the adsorption performance test, the evaporating temperature of the ammonia inside the condenser/evaporator is controlled at -10 ^{o}C, 0 ^{o}C and 10 ^{o}C by this equipment.

Figure 4-5 Picture of the cryostat for condenser/evaporator

Differential pressure transmitter

Figure 4-6 Picture of the differential pressure transmitter

The differential pressure transmitter in this test bench is supplied by Rosemount with the range of -623 mbar to 623 mbar, which is shown in Figure 4-6. The output of the differential pressure transmitter is 4~20 mA.

The overall mass of ammonia inside the condenser/evaporator can be calculated by the Equation 4-1. The adsorption and desorption rate for the metal chloride is determined by Equation 4-2.

$$m = \frac{\rho_f(Te) - \rho_g(Te)}{\rho_f(Te)} \times \frac{A_c}{g} \times \rho_f(Te) \times g \times \Delta h + V \times \rho_g(Te)$$
$$= \rho_f(Te) \times A_c \times \Delta h - \rho_g(Te) \times A_c \times \Delta h + m_g(Te) \qquad \text{Equation 4-1}$$
$$= \Delta m_f(Te) - \Delta m_g(Te) + m_g(Te)$$

$$\Delta x = \frac{\Delta m}{m_{am}} \qquad \text{Equation 4-2}$$

A_c : Internal area of the Condenser & Evaporator (A_c=4.524×10^{-4}m^2)

g : Gravitational acceleration (g=9.80 m/s^2)

V : Volume of the Condenser & Evaporator (V=4.524×10^{-4} m^3)

Δx : Adsorption capacity (kg/kg)

Δm : Adsorption or desorption quantity of ammonia (kg)

m_{am}: Theoretical transferable ammonia of the adsorbent (kg)

Δp : Pressure difference between Condenser & Evaporator (kPa)

m : Gross mass of liquid and gas state ammonia inside the Condenser & Evaporator (kg)

$\rho_f(Te)$ & $\rho_g(Te)$: Density of saturated liquid state ammonia and gas state ammonia (m^3/kg) [144]

Data acquisition system

The data acquisition system of the adsorption performance test rig includes a DC power supply, a resistor load bank and a data logger. The DC power supply maintains the constant voltage of the pressure sensor and the differential pressure sensor. The real reading from two pressure sensors and differential pressure sensor are converted into 4-20 mA recorded by the data taker DT85. Conversion equations were pre-set in the data logger by the computer. In order to achieve the more accurate reading of the temperature value inside the adsorbent bed, a 4 wire Pt 100 was selected as the temperature sensor. All the other temperature sensors on the pipe lines are K-type thermocouples. The detailed settings of the sensors recorded by the data taker are list in Table 4-1

Table 4-1 Recorded data of the data acquisition system

No	Location	Measured data	Symbol	Type of signal	Measuring error
1	Inlet of the adsorbent bed	Temperature	T_{ad_inlet}	K type thermocouple	0.4%
2	Outlet of the adsorbent bed	Temperature	T_{ad_outlet}	K type thermocouple	0.4%
3	Inside the adsorbent bed	Temperature	T_{RTD}	RTD PT100	±0.01℃
4	Pipeline on the top of the adsorbent bed	Temperature	T_{ad_top}	K type thermocouple	0.4%
5	Pipeline on the top of the condenser/evaporator	Temperature	T_{con_top}	K type thermocouple	0.4%
6	Top of the electric heating coil	Temperature	T_{ele_top}	K type thermocouple	0.4%
7	Bottom of the electric heating coil	Temperature	T_{ele_bot}	K type thermocouple	0.4%
8	Inlet of the condenser/evaporator	Temperature	T_{con_inlet}	K type thermocouple	0.4%
9	Outlet of the condenser/evaporator	Temperature	T_{con_outlet}	K type thermocouple	0.4%
10	Top of the adsorbent bed	Pressure (bar)	P_{ad}	4-20 mA	0.25% FS
11	Top of the condenser/evaporator	Pressure (bar)	P_{con}	4-20 mA	0.25% FS
12	Bottom of the condenser/evaporator	Pressure difference (kPa)	Δp	4-20 mA	0.1%

4.3 Preparations

4.3.1. Manufacture processes of porous matrix using natural expandable graphite

Expanded graphite is originally manufactured from natural graphite flake. Figure 4-7 shows the electron microscope images of expandable and expanded graphite. Compared with expandable graphite, the microstructure of the expander graphite shows more uniform structure.

The characteristics of expanded graphite can be summarised as: large specific surface area, small density, and strong surface adsorption force. Due to the special structure, the expanded graphite can be directly compressed and adhered with each other. The expanded graphite, which will not participate in the chemical reaction, is an inert medium, when it is compounded with pure chemical salts.

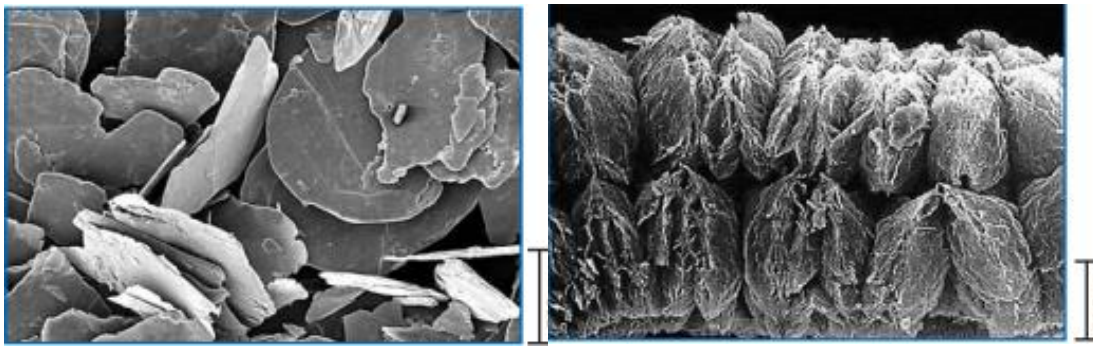

(a) (b)

Figure 4-7 Electron microscope image of expandable and expanded graphite [145] (a) Expandable graphite, 200μm, (b) Expanded graphite, 200μm

Tools

The manufacturing process of the expanded graphite requires several tools includes, a temperature controlled oven (Figure 4-8), an electronic balance (Figure 4-9), a measuring pot, a stainless steel box, etc.

Figure 4-8 Photo of oven

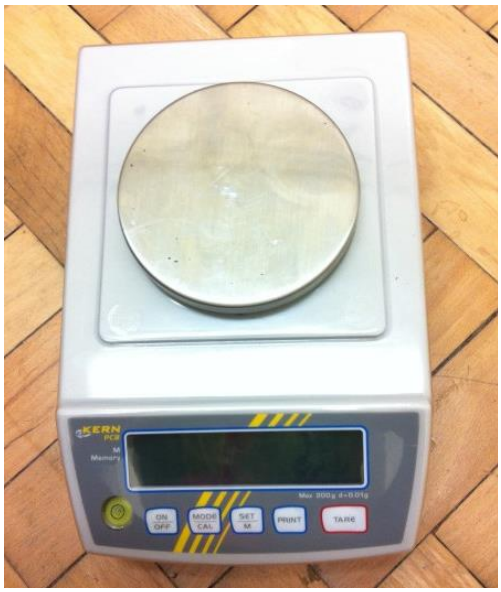

Figure 4-9 Photo of electronic balance

The interlayer bonding force of natural flake graphite is relatively low, which enables it is easy to be transformed into intercalated compounds after using chemical or electrochemical methods. The volume of the expanded graphite is around 100 to 400 times of that of the expandable graphite. The expanded graphite inherits all the properties from natural graphite. Moreover, the expanded graphite possesses good plasticity, extensibility and tightness. The density of the expanded graphite is highly related with the heating temperature and duration of heating. The fibre of the graphite could be destroyed, if the graphite has been overheated. Therefore, the temperature and heating time should be specific considered and controlled.

The manufacture processes of the expanded graphite are described as follows

1. Pre heat the oven to the required temperature (600 ^{o}C)
2. Measure 20 gram of expandable graphite into the steel box by electronic balance shown as Figure 4-10 (a)
3. The steel box is left inside the over for 10 minutes
4. The expandable graphite is ready to be used and can be collected from the oven shown as Figure 4-10 (b)

Figure 4-10 Photo of expandable graphite and expanded graphite

(a) Expandable graphite (b) Expanded graphite

4.3.2. Making composite adsorbents

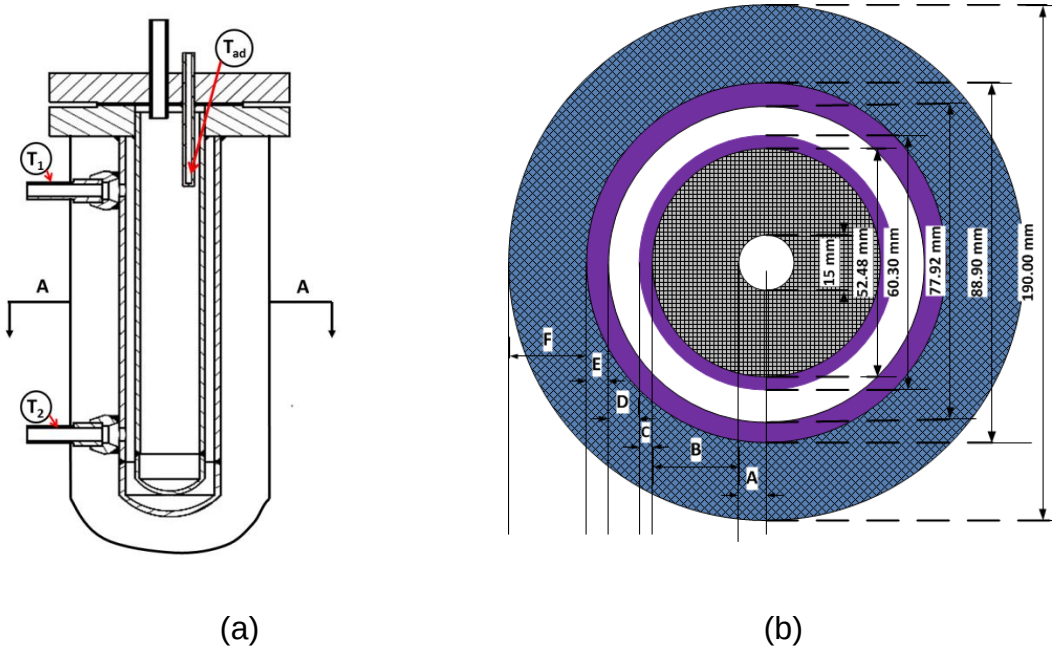

(a) (b)

Figure 4-11 Detailed information about the adsorbent and adsorbent bed

(a) Layout of the temperature sensors
T_1- K type thermocouple, T_2 – K type thermocouple, T_{ad} – RTD
(b) Cross section view (Surface A-A) of the adsorbent bed,
A – Gas flow channel, B - Adsorbent layer, C – Stainless steel, D – Heat transfer fluid, E – Stainless steel, F – Insulation material (Rockwool)

The selected salt is dissolved in the water and mix with the expanded graphite made previously. The mixture of salt, expanded graphite and water is left inside the pre heated oven, which has set the temperature at 120 ^{o}C. The evaporating duration of the water should at least last for 8 to 10 hours based on our experience. The powder state of composite adsorbent is then compressed into the adsorbent bed. A mass flow channel has been left in the centre of the adsorbent bed to let the ammonia freely adsorbed and desorbed from the composite adsorbent. We applied 120 stainless steel mesh in the centre of the adsorbent to prevent the collapse problem and stop the adsorbent flowing into the condenser/evaporator

during the test. The layout of the temperature sensors on the adsorbent bed and the cross section view of the adsorbent bed are indicated in Figure 4-11.

4.3.3. Test plan and procedure

Pressure test

System needs to be checked by compressed air or nitrogen to avoid leakage problem before running with ammonia. Before filling compressed nitrogen into the system, the pipe lines have to be vacuumed by a chemical resistant pump. V_1, V_2 and V_3 were left open during the vacuum process. The compressed nitrogen is then filled into the pipe lines. The test bench was left for at least half a day. If there the leakage problem exists, the pressure drop can be detected from the pressure sensor.

Ammonia filling process

As shown in Figure 4-1，the temperature of the condenser/evaporator will be controlled by the cryostat at -25 ^{0}C. A leak detector or some test papers will ensure there is no leak between the ammonia tank and V_2. The ammonia will evaporates slowly inside the ammonia tank and condenses in the condenser/evaporator. A balance will measure the filling quantity of ammonia (303.62g).

The control processes are,

- V_2 open, V_1,V_3 close
- Control the condenser/evaporator temperature at -25^{o}C by the cryostat
- Connect the ammonia cylinder with the system

- Gradually open V_2 to allow ammonia entering in the system
- Close V_2 when the transfer is complete (determined by the differential pressure sensor and the balance from the ammonia cylinder)
- Disconnect ammonia cylinder
- The condenser/evaporator is fully filled with liquid ammonia.

Testing process

There are two processes during the test of the adsorbent-adsorption process and desorption process. The adsorbent adsorbs the ammonia evaporated from the condenser/evaporator and desorbs the ammonia when the heat circulator increases the temperature. The adsorption/desorption performance can be measured by the test bench. The control processes for the test are as follows,

Adsorption process:

- V_1, V_2 close, V_3 open
- Set Cryostat to desired vessel temperature (above -25 ^{0}C)
- Oil bath running at ambient temp – (OV_1,OV_2 open)
- When the adsorbent temperature reaches the ambient temperature, gradually open V_1.
- Ammonia will evaporate from condenser vessel and be adsorbed into adsorbent.
- Adsorption heat will be removed by cooling effect of recirculating oil. Ensure temperature does not rise above limits.
- Monitor differential pressure gauge
- When the adsorption process finishes, close V_1, V_3

Desorption process:

- V_1,V_2,V_3 close
- Start recirculating oil heater – set at 150 ^{o}C (OV_1, OV_2 close)

- Start cryostat to maintain condenser temperature to ambient temperature.
- Switch on the electric heating wire on condenser pipe– to maintain above 10 ^{o}C.
- When heating oil reaches set point temperature, open OV_1 and OV_2
- The temperature of the adsorbent will begin to rise.
- When temperature inside the adsorbent vessel reaches set-point, open V_1 and V_3 to allow ammonia gas to enter condenser vessel where it condenses to liquid phase.
- Read differential pressure gauge (liquid level measurement) to monitor when full ammonia transfer has occurred.
- Close V_1, V_3

4.4 Experimental investigate of the high temperature composite salt - $MnCl_2$

4.4.1. Heat transfer performance of the composite HTS

In the resorption cogeneration, the composite salt making from $MnCl_2$ and natural expandable graphite has been selected as the high temperature adsorbent. The chemical reaction equation of the $MnCl_2$ is displayed as Equation 4-3. In order to investigate the heat transfer performance of the composite HTS and the effects of heat source temperature, the adsorbent was tested under the inlet oil temperature at 150 ^{o}C, 160 ^{o}C, 170 ^{o}C and 180 ^{o}C while the temperature of the condenser/evaporator was controlled at 20 ^{o}C. The results are plotted in the Figure 4-12.

$$MnCl_2 \cdot 2NH_3 + 4NH_3 \Leftrightarrow MnCl_2 \cdot 6NH_3 + 4\Delta H_{MnCl_2} \quad \text{Equation 4-3}$$

It can be found that the temperature evolution of the adsorbent under different heat source temperature is quite similar with each other except the start point for the chemical reaction. In the first 1 to 2 minutes, the temperature of the adsorbent increases rapidly with the increase of the temperature of the heating oil. This indicates the heat from the oil has only been consumed by the adsorbent bed as the form of sensible heat of the metal and sensible heat of the composite adsorbent. When the adsorbent temperature reaches around 110 ^{o}C, the adsorbent $MnCl_2 \cdot 6NH_3$ starts to release ammonia and transform into $MnCl_2 \cdot 2NH_3$. Large amount of heat has been consumed by the adsorbent bed during the chemical reaction process, which could be explained by the chemical reaction equation of the $MnCl_2$. Furthermore, the adsorbent temperature is very close to the temperature oil temperature, which means the heat transfer between the fluid and the adsorbent is quite well. Therefore the conclusion is the composite HTS has a good heat transfer performance based on the experimental results.

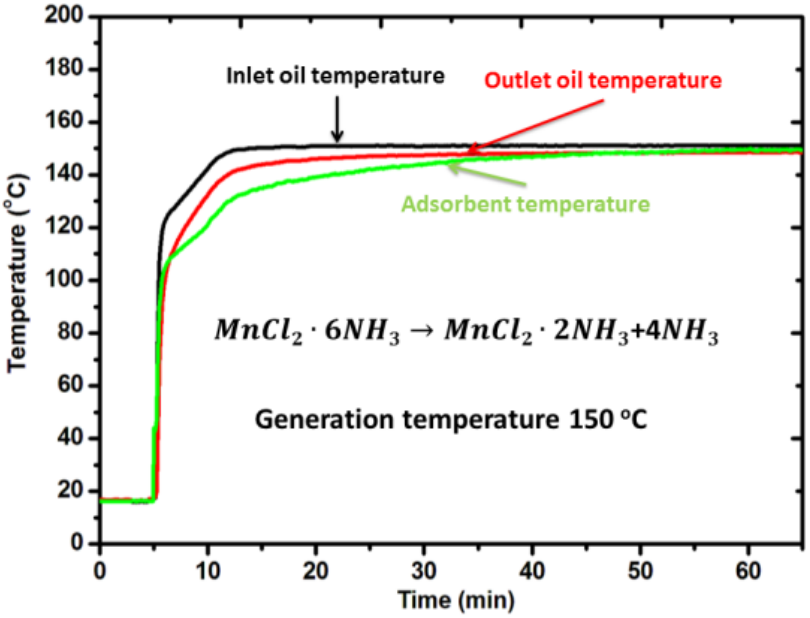
Inlet oil temperature
Outlet oil temperature
Adsorbent temperature
$MnCl_2 \cdot 6NH_3 \rightarrow MnCl_2 \cdot 2NH_3 + 4NH_3$
Generation temperature 150 °C
Temperature (°C)
Time (min)

(a)

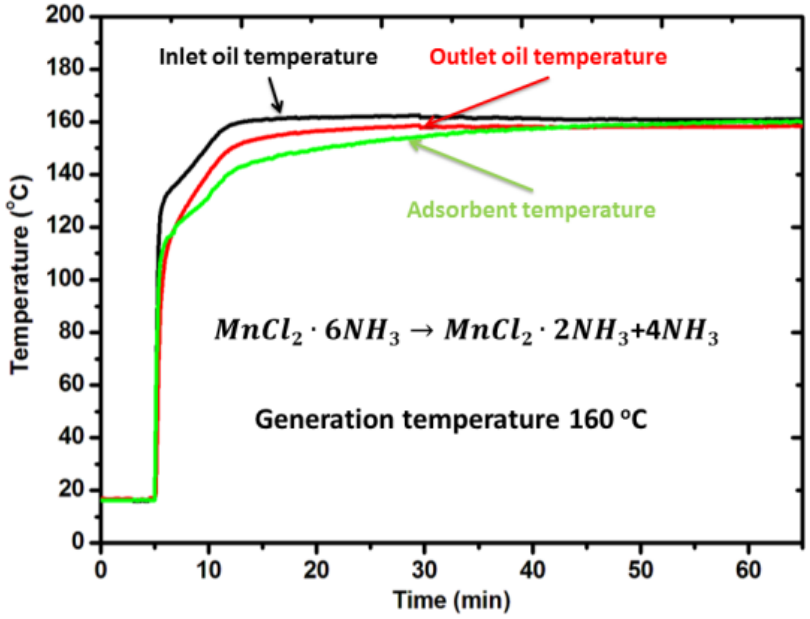
Inlet oil temperature
Outlet oil temperature
Adsorbent temperature
$MnCl_2 \cdot 6NH_3 \rightarrow MnCl_2 \cdot 2NH_3 + 4NH_3$
Generation temperature 160 °C
Temperature (°C)
Time (min)

(b)

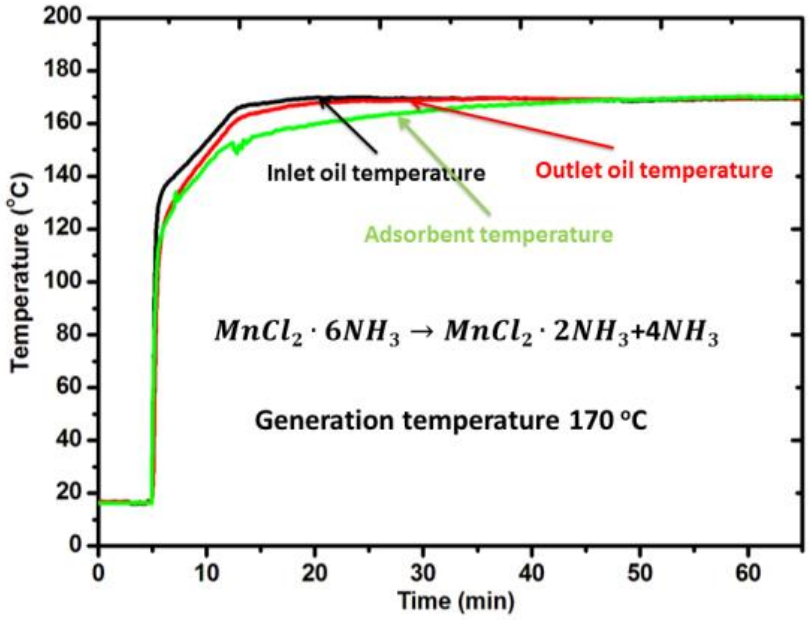

(c)

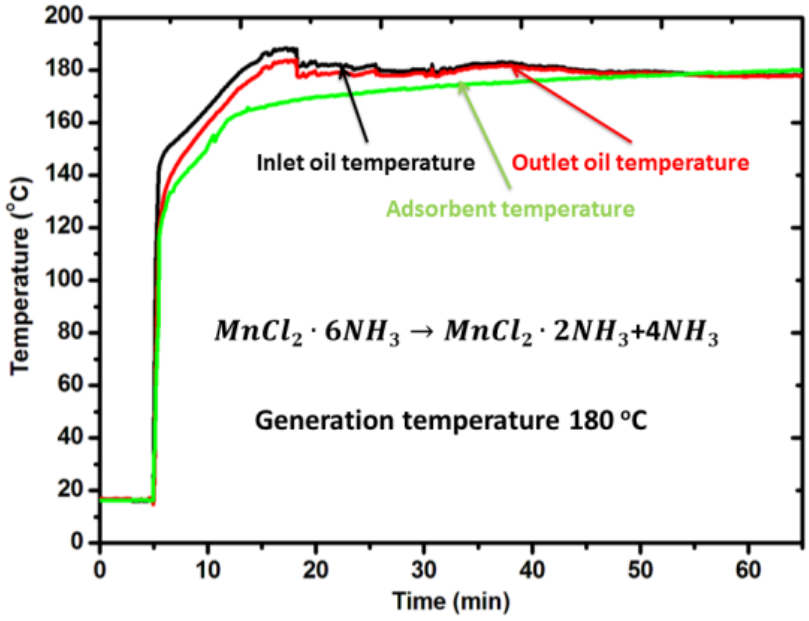

(d)

Figure 4-12 Temperature evolution of the composite HTS under the heat source temperature at (a) 150 ^{o}C, (b) 160 ^{o}C, (c) 170 ^{o}C, (d) 180 ^{o}C; condensing temperature 20 ^{o}C

Figure 4-13 illustrates the temperature evolution of the composite HTS under different heat source temperatures. The results indicate the strongest chemical reaction happens within the first 10 minutes under the tested conditions. The temperature evolution between two dot dash lines illustrated in Figure 4-13 indicates that the chemical reaction process inside the adsorbent bed consumes huge amount of heat compared with the heat required as the form of sensible heat of adsorbent and metal part.

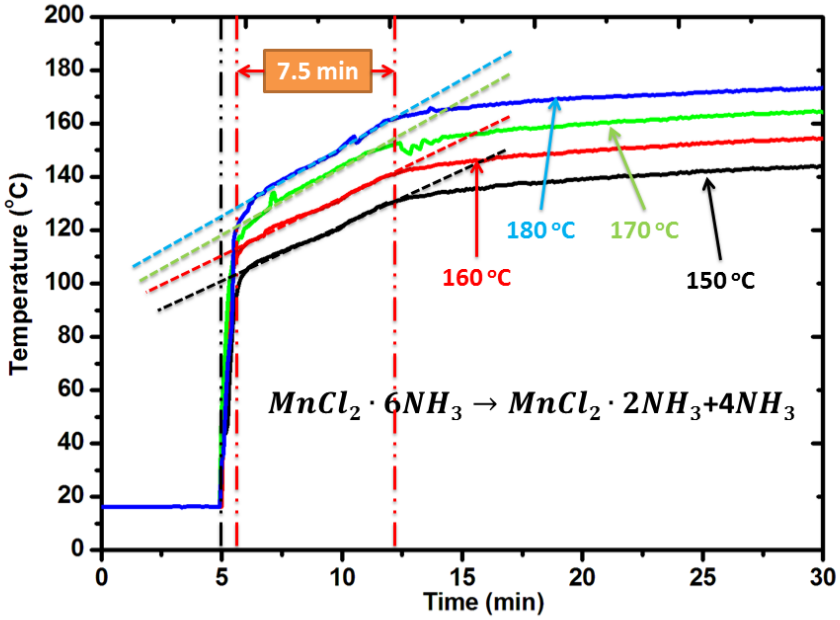

Figure 4-13 Adsorbent temperature under different heating source temperatures

4.4.2. Reaction kinetics of the composite HTS

The chemical reaction rate of the composite HTS under different temperature of heat source has been illustrated in Figure 4-14. When the global conversion ratio is 0.2, the required duration of reaction for the composite HTS under the heat source temperature at 150 ^{o}C, 160 ^{o}C, 170

^{o}C and 180 ^{o}C is around 36 min, 24 min, 17 min and 10 min, respectively. The phenomenon is caused by the difference of the driving temperature under different heat source temperature. The results indicated within the same cycle time, the higher of the heat source temperature, the faster of the chemical reaction of the composite HTS can be obtained.

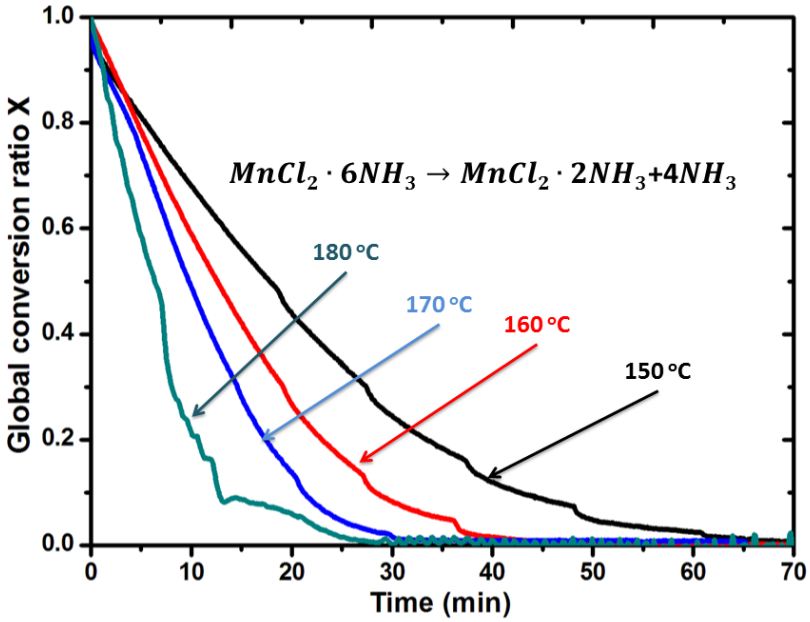

Figure 4-14 The global conversion ratio of the composite HTS during desorption process under different heating temperature

In order to identify the duration of the desorption process of the composite HTS under different heat source temperatures, the temperature sensor has been installed on the top of the condenser/evaporator. The temperature evolution at the top of the condenser/evaporator has been recorded and the results are plotted in Figure 4-15. The results indicated the temperature all increases in the beginning of the desorption process under these four heat source temperature. Under the heat source temperature at 180 ^{o}C, the temperature starts to drop after 20 minutes, which indicates desorption

process of the composite HTS has been ended and no more ammonia flows from the adsorbent bed into the condenser/evaporator. The duration of desorption process of the composite HTS under 150 ^{o}C, 160 ^{o}C and 170 ^{o}C is around 51 min, 38 min and 26 min, respectively. These results demonstrated and verified the required desorption duration of the composite HTS observed from Figure 4-14. The conclusions drawn from the analysis of Figure 4-14 can also been proven by Figure 4-15.

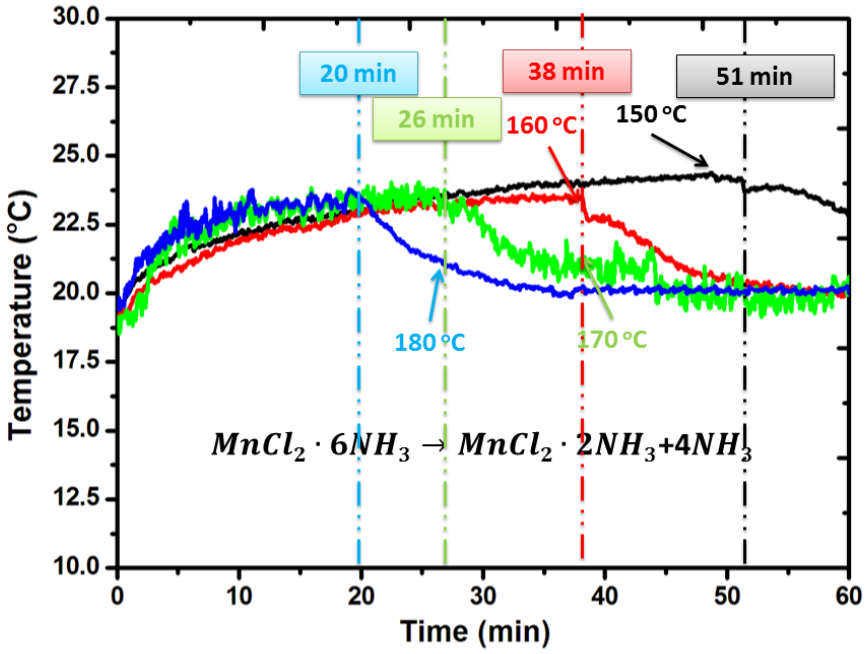

Figure 4-15 Temperature evolution on the top of the Evaporator/condenser during desorption process under different heating source temperatures

The global conversion ratio of the composite HTS during adsorption process under three evaporation temperatures 10 ^{o}C, 0 ^{o}C and -10 ^{o}C has been tested and the results are shown in Figure 4-16. Results indicate in the first ten minutes of the adsorption process, the speed of the chemical reaction increase rapidly. After 15 minutes of cycle time, the global conversion ratio of the evaporation temperature at 10 ^{o}C, 0 ^{o}C and -10 ^{o}C is

around 0.9, 0.83, and 0.81, respectively. Results also indicate under the same heat sink temperature, the higher of the evaporation temperature, the driving temperature for adsorption process is higher. The high driving temperature for adsorption process leads to a relatively fast conversion rate.

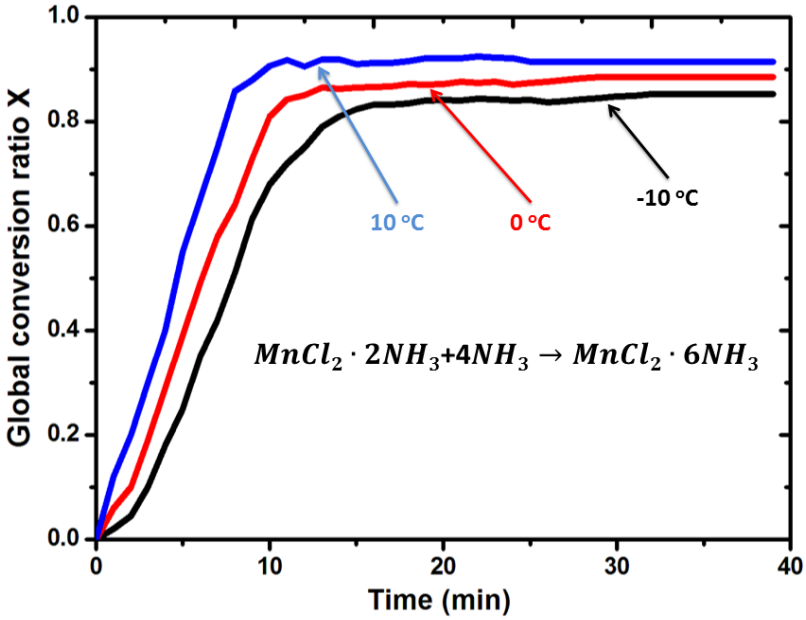

Figure 4-16 The global conversion ratio of the composite HTS during adsorption process under different refrigeration temperature

4.4.3. Isobaric sorption performance of the composite HTS

The isobaric sorption performance of the composite HTS under different working conditions has been shown in Figure 4-17. The isobaric desorption performance is illustrated by Figure 4-17 (a), which indicates under the same restricted pressure P_c controlled by the condenser/evaporator, the composite HTS starts to generate ammonia when the adsorbent temperature reaches about 100 ^{o}C. The decomposition phase of the

composite HTS is almost ended when the adsorbent temperature arrives at 140 ^{o}C.

The isobaric adsorption performance of the composite HTS under three adsorption pressures is shown in Figure 4-17 (b). As the results show, the higher of the adsorption pressure controlled by the condenser/evaporator, the more ammonia can be adsorbed by the composite adsorbent. After several times of tests, the adsorption capacity of the composite HTS is still as high as 81%, 85% and 92% under the adsorption pressure at 292kPa, 429kPa and 612kPa, respectively. These results indicate with the help of porous matrix the agglomeration problem of the chemical adsorbent has been effectively overcome and the repeatable adsorption performance has been effectively improved.

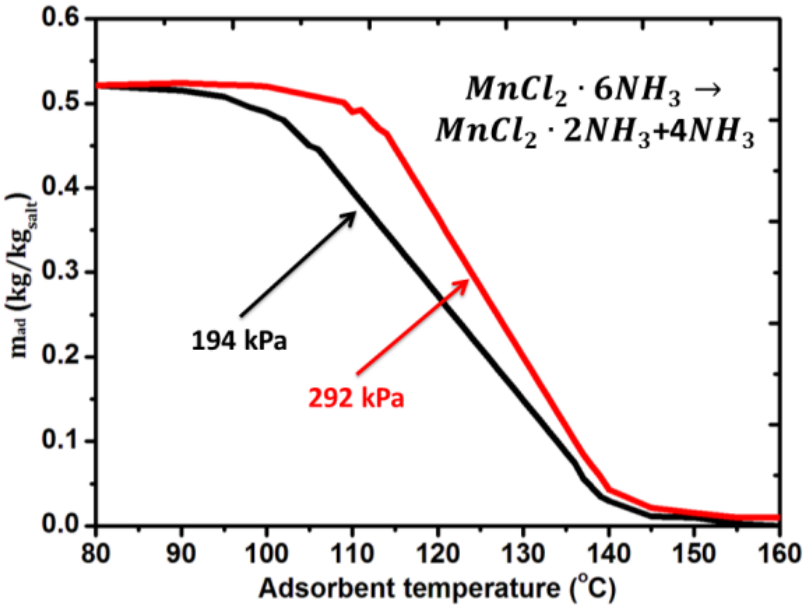

(a)

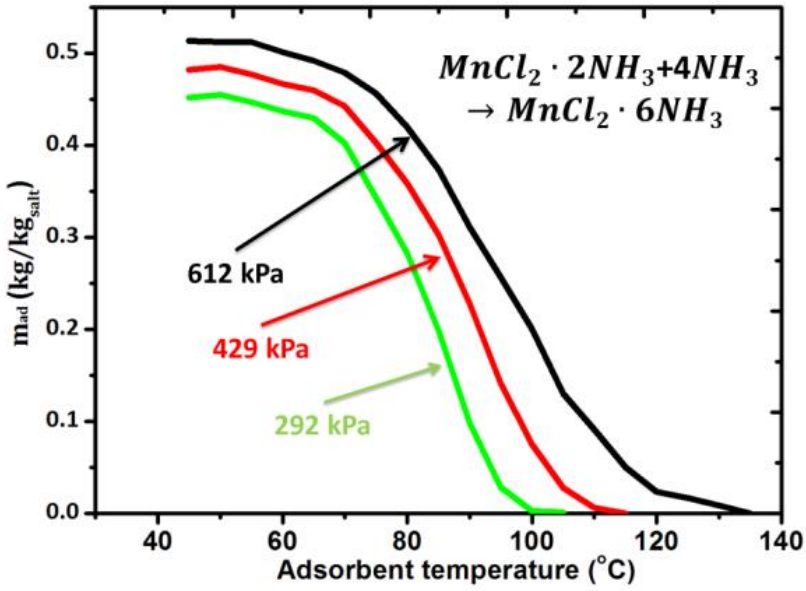

(b)

Figure 4-17 Isobaric sorption performance of the composite HTS
(a) decomposition phase (b) synthesis phase

The adsorption and desorption curves under the tested conditions are shown in Figure 4-18, which illustrate the relationship between the adsorbent temperature and conversion ratio. The global conversion ratio shows linear relationship with the temperature of adsorbent within the specific temperature ranges. The fitted lines are added on the curves and the relationships are presented by the equations from Equation 4-4 to Equation 4-8.

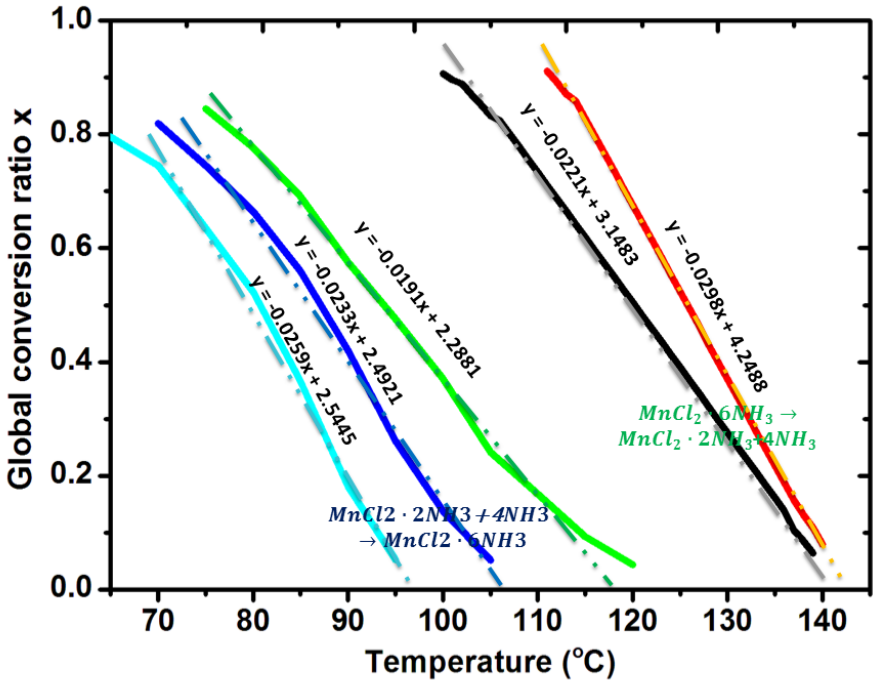

Figure 4-18 Relationship between global conversion ratio and adsorbent temperature of the composite HTS

Desorption curve

$$x = -0.0298T + 4.2488,\ P_c = 2.89\text{bar}, 110℃ \le T \le 140℃$$ Equation 4-4

$$x = -0.0221T + 3.1483,\ P_c = 1.91\text{bar}, 100℃ \le T \le 140℃$$ Equation 4-5

Adsorption curve

$$x = -0.0191T + 2.2881,\ P_c = 6.04\text{bar}, 75℃ \le T \le 115℃$$ Equation 4-6

$$x = -0.0233T + 2.4921,\ P_c = 2.89\text{bar}, 75℃ \le T \le 105℃$$ Equation 4-7

$$x = -0.0259T + 2.5445,\ P_c = 1.91\text{bar}, 70℃ \le T \le 95℃$$ Equation 4-8

4.4.4. SCP of the composite HTS

The evolution of the specific cooling power (SCP) of the composite HTS has been shown in Figure 4-19. The heat sink temperature is maintained at 20 ^{o}C and the evaporating temperature of the ammonia is controlled under three different temperature. The SCP of the composite is calculated by the Equation 4-9.

Equation 4-9

$$SCP_{HTS} = \frac{Qref}{m_{HTS} \times (t - t_0)} = \frac{m_{HTS} \times \Delta x_{HTS} \times L_{am}}{m_{HTS} \times (t - t_0)} = \frac{\Delta x_{HTS} \times L_{am}}{(t - t_0)}$$

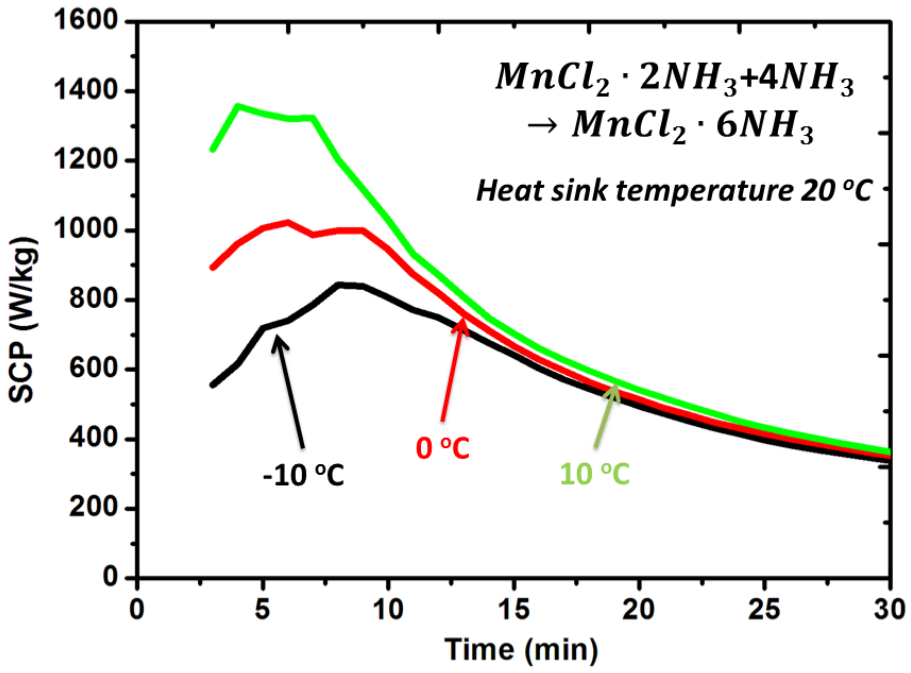

Figure 4-19 SCP evolution of the HTS composite adsorbent at different refrigeration temperature

In the Equation 4-9, SCP_{HTS} is the specific cooling power of the composite HTS, Δx_{HTS} is the conversion ratio of the ammonia, L_{am} is the latent heat of ammonia and $(t-t_0)$ is the duration of the adsorption process.

The results indicate that in the beginning of the adsorption process, the value of the SCP increase quickly until a peak point has been achieved. The highest SCP achieved by the composite under -10 ^{o}C refrigeration temperature is 820 W/kg at 8 minutes of adsorption cycle time. With the increase of cycle time, the SCP slowly decreases after the peak point. The reason of this phenomenon is that the chemical reaction speed is relatively fast in the beginning of adsorption process, which leads to the sharp increase of adsorption capacity.

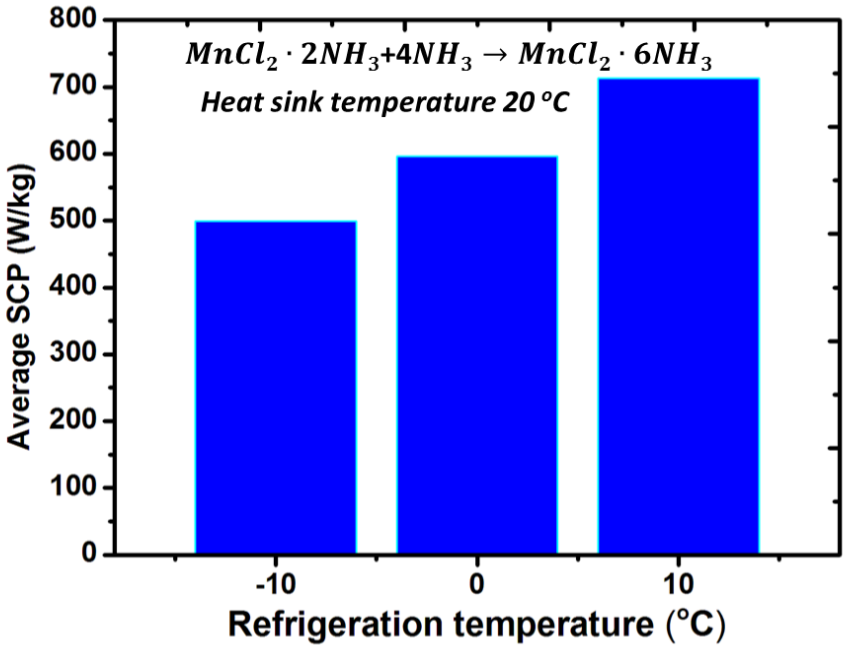

Figure 4-20 Average SCP of the HTS composite adsorbent at different refrigeration temperature

The average SCP of the composite HTS under different refrigeration temperature is illustrated as Figure 4-20. When the heat sink temperature is controlled at 20 ^{o}C, the average SCP of the composite HTS under the refrigeration temperature at -10 ^{o}C, 0 ^{o}C and 10 ^{o}C, is 500 W/kg, 600 W/kg and 700 W/kg, respectively.

4.5 Experimental investigation of the low temperature composite salt - $SrCl_2$

4.5.1. Heat transfer performance of the composite LTS

The composite LTS selected in this study is $SrCl_2$ and the chemical reaction equation can be presented by Equation 4-10

$$SrCl_2 \cdot NH_3 + 7NH_3 \Leftrightarrow SrCl_2 \cdot 8NH_3 + 7\Delta H_{SrCl_2} \quad \text{Equation 4-10}$$

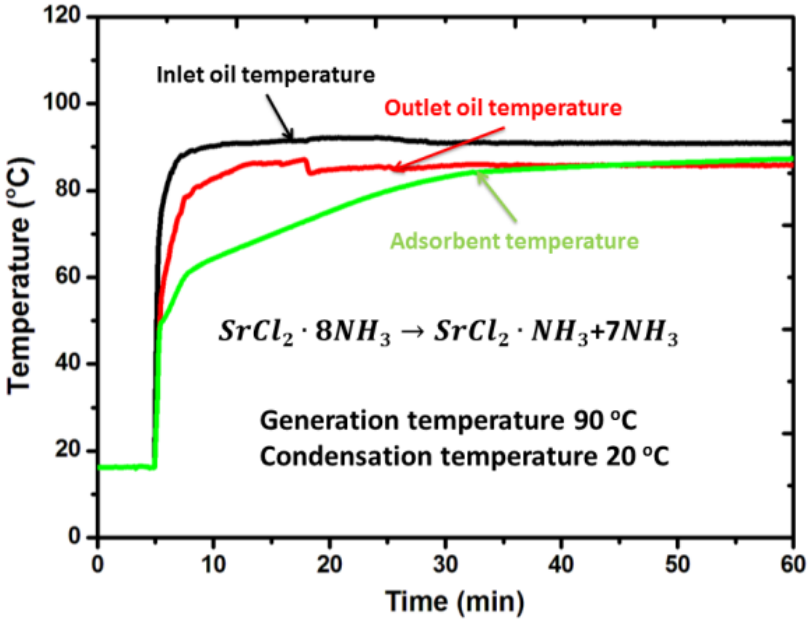

(a)

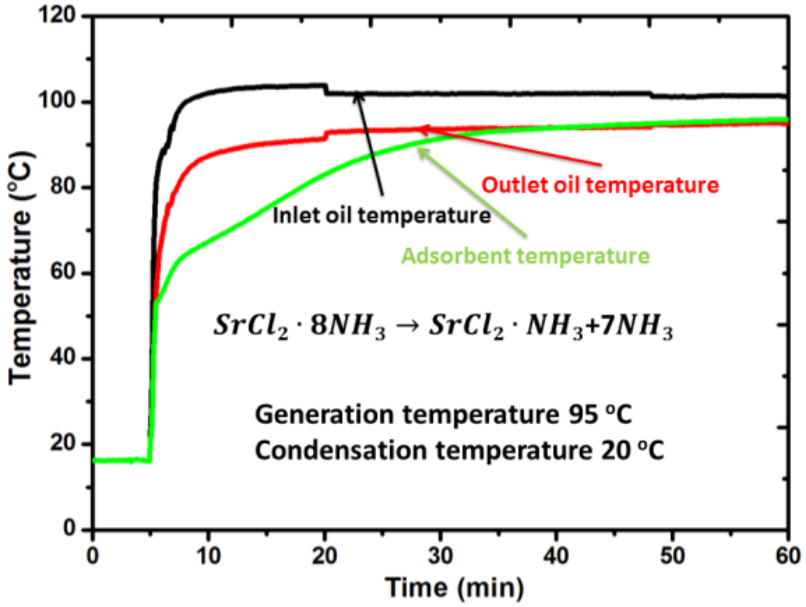
Temperature (°C)
Time (min)
Outlet oil temperature
Inlet oil temperature
Adsorbent temperature
$SrCl_2 \cdot 8NH_3 \rightarrow SrCl_2 \cdot NH_3 + 7NH_3$
Generation temperature 95 °C
Condensation temperature 20 °C

(b)

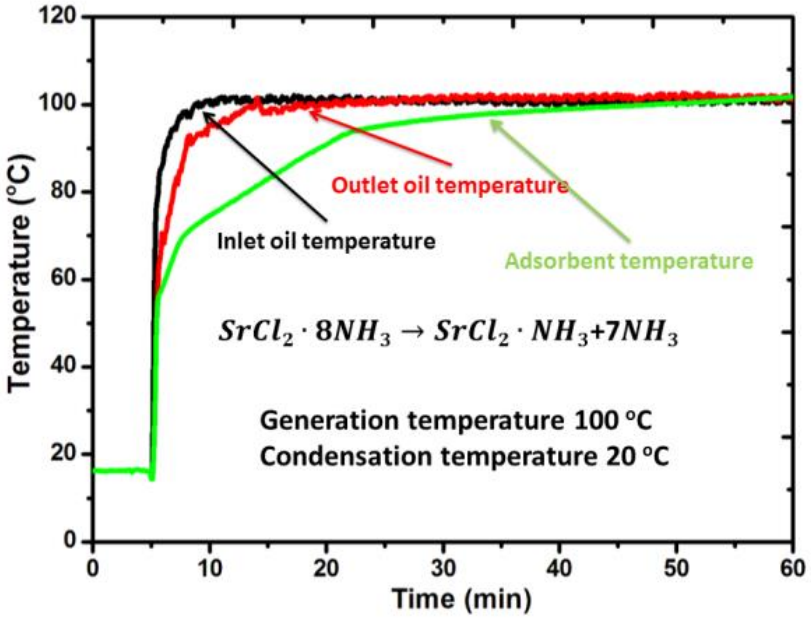
Temperature (°C)
Time (min)
Outlet oil temperature
Inlet oil temperature
Adsorbent temperature
$SrCl_2 \cdot 8NH_3 \rightarrow SrCl_2 \cdot NH_3 + 7NH_3$
Generation temperature 100 °C
Condensation temperature 20 °C

(c)

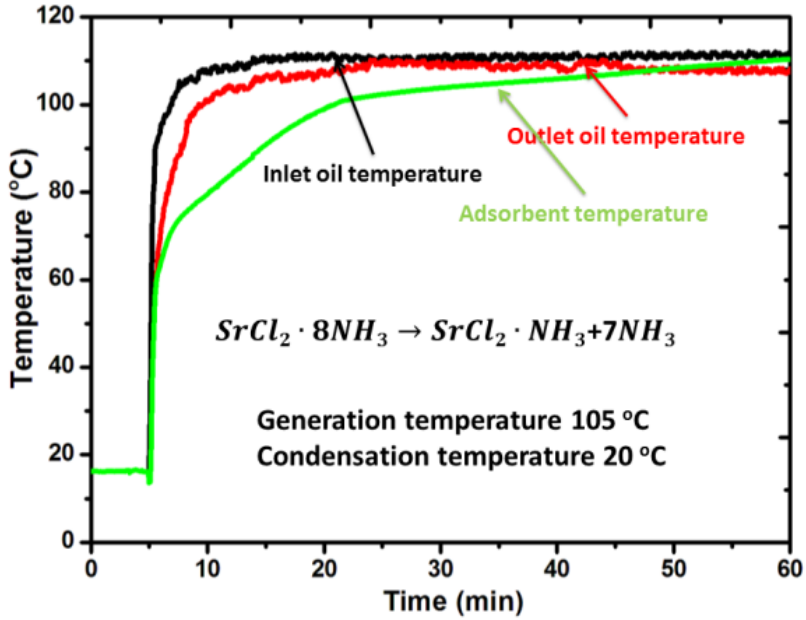

(d)

Figure 4-21 Temperature evolution of the LTS composite adsorbent under the heat source temperature at (a) 90 ^{o}C, (b) 95 ^{o}C, (c) 100 ^{o}C, (d) 105 ^{o}C

The composite LTS was tested under the heating oil temperature at 90 ^{o}C, 95 ^{o}C, 100 ^{o}C and 105 ^{o}C, when the heat sink temperature was maintained at 20 ^{o}C. The results pointed out the adsorbent temperature of the composite LTS increases sharply when the heating oil flows into the adsorbent bed. The temperature of the composite LTS requires more time to be stable compared with the composite HTS. This can be explained by the chemical reaction equations of the HTS and LTS, which is indicated by Equation 4-3 and Equation 4-10. The salts in the tested sample are all 210 g, which is around 1.67 mol of $MnCl_2$ and 1.32 mol $SrCl_2$. The reaction enthalpy of these two salts is very close to each other. Therefore, the composite LTS requires almost twice of the chemical reaction heat from the heat source compared with the reaction heat required for the composite HTS. The majority of the supplied heat was consumed to provide the desorption heat of the composite LTS when the adsorbent temperature slowly increases after 1 to 2 minutes of desorption cycle time as shown in Figure 4-21. After 25 minutes of desorption cycle time, the temperature of

the adsorbent starts to be stable and is very close to the supplied oil temperature.

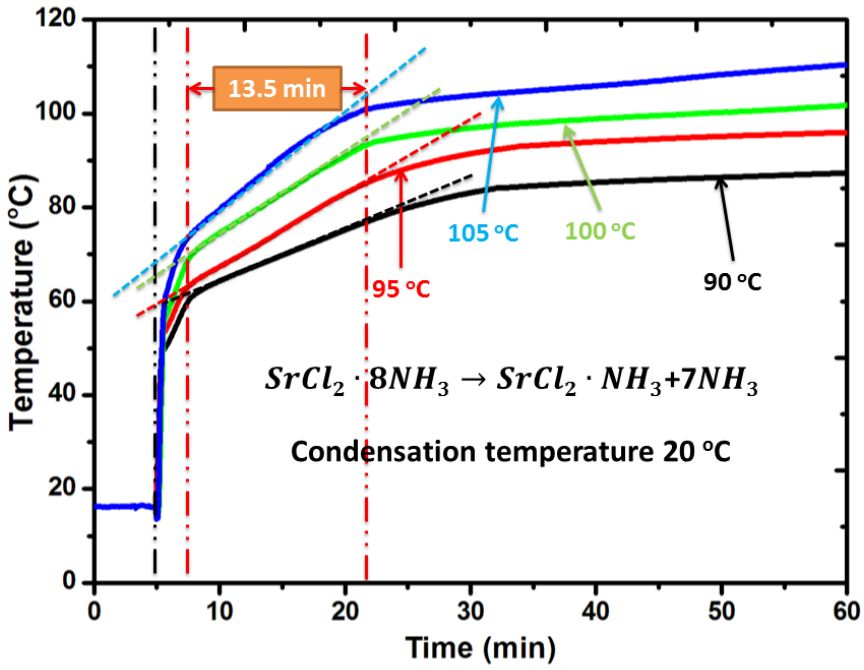

Figure 4-22 Adsorbent temperature under different heating source temperatures

Figure 4-22 compares the temperature variation of the composite LTS under four different heating oil temperature. The results indicate the average duration for the desorption process of the composite LTS under the tested conditions is around 13.5 minutes. Mover, the results also indicated the higher of the heating oil temperature, the quicker of the adsorbent temperature can reach the steady process.

4.5.2. Reaction kinetics of the composite LTS

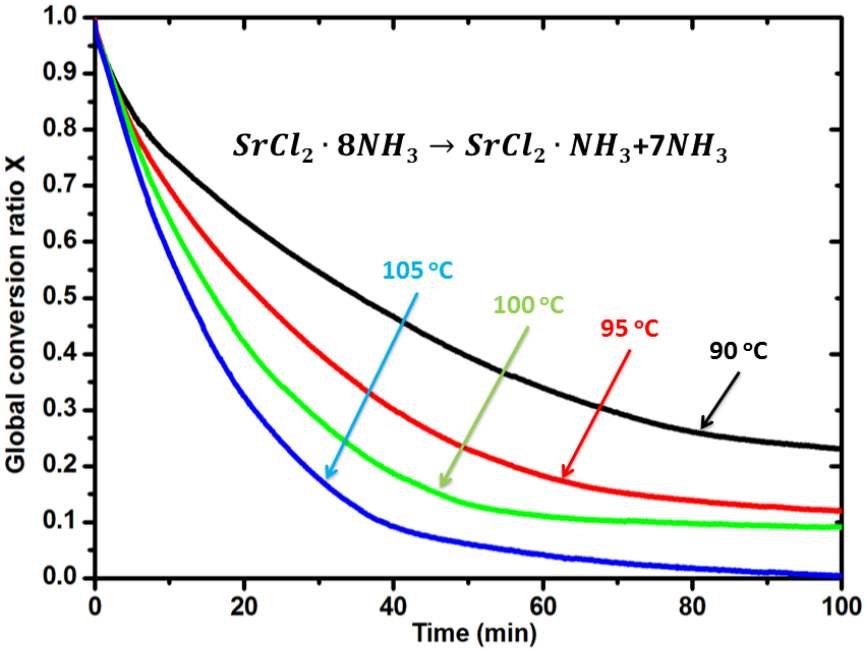

Figure 4-23 The global conversion ratio of the LTS during desorption process under different heating temperature

The global conversion ratio of the composite LTS under different heating oil temperatures are illustrated in Figure 4-23. Under the same heat sink temperature controlled by the condenser/evaporator, the difference between the global conversion ratio of the composite LTS under different heat source temperature is caused by desorption driving temperature. Within the same time, the higher of the heat source temperature, the higher desorption driving temperature can be obtained. At 60 minutes of desorption cycle time, almost 95% of $SrCl_2 \cdot 8NH_3$ has been converted into $SrCl_2 \cdot NH_3$, when the heating oil temperature is supplied at 105 ^{o}C. The global conversion ratio of the composite LTS under the heating oil

temperature at 90 ^{o}C, 95 ^{o}C and 100 ^{o}C is around 0.35, 0.22 and 0.15, respectively.

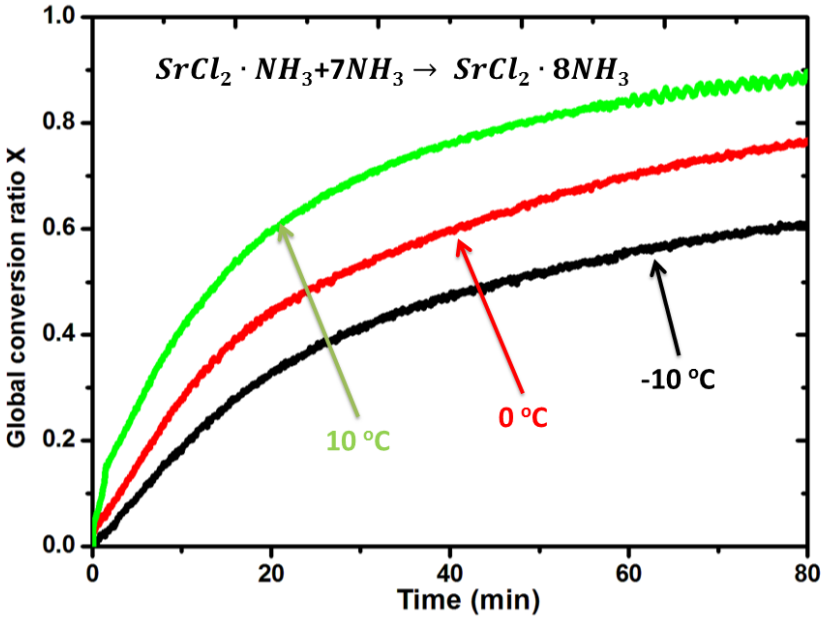

Figure 4-24 The global conversion ratio of the LTS during adsorption process under different refrigeration temperature

The adsorption performance of the composite LTS was tested under three evaporating temperature -10 ^{o}C, 0 ^{o}C and 10 ^{o}C. The results are plotted in Figure 4-24. Within the same adsorption cycle time, the higher of the evaporating temperature of ammonia, the higher global conversion ratio can be obtained. The higher of the evaporating temperature leads to higher restricted pressure P_c from the condenser/evaporator. The equilibrium pressure P_{eq} of the adsorbent during adsorption process is controlled by the heat sink temperature. The driving pressure $(P_c - P_{eq})$ results to the start of adsorption process. The results indicated under the refrigeration temperature at -10 ^{o}C, 0 ^{o}C and 10 ^{o}C, the global conversion ratio of the

composite LTS at 60 minutes cycle time is around 0.55, 0.70 and 0.82, respectively.

4.5.3. Isobaric sorption performance of the composite LTS

In order to evaluate the relationship between the adsorbent temperature and the adsorbed/desorbed quantity of the composite LTS, the isobaric sorption curves during the decomposition phase and synthesis phase are plotted as Figure 4-25 (a) and (b).

The composite LTS starts to generate ammonia, when the adsorbent temperature arrives at 60 ^{o}C under the restricted pressure set at 194 kPa and 292 kPa. The decomposition phase is almost ended when the adsorbent temperature is at 100 ^{o}C. This indicates that in order to fully transform $SrCl_2 \cdot 8NH_3$ into $SrCl_2 \cdot NH_3$, the minimum heat source temperature supplied to the composite LTS should be higher than 100 ^{o}C.

The isobaric adsorption performance of the composite LTS under the restricted pressure at 292 kPa, 429 Kpa and 612 kPa are illustrated in Figure 4-25 (b). When the restricted pressure is set at 612 kPa, the composite LTS starts to adsorb ammonia at the adsorbent temperature 75 ^{o}C. The start point to react with ammonia for the composite LTS under the restricted pressure at 292 kPa and 429 kPa is around 55 ^{o}C and 70 ^{o}C, respectively. The results also indicate the adsorption capacity of the composite LTS under the restricted pressure at 612 kPa can be as high as 0.68 kg/kg salt, which is about 93% of the theoretically adsorption capacity of the $SrCl_2$. These results indicate the composite adsorbent has successfully overcome the swelling and agglomeration phenomenon,

which can lead the reduction of adsorption performance of the chemical adsorbent.

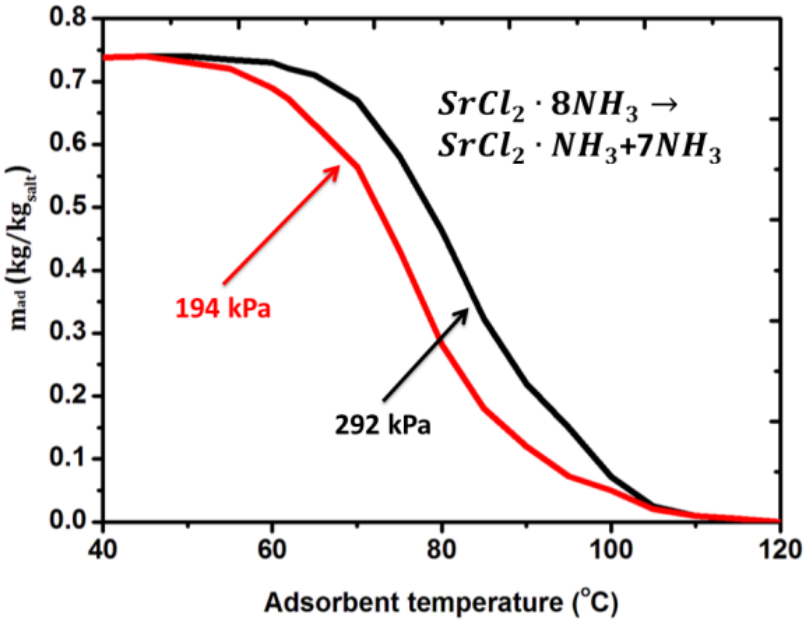

(a)

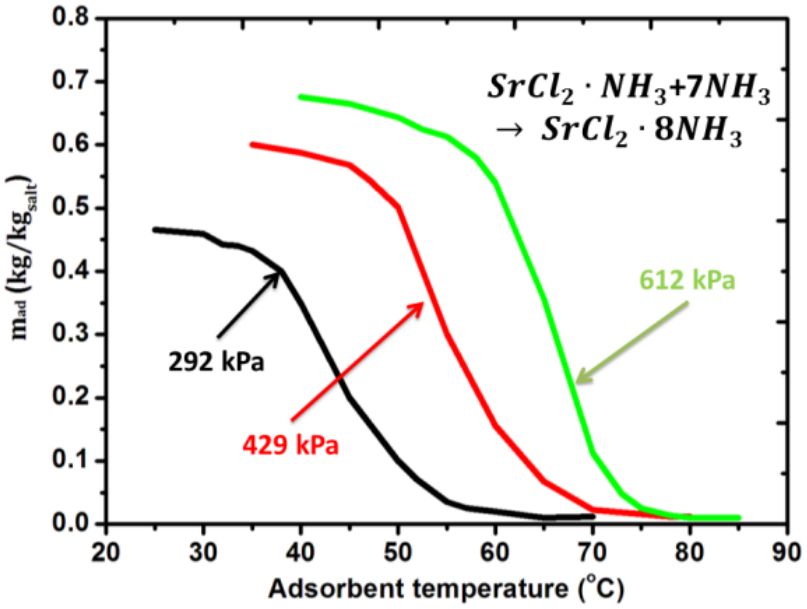

(b)

Figure 4-25 Isobaric sorption performance of the composite LTS

(a) decomposition phase (b) synthesis phase

The relationship between the adsorbent temperature and global conversion ratio under the tested conditions are drawn in Figure 4-26. The black and read lines are the relationships during desorption process, when the restricted pressure of the condenser/evaporator is 194kPa and 292kPa. The global conversion ratio of the adsorption performance for $SrCl_2$ under 292 kPa, 429 Kpa and 612 kPa is indicated as blue, green and pink lines in Figure 4-26. Five fitted lines are added to illustrate the linear relationship between the adsorbent temperature and global conversion ratio. The fitted equations are shown from Equation 4-11 to Equation 4-15.

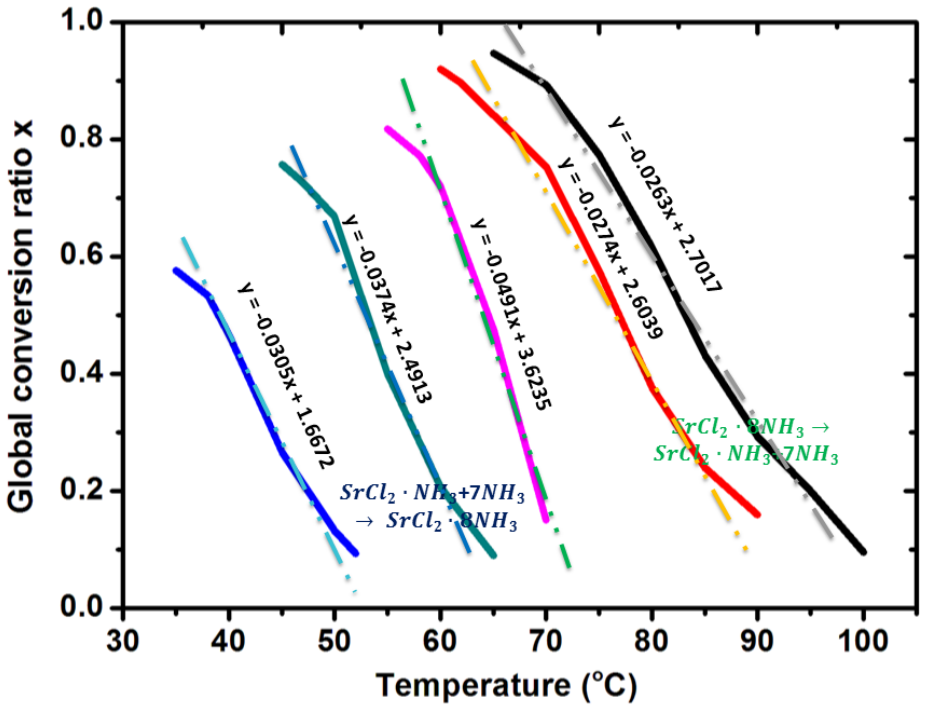

Figure 4-26 Relationship between global conversion ratio and adsorbent temperature of the composite LTS

Desorption

$$x = -0.0263T + 2.7017,\ P_c = 2.89\text{bar},\ 65℃ \le T \le 100℃ \qquad \text{Equation 4-11}$$

$$x = -0.0274T + 2.6039,\ P_c = 1.91\text{bar},\ 60℃ \le T \le 90℃ \qquad \text{Equation 4-12}$$

Adsorption

$$x = -0.0491T + 3.6235,\ P_c = 6.04\text{bar},\ 55℃ \le T \le 75℃ \qquad \text{Equation 4-13}$$

$$x = -0.0374T + 2.4913,\ P_c = 2.89\text{bar},\ 45℃ \le T \le 65℃ \qquad \text{Equation 4-14}$$

$$x = -0.0305T + 1.6672,\ P_c = 1.91\text{bar},\ 35℃ \le T \le 55℃ \qquad \text{Equation 4-15}$$

4.5.4. SCP of the composite LTS

The specific cooling power of the composite LTS is evaluated by the Equation 4-16.

$$SCP_{LTS} = \frac{Q_{ref}}{m_{LTS} \times (t - t_0)} = \frac{m_{LTS} \times \Delta x_{LTS} \times L_{am}}{m_{LTS} \times (t - t_0)} = \frac{\Delta x_{LTS} \times L_{am}}{(t - t_0)} \qquad \text{Equation 4-16}$$

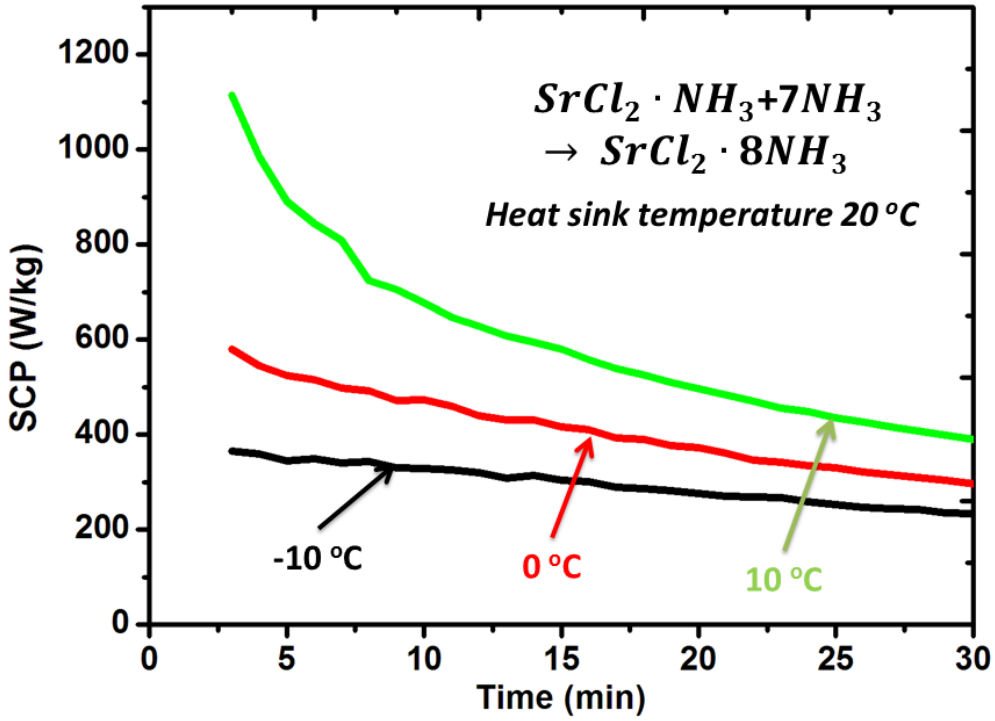

Figure 4-27 SCP evolution of the composite LTS at different refrigeration temperature

Figure 4-27 shows the SCP evolution of the composite LTS under three refrigeration temperature controlled by the condenser/evaporator. The results indicate the SCP decreases with the increase of cycle time. This phenomenon is caused by the relatively strong and fast chemical reaction in the beginning of the adsorption process. The average SCP of the composite LTS under the refrigeration temperature at -10 ^{o}C, 0 ^{o}C and 10 ^{o}C is around 260 W/kg, 360 W/kg and 540 W/kg, which is shown in Figure 4-28.

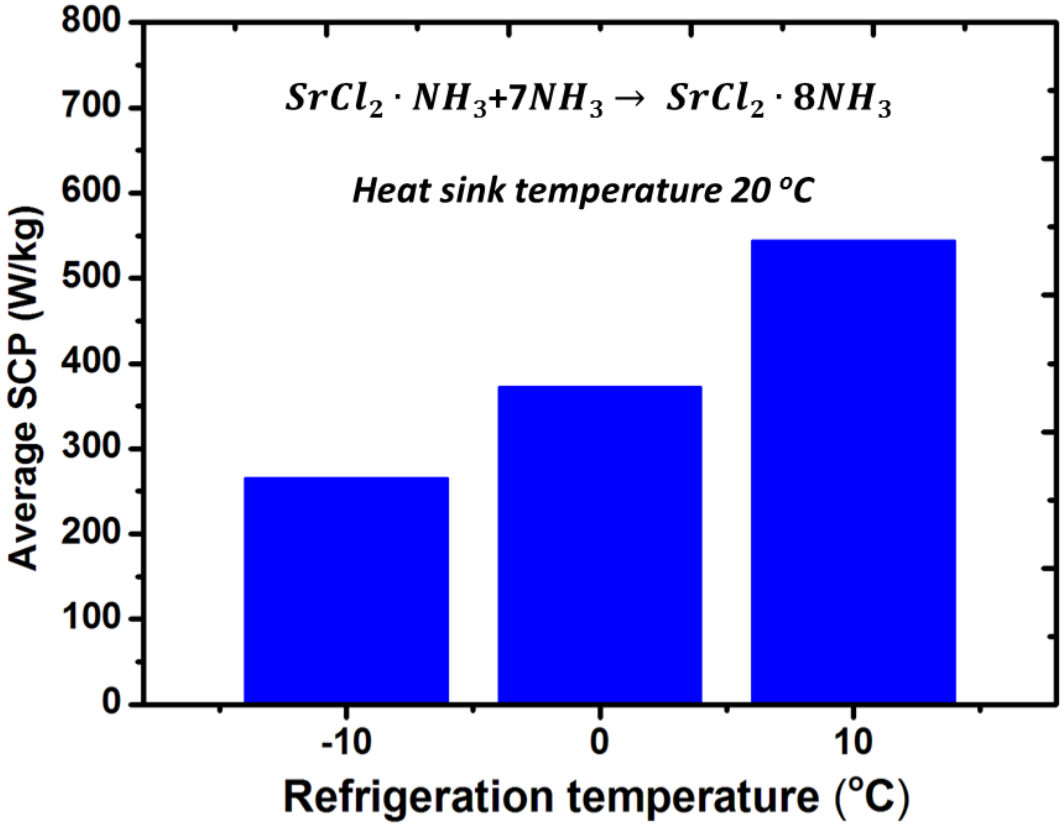

Figure 4-28 Average SCP of the composite LTS at different refrigeration temperature

4.6 Summary

This chapter describes the design and construction work on an adsorption performance test rig applying volumetric method. The manufacturing processes of composite adsorbent using expandable graphite as matrix has been developed. The adsorption and desorption performance of the $MnCl_2$ and $SrCl_2$, which has been selected as the HTS and LTS of the resorption cogeneration system, are tested and evaluated. The heat transfer performance, reaction kinetics, isobaric sorption performance and specific cooling capacity of the composite adsorbent are studied and investigated. The main conclusions can be summarised as

- The composite adsorbent shows a good heat transfer performance under the tested conditions. The chemical reaction can only start when the temperature of the adsorbent reaches the equilibrium temperature at the restricted pressure controlled by the condenser/evaporator. Huge amount of heat has been consumed/rejected during desorption/adsorption process of the adsorbent. During the desorption process, the heat supplied from the oil has been mainly consumed as the desorption heat of the adsorbent. The sensible heat required for the adsorbent bed is quite limited during the chemical reaction process.

- The study of reaction kinetics of the composite adsorbent shows the chemical reaction rate is mainly affected by the restrained temperature. The desorption performance is affected by the heat source temperature and the adsorption performance is influenced by the heat sink temperature. In order to improve the adsorption and desorption performance of the adsorbent, the increase of the difference of driving temperature could effectively achieve this target.

- The composite adsorbent using expandable graphite has effectively overcome the swelling and agglomeration problems, which can be commonly occurred in chemical adsorbent. After several times of tests, the regeneration performance of the composite adsorbent is still very good. Under the restricted pressure at 612 kPa, the adsorption capacity of the composite HTS is as high as 92% and the adsorption capacity of the composite LTS is around 93%. The SCP of the adsorbent increases with the increase of refrigeration temperature. When the evaporating temperature changes from -10 ^{o}C to 10 ^{o}C, the average SCP of the composite LTS increases from 260 W/kg to 540 W/kg.

Chapter 5. Investigation of scroll expander

5.1 Introduction

Expansion machine plays a key role in power generation system. The scroll expander has been identified as one of the most proper expanders to be integrated with adsorption system because of its high efficiency, reliability, wide output power range under relatively low flow rate.

A scroll expander test bench has been designed, constructed and experimentally tested within this study. This chapter describes all the processes about the rig design, experimental testing results and the geometric study on the tested machine. The results collected in this chapter will be used in Chapter 6 for the simulation work on the scroll expansion machine.

5.2 Design and construction of a scroll expander test bench

5.2.1. System design

An open-drive scroll expander test rig has been designed to test the performance of this type of expansion machine. The schematic diagram of the designed system has been illustrated in Figure 5-1.Compressed air is used to drive the expander for power generation and the compressed air is supplied by the compressed air line through the building. The supplied pressure and flow rate of the system has been controlled by a control valve locating between the air compressor and flow meter. An electrical heating

unit was designed at the inlet of the expansion machine to test the power generation performance of the expander under different supplied inlet temperature.

The inlet and outlet working conditions of the expander are measured by two temperature and pressure sensors. A belt was used to transfer the mechanical power from the scroll expander to electricity produced from a generator. The generated electricity is consumed by load lamps and measured by a power meter.

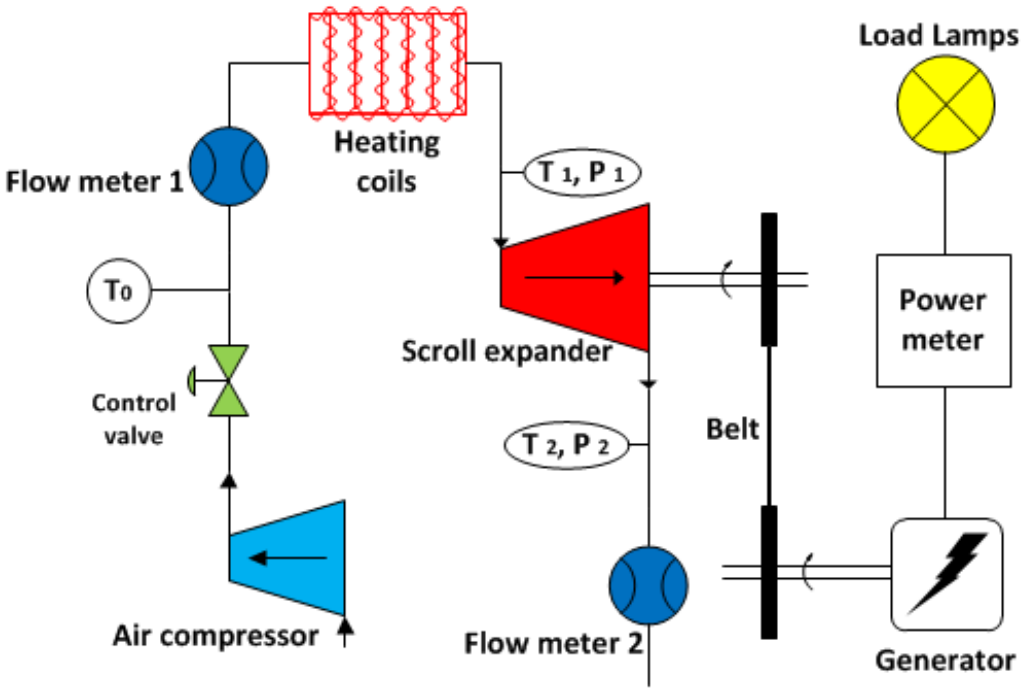

Figure 5-1 Schematic diagram of the scroll expander test bench

5.2.2. System components

Inlet flow meter

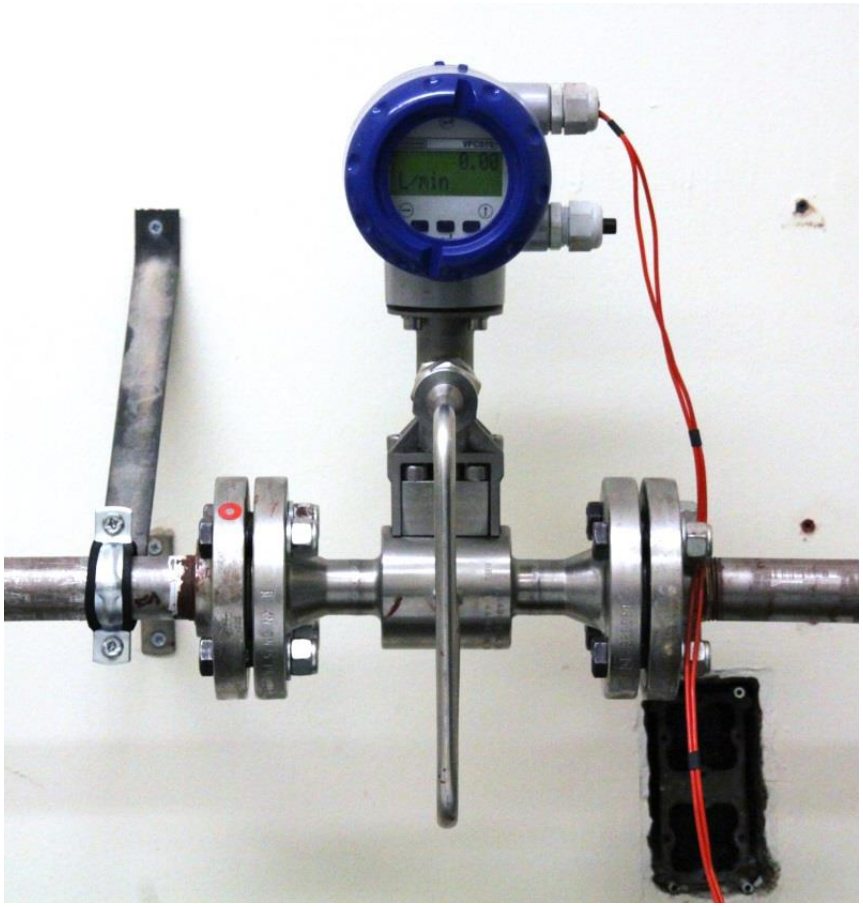

Figure 5-2 Flow meter to measure the inlet flow rate

The inlet volume flow rate is measured by a flow meter manufactured by KROHNE Group with the model of OPTISWIRL 4070. This equipment is designed to accurately measure both liquid and gas phase working fluid with an integrated pressure and temperature sensors to self-calibrate the collected results. The flow rate converts the data into4-20 mA signal, which is collected by the data acquisition system.

Outlet flow meter

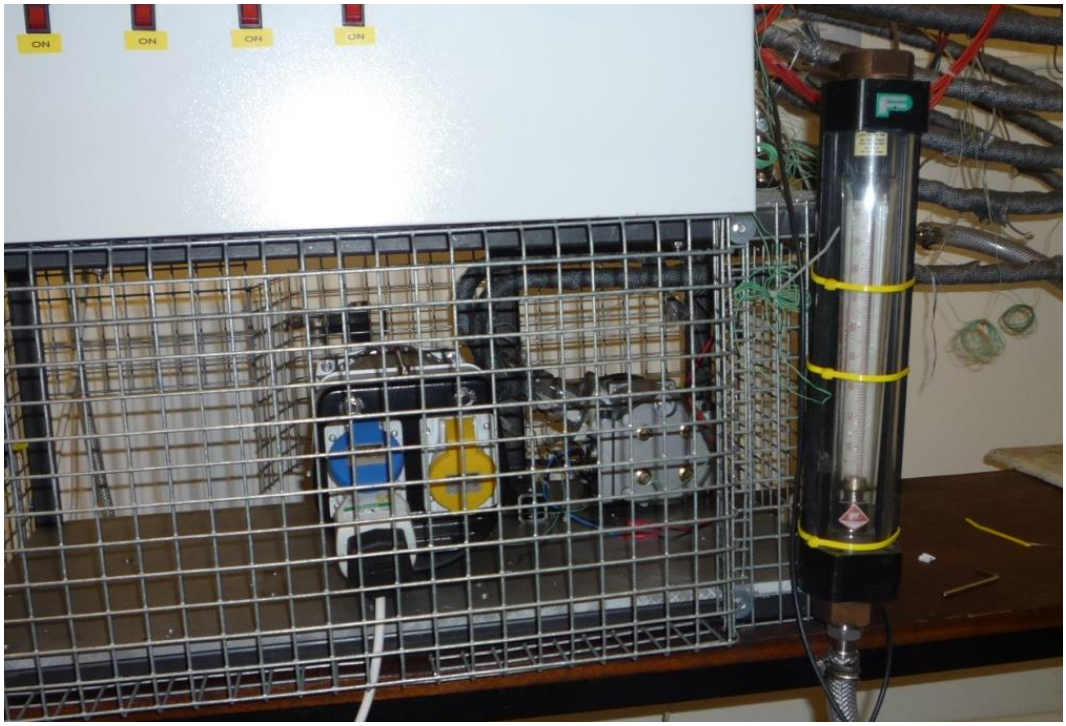

Figure 5-3 Flow meter to measure the outlet flow rate of the expander

The volumetric expansion ratio is one of the most critical parameters of scroll expander. A second volumetric flow meter has therefore been placed at the outlet of the scroll expander to test the exhaust flow rate. This flow meter has been connected to the stainless pipe line through a flexible pipe. The second function of the measuring the exhaust flow rate of the expander is to be used to calculated the real exhaust pressure at the exhaust port of the expander. Because this designed rig is an open driven system the real pressure at the exhaust port of the scroll expander can hardly been measured by the pressure sensor locates at the outlet. The calculation methods will be introduced in the next section

Generator

The generator selected for the test bench is manufactured by Mecc Alte with the model number of S15W-85/A, which has the rated power of 2.4 kW at 50 Hz and 2.9 kW at 60 Hz. This generator has two types of output as indicated in Figure 5-4 (a). Belt is used to connect the scroll expander with the generator to convert mechanical power into electricity. The electricity produced from the generator is consumed by a load bank using 6 lamps to consume the power and illustrate the electricity production of this tested bench.

(a) (b)

Figure 5-4 Electrical generator (a) front view ; (b) side view

Simulated heat source unit

(a) (b)

Figure 5-5 Photo of the electrical heat unit

(a)heat ropes on the pipes (b) control box

An electrical heating unit is designed to simulate the heating source temperature and is located between the inlet of the scroll expander and outlet of the flow meter unit. The heat source unit includes five heat ropes, five temperature process controllers, bended stainless steel pipes, five K type temperature sensors and some accessories. Heat ropes are rolled on the bended pipes and the temperature sensors are covered by the heat ropes (OMEGA: STH102-080). The temperature sensors are evenly distributed in the heat unit. Five separated electric circulators are installed inside the control box for the heat ropes. The heat temperature is controlled by the temperature process controller supplied from OMEGA. Each of the heat circulator could be switched on or off by the switch shown in Figure 5-5 (b). Insulation ropes are wrapped on the top of heat ropes to reduce the heat losses.

Scroll expander

The scroll device chosen for the system is originally designed as a scroll compressor for car air condition application with the model number Sanden: TRSE09 as shown in Figure 5-6. As mentioned in the literature review, scroll compressor could be run as the expander as long as the inlet and outlet been switched with each other. Several modifications have to be done before the test as described in the following paragraphs.

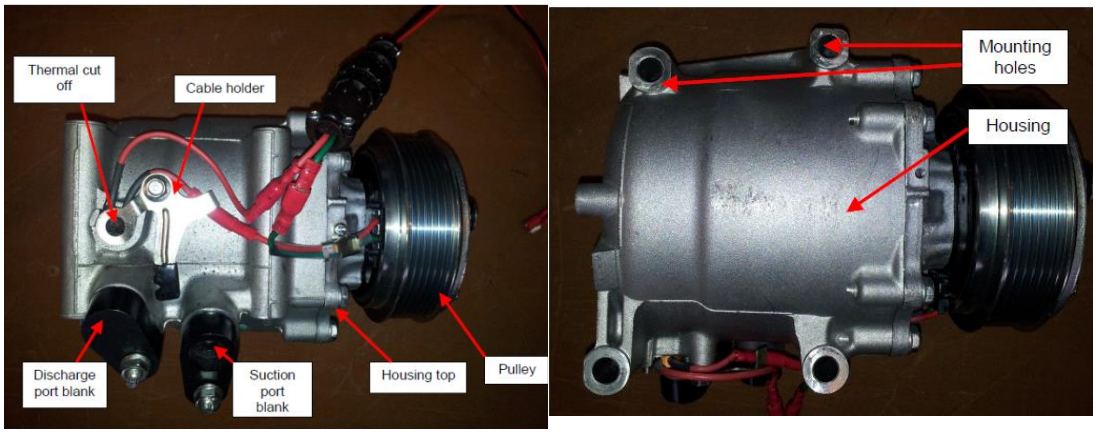

(a) (b)

Figure 5-6 Picture of the Sanden TRSA09 Scroll Compressor
(a) front view (b) side view

A check valve was originally installed in the scroll device to stop the discharged high pressure working fluid flowing back to the device and prevent the reverse rotation of the scrolls in compressor mode [146, 147]. However, in the expander mode, the check vale stops the fluid flowing into the scrolls, which should be removed before operation. Figure 5-7 shows the photo of the scroll before and after the removal of check valve. Moreover, the Sanden TRSA09 is factory lubricated with SP-15 oil, which has the function of lubricate the contacted seals between two scrolls and bearings to reduce the heat and mass losses. The investigation of the performance of scroll expander is to simulate the real working conditions of

the cogeneration system proposed in Chapter 3. The resorption cogeneration contains chemical adsorbents in the system. Oil should be forbidden to be used in the cogeneration system, because the oil will contaminate the adsorbents and reduce the system performance. Therefore, the oil has been drained from the expander. The detailed information about the components of the test rig is list in Appendix 2.

Figure 5-7 Removal process of the check valve from the stationary scroll

(a) Stationary scroll with check valve (b) Stationary scroll without check valve

Data acquisition system

The data of this test rig are collected and recorded by a data logger-dataTaker DT85 manufactured by Grant. This data acquisition system can record temperature, Voltage, current, 4-20 mA loops, different resistance, and frequency. In this rig, all the thermocouples are K-type with the ranges from 0 ^{o}C to 275 ^{o}C. The two pressure sensors are connected into the data logger on Channel 9 and 10, respectively. The conversion

equations for the pressure sensor were pre-set in to the data logger by the computer. The recorded interval for this test rig was set at 5 second. Detailed information about the recorded data are listed in the Table **5-1**

Table 5-1 Recorded data of the data acquisition system

No	Location	Measured data	Symbol	Type of signal	Error
1	Inlet of flow meter	Temperature	T_0	K type thermocouple	0.4%
2	Inlet of scroll expander	Temperature	T_{inlet}	K type thermocouple	0.4%
3	Outlet of scroll expander	Temperature	T_{outlet}	K type thermocouple	0.4%
4	First heat unit control process	Temperature	T_1	K type thermocouple	0.4%
5	Second heat unit control process	Temperature	T_2	K type thermocouple	0.4%
6	Third heat unit control process	Temperature	T_3	K type thermocouple	0.4%
7	Forth heat unit control process	Temperature	T_4	K type thermocouple	0.4%
8	Fifth heat unit control process	Temperature	T_5	K type thermocouple	0.4%

9	Inlet of scroll expander	Pressure	P_{inlet}	4-20 mA	1% FS
10	Outlet of scroll expander	Pressure	P_{outlet}	0-10V	1% FS
11	After control valve	Inlet volumetric flow rate	$\dot{V}_{inlet}$	4-20 mA	4%

5.3 Geometric study and measurement of the scroll unit

5.3.1. Geometric study of the scroll unit

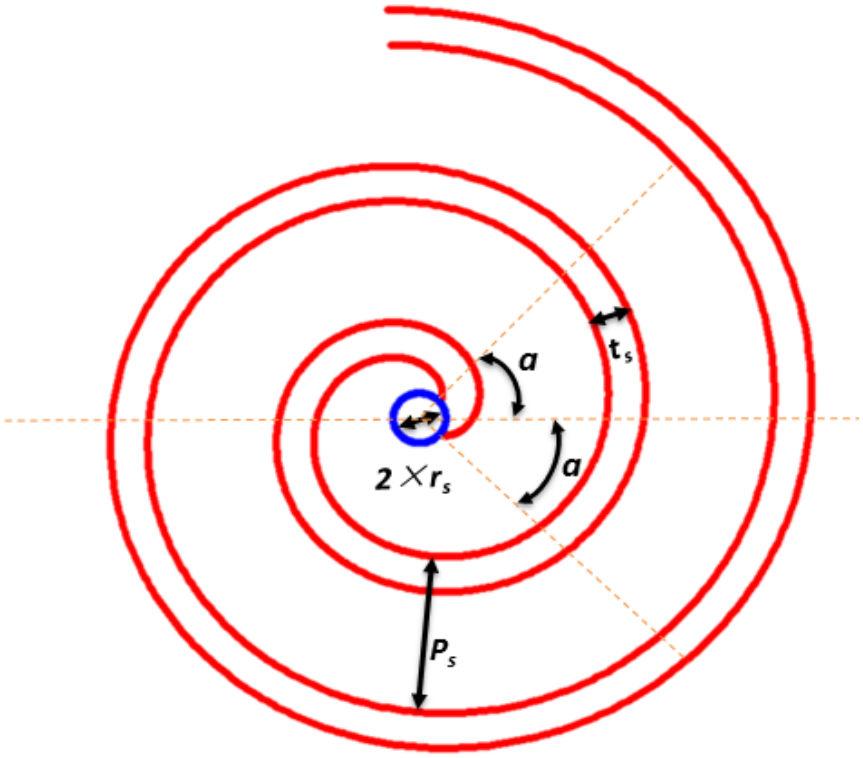

Figure 5-8 The internal and external involute lines of scroll unit

A detailed geometric study on scroll blade not only can accurately calculate the physical parameters of the scroll machine such as the swept areas,

volumes and designed volumetric expansion ratio. Moreover， the relationships between the situational and orbiting scrolls during expansion process can be studied.

The geometric shape of the scroll blade can be described by circle involute equation as indicated in Equation 5-1, where r_s is the radius of the basic circle, ϕ is the involute angle and α is the start angle of the involute.

$$x = r_s\left[\cos(\phi+\alpha)+\phi\sin(\phi+\alpha)\right]$$
$$y = r_s\left[\sin(\phi+\alpha)-\phi\cos(\phi+\alpha)\right] \qquad \text{Equation 5-1}$$

Other important parameters of the geometric shape of the scroll blade include pitch of the scroll P_s, thickness of the scroll blade t_s and height of the scroll H_s. The radius of gyration of the orbiting scroll is R_{gy}. The relationships between these parameters have been illustrated as

$$t_s = 2\times r_s\times\alpha \qquad \text{Equation 5-2}$$

$$P_s = 2\times\pi\times r_s \qquad \text{Equation 5-3}$$

$$R_{gy} = \frac{1}{2}\times(P_s - 2\times t_s) \qquad \text{Equation 5-4}$$

The scroll unit of the machine includes the internal involute lines and external line with different start angle as $+\alpha$ and $-\alpha$, respectively. Based on the circle involute equation shown as Equation 5-1, the internal and external involute lines of scroll unit have been drawn and indicated as Figure 5-8.

5.3.2. Measurement of the scroll unit

Physical dimensions of the scroll unit determine the performance of the expansion machine and can be used to compare/validate the experimental results. The experimental used scroll machine was fully disassembled to retrieve some critical data as indicated in Figure 5-9. The measured parameters were used to draw the geometric shape of the scroll unit. The designed parameters such as start angle of the involute, swept volumes, areas and volumetric expansion ratio of this scroll unit could be obtained and compared with the experimental results.

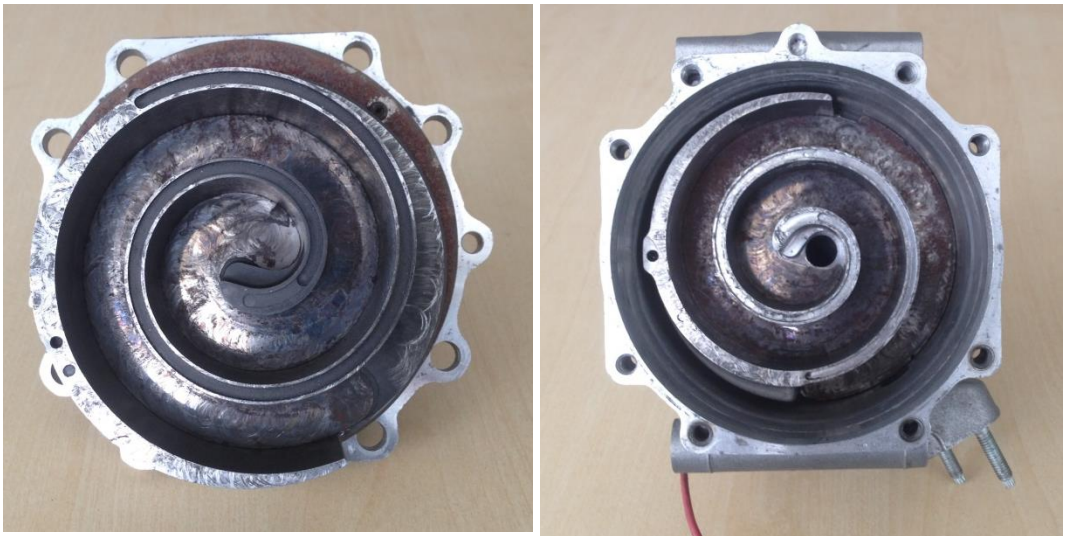

(a) (b)

Figure 5-9 Picture of the dissembled scroll expander
(a) orbiting scroll, (b) stationary scroll

The measured parameters of the experimental used scroll unit have been listed in Table 5-2. The start angle of the involute, pitch of the scroll blade and the radius of gyration of the orbiting scroll are calculated by the Equation 5-2 to Equation 5-4.

Table 5-2 Physical parameters of the Sanden TRSA 09

Name	Symbol	Value
Height of the scroll wrap	H_s	33.3mm
Thickness of the scroll	t_s	4.5 mm
Scroll turns	$\mathrm{N_s}$	2.5
Radius of the basic circle	r_s	3.2 mm
Pitch of the scroll blade	P_s	20.1 mm
Start angle of the involute	α	40.29 °
Radius of gyration	R_{gy}	5.553 mm
Diameter of the inlet port as expander	D_{in}	10.2 mm
Diameter of the outlet port as expander	D_{out}	12.7 mm
Diameter of the inlet port of the stationary scroll	D_{inner}	11.9 mm
Swept volume of the scroll machine	V_{SV}	85.7 cm^3[148]

The comparison of geometric scroll unit and real scroll has been drawn in Figure 5-10, which indicated the geometric drawn scroll blade has fitted the stationary scroll unit well. The geometric scroll blade can therefore be used to illustrate the expansion process of the scroll machine as shown in Figure 5-11 and some physical parameters can be calculated using this geometric model.

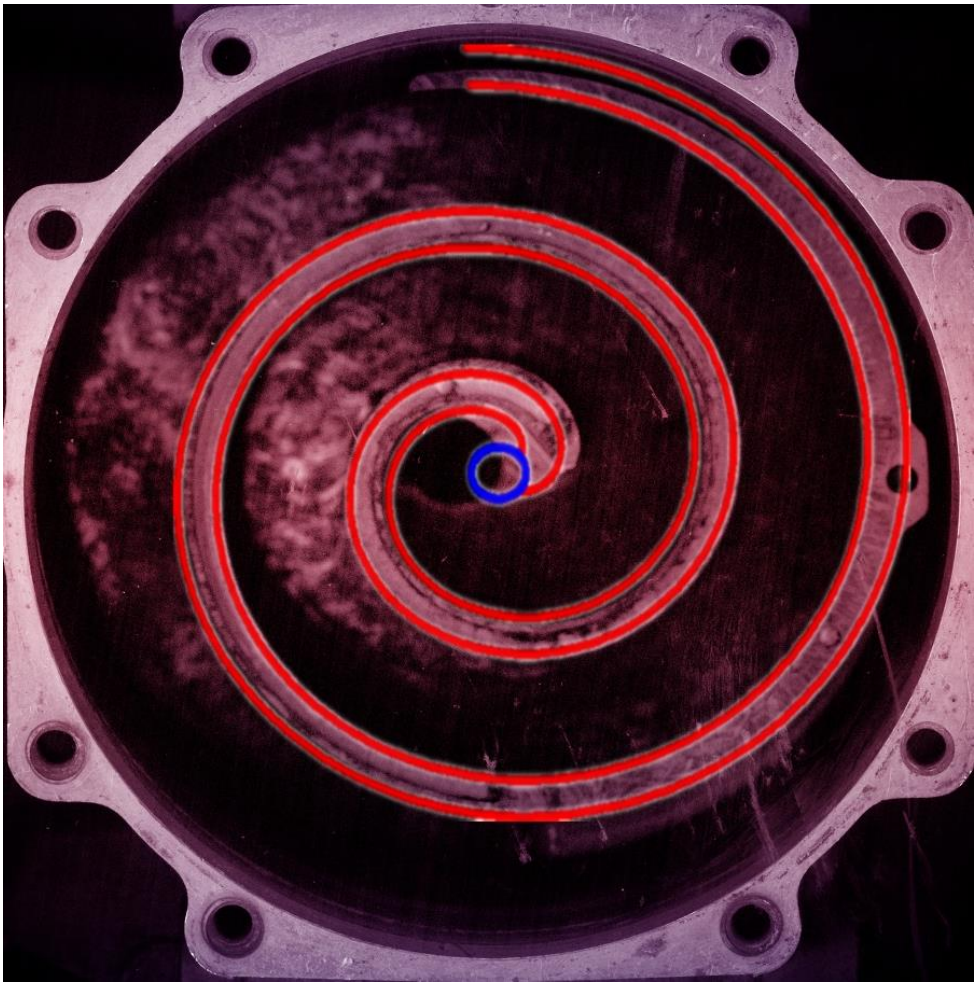

Figure 5-10 Comparison of the geometric scroll blade and real scroll unit

The geometric model can indicates the expansion process inside the experimentally used scroll unit under different crank angle as shown in Figure 5-11. The stationary scroll has been indicated as red lines and the orbiting scroll has been illustrated as cyan lines. Two central lines of the stationary scroll and orbiting scroll are represented as black dot lines. Basic circles of the stationary and orbiting scrolls are shown as the blue circle and pink circle, respectively. The expansion chambers of the scroll unit are numbed as A1, A2, B1, B2, C1 and C2 as illustrated in Figure 5-11.

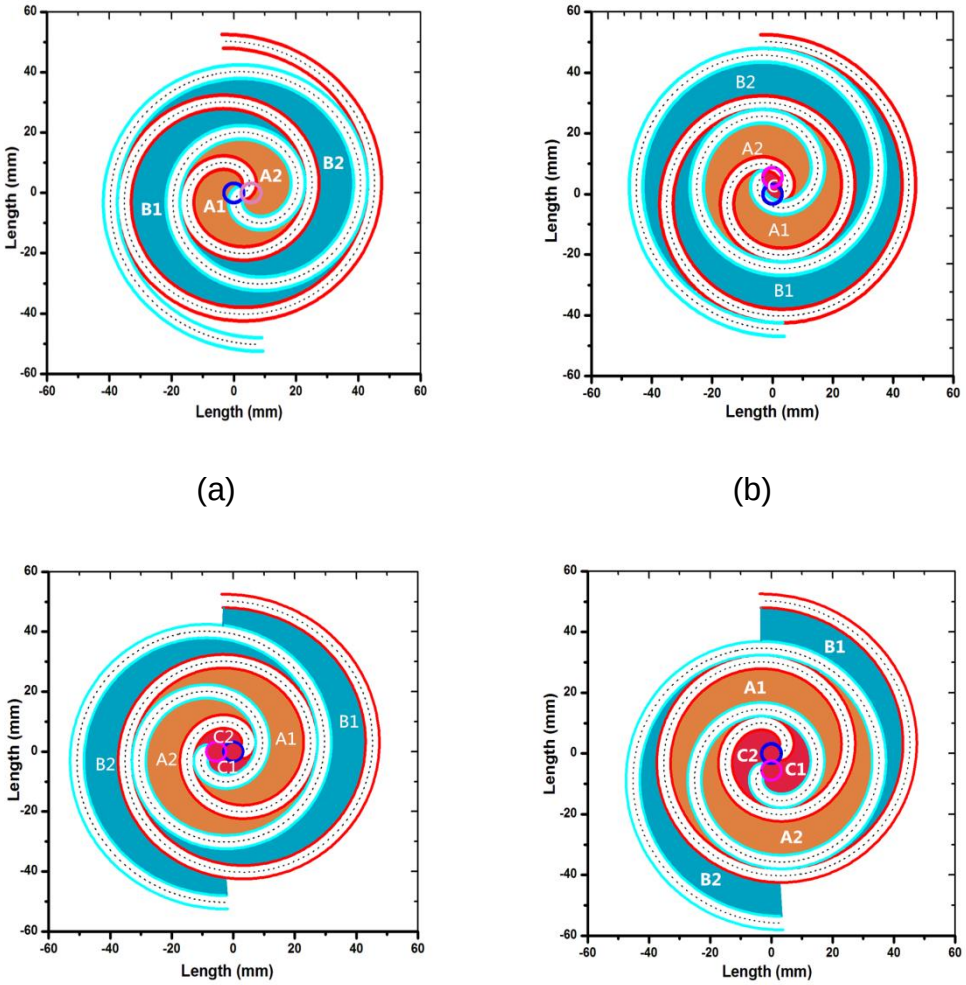

Figure 5-11 Schematic diagram of the expansion process of the scroll expander under different crank angle

(a) $\theta = 0$; (b) $\theta = \frac{1}{2}\pi$; (c) $\theta = \pi$; (d) $\theta = \frac{3}{2}\pi$

The suction process in the centre of the expansion machine is ended and another chamber will appear when the orbiting scroll moves as shown in Figure 5-11 (a). The locations of the expansion chambers of the scroll machine have been well illustrated by the Figure 5-11. The tested scroll machine has 2.5 scroll turns as shown in Figure 5-10. The exhaust process starts when the working fluid reaches the end of the scroll blade as indicated in Figure 5-11 (b). The geometric exhaust volume of the scroll

expander $V_{exhaust}$ can be calculated as the equation[149], where θ_{end} is the end angle of the expansion process. Based on the measured parameters of this expansion machine shown in Table 5-2, the $V_{exhaust}$ is 105.12 cm^3.

$$V_{exhaust} = \pi \times P_s \times (P_s - 2t_s) \times H_s \times (2N_s - 1 - \frac{\theta_{end}}{\pi}) \qquad \text{Equation 5-5}$$

The volume of the expansion chambers of the scroll expansion machine can be calculated by the following equation, where θ is the crank angle between the stationary scroll and orbiting scroll [149]. The number of the expansion chambers has been illustrated as i in this equation. The suction volume of this scroll machine can therefore be calculated and the $V_{suction}$ is 35.04 cm^3.

$$V_i = \pi \times P_s \times (P_s - 2t_s) \times H_s \times (2 \times i - 1 - \frac{\theta}{\pi}) \qquad \text{Equation 5-6}$$

The internal volumetric expansion ratio of this scroll machine can be calculated by Equation 5-7. Based on the results of $V_{exhaust}$ and $V_{suction}$, the internal volumetric expansion ratio of this scroll machine equals to 3.0.

$$\gamma_{v\_in} = \frac{V_{exhaust}}{V_{suction}} \qquad \text{Equation 5-7}$$

5.4 Experimental test of the scroll expander

The constructed scroll expander test bench as show in Figure 5-12 mainly includes an inlet flow meter, heating coils, a scroll expander, a generator, an outlet flow meter and the control box.

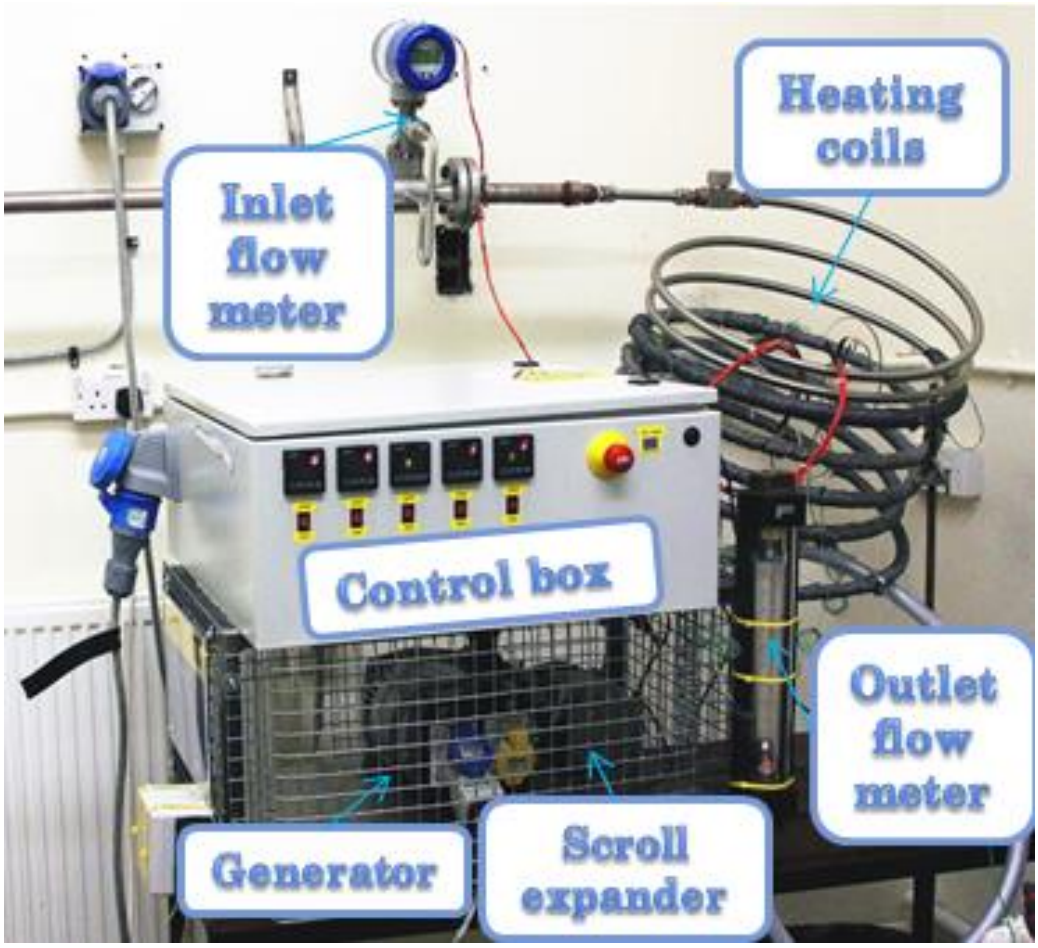

Figure 5-12 Photo of the scroll expander test rig

5.4.1. Test plan

As mentioned previously, the scroll expander is selected to be integrated into the resorption cogeneration for the power generation part. The working conditions of the expansion machine are highly determined by the adsorbent. The experimental results reported by Li et al. [150] pointed out that the highest system pressure achieved by the resorption working pair $MnCl_2$-$BaCl_2$ is around 7 bar and the high pressure can only last for 1 to 2 minutes.

The thermodynamic analysis and comparison of different resorption working pairs as introduced in Chapter 3 pointed out that $BaCl_2$ has higher equilibrium pressure than the $SrCl_2$ under the same temperature. The system pressure of a resorption system using $MnCl_2$-$SrCl_2$ should be lower than 7 bar as reported by the experimental data obtained from MnCl2-BaCl2 system [150]. Therefore, the experimental investigation of the power generation part of the resorption cogeneration using $MnCl_2$-$SrCl_2$ as the working pair should mainly focus on low pressure ranges. The equilibrium pressures of the $MnCl_2$ under the heat source temperature from 70 ^{o}C to 125 ^{o}C and the estimated working conditions for the power generation part of the resorption cogeneration are listed in Table 5-3.

The designed testing points of the scroll expander are from 50 kPa to 500 kPa under the controlled temperature from 70 ^{o}C to 125 ^{o}C. The real operational working conditions of the cogeneration using $MnCl_2$-$SrCl_2$ as working pair can be covered under the designed testing points.

Table 5-3 Working conditions of the resorption cogeneration under the heat source temperature from 70 to 125 ^{o}C

No	Heat source temperature	Equilibrium pressure of $MnCl_2$ (kPa)	Equilibrium pressure of $SrCl_2$ at 20 ^{o}C (kPa)	Pressure difference Δp (kPa)
1	70	49.8	36.7	13.1
2	75	63.3	36.7	26.6
3	80	79.8	36.7	43.1
4	85	100	36.7	63.3
5	90	124.6	36.7	87.9
6	95	154.2	36.7	117.5
7	100	189.8	36.7	153.1
8	105	232.4	36.7	195.7
9	110	282.9	36.7	246.2
10	115	342.8	36.7	306.1
11	120	413.3	36.7	376.6
12	125	495.9	36.7	459.2

5.4.2. Description of the test procedure

The experimental procedures of the test bench are described as follows

1) Leakage test: Block the outlet of the expander and open the compressed air control valve. If the pressure of the system drops within 5 minutes, check all the connectors and parts to detect the leakage.
2) Remove the block plug, read the ambient temperature first and then set the required temperature on five temperature control panels
3) switch on the electrical heater and set the temperature to the desirable degree
4) Until the temperature reaches to the required level, open the control valve and let compressed air flowing through the system until the inlet temperature and outlet temperature of the scroll expander are stable. The duration of this process requires about 30 minutes. During the test, six bulbs with two of 25W, two of 50W and two of 200W were used as load bank.
5) The temperature control panels need to be switched off first and then close the control valve
6) Switch off the air supply line and then collect all the test data from the computer.
7) Switch off the power supply to the control box

5.5 Results and discussion of the experimental tests

5.5.1. Identification of real volumetric expansion ratio

In order to achieve the real volumetric expansion ratio of the expander, two volumetric flow meters are designed in the inlet and outlet of the expansion

machine as indicated in Figure 5-12. The tests to measure the volumetric expansion ratio of the expander are all conducted without switching on the heating unit, because the volume flow rate is highly related with the temperature conditions. Without using the heating unit can reduce the complexity of the tests and reduce the numbers of uncertainty parameters. The relationships between inlet pressure and volume flow rate at the inlet and outlet of the expander have been drawn in Figure 5-13. It indicates that the inlet and outlet volume flow rate increases with the increase of inlet pressure. Two linear lines have been added in Figure 5-13, which indicate the linear relationships between inlet pressure and volume flow rate of the expander. The red points and black points in Figure 5-13 are the tested results of the outlet and inlet volume flow rate of the expander. The equations of the fitted lines have also been listed in Figure 5-13

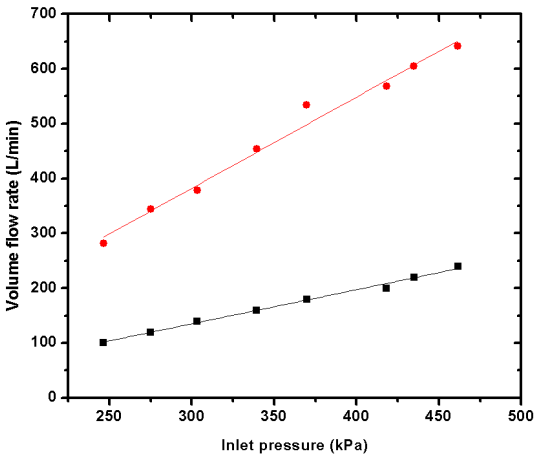

Equation	y = a + b*x		
Adj. R-Square	0.99245	0.98281	
		Value	Standard Error
Inlet volume flow rate	Intercept	-51.57341	7.45408
Inlet volume flow rate	Slope	0.62237	0.02051
Outlet volume flow rate	Intercept	-116.71936	30.18655
Outlet volume flow rate	Slope	1.66338	0.08304

Figure 5-13 Relationship between inlet pressure and volume flow rate at the inlet and outlet of the expander

The real volumetric expansion ratio of expander should be lower than theoretical volumetric expansion ratio calculated by the geometric model as indicated in Figure 5-11 because of the internal leakage of expander. The experimental results are plotted in Figure 5-14 and the real volumetric expansion ratio γ_{v_real} of the expander is calculated by Equation 5-8. The volumetric expansion ratio achieved under the tested conditions fluctuates

from 2.67 to 2.96, which is slightly lower than the theoretical volumetric expansion ratio 3.0 as calculated in Equation 5-7.

$$\gamma_{v\_real} = \frac{V_{inlet\_volume\_flow\_rate}}{V_{outlet\_volume\_flow\_rate}} \qquad \text{Equation 5-8}$$

A linear line has been fitted in Figure 5-14 to reveal the relationship between inlet pressure and real volumetric expansion ratio of the expander. The standard error between the experimental results and the volumetric expansion ratio calculated by the equation of the fitted line is 0.17452 as indicated. The average value of the real volumetric expansion ratio based on the calculation of the fitted line is 2.929, which is slightly lower than theoretical result obtained from the geometric model.

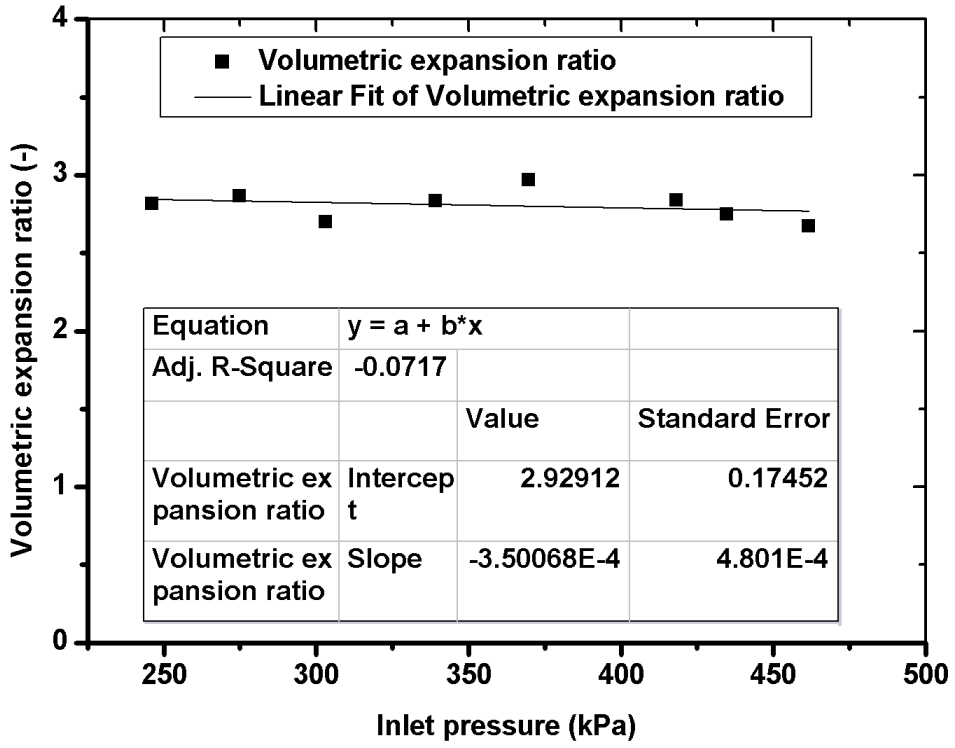

Figure 5-14 Relationship between inlet pressure and volumetric expansion ratio

5.5.2. Electrical generation and friction losses

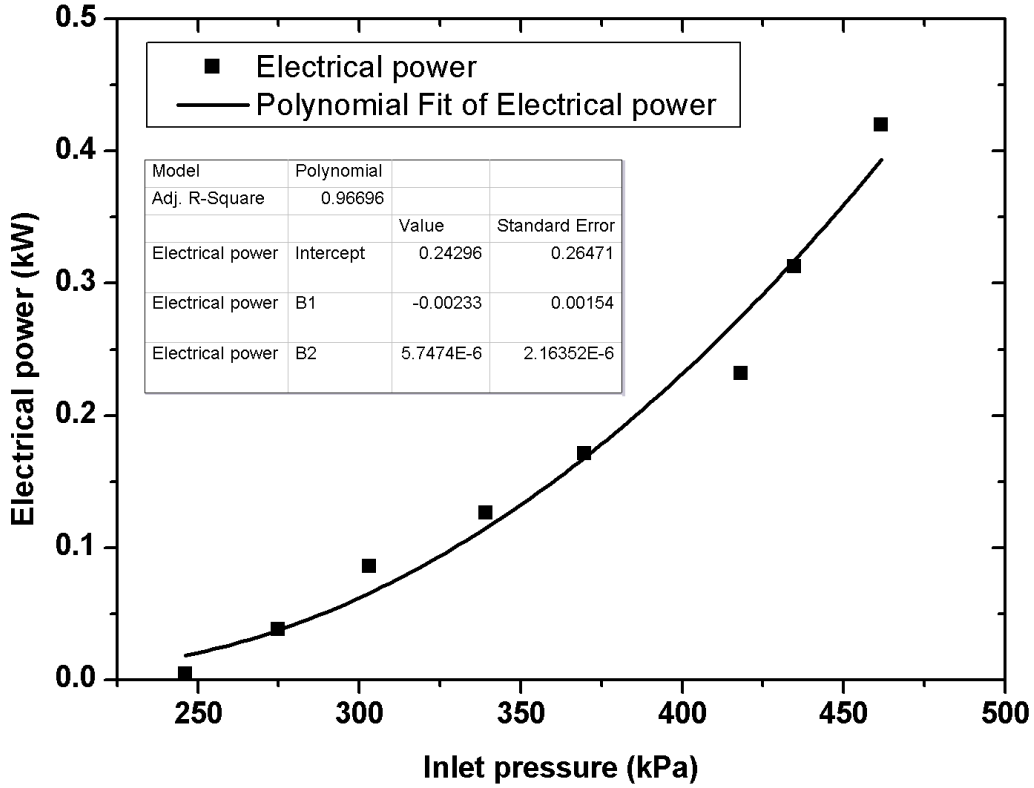

Figure 5-15 Relationship between inlet pressure and average generated electricity

In order to produce electricity, the expansion machine has to overcome the internal friction, mechanical losses between the shafts, and electrical losses in the generator. Figure 5-15 illustrates the relationship between the inlet pressure and the average generated electricity. The scroll expander starts to produce electricity when the inlet pressure is higher than 245 kPa and the highest electricity obtained from this expander is about 420W with the supplied pressure at 360 kPa. The fitted line as shown in Figure 5-15 indicates that the electrical generation is not linearly related to the inlet pressure, which means the friction losses should also not be linearly related to the supply pressure.

Friction loss defined in this study is a combination of the losses of internal friction of the expander, mechanical loss between the shafts and electrical losses of the generator, which will be introduced in the Chapter 6. The friction torque can therefore be calculated by

$$\dot{W}_{loss} = \dot{W}_{in} - \dot{W}_{net} \qquad \text{Equation 5-9}$$

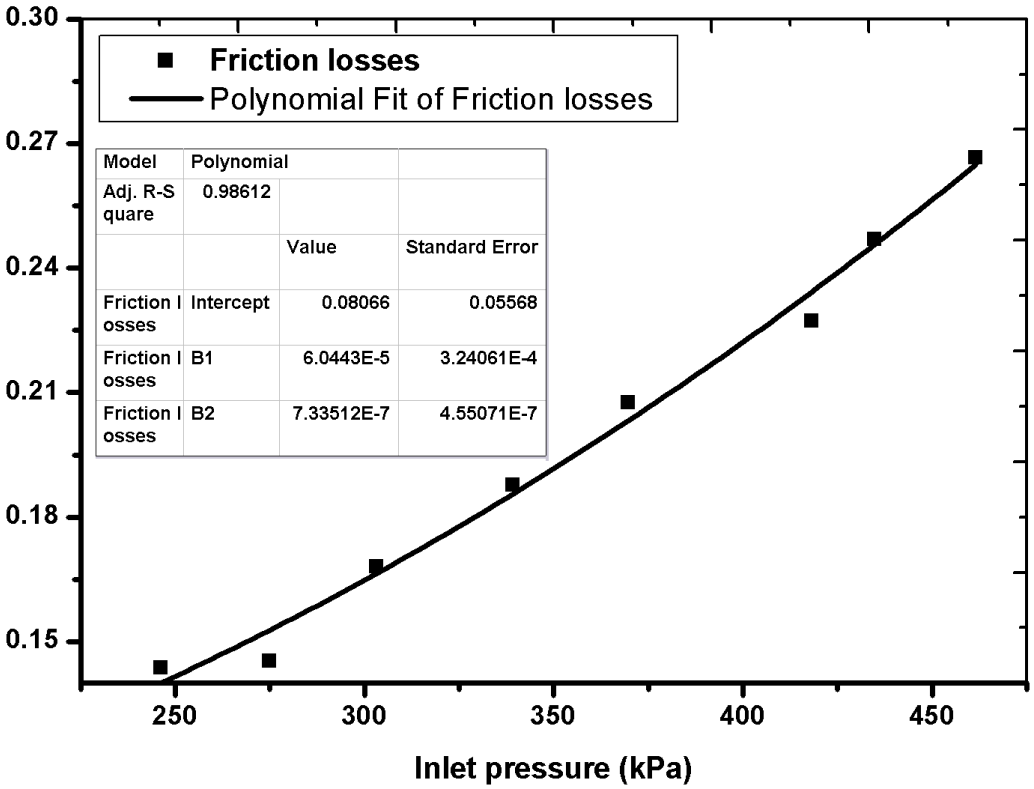

Figure 5-16 Relationship between inlet pressure of the expander and friction torque

The input energy into the expander is defined as $\dot{W}_{in}$, which equals to the net electrical power output $\dot{W}_{net}$ plus the friction losses $\dot{W}_{loss}$ as shown in Equation 5-9. The calculation method for input energy will be introduced in Chapter 6. The relationship between friction losses and inlet pressure has

been indicated in Figure 5-16. Results indicated the friction loss to start the generator is about 0.145 kW. The friction loss of the expander increases with the increase of inlet pressure. A polynomial fitted line has been added and the equation of the polynomial line is illustrated in Figure 5-16.

5.5.3. Performance under different inlet temperature and pressure

Electricity performance

Figure 5-17 shows the relationship between the inlet temperature and the average electricity achieved driven by two different supplied pressures. The red points illustrate the variation of the electricity produced from the scroll expander under the supply pressure at 339.0 kPa and the black points are the achieved data under the inlet pressure at 418 kPa. Both of the testing results under different supplied pressures have been fitted by two polynomial lines as indicated in the figure.

Results indicate that with the supply pressure at 339.0 kPa, the electricity increases from 180 W to 250 W with the increase of temperature from 65 ^{o}C to 105 ^{o}C. The electricity production is stable at 250 W when the temperature increases from 105 ^{o}C to 125 ^{o}C. When the inlet pressure is 418 kP, the electricity generation shows similar tendency as that of the inlet pressure at 339.0 kPa. The stable point appears at 90 ^{o}C.

Results indicate that the temperature factor has limited influence on the electricity production of the scroll expander. Adding insulation materials for scroll expander may prevent the heat losses when the inlet temperature is higher than 90 ^{o}C.

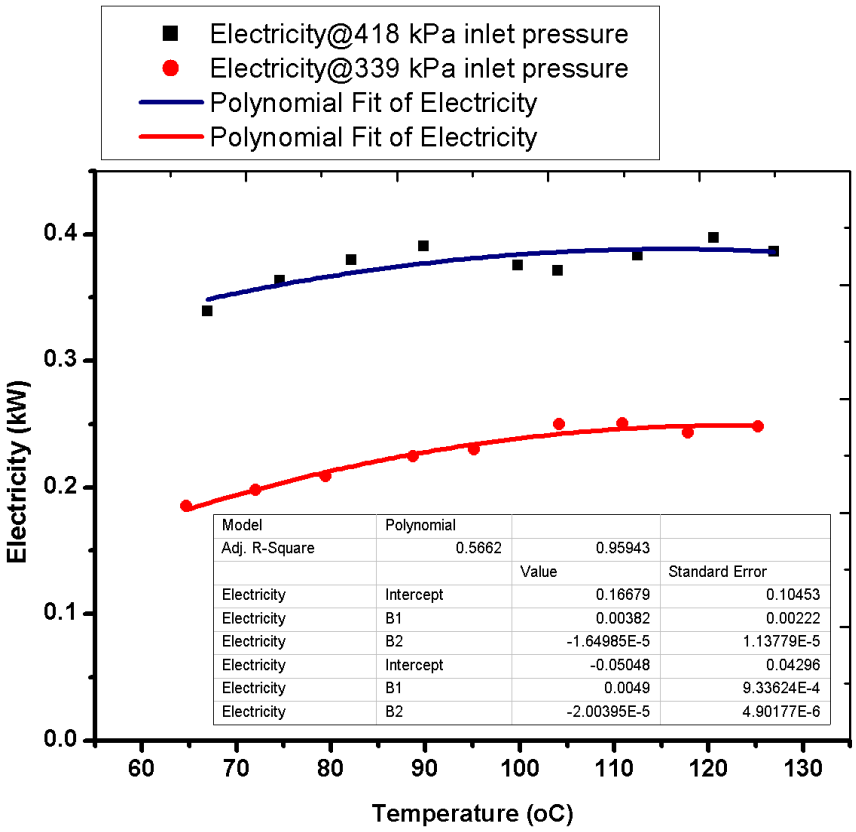

Figure 5-17 Relationship between the inlet temperature and achieved electricity

Isentropic efficiency

The isentropic efficiency presents the relationship between the reversible work and irreversible work during the expansion process. The isentropic efficiency of the scroll expander is calculated by Equation 5-10. The specific enthalpy of the inlet and outlet of the scroll expander is presented by h_{inlet} and h_{outlet}, respectively. h_{outlet_s} is the specific enthalpy at the outlet of the expander during isentropic expansion process.

$$\eta_{isen} = (h_{inlet} - h_{outlet}) / (h_{inlet} - h_{outlet\_s}) \qquad \text{Equation 5-10}$$

The inlet specific enthalpy is identified from two parameters T_{inlet} and P_{inlet}. Due to the fact that this test rig is an open driven system, the pressure at the outlet port of the scroll expander can hardly been measured by the sensor. Therefore the specific enthalpy at the outlet of the expander is identified by the density at the outlet of the expander ρ_{outlet} and the temperature at the outlet port T_{outlet}. The outlet density is calculated by the Equation 5-11. The volume flow rate at the inlet and outlet of the expander is presented as $\dot{V}_{inlet}$ and $\dot{V}_{outlet}$, respectively. The volumetric expansion ratio r_{v_in} used in this calculation was 2.93, which was obtained by the experimental test mentioned in the early part of this chapter.

$$\rho_{outlet} = \rho_{inlet} \times \frac{\dot{V}_{inlet}}{\dot{V}_{outlet}} = \rho_{inlet} \times r_{v\_in} \qquad \text{Equation 5-11}$$

The isentropic efficiency achieved by this scroll expander fluctuates from 0.56 to 0.64 under two different inlet pressures, which is shown in Figure 5-18. The isentropic efficiency of the inlet pressure 418.0 kPa is slightly higher than that of the inlet pressure 339.0 kPa. The overall isentropic efficiency of the scroll expander under the tested conditions is around 0.6, which is very close as reported in the literature[139].

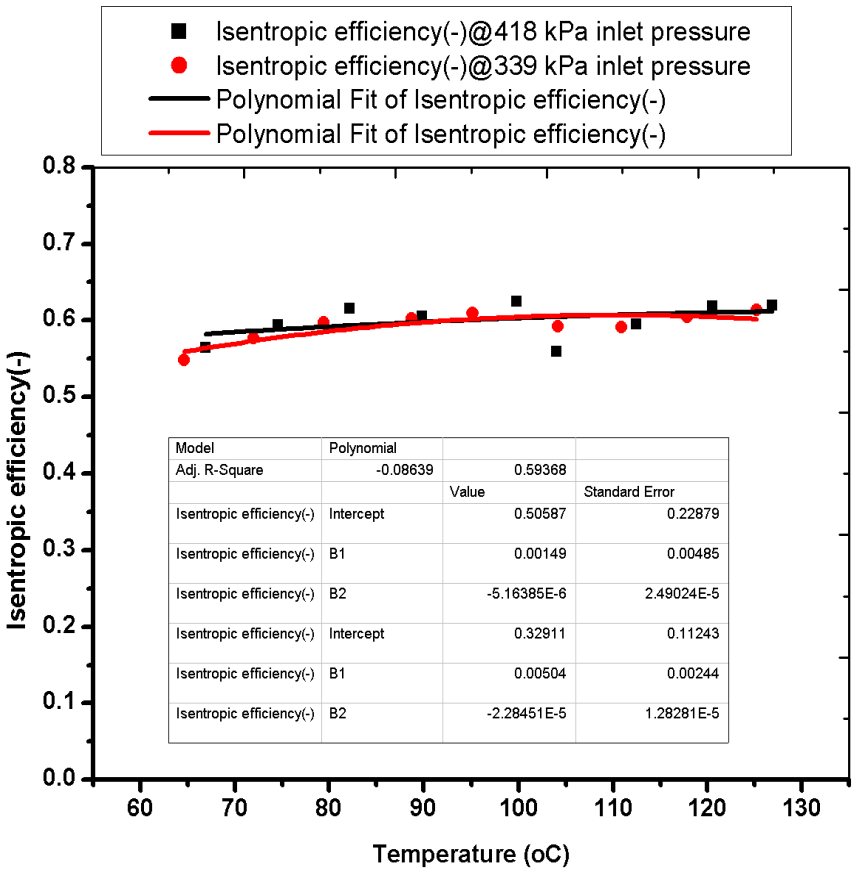

Figure 5-18 Relationship between isentropic efficiency of the scroll expander and the inlet temperature

Electrical efficiency

In order to evaluate the conversation ratio of mechanical work into electricity by the scroll expander. The internal energy efficiency was introduced here for the calculation of electrical efficiency of the scroll expander.

The mass flow rate multiple the enthalpy difference between the inlet and outlet of the expander is the overall energy received by the expansion machine, which can be calculated as Equation 5-12.

$$\dot{W}_{rec} = \dot{m} \times (h_{inlet} - h_{outlet})$$ Equation 5-12

The volume flow rate multiply by the density equals to the mass flow rate, which is presented as Equation 5-13.

$$\dot{m} = \dot{V}_{inlet} \times \rho_{inlet} = \dot{V}_{outlet} \times \rho_{outlet}$$ Equation 5-13

The electrical efficiency of the scroll expander is determined by

$$\eta_{\text{int}} = \dot{W}_{el} / \dot{W}_{rec}$$ Equation 5-14

The experimental results showed the electrical efficiency under the inlet pressure at 339.0 kPa was around 0.22. When the inlet pressure was 418.0 kPa, the electrical efficiency is stable under the inlet temperature ranging from 65 ^{o}C to 90 ^{o}C and started to drop from 90 ^{o}C to 125 ^{o}C. Results indicated the ratio of the heat loss under the supply pressure at 418.0 kPa was higher than that at 339.0 kPa, when the inlet temperature was higher than 90 ^{o}C. This phenomenon proved the heat loss of the expander is one of the main losses affecting the power generation of the expander.

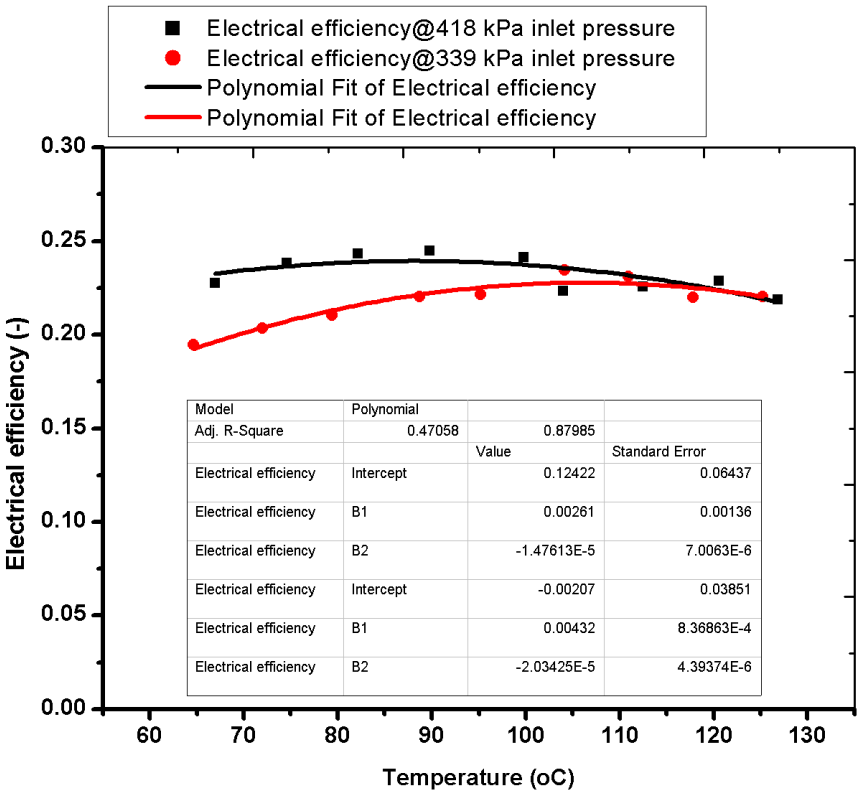

Figure 5-19 Relationship between electrical efficiency and inlet temperature

For scroll type of expansion machine, there are two main losses - internal leakage inside the expander and heat losses during expansion process. This tested scroll expander was modified from an original scroll compressor with factory lubricate oil, which has the function of lubricating the contact faces of the two scrolls and the bearings inside the expander to reduce the mechanical friction. Moreover, the lubricate oil could seal the working fluid between two scrolls and reduce the radial leakage. On the other hand, the scroll expander was installed without insulation, which could cause large amount of heat losses from the scroll expander to the environment.

5.6 Summary

A scroll expander rig was designed, constructed and used to obtain the operational working conditions of the tested unit under similar working conditions of the cogeneration. The constructed rig was used to test the performance of the scroll expander and measure the required parameters such as isentropic efficiency, real volumetric expansion ratio and electrical efficiency under different working conditions.

The geometric study and investigation of the tested scroll unit as introduced in 5.3 has been used to explore the expansion process inside the scroll expander. The physical parameters obtained from the geometric model were used to compare with the tested results obtained by experiments. Results indicated the geometric model can effectively be reveal the real expansion process inside the tested machine. The geometric model built in this chapter will also be used in Chapter 6 for the simulation model of scroll expander.

The tested scroll machine was modified from a scroll compressor used in conventional vehicle air-condition system. Several modifications have been conducted to run the scroll type of machine in expander mode and the detailed modification processes were introduced in the Chapter. The modified scroll machine was integrated with the designed test bench and the scroll expander have been tested under similar working conditions of the resorption cogeneration using $MnCl_2$-$SrCl_2$ as resorption working pair as introduced and analysed in Chapter 3. Based on the achieved results, following conclusions can therefore be drawn,

- The scroll expander test bench was first tested without switching on the heating unit in order to investigate the performance of the tested unit under various supplied pressures. The real internal volumetric expansion ratio of the scroll expander was experimentally achieved and compared with the data achieved from the geometric model. The average volumetric expansion ratio of the tested unit is 2.929, which is very close with the data obtained from geometric model 3.0. The results indicated that the geometric model can effectively be used to reveal the real expansion process inside this scroll machine and there is around 2.366% difference between the data obtained from the experimental results and from the geometric model.

- In order to run the scroll expander to generate electricity, the internal friction of the expander, mechanical frictions between the expander and generator, friction of the generator and internal leakage of the expander have to be overcome. There is a minimum start state for this tested unit based on the experimental investigation, which is about 245 kPa.

- To simulate the real working conditions of the power generation part of the resorption cogeneration, a heating unit was designed and installed to supply heated compressed air into the expander. The selected scroll expander was tested under two inlet pressures with various inlet temperatures. The achieved electricity from the generator is abound 220 W and 360 W under the inlet port pressure at 339.0 and 418.0 kPa, respectively. The results also indicated the inlet temperature has limited effects for the final electricity production from the expander.

- The isentropic efficiency of the expander has been evaluated to identify the relationship between the reversible work and irreversible work of the expander. The results indicated the isentropic efficiency of the expander fluctuates from 0.56 to 0.64 under the tested conditions.

- The electrical efficiency shows the conversion rate from the work of the expander to the generator. When the inlet temperature is higher than 90 ^{o}C, the electrical efficiency drops from 0.4 to 0.35 under the inlet pressure at 418.0 kPa. On the other hand, the electrical efficiency at 339.0 kPa shows a stable tendency with the increase of inlet temperature, which is around 0.35.

In summary, the geometric model built in this chapter can effectively identify the expansion process inside the tested machine. The experimental investigation of the scroll expander identified the real volumetric expansion ratio, internal electrical efficiency and isentropic efficiency of the expander under various working conditions. Heat losses start to be noticeable when the inlet temperature of the expander is higher than 90 ^{o}C. The average isentropic efficiency and electrical efficiency obtained from the experimental is around 60% and 38%, respectively. The parameters achieved from the geometric model and the experimental results obtained from the rig will be used for the simulation model, which will be introduced in Chapter 6.

Chapter 6. Assessment of the resorption cogeneration based on the experimental results

6.1. Introduction

The system performance the resorption cogeneration under various working conditions is critical to explore the potential applications of the system to meet different requirements. This chapter first describes the simulation model of a tube type adsorption unit and a scroll expander. These two component simulation models have been conducted based on the real physical parameters as described in Chapter 4 and Chapter 5. Engineering Equation Solver (EES), which has been widely used by many researchers and industry [151], was selected as the software to code the adsorption model and expander model. The simulations of these two models are used to predict and explore the performance of the four-bed resorption cogeneration system for continuous power and refrigeration generation. The size and weight of a small scale resorption cogeneration have also been discussed and reported.

6.2. Mathematical model of an adsorption unit

6.2.1. Adsorption kinetic

The chemisorption simulation models are commonly conducted by integrating adsorption kinetic model with heat/mass transfer model to predict the adsorption/desorption performance. The chemisorption kinetic models can be classified as three types: global, local and analytical models[7]. Global kinetic model requires several parameters of the

adsorbent unit such as permeability, conductivity, specific heat capacity, detailed dimensions of the reactor and several variables. The variable of the model can be solved using numerical analysis[7], such as a global reaction model proposed by Mazet et al.[12]. The local kinetic model mainly consider the heat and mass transfer performance of the material, which will can be solved by several partial differential equations[7]. The analytical only consider the average value of the variable parameters and can be used to dynamic relationships between the variable parameters, which is an efficient and effective method to predict the adsorption performance[7]. The chemisorption kinetic model used in this study applies one of the analytical model, which has been widely used by previous researcher sand have been proven as an effective model to predict the overall performance [152-154].

$$\frac{dx}{dt} = Ar \cdot (1-x)^{Mr} \cdot \frac{P_c - P_{eq,syn}}{P_c} \qquad \text{Equation 6-1}$$

$$\frac{dx}{dt} = Ar \cdot x^{Mr} \cdot \frac{P_c - P_{eq,syn}}{P_c} \qquad \text{Equation 6-2}$$

The chemical kinetic adsorption model used in this study is expressed as Equation 6-1, where Ar is the Arrhenius factor showing the correlation between the chemical reaction speed and working temperature and Mr reflects the influence of chemical reaction vacant sites [152-155]. Likewise the principle of kinetic adsorption model, the kinetic model for desorption process can be written as Equation 6-2.

The equilibrium pressure of the chemical adsorbent corresponding with the working temperature is calculated by the Clausius - Clapeyron equation as described in Equation 6-3.

$$P_{eq} = \exp(\frac{-\Delta H_r}{RT_c} + \frac{\Delta S}{R})$$ Equation 6-3

The complex reaction between metal chlorides and ammonia can be displayed as following equation, where M expresses the metallic element.

$$M_aCl_b(NH_3)_c + (d-c)NH_3 \underset{desorption}{\overset{adsorption}{\rightleftharpoons}} M_aCl_b(NH_3)_d$$ Equation 6-4

6.2.2. Physical model of one adsorption unit

In order to build the analytical equations for the heat transfer analysis, the physical model has to be built to obtain the required parameters. The physical dimensions of one tube type of adsorption unit used in this simulation are obtained from the real parameters of the tube type adsorbent bed, which has been designed, constructed and used as reported in Chapter 4. The schematic diagram of this one tube unit adsorption model has been illustrated in Figure 6-1. The tube unit includes central gas channel for ammonia getting in and out of the adsorbent, composite adsorbent shown in orange colour, stainless steel tube to isolate thermal fluid and adsorbent, thermal fluid and insulation materials. The detailed dimensions of the tube unit are listed in

Table **6-1**

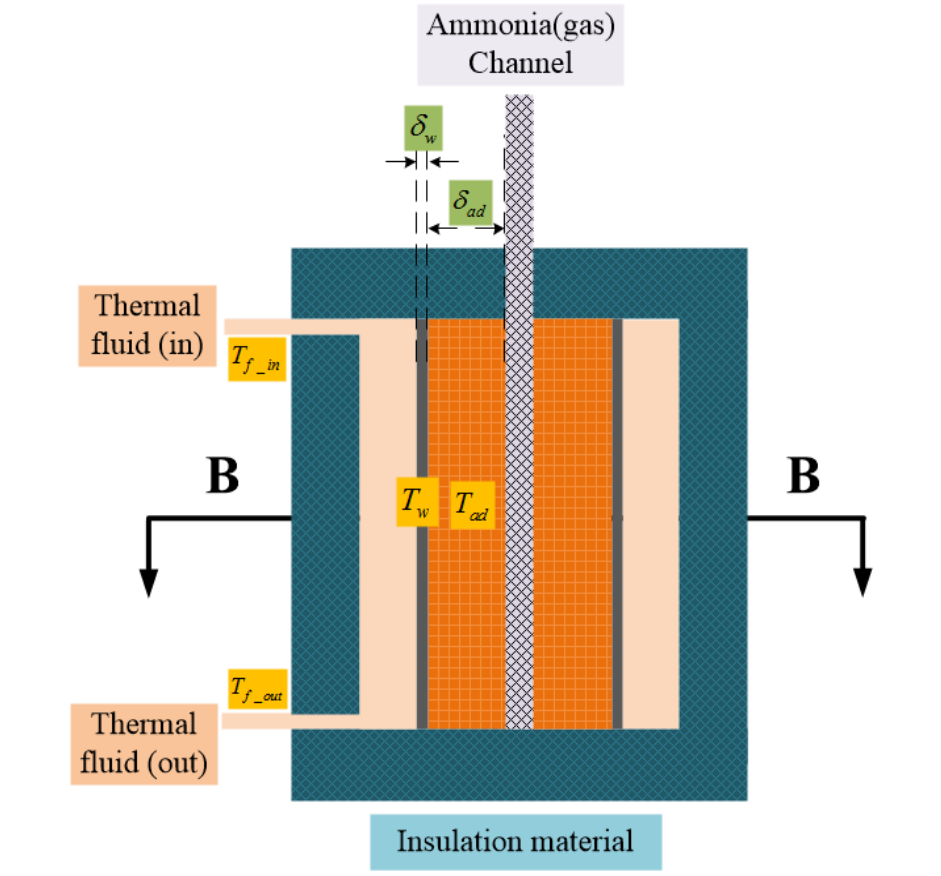

(a)

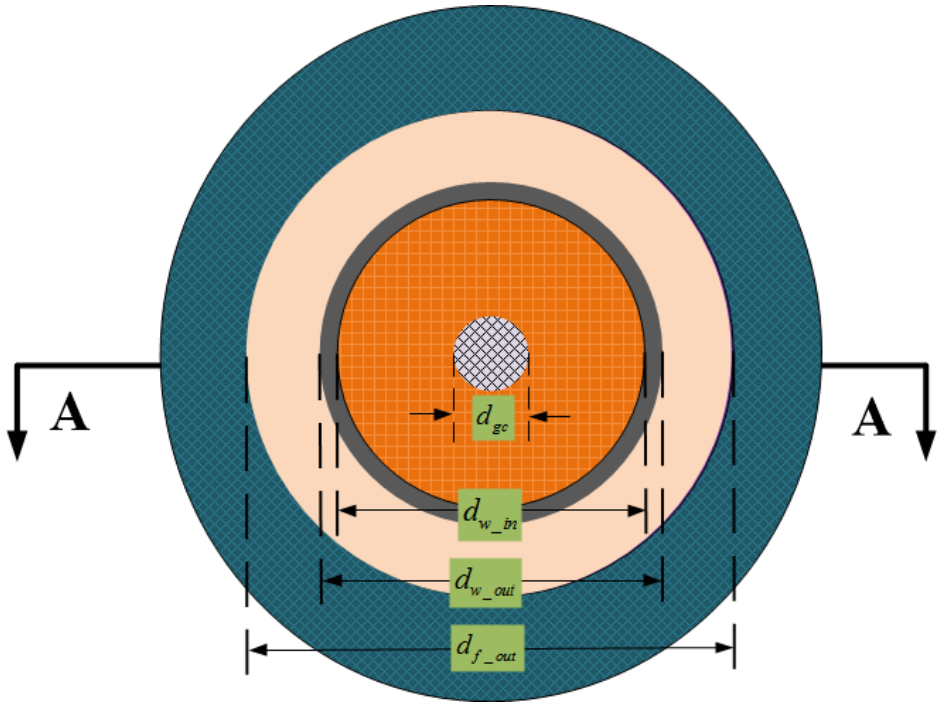

(b)

Figure 6-1 Schematic diagram of the physical model
and temperature of one adsorption unit (a) Section A-A (b) Section B-B

Table 6-1 Physical dimensions of the one tube adsorption unit

Symbol	Description	Value
δ_{ad}	thickness of adsorbent	18.74mm
δ_{w}	thickness of wall	3.91mm
d_{gc}	diameter of gas channel	15.00mm
d_{w_in}	inner diameter of wall	52.48mm
d_{w_out}	outer diameter of wall	60.30mm
d_{f_out}	outer diameter of thermal fluid	77.92mm
λ_{w}	thermal conductivity of wall material - 304 Stainless Steel	16.2W/(m.K)
λ_{ad} [156]	thermal conductivity of the selected composite salts	1.5 W/(m.K) EG-$MnCl_2$ 1.4 W/(m.K) EG-$SrCl_2$
L	Length of tube unit	300mm

6.2.3. Heat transfer equations

The heat transfer processes between the thermal fluid and adsorbent of the cylindrical tube during desorption process can be divided into two parts: thermal fluid to wall and wall to adsorbent. In order to simplify the calculation of the heat transfer process of the tube unit, one-dimensional analysis is used. The one-dimensional heat flow though the cylindrical tube adsorption unit can be further divided into four parts: convection between thermal fluid and outer side of the wall, conduction between outer and centre of the wall, conduction between centre and inner side of the wall, conduction between centre of the wall and centre of the adsorbent. The

thermal resistances from thermal fluid to the adsorbent are illustrated and the equations of the thermal resistances are described in Figure 6-2.

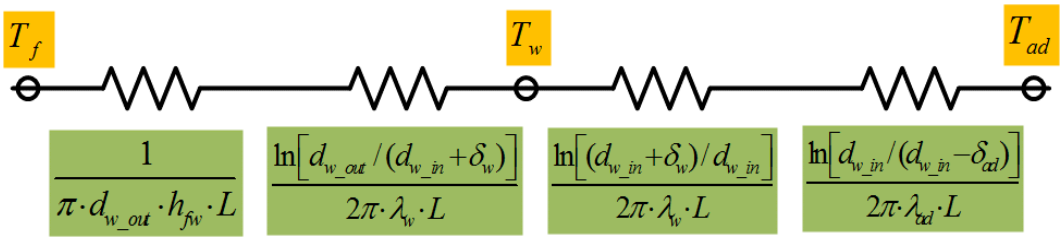

Figure 6-2 One-dimensional heat flow through cylindrical one adsorption unit

R_{f_w} is the thermal resistance between thermal fluid and wall as illustrated in Equation 6-5. And the thermal resistance between wall and adsorbent is described in Equation 6-6 as R_{w_ad}. These parameters are used in the energy equations of the simulation model.

$$R_{f\_w} = \frac{1}{\pi d_{w\_out} h_{f\_w} L} + \frac{\ln\left[d_{w\_out}/(d_{w\_in}+\delta_w)\right]}{2\pi\lambda_w L} \qquad \text{Equation 6-5}$$

$$R_{w\_ad} = \frac{\ln\left[(d_{w\_in}+\delta_w)/d_{w\_in}\right]}{2\pi\lambda_w L} + \frac{\ln\left[d_{w\_in}/(d_{w\_in}-\delta_{ad})\right]}{2\pi\lambda_{ad} L} \qquad \text{Equation 6-6}$$

The log mean temperature difference between the heat transfer fluid and the wall during the convection heat transfer process can be written as

$$LMTD_{f\_w} = \frac{T_{f\_in} - T_{f\_out}}{\ln \frac{T_{f\_in} - T_w}{T_{f\_out} - T_w}} \qquad \text{Equation 6-7}$$

6.2.4. Energy balance equations

The lumped parameter model is selected and used in this study to reveal the unsteady-state heat transfer process of one tube adsorption unit. This calculation method assumes the temperatures of the materials are all uniform, which can effectively predict the global changes of the heat transfer processes.

The heat transfer between the thermal fluid and wall can be described by Equation 6-8. The left of the equation is the internal energy change of the thermal fluid. And right of the equation includes the overall energy provided/removed by thermal fluid through convection and the energy changes through conduction between fluid and wall. The specific heat capacity, volume, density, and mass flow rate of the thermal fluid is shown as C_{p_f}, V_f, ρ_f and $\dot{m}_f$, respectively.

$$\rho_f C_{p\_f} V_f \frac{\partial T_f}{\partial t} = \dot{m}_f C_{p\_f} (T_{f\_in,j} - T_{f\_out,j}) - \frac{LMTD_{f\_w,j}}{R_{f\_w}} \qquad \text{Equation 6-8}$$

Equation 6-9 describes the heat transfer between the wall and adsorbent, which only includes two convection processes. The left side of the equation is the internal energy change of the wall and the right side describes two convection heat transfer processes: fluid-wall and wall-adsorbent as written below

$$\rho_w C_{p\_w} V_w \frac{\partial T_w}{\partial t} = \frac{LMTD_{f\_w,j}}{R_{f\_w}} - \frac{T_{w,j} - T_{ad,j}}{R_{w\_ad}} \qquad \text{Equation 6-9}$$

The energy balance equation of the adsorbent can be written as Equation 6-10. The first element of this equation is the internal energy change of the adsorbent and the second element is the energy of the adsorbed/desorbed ammonia through the adsorbent. n_{ad} is number of moles of chemical adsorbent and $(d-c)$ can be found in the chemical reaction equation in Equation 6-4.

$$(\sum_{i=1}^{N}\rho_i C_{p\_i})V_{ad}\frac{\partial T_{ad}}{\partial t}-(d-c)n_{ad}M_{r\,NH_3}\Delta H_{ad}\frac{dx}{dt}=\frac{T_{w,j}-T_{ad,j}}{R_{w\_ad}} \qquad \text{Equation 6-10}$$

The specific volumetric heat capacity is expressed as ρC_p. The sum of specific volumetric heat capacity of the composite same can therefore be written as $\sum_{i=1}^{N}\rho_i C_{p\_i}$, which includes the specific volumetric heat capacity of graphite, adsorbent and ammonia as shown in Equation 6-11.

$$\sum_{i=1}^{N}\rho_i C_{p\_i}=\underbrace{\rho_{\mathrm{EG}}C_{p\_EG}}_{Graphite}+\underbrace{\rho_{ad}C_{p\_ad}}_{Adsorbent}+\underbrace{x(d-c)n_{ad}Mr_{NH_3}C_{p\_NH_3}/V_{ad}}_{Ammonia} \qquad \text{Equation 6-11}$$

In order to simplify the calculation and improve the applicability of the simulation model, the thermal mass of the fluid and wall is lumped together[14], which means the slope of the changes of T_f and T_w is the same. Therefore the Equation 6-8 and Equation 6-9 can be written as the following equation

$$(\rho_f C_{p\_f} V_f + \rho_w C_{p\_w} V_w)\frac{\partial T_w}{\partial t} = \dot{m}_f C_{p\_f}(T_{f\_in,j} - T_{f\_out,j}) - \frac{T_{w,j} - T_{ad,j}}{R_{w\_ad}}$$ Equation 6-12

Table 6-2 Parameters of the adsorption tube unit model [151]

Symbol	Parameter	Value
m_{ad}	Mass of adsorbent in one tube unit	210 g
m_{EG}	Mass of expendable graphite in one tube unit	105 g
C_{P_f}	Specific heat capacity of heat transfer fluid	1.6 kJ/(kg.K)
C_{P_w}	Specific heat capacity of metallic wall (304 ss)	0.5 kJ/(kg.K)
$C_{p\_NH_3}$	Specific heat capacity of ammonia	2.06 kJ/(kg.K)
C_{p_EG}	Specific heat capacity of graphite	0.71 kJ/(kg.K)
ρ_f	Average density of the thermal fluid	0.88 g/cm^3
ρ_w	Density of the metallic wall (304 ss)	7.99 g/cm^3
V_{ad}	Volume of the composite adsorbent	595.9 cm^3
$\dot{V}_f$	Volume flow rate of the thermal fluid	26 L/min
V_f	Volume of the thermal fluid	573.8 cm^3
V_w	Volume of the wall	207.8 cm^3

The assumptions apply in this simulation model can be described as

1) The pressure and temperature of the adsorbent are both homogeneous.
2) The ammonia is evenly adsorbed and desorbed by the adsorbent during the chemical reaction process.
3) The working conditions of the ammonia are calculated as ideal gases.
4) The heat losses from the heat transfer fluid to the adsorbent and environment are ignored
5) The pressure losses of the system are ignored.

6.3. Simulation model of scroll expander

6.3.1. Description of the scroll expander model

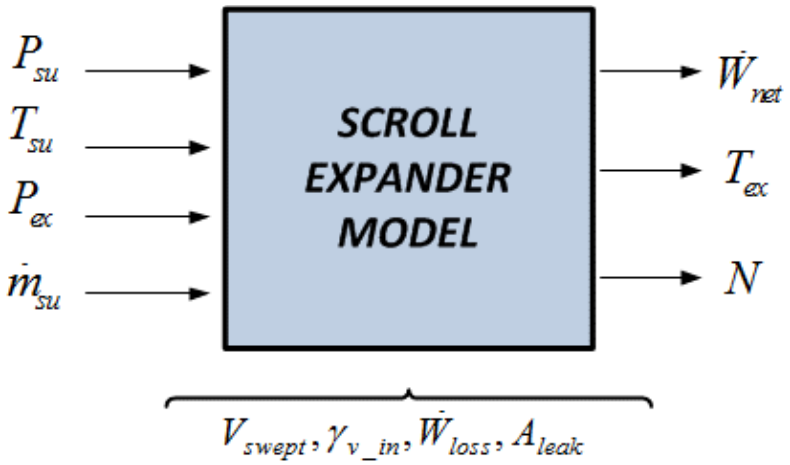

Figure 6-3 Schematic diagram of the parameters of the scroll expander model

The scroll expander model applied here was first proposed by Lemort et al [139]. This semi-empirical model has been used by many researchers and

has been proven as a very effective model to predict the performance of scroll expander within a specific operational range [127, 129, 130, 133, 134, 157]. The schematic diagram of the semi-empirical model has been shown in Figure 6-3. This simplified scroll expander model requires four input values have to be obtained either from experimental results and from the geometric model as introduced in Chapter 5 including supplied pressure P_{su} , supplied temperature T_{su} , exhaust pressure P_{ex} and supplied mass flow rate $\dot{m}_{su}$. Four semi-empirical parameters including friction loss (sum of mechanical losses and driven torque of the generator) $\dot{W}_{loss}$, internal leakage area A_{leak}, internal volumetric expansion ratio γ_{v_in} and swept volume V_{swept}.

The expansion process of the scroll expander can be divided and described into five steps, which has been illustrated in Figure 6-4.

1) Supply mass leakage from su to in, during this process the supply mass flow rate equals to the internal supply mass flow rate plus leaking mass flow rate
2) Isentropic expansion process from in to int, the first part of internal expansion process inside the expander has been recognized as isentropic process
3) Isochoric expansion process inside the expander from int to ex_2, during the process, the working fluid is expanded in constant volume.
4) Mixing process at the exhaust of expander when the internal leakage mixes with the working fluid involving the expansion process. The condition changes has been illustrate as from ex_2 to ex_1
5) Exhaust losses from condition ex_1 to ex

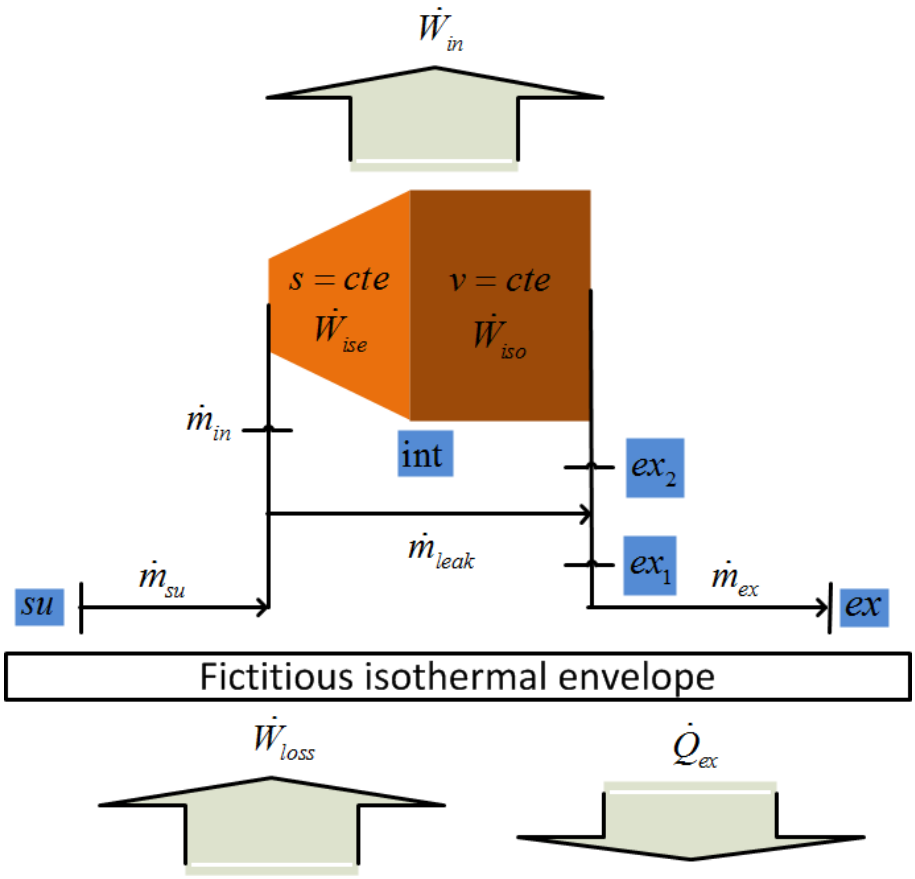

Figure 6-4 Schematic diagram of the scroll expander model

The working condition at int point is calculated by v_{int} and P_{int}. The specific volume at int point can be calculated by Equation 6-13. And the pressure at this point can be defined from Equation 6-14.

$$\gamma_{v\_in} = \frac{V_{s\_cp}}{V_{s\_exp}} = \frac{v_{int}}{v_{su}} \qquad \text{Equation 6-13}$$

$$P_{int} = f(v_{int}, s_{su}) \qquad \text{Equation 6-14}$$

The theoretical obtained energy, which has been converted as mechanical power, of the expander can therefore be calculated by the combination of

the mechanical power during isentropic and isochoric processes as illustrated in Equation 6-15.

$$\dot{W}_{in} = \underbrace{\dot{m}_{in} \times (h_{su} - h_{int})}_{\dot{W}_{ise}} + \underbrace{\dot{m}_{in} \times v_{int} \times (P_{int} - P_{ex})}_{\dot{W}_{iso}} \qquad \text{Equation 6-15}$$

The relationship between the supply mass flow rate and rotational speed of the expander has been calculated by Equation 6-16. V_{swept} is the swept volume per turn of the expander, which is 85.7 cm^3 based on the data provided by the SANDEN. v_{su} is the specific volume of the compressed air at the supply point.

$$\dot{m}_{su} = \frac{\dot{V}_{su}}{v_{su}} = \frac{N \times V_{swept}}{60 \times v_{su}} = \dot{m}_{ex} \qquad \text{Equation 6-16}$$

The mass balance of the simulation model can be defined as Equation 6-17. The displaced mass flow rate of the expander $\dot{m}_{in}$ equals to the overall mass flow rate $\dot{m}_{su}$ minus the internal leakage mass flow rate $\dot{m}_{leak}$. The leakage mass flow rate leaking between the clearances in the scroll can be modelled by assuming an isentropic flow through a convergent nozzle [158]. A_{leak} is the leakage area and C_{throat} is the velocity at the throat of the nozzle model.

$$\dot{m}_{in} = \underbrace{\frac{N \times V_{swept}}{60 \times v_{su}}}_{\dot{m}_{su}} - \underbrace{A_{leak} \times \frac{C_{throat}}{v_{throat}}}_{\dot{m}_{leak}} \qquad \text{Equation 6-17}$$

The velocity of the working fluid at the throat of nozzle can be calculated by Equation 6-18 and the specific enthalpy at the throat is defined by two parameters the pressure P_{throat} and the specific entropy at the throat s_{throat}. Because the specific entropy at the throat equals to the specific entropy at the supply point s_{su}, the specific enthalpy at the throat can be calculated by Equation 6-19.

$$C_{throat} = \sqrt{2(h_{su} - h_{throat})} \qquad \text{Equation 6-18}$$

$$h_{throat} = f(P_{throat}, s_{su}) \qquad \text{Equation 6-19}$$

The pressure at the throat of nozzle is defined as the critical pressure when the fluid is in choked flow regime where the critical pressure is larger than the exhaust pressure. When the fluid is not in choked flow regime, the throat pressure equals to the exhaust pressure. The definition of throat pressure can therefore been illustrated as Equation 6-20. The critical pressure of choked flow can be calculated by Equation 6-21, where γ is the heat capacity ratio of the fluid as indicated in Equation 6-22.

$$P_{throat} = MAX(P_{critical}, P_{ex}) \qquad \text{Equation 6-20}$$

$$P_{critical} = P_{su} \times \left(\frac{2}{r+1}\right)^{\frac{r}{r-1}} \qquad \text{Equation 6-21}$$

$$r = \frac{C_{p\_su}}{C_{v\_su}} \qquad \text{Equation 6-22}$$

The energy balances when the fluid mixes with the leakage flow at the exhaust point of the expander is calculated by the Equation 6-23, where h_{ex1} is the specific enthalpy at the exhaust point before mixing with the leakage flow, h_{ex2} is the specific enthalpy of the fluid after the mixing process and h_{su} is the specific enthalpy of the leakage flow. The specific enthalpy at the exhaust point of the expander can therefore be calculated by the Equation 6-24. The specific enthalpy at the exhaust point has been represented as h_{ex} and $\dot{Q}_{ex}$ is the overall heat losses of the expander to the environment.

$$\dot{m}_{ex} \times h_{ex1} = \dot{m}_{in} \times h_{ex2} + \dot{m}_{leak} \times h_{su} \qquad \text{Equation 6-23}$$

$$h_{ex} = h_{ex1} + \frac{\dot{Q}_{ex}}{\dot{m}_{su}} \qquad \text{Equation 6-24}$$

The net power output as the form of electricity equals to the theoretical power obtained by the expander minus the friction losses. The friction losses are defined as a sum of internal friction of the expander and the friction of electrical generator. The friction losses are assumed to be converted as heat losses of the expansion machine. Therefore the overall net power output from the expander can be calculated by the following equation.

$$\dot{W}_{net} = \dot{W}_{in} - \dot{W}_{loss} = \dot{m}_{in} \times [(h_{su} - h_{int}) + v_{int} \times (P_{int} - P_{ex})] - \dot{Q}_{ex} \qquad \text{Equation 6-25}$$

6.3.2. Determination of the parameters of the simulation model

This semi-empirical simulation model requires identifying four parameters including the friction loss $\dot{W}_{loss}$, internal leakage area A_{leak}, volumetric expansion ratio γ_{v_in} and swept volume of the expander V_{swept}.

The identification of the internal volumetric expansion ratio of the expander using the geometric model has been introduced in Chapter 5. The geometric model identified the suction volume of this scroll machine $V_{suction}$ is 35.04 cm^3, the exhaust volume of at the end of expansion chambers $V_{exhaust}$ is 105.12 cm^3 and the volumetric expansion ratio γ_{v_in} is 3.0. The swept volume of the equipment is provided by the manufacturer, which is 85.7 cm^3 per turn.

The other two parameters leakage area A_{leak} and friction losses $\dot{W}_{loss}$ of the expander have to be obtained by the experimental tests, which have been introduced in the next.

Determination of friction losses

The scroll type of expansion machine can be recognized as a heat power generation engine. Likewise conventional internal combustion engine, the friction losses of heat power engine has a relationship with the rotational speed of the engine.

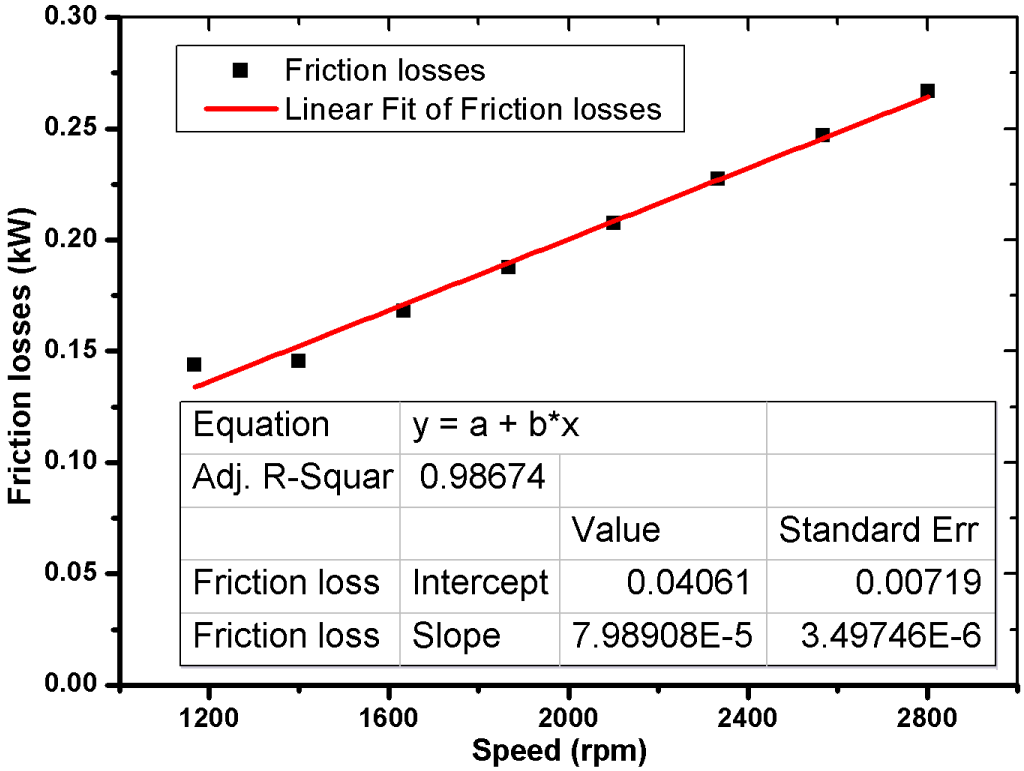

Figure 6-5 Relationship between friction losses and rotational speed

The overall friction losses include the internal friction of expander, mechanical losses between the shafts and electrical losses in the generator. The relationship between the rotational speed of the expander and friction losses based on eight stead state experimental tests has been illustrated in Figure 6-5. Results indicated that the friction losses linearly increase with the increase of rotational speed of expander. A linear fitted line has been added in the figure and the R squared of this fitted line is as high as 0.98674 as shown in the figure. Equation 6-26 illustrates the linear equation to illustrate the relationship between rotational speed and friction losses of the expander.

$$\dot{W}_{loss} = 0.04061 + 7.98908 \times 10^{-5} \times N \qquad \text{Equation 6-26}$$

Determination of leakage area

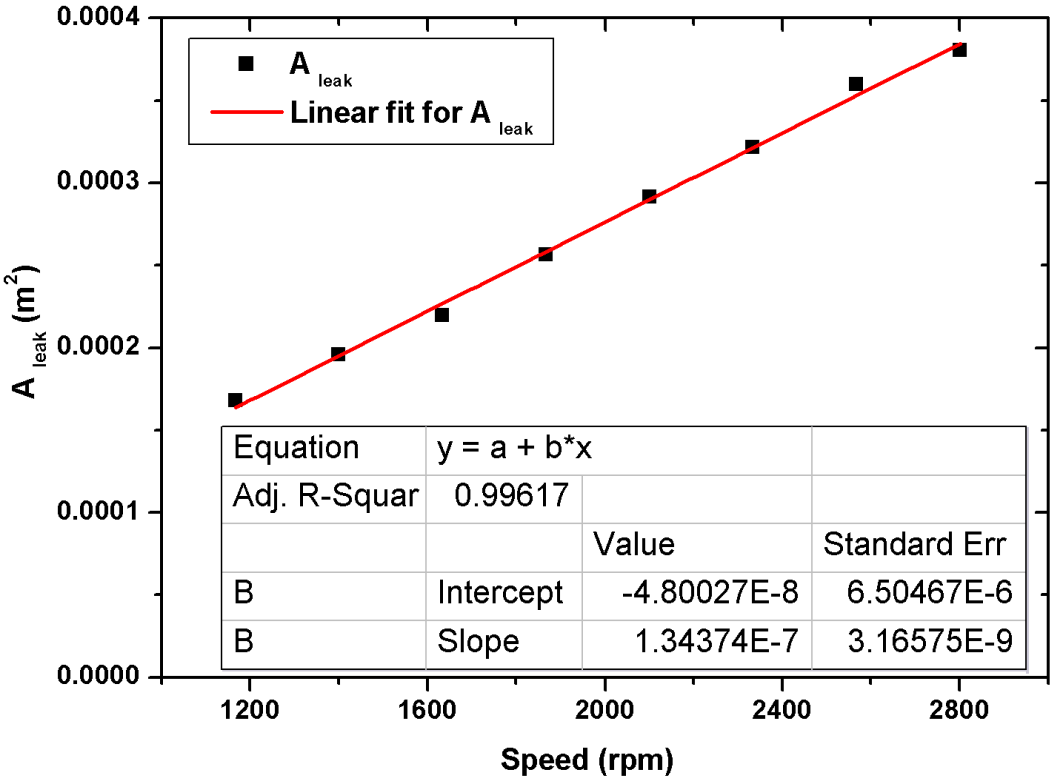

Figure 6-6 Relationship between leakage area and rotational speed

Leakage area is a predefined parameter in the nozzle model of the scroll expander simulation mode. The leakage area is used to calculate the leakage mass flow rate inside the expansion machine, which is also related to the rotational speed. The relationship between the rotational speed of the expander and leakage area under the experimental conditions has been drawn in Figure 6-6. The R squared of the fitted line is 0.99617 as indicated in the figure. The linear equation has been listed in Equation 6-27. The parameters used in the simulation model can be found in Table 6-3.

$$A_{leak} = -4.80027 \times 10^{-8} + 1.34374 \times 10^{-7} \times N \qquad \text{Equation 6-27}$$

Table 6-3 Sum of the parameters of the scroll expander model

Parameter	Symbol	Value
Swept volume	V_{swept}	85.7 cm^3 per turn
Internal volumetric expansion ratio	r_{v_in}	3.0
Suction area of the expander	$V_{suction}$	35.04 cm^3
Exhaust area of the expander	$V_{exhaust}$	105.12 cm^3
Friction losses	$\dot{W}_{loss}$	$0.04061 + 7.98908 \times 10^{-5} \times N$ (kW)
Leakage area	A_{leak}	$-4.80027 \times 10^{-8} + 1.34374 \times 10^{-7} \times N$ (m^2)

6.4. Performance evaluation of the cogeneration

Due to the intermittent performance of adsorption technology and various chemical reactions of chemisorption adsorbent, the power and refrigeration production from the cogeneration system are highly related and are various with the time. A case study of a resorption cogeneration system using 120 tubes of $MnCl_2$ as HTS and 90 tube units of $SrCl_2$ as LTS is selected to

evaluate the system performance. The detailed parameters of this case study can be found in Table 6-4

Table 6-4 Parameters of the evaluated cogeneration

Symbol	Description	Value
m_{MnCl_2}	Mass of $MnCl_2$	25.2 kg
m_{SrCl_2}	Mass of $SrCl_2$	18.9 kg
m_{ad} / m_{EG}	Mass ratio of adsorbent and graphite	2:1
m_{am}	Maximum transferable ammonia	13.6 kg
T_h	Heat source temperature	180 ^oC
T_0	Heat sink temperature	20 ^oC
T_{ref}	Refrigeration temperature	10 ^oC

6.5.1. Evaluation methods

The supplied heat power is calculated by the Equation 6-28, where $T_{f\_h\_in,j}$ is the supplied heat source temperature to the HTS and $T_{f\_h\_out,j}$ is the exhaust temperature from the HTS adsorbent bed.

$$Q_h = \frac{\int_0^{t_{cycle}} \dot{m}_f C_{p\_f} (T_{f\_h\_in,j} - T_{f\_h\_out,j}) dt}{t_{cycle}}$$ Equation 6-28

The electrical power of the system is evaluated by the Equation 6-29. η_{ele} is the electrical efficiency of the scroll expander, which is retrieved by the model described in Chapter 6.3. $h_{HTS\_T_{ad}}$ is the specific enthalpy of the ammonia at the inlet of the scroll expander under the heat source temperature and equilibrium pressure of the HTS. The calculation method of equilibrium pressure has been introduced in Chapter 3. $h_{LTS\_T_0}$ is the specific enthalpy of the ammonia at the outlet of the scroll expander, which is defined by the equilibrium pressure of the LTS under heat sink temperature and the entropy at the inlet of the expander.

$$W_{ele} = \frac{m_{am} \Delta x (h_{HTS\_T_{ad}} - h_{LTS\_T_0}) \eta_{ele}}{t_{cycle}}$$ Equation 6-29

The refrigeration power of this cogeneration system is defined by Equation 6-30, where the inlet and outlet temperature of the LTS during refrigeration process is presented as $T_{f\_ref\_in,j}$ and $T_{f\_ref\_out,j}$, respectively.

$$Q_{ref} = \frac{\int_0^{t_{cycle}} \dot{m}_f C_{p\_f} (T_{f\_ref\_in,j} - T_{f\_ref\_out,j}) dt}{t_{cycle}}$$ Equation 6-30

6.5.2. Performance of power generation

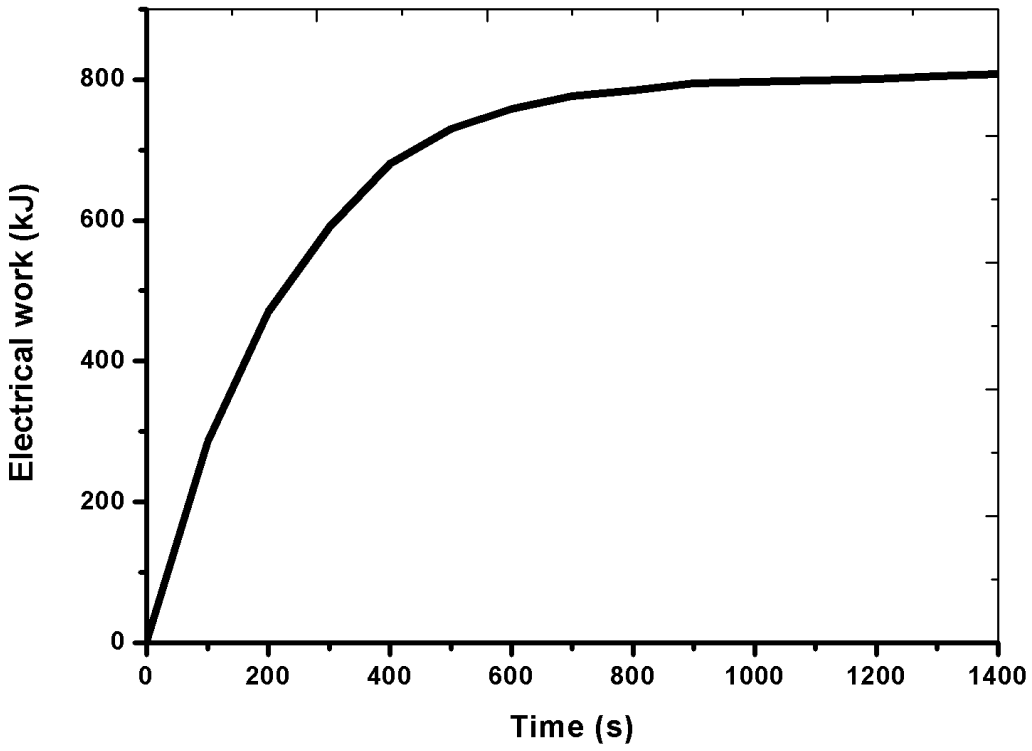

Figure 6-7 Relationship between electrical work and time under the heat source temperature at 180 ^{o}C and heat sink temperature at 20 ^{o}C

Under the heating temperature at 180 ^{o}C, the equilibrium pressure of $MnCl_2$ is as high as 26.87 bar calculated from the Equation 3-11, which is sufficient to start the scroll expander and generate electricity. The electrical work of this cogeneration using $MnCl_2$-$SrCl_2$ as the working pair has been evaluated and the results is illustrated in Figure 6-7. Results indicated that this maximum electrical work produced from this system is around 800 kJ. The increase of electrical work is quite rapid in the first 400 seconds. After ten minutes, the increase of electrical work is almost ignorable.

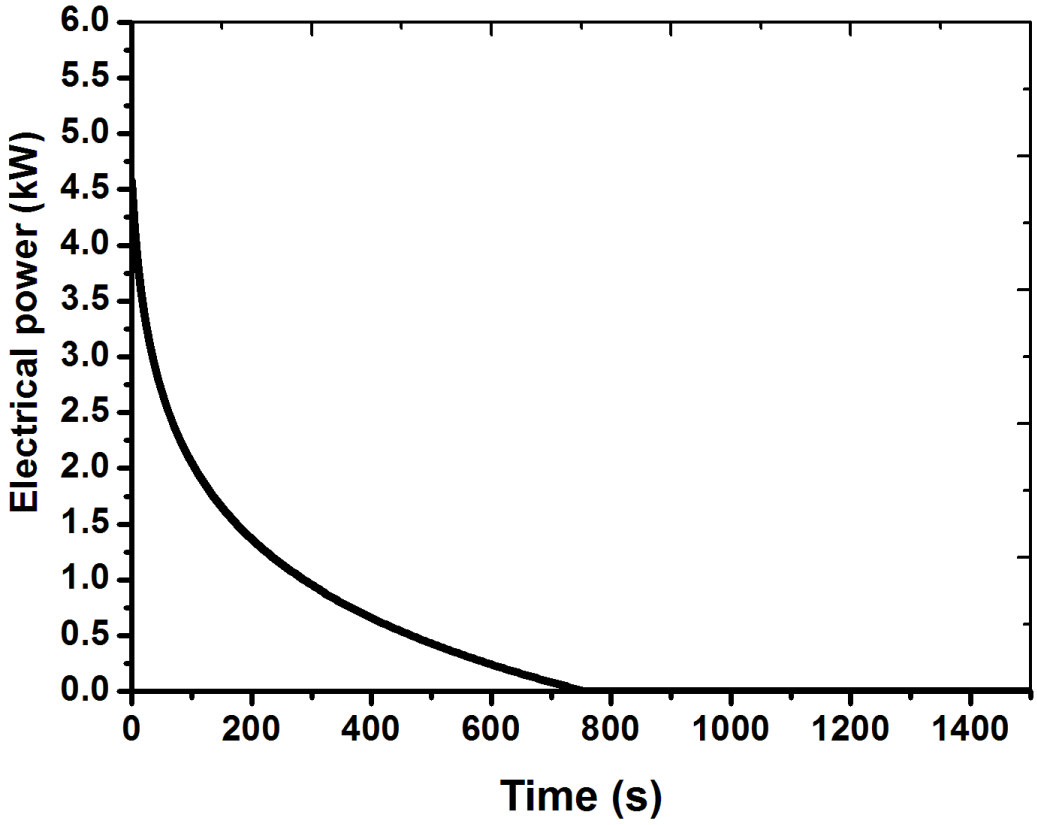

Figure 6-8 Relationship between the electrical power and time under the heat source temperature at 180 ^{o}C and heat sink temperature at 20 ^{o}C

The electrical power of the system is calculated by the Equation 6-29 and the variation of the electrical power is shown in Figure 6-8. The highest electrical power generated from the system is around 3 kW, which could be found in the first 1 to 2 minutes of the power generation process. The average electrical power from this scale of system is about 1 kW. The results pointed out the effectively production of power from this designed system is about 10 minutes.

Influences of heating source temperature

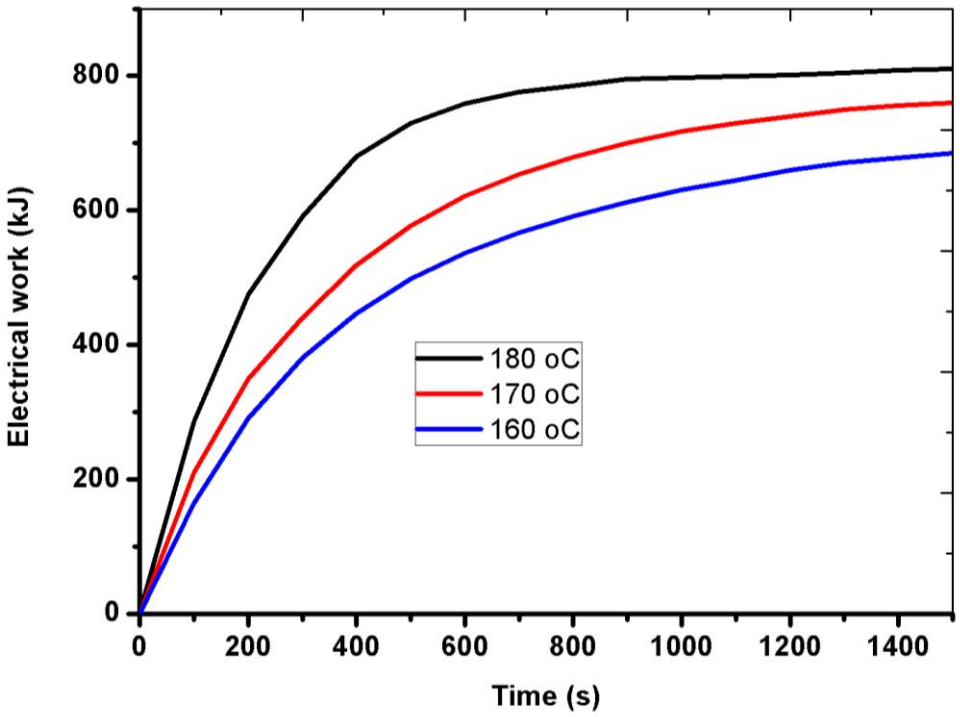

Figure 6-9 Relationship between the electrical work and time under different heat source temperature

The electrical work of the cogeneration under three different heat source temperature are compared and the results have been plotted in Figure 6-9. The blue line is the electrical work under 160 ^{o}C, the red line is the electrical work under 170 ^{o}C and the black line indicates the electrical work under the heat source temperature at 180 ^{o}C. Within 25 minutes, the electrical work generated by the system under 160, 170 and 180 ^{o}C is about 650kJ, 730 kJ and 800 kJ, respectively. The results also indicated that in order to speed up the chemical reaction of this resorption working pair within 10 minutes, 180 ^{o}C heat source temperature is the minimum required temperature.

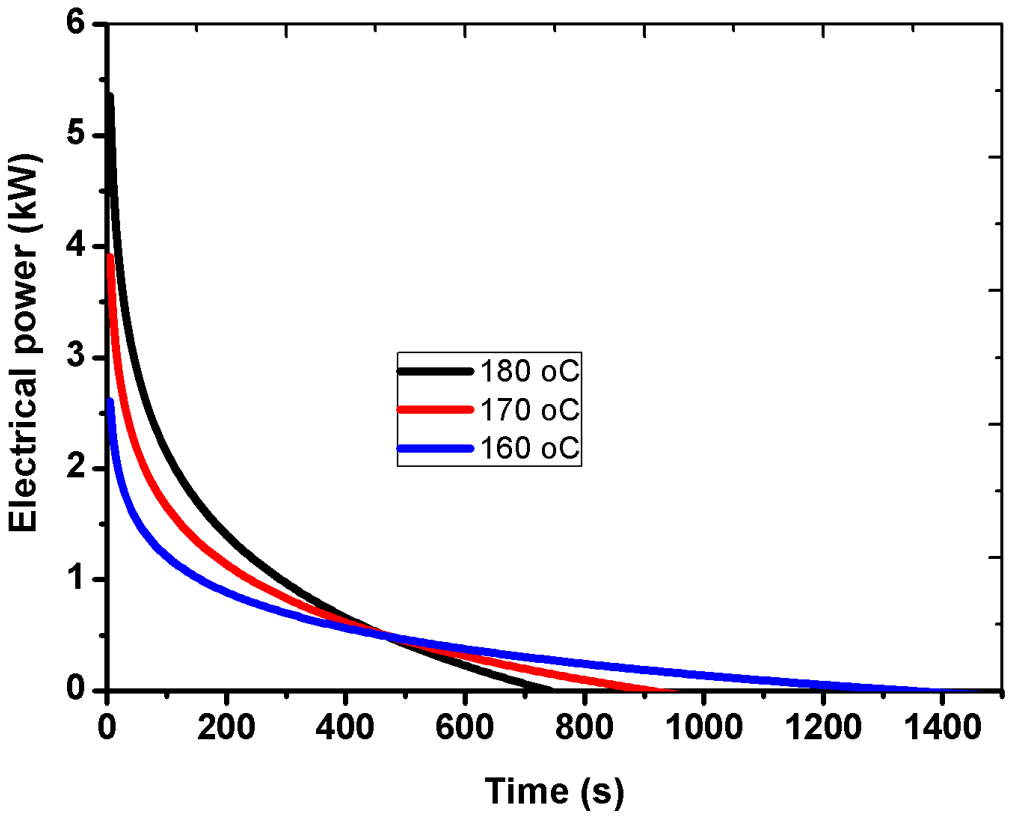

Figure 6-10 Relationship between the electrical power and time under different heat source temperature

The variation of electrical power within 25 minutes of cycle time at three different heat source temperatures are drawn in Figure 6-10. In the first 1 to 2 minutes, the average electrical power of 160 ^{o}C, 170 ^{o}C and 180 ^{o}C heat source temperature is about 1.5kW, 2.5kW and 3.5kW, respectively. At 500 second, the electrical power of this system is about 500 W.

6.5.3. Performance of refrigeration

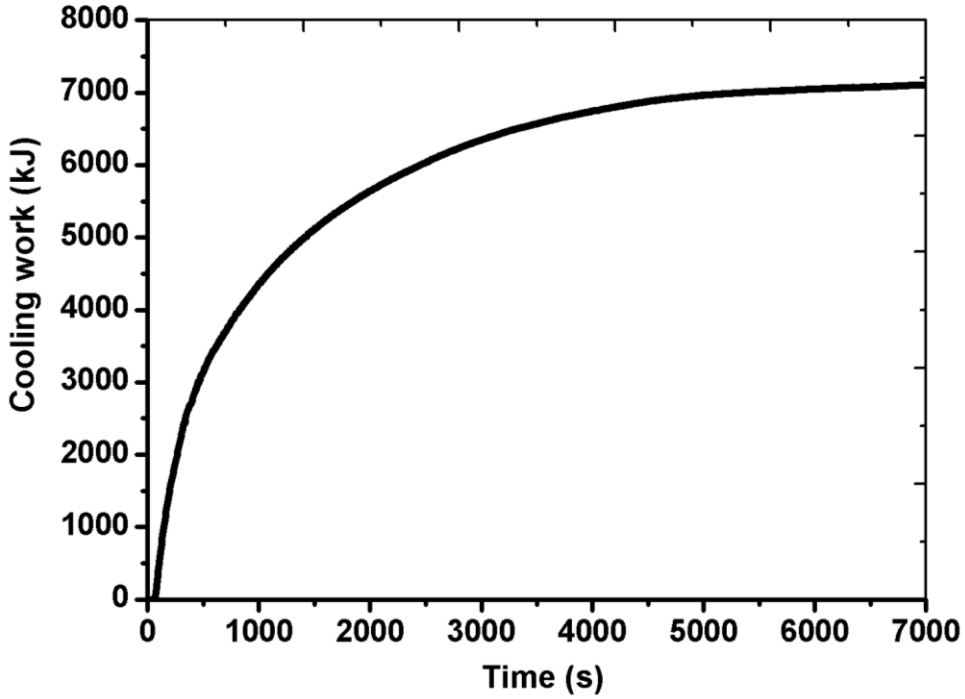

Figure 6-11 Relationship between cooling work and time under refrigeration temperature at 10 ^{o}C and heat sink temperature at 20 ^{o}C

The refrigeration process of the resorption part is generated from the LTS. The refrigeration generation is highly related with the pressure difference between the HTS and LTS. The resorption working pair selected in this study is $MnCl_2$-$SrCl_2$, which has 0.2 bar pressure difference between the two beds. Therefore, the reaction time for refrigeration generation part of the system requires more than that for power generation. The variation of cooling capacity is shown in Figure 6-11. During the first 15 to 20 minutes, the cooling capacity rapidly increases with the increase of time. The refrigeration capacity at 15 and 20 minutes of the system is about 3500 kJ and 4600kJ, respectively.

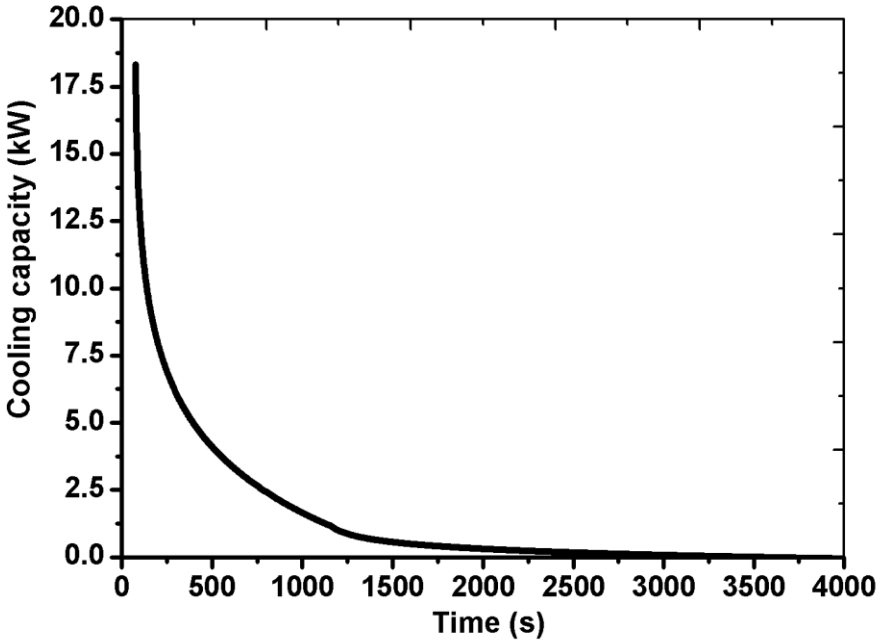

Figure 6-12 Relationship between the cooling capacity and time under refrigeration temperature at 10 ^{o}C and heat sink temperature at 20 ^{o}C

The refrigeration performance of the cogeneration system shows similar tendency compared with the electrical power, except the first two to three minutes, which is illustrated in Figure 6-12. During this time, the refrigeration has been consumed by the adsorbent bed to cool down the bed to the refrigeration temperature. The results indicated that the refrigeration generated by the system after 25 minutes is not worth to recovery although the overall cooling capacity of the system is still increasing as shown in Figure 6-12. The average refrigeration achieved from this scale of system is around 2.5 kW at 10 ^{o}C refrigeration temperature.

6.5.4. *Performance of the full cycle*

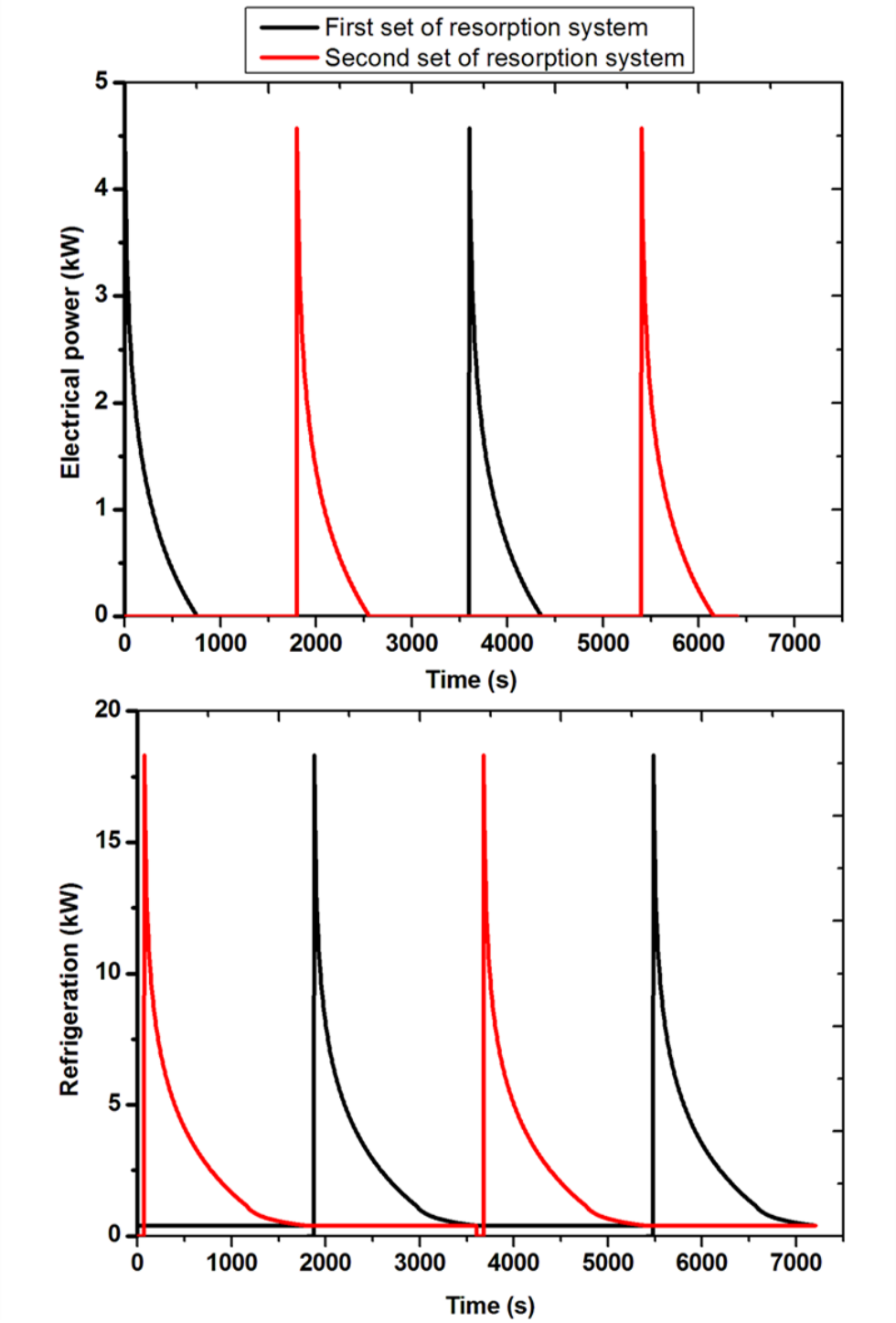

Figure 6-13 Performance of two sets of resorption system under the heat source temperature at 180 ^{o}C and refrigeration temperature at 10 ^{o}C

Based on the results from the independent resorption system, the performance of two sets of resorption system was plotted in Figure 6-13. The refrigeration duration is chosen at 30 minutes, when the refrigeration temperature is 10 ^{o}C. The heat source temperature is selected at 180 ^{o}C. The cogeneration performance of the first set of the resorption system is indicated as the black line in Figure 6-13. The red line indicates the power and refrigeration performance of the second set of resorption system. The power generation part of the resorption cogeneration could be recognised as the regeneration to produce refrigeration. The regeneration time for the resorption system under the heat source temperature at 180 ^{o}C is around 14 minutes, which indicates more sets of resorption system is required in order to continuously produce electricity and refrigeration. The other practical option to maintain stable output using two sets of system is to reduce the heat source temperature, which can enlarge the regeneration duration to meet the required time for refrigeration generation of the resorption system. The average generated electricity of these two sets of resorption system is around 250 W and the average refrigeration production from the system is about 2.5 kW at 10 ^{o}C refrigeration temperature.

6.5. Summary

This chapter describes the evaluation of the resorption cogeneration based on the experimental results achieved from Chapter 4 and Chapter 5. The adsorption model was conducted by integrating the experimental kinetic equations and heat transfer equation to predict the performance of the adsorbent bed. A scroll expander model was built based on the physical dimensions of the scroll expander and several parameters obtained from the experimental test in Chapter 5. The dynamic performance of the resorption cogeneration using $MnCl_2$-$SrCl_2$ as the working pair is then evaluated.

Results indicated the power generation performance of the cogeneration system is quite good in the first 400 s of the cycle time and after 600 seconds the power produced from the system can be ignored. In order to averagely generate 1 KW of power, the required quantity of $MnCl_2$ and $SrCl_2$ in the system is around 25.2 kg and 18.9 kg, respectively. Moreover, the effects of heating source temperature has been evaluated, the minimum heating source temperature for the system to operate within 10 minutes is 180 ^oC. The evaluation of the dynamic refrigeration performance of the $MnCl_2$-$SrCl_2$ cogeneration indicated that the reasonable cycle time for refrigeration production is lower than 25 minutes. The average refrigeration achieved from this system is around 2.5 KW at 10 ^oC refrigeration temperature. The full cycle performance using two sets of resorption system under the heat source temperature at 180 ^oC and refrigeration temperature at 10 ^oC was evaluated. The results indicated more sets of resorption system are required to continuous produce power and refrigeration. The average electricity produced from this two sets system is about 250 W and the refrigeration is around 2.5 kW, when the cycle time is 1 hour.

Chapter 7. Conclusions and Recommendations

7.1. Summary of main conclusions

This study focuses on the feasibility investigation on a resorption cogeneration system to continuously produce power and refrigeration using the combination of adsorption technology and expansion machine. The conducted methodologies include:

1) Design and analysis the system performance of the resorption cogeneration to identify the optimal working pair and investigate potential system improvement methods by using the first and second law analysis,

2) Design and construct an adsorption performance test rig to experimentally test the adsorption/desorption performance of the candidate adsorbents,

3) Design and construct a scroll expander test rig to test the performance of this type of expansion machine to be used in the resorption cogeneration system,

4) Evaluation on a small scale resorption cogeneration system using the obtained experimental results to predict the size/weight, variation performance and potential application fields of the system. The main conclusions of this study are as follows,

- The analysis of the proposed resorption cogeneration shows attractive performance. Twelve resorption working pairs were selected and studied under the heat source temperature from 100 ^{o}C to 300 ^{o}C. Results identified the $MnCl_2$-$SrCl_2$ achieve the highest COP at 0.7 without using system optimisation methods under the heat source

temperature at 110 ^{o}C. The highest electrical production is achieved at 12.49%, when the resorption working pair is $PbCl_2$-$NiCl_2$ under the heat source temperature at 300 ^{o}C.

- The exergy analysis conducted on four resorption working pairs pointed out that the advanced optimisation methods using heat and mass recovery processes can potentially improve the average COP by 35% for the HTS-$MnCl_2$ and by 38% for the HTS-$NiCl_2$. Moreover, the electrical energy efficiency of the system using $MnCl_2$ and $NiCl_2$ as the HTS is by 3% and 1.5%, when the heat recovery process is used in the system. The candidate resorption working pair driven by low grade heat source for the main purpose of refrigeration generation has been pointe out as $MnCl_2$-$SrCl_2$.

- The manufacture processes of expanded graphite, which is to be used as a matrix for the salts to overcome the swelling and agglomeration commonly existing in chemical adsorbents, were conducted in the study,. Different mixture methods have been studied and applied to make the composite adsorbents. The heat transfer performance and reaction speed of the composite adsorbents are not effected after repeated times, which indicated the swelling and agglomeration problems are effectively solved by applying the composite adsorbents.

- A scroll expander has been modified from a scroll compressor originally used in car air condition system. The experimental investigation on this expansion machine obtained the volumetric expansion ratio of the equipment, electrical efficiency, isentropic efficiency of the tested unit under various conditions are conducted. A geometric model of the tested unit to obtain the physical parameter has also been conducted and the volumetric expansion ratio obtained from the geometric model and experimental results shows very well agreement. The average isentropic efficiency of this tested unit expander fluctuates from 0.56 to 0.64 under

the tested conditions. The electrical efficiency of the scroll expander is around 0.35.

- A case study of a small scale resorption cogeneration system is established in Chapter 6 to evaluate the variation performance of the system. In order to produce the average 1kW power and 2.5kW cooling capacity at 10 ^{o}C refrigeration temperature, the minimum quantity of the $MnCl_2$ and $SrCl_2$ is around 25.2 kg and 18.9 kg, respectively. The results pointed out that huge amount of power and refrigeration production could be achieved in the first 1 to 2 minutes of cycle time, which is caused by the huge chemical reaction of the chemical adsorbent and ammonia. The resorption cogeneration system has high potential to be used for some place requires both refrigeration and power such as supermarket and swimming pool.

7.2. Recommendations for future work

The resorption cogeneration shows promising applications to recovery low grade heat such as solar energy and industry waste heat into refrigeration and power. Furthermore, the cogeneration system has the advantages of simple construction, dual energy generation, wide flexibility for different heat source temperature, etc. However, the intermittent performances of the chemical adsorption which cannot stably control the inlet conditions of the expansion machine and produce stable power output. More detailed studies on the integration of these two technologies are required.

The investigation and development on novel composite adsorbent can be one of the solutions to improve the mass and heat transfer performance of the adsorbent, which could potentially improve the overall energy efficiency of the cogeneration system.

The scroll expander used in this study was modified from a scroll compressor, which requires oil to lubricate the equipment and seal the working fluid to reduce the losses inside the expansion machine. Oil free scroll expander may be one of the solutions to be integrated with ammonia system. A specific designed oil free expander is suggested to be used under the working conditions of resorption cogeneration system. Variable geometry turbine can also be a good choice as long as the operational working conditions of the resorption system have been experimentally identified and controlling strategies of the turbine machine have been developed.

In this study, the resorption cogeneration was evaluated based on the component level results obtained from the adsorption performance test rig and scroll expander rig. A demonstration rig of one pair of resorption cogeneration is suggested to explore the real performance of this system when the component level exploration and study on the system have been accomplished.

References

[1] BP:. Statistical Review of World Energy,Workbook (xlsx). 2013.
[2] IPCC. CLIMATE CHANGE 2014: Synthesis Report. Summary for Policymakers. 2015;2015.
[3] Hansen J, Ruedy R, Sato M, Lo K. GLOBAL SURFACE TEMPERATURE CHANGE. Reviews of Geophysics. 2010;48.
[4] Wang RZ, Oliveira RG. Adsorption refrigeration - An efficient way to make good use of waste heat and solar energy. Prog Energ Combust. 2006;32:424-58.
[5] Energy Policies of IEA Countries - The United Kingdom 2012 Review. International Energy Agency.
[6] UK renewable Energy Roadmap Update 2013. Department of Energy & Climate Change.
[7] Ruzhu Wang, Liwei Wang, Wu J. Adsorption Refrigeration Technology: Theory and Application2014.
[8] Spinner B. Ammonia-based thermochemical transformers. Heat Recovery Systems and CHP. 1993;13:301-7.
[9] Wang LW, Li D, Roskilly AP, Wang YD, Wang RZ. A novel type resorption cycle for electrical generation and refrigeration. SusTEM2011, Newcastle, UK2011.
[10] Lu YZ, Wang RZ, Zhang M, Jiangzhou S. Adsorption cold storage system with zeolite–water working pair used for locomotive air conditioning. Energy Conversion and Management. 2003;44:1733-43.
[11] Wang RZ. Adsorption refrigeration research in Shanghai Jiao Tong University. Renewable and Sustainable Energy Reviews. 2001;5:1-37.
[12] Mazet N, Amouroux M, Spinner B. ANALYSIS AND EXPERIMENTAL STUDY OF THE TRANSFORMATION OF A NON-ISOTHERMAL SOLID/GAS REACTING MEDIUM. Chemical Engineering Communications. 1991;99:155-74.
[13] Thamm H. Adsorption site heterogeneity in silicalite: a calorimetric study. Zeolites. 1987;7:341-6.
[14] Metcalf SJ, Tamainot-Telto Z, Critoph RE. Application of a compact sorption generator to solar refrigeration: Case study of Dakar (Senegal). Applied Thermal Engineering. 2011;31:2197-204.
[15] Lu Y, Bao H, Yuan Y, Wang Y, Wang L, Roskilly AP. Optimisation of a Novel Resorption Cogeneration Using Mass and Heat Recovery. Energy Procedia. 2014;61:1103-6.
[16] Lu Y, Wang Y, Bao H, Wang L, Yuan Y, Roskilly AP. Analysis of an optimal resorption cogeneration using mass and heat recovery processes. Applied Energy. 2015;160:892-901.
[17] Jiang L, Wang LW, Roskilly AP, Wang RZ. Design and performance analysis of a resorption cogeneration system. International Journal of Low-Carbon Technologies. 2013;8:85-91.
[18] Lu Y, Wang Y, Wang L, Yuan Y, Liu Z, Roskilly AP. Experimental Investigation of a Scroll Expander for Power Generation Part of a Resorption Cogeneration. Energy Procedia. 2015;75:1027-32.

[19] Srivastava NC, Eames IW. A review of adsorbents and adsorbates in solid–vapour adsorption heat pump systems. Applied Thermal Engineering. 1998;18:707-14.
[20] Ammar Y, Joyce S, Norman R, Wang Y, Roskilly AP. Low grade thermal energy sources and uses from the process industry in the UK. Applied Energy. 2012;89:3-20.
[21] Tchanche BF, Lambrinos G, Frangoudakis A, Papadakis G. Low-grade heat conversion into power using organic Rankine cycles – A review of various applications. Renewable and Sustainable Energy Reviews. 2011;15:3963-79.
[22] Critoph RE, Zhong Y. Review of trends in solid sorption refrigeration and heat pumping technology. Journal of Process Mechanical Engineering. 2004:285-300.
[23] Critoph RE. Performance limitations of adsorption cycles for solar cooling. Solar Energy. 1988;41:21-31.
[24] Pons M, Feng Y. Characteristic parameters of adsorptive refrigeration cycles with thermal regeneration. Applied Thermal Engineering. 1997;17:289-98.
[25] Teng Y, Wang RZ, Wu JY. Study of the fundamentals of adsorption systems. Applied Thermal Engineering. 1997;17:327-38.
[26] Srikhirin P, Aphornratana S, Chungpaibulpatana S. A review of absorption refrigeration technologies. Renewable and Sustainable Energy Reviews. 2001;5:343-72.
[27] Wang LW, Wang RZ, Wu JY, Wang K, Wang SG. Adsorption ice makers for fishing boats driven by the exhaust heat from diesel engine: choice of adsorption pair. Energy Conversion and Management. 2004;45:2043-57.
[28] Jiangzhou S, Wang RZ, Lu YZ, Xu YX, Wu JY. Experimental investigations on adsorption air-conditioner used in internal-combustion locomotive driver-cabin. Applied Thermal Engineering. 2002;22:1153-62.
[29] DallBauman LA, Finn JE. Adsorption processes in spacecraft environmental control and life support systems. In: Dąbrowski A, editor. Studies in Surface Science and Catalysis: Elsevier; 1999. p. 455-71.
[30] Wang K, Wu JY, Wang RZ, Wang LW. Composite adsorbent of CaCl2 and expanded graphite for adsorption ice maker on fishing boats. International Journal of Refrigeration. 2006;29:199-210.
[31] Tchernev D. I., Emerson D. T. High-efficiency regenerative zeolite heat pump. ASHRAE Transactions1988. p. 2024-32.
[32] Shelton S V. Solid adsorbent heat pump system. US Patent, US4610148; 1986.
[33] Dai YJ, Wang RZ, Xu YX. Study of a solar powered solid adsorption–desiccant cooling system used for grain storage. Renewable Energy. 2002;25:417-30.
[34] Jain S, Dhar PL, Kaushik SC. Evaluation of solid-desiccant-based evaporative cooling cycles for typical hot and humid climates. International Journal of Refrigeration. 1995;18:287-96.
[35] Saha BB, Koyama S, Kashiwagi T, Akisawa A, Ng KC, Chua HT. Waste heat driven dual-mode, multi-stage, multi-bed regenerative adsorption system. International Journal of Refrigeration. 2003;26:749-57.
[36] Saha BB, Koyama S, Choon Ng K, Hamamoto Y, Akisawa A, Kashiwagi T. Study on a dual-mode, multi-stage, multi-bed regenerative adsorption chiller. Renewable Energy. 2006;31:2076-90.
[37] Chua HT, Ng KC, Malek A, Kashiwagi T, Akisawa A, Saha BB. Multi-bed regenerative adsorption chiller — improving the utilization of waste heat and reducing the chilled water outlet temperature fluctuation. International Journal of Refrigeration. 2001;24:124-36.
[38] Douss N, Meunier F. Experimental study of cascading adsorption cycles. Chemical Engineering Science. 1989;44:225-35.

[39] Critoph RE. Performance estimation of convective thermal wave adsorption cycles. Applied Thermal Engineering. 1996;16:429-37.
[40] Sward BK, LeVan MD, Meunier F. Adsorption heat pump modeling: the thermal wave process with local equilibrium. Applied Thermal Engineering. 2000;20:759-80.
[41] Taylan O, Baker DK, Kaftanoğlu B. COP trends for ideal thermal wave adsorption cooling cycles with enhancements. International Journal of Refrigeration. 2012;35:562-70.
[42] Akahira A, Alam KCA, Hamamoto Y, Akisawa A, Kashiwagi T. Experimental investigation of mass recovery adsorption refrigeration cycle. International Journal of Refrigeration. 2005;28:565-72.
[43] Akahira A, Alam KCA, Hamamoto Y, Akisawa A, Kashiwagi T. Mass recovery adsorption refrigeration cycle—improving cooling capacity. International Journal of Refrigeration. 2004;27:225-34.
[44] Oliveira RG, Silveira Jr V, Wang RZ. Experimental study of mass recovery adsorption cycles for ice making at low generation temperature. Applied Thermal Engineering. 2006;26:303-11.
[45] Wang LW, Wang RZ, Lu ZS, Chen CJ, Wu JY. Comparison of the adsorption performance of compound adsorbent in a refrigeration cycle with and without mass recovery. Chemical Engineering Science. 2006;61:3761-70.
[46] Wang RZ. Performance improvement of adsorption cooling by heat and mass recovery operation. International Journal of Refrigeration. 2001;24:602-11.
[47] T. X. Li, R. Z. Wang*, R. G. Oliveira, Wang LW. Performance analysis of an innovative multimode, multisalt and multieffect chemisorption refrigeration system. AIChE Journal. December 2007;53:3222-30.
[48] Oliveira RG, Wang RZ, Li TX. Transient analysis of a chemisorption air conditioning system operating under different kinds of cycle. Industrial & Engineering Chemistry Research. 2008;47:1102-10.
[49] Wang LW, Bao HS, Wang RZ. A comparison of the performances of adsorption and resorption refrigeration systems powered by the low grade heat. Renewable Energy. 2009;34:2373-9.
[50] Lu Y, Wang L, Tian G, Roskilly AP. Study on A Small Scale Solar Powered Organic Rankine Cycle Utilizing Scroll Expander. International Conference on Applied Energy. Suzhou, China, July 5-8, 2012.
[51] Hung TC, Shai TY, Wang SK. A review of organic rankine cycles (ORCs) for the recovery of low-grade waste heat. Energy. 1997;22:661-7.
[52] Tchanche BF, Papadakis G, Lambrinos G, Frangoudakis A. Fluid selection for a low-temperature solar organic Rankine cycle. Applied Thermal Engineering. 2009;29:2468-76.
[53] Chen H, Goswami DY, Stefanakos EK. A review of thermodynamic cycles and working fluids for the conversion of low-grade heat. Renewable and Sustainable Energy Reviews. 2010;14:3059-67.
[54] Heberle F, Brüggemann D. Exergy based fluid selection for a geothermal Organic Rankine Cycle for combined heat and power generation. Applied Thermal Engineering. 2010;30:1326-32.
[55] Kalina AI. Combined-Cycle System With Novel Bottoming Cycle. Journal of Engineering for Gas Turbines and Power. 1984;106:737-42.
[56] Zhang X, He M, Zhang Y. A review of research on the Kalina cycle. Renewable and Sustainable Energy Reviews. 2012;16:5309-18.

[57] Leibowitz HM, Micak HA. Design of a 2 MW Kalina cycle binary module for installation in Husavik, Iceland. Transactions - Geothermal Resources Council. 1999;23:75-80.
[58] Bombarda P, Invernizzi CM, Pietra C. Heat recovery from Diesel engines: A thermodynamic comparison between Kalina and ORC cycles. Applied Thermal Engineering. 2010;30:212-9.
[59] Zhang Z, Guo Z, Chen Y, Wu J, Hua J. Power generation and heating performances of integrated system of ammonia–water Kalina–Rankine cycle. Energy Conversion and Management. 2015;92:517-22.
[60] Fontalvo A, Pinzon H, Duarte J, Bula A, Quiroga AG, Padilla RV. Exergy analysis of a combined power and cooling cycle. Applied Thermal Engineering. 2013;60:164-71.
[61] Goswami DY, Xu F. Analysis of a new thermodynamic cycle for combined power and cooling using low and mid temperature solar collectors. Journal of Solar Energy Engineering, Transactions of the ASME. 1999;121:91-7.
[62] Xu F, Yogi Goswami D, S. Bhagwat S. A combined power/cooling cycle. Energy. 2000;25:233-46.
[63] Hasan AA, Goswami DY, Vijayaraghavan S. First and second law analysis of a new power and refrigeration thermodynamic cycle using a solar heat source. Solar Energy. 2002;73:385-93.
[64] Lu S, Goswami DY. Optimization of a Novel Combined Power/Refrigeration Thermodynamic Cycle. Journal of Solar Energy Engineering. 2003;125:212-7.
[65] Tamm G, Goswami DY, Lu S, Hasan AA. Theoretical and experimental investigation of an ammonia–water power and refrigeration thermodynamic cycle. Solar Energy. 2004;76:217-28.
[66] Hasan AA, Goswami DY. Exergy Analysis of a Combined Power and Refrigeration Thermodynamic Cycle Driven by a Solar Heat Source. Journal of Solar Energy Engineering. 2003;125:55-60.
[67] W.M. Haynes. Handbook of Chemistry and Physics93RD EDITION 2012-2013.
[68] Chua HT, Ng KC, Malek A, Kashiwagi T, Akisawa A, Saha BB. Modeling the performance of two-bed, sillica gel-water adsorption chillers. International Journal of Refrigeration. 1999;22:194-204.
[69] Saha BB, Koyama S, Lee JB, Kuwahara K, Alam KCA, Hamamoto Y, et al. Performance evaluation of a low-temperature waste heat driven multi-bed adsorption chiller. International Journal of Multiphase Flow. 2003;29:1249-63.
[70] Critoph RE, Metcalf SJ. Specific cooling power intensification limits in ammonia–carbon adsorption refrigeration systems. Applied Thermal Engineering. 2004;24:661-78.
[71] Sumathy K, Zhongfu L. Experiments with solar-powered adsorption ice-maker. Renewable Energy. 1999;16:704-7.
[72] Wang RZ, Li M, Xu YX, Wu JY. An energy efficient hybrid system of solar powered water heater and adsorption ice maker. Solar Energy. 2000;68:189-95.
[73] Wang LW, Wang RZ, Lu ZS, Chen CJ, Wang K, Wu JY. The performance of two adsorption ice making test units using activated carbon and a carbon composite as adsorbents. Carbon. 2006;44:2671-80.
[74] Florence Poyelle J-JG, Meunier F. Experimental Tests and Predictive Model of an Adsorptive Air Conditioning Unit. Industrial & Engineering Chemistry Research. 1999;38:298-309.
[75] Lai H-M. An enhanced adsorption cycle operated by periodic reversal forced convection. Applied Thermal Engineering. 2000;20:595-617.
[76] Saha BB, Akisawa A, Kashiwagi T. Silica gel water advanced adsorption refrigeration cycle. Energy. 1997;22:437-47.

[77] Saha BB, Boelman EC, Kashiwagi T. Computational analysis of an advanced adsorption-refrigeration cycle. Energy. 1995;20:983-94.
[78] Wang DC, Xia ZZ, Wu JY, Wang RZ, Zhai H, Dou WD. Study of a novel silica gel–water adsorption chiller. Part I. Design and performance prediction. International Journal of Refrigeration. 2005;28:1073-83.
[79] Wang DC, Wu JY, Xia ZZ, Zhai H, Wang RZ, Dou WD. Study of a novel silica gel–water adsorption chiller. Part II. Experimental study. International Journal of Refrigeration. 2005;28:1084-91.
[80] Wang LW, Wang RZ, Oliveira RG. A review on adsorption working pairs for refrigeration. Renewable and Sustainable Energy Reviews. 2009;13:518-34.
[81] Willers E, Groll M. Evaluation of metal hydride machines for heat pumping and cooling applications: Evaluation des machines à hydrure métallique dans les applications de pompes à chaleur et de refroidissement. International Journal of Refrigeration. 1999;22:47-58.
[82] L.L. V, D.A. M, Jr V. Multi-effect complex compound/ammonia sorption machines. Proceedings of the International Absorption Heat Pump Conference Montreal. Quebec, Canada1996. p. 3-7.
[83] Dellero T, Sarmeo D, Touzain P. A chemical heat pump using carbon fibers as additive. Part I: enhancement of thermal conduction. Applied Thermal Engineering. 1999;19:991-1000.
[84] Dellero T, Touzain P. A chemical heat pump using carbon fibers as additive. Part II: study of constraint parameters. Applied Thermal Engineering. 1999;19:1001-11.
[85] Wang LW, Wang RZ, Wu JY, Wang K. Compound adsorbent for adsorption ice maker on fishing boats. International Journal of Refrigeration. 2004;27:401-8.
[86] Oliveira RG, Wang RZ, Wang C. Evaluation of the cooling performance of a consolidated expanded graphite–calcium chloride reactive bed for chemisorption icemaker. International Journal of Refrigeration. 2007;30:103-12.
[87] Bao HS, Wang RZ, Wang LW. A resorption refrigerator driven by low grade thermal energy. Energy Conversion and Management. 2011;52:2339-44.
[88] Bao HS, Wang RZ, Oliveira RG, Li TX. Resorption system for cold storage and long-distance refrigeration. Applied Energy. 2012;93:479-87.
[89] Vasiliev LL, Mishkinis DA, Antukh AA, Kulakov AG. Resorption heat pump. Applied Thermal Engineering. 2004;24:1893-903.
[90] Goetz V, Spinner B, Lepinasse E. A solid-gas thermochemical cooling system using BaCl2 and NiCl2. Energy. 1997;22:49-58.
[91] Oliveira RG, Wang RZ, Kiplagat JK, Wang CY. Novel composite sorbent for resorption systems and for chemisorption air conditioners driven by low generation temperature. Renewable Energy. 2009;34:2757-64.
[92] Xu J, Oliveira RG, Wang RZ. Resorption system with simultaneous heat and cold production. International Journal of Refrigeration. 2011;34:1262-7.
[93] Lépinasse E, Marion M, Goetz V. Cooling storage with a resorption process. Application to a box temperature control. Applied Thermal Engineering. 2001;21:1251-63.
[94] Castaing-Lasvignottes J, Neveu P. Equivalent Carnot cycle concept applied to a thermochemical solid/gas resorption system. Applied Thermal Engineering. 1998;18:745-54.
[95] Li TX, Wang RZ, Oliveira RG, Kiplagat JK, Wang LW. A combined double-way chemisorption refrigeration cycle based on adsorption and resorption processes. International Journal of Refrigeration. 2009;32:47-57.

[96] Xu L, Wang RZ, Li TX, Wang LW. Experimental study on a combined double-way chemisorption refrigeration system. International Journal of Refrigeration. 2011;34:914-21.
[97] Bao HS, Oliveira RG, Wang RZ, Wang LW, Ma ZW. Working pairs for resorption refrigerator. Applied Thermal Engineering. 2011;31:3015-21.
[98] Eic M, Ruthven DM. A new experimental technique for measurement of intracrystalline diffusivity. Zeolites. 1988;8:40-5.
[99] Buss E. Gravimetric measurement of binary gas adsorption equilibria of methane—carbon dioxide mixtures on activated carbon. Gas Separation & Purification. 1995;9:189-97.
[100] Linders MJG, Van Den Broeke LJP, Van Bokhoven JJGM, Duisterwinkel AE, Kapteijn F, Moulijn JA. Effect of the adsorption isotherm on one- and two-component diffusion in activated carbon. Carbon. 1997;35:1415-25.
[101] Dawoud B, Aristov Y. Experimental study on the kinetics of water vapor sorption on selective water sorbents, silica gel and alumina under typical operating conditions of sorption heat pumps. International Journal of Heat and Mass Transfer. 2003;46:273-81.
[102] Wang L, Ziegler F, Roskilly AP, Wang R, Wang Y. A resorption cycle for the cogeneration of electricity and refrigeration. Applied Energy. 2013;106:56-64.
[103] Brennison MT. Development and Testing of A Low Cost Linear Slot Impulse Turbine: University of Kansas; 2010.
[104] B APW. Volumetric expander versus turbine-Which is the better choice for small ORC plants? 3rd International Seminar on ORC Power Systems. Brussels, Belgium2015.
[105] Barber-nichols. Turbines. http://www.barber-nichols.com/products/turbines Last achieved 26th August, 2012.
[106] Kang SH. Design and experimental study of ORC (organic Rankine cycle) and radial turbine using R245fa working fluid. Energy. 2012;41:514-24.
[107] Yamamoto T, Furuhata T, Arai N, Mori K. Design and testing of the Organic Rankine Cycle. Energy. 2001;26:239-51.
[108] Nguyen VM, Doherty PS, Riffat SB. Development of a prototype low-temperature Rankine cycle electricity generation system. Applied Thermal Engineering. 2001;21:169-81.
[109] Yagoub W, Doherty P, Riffat SB. Solar energy-gas driven micro-CHP system for an office building. Applied Thermal Engineering. 2006;26:1604-10.
[110] Pei G, Li J, Li Y, Wang D, Ji J. Construction and dynamic test of a small-scale organic rankine cycle. Energy. 2011;36:3215-23.
[111] Li J, Pei G, Li Y, Wang D, Ji J. Energetic and exergetic investigation of an organic Rankine cycle at different heat source temperatures. Energy. 2012;38:85-95.
[112] G. Pei YZL, J. Li, J. Ji. A High-Speed Micro Turbine for Organic Rankine Cycle. World Society of Sustainable Energy Technologies (WSSET)-Newsletter2009.
[113] Wang T, Zhang Y, Peng Z, Shu G. A review of researches on thermal exhaust heat recovery with Rankine cycle. Renewable and Sustainable Energy Reviews. 2011;15:2862-71.
[114] Zhang X, Xu Y, Xu J, Xue H, Chen H. Study of a single-valve reciprocating expander. Journal of the Energy Institute. 2016.
[115] Zhang B, Peng X, He Z, Xing Z, Shu P. Development of a double acting free piston expander for power recovery in transcritical CO2 cycle. Applied Thermal Engineering. 2007;27:1629-36.
[116] Tang H, Wu H, Wang X, Xing Z. Performance study of a twin-screw expander used in a geothermal organic Rankine cycle power generator. Energy. 2015;90, Part 1:631-42.

[117] Xia G-D, Zhang Y-Q, Wu Y-T, Ma C-F, Ji W-N, Liu S-W, et al. Experimental study on the performance of single-screw expander with different inlet vapor dryness. Applied Thermal Engineering. 2015;87:34-40.
[118] Imran M, Usman M, Park B-S, Lee D-H. Volumetric expanders for low grade heat and waste heat recovery applications. Renewable and Sustainable Energy Reviews. 2016;57:1090-109.
[119] H. Leibowitz, K. Smith, Stosic N. Cost effective small scale ORC systems for power recovery from low grade heat sources. Chicago, Illinois, USA.November 5-10, 2006.
[120] Smith IK, Stosic N, Kovacevic A. Screw expanders increase output and decrease the cost of geothermal binary power plant systems. Reno, NV2005. p. 787-94.
[121] Qiu G, Liu H, Riffat S. Expanders for micro-CHP systems with organic Rankine cycle. Applied Thermal Engineering. 2011;31:3301-7.
[122] Carrier Corporation Syracuse NY. Scroll compressor, High efficiency compression for commercial and industrial applications. October 2004.
[123] Qiang J. Study on basic parameters of scroll fluid machine based on general profile. Mechanism and Machine Theory. 2010;45:212-23.
[124] Scroll-compressor. <http://en.wikipedia.org/wiki/Scroll_compressor>. retrived 20 Nov 2011.
[125] Guangbin L, Yuanyang Z, Liansheng L, Pengcheng S. Simulation and experiment research on wide ranging working process of scroll expander driven by compressed air. Applied Thermal Engineering. 2010;30:2073-9.
[126] Quoilin S, Broek MVD, Declaye S, Dewallef P, Lemort V. Techno-economic survey of Organic Rankine Cycle (ORC) systems. Renewable and Sustainable Energy Reviews. 2013;22:168-86.
[127] Quoilin S, Aumann R, Grill A, Schuster A, Lemort V, Spliethoff H. Dynamic modeling and optimal control strategy of waste heat recovery Organic Rankine Cycles. Applied Energy. 2011;88:2183-90.
[128] Morini M, Pavan C, Pinelli M, Romito E, Suman A. Analysis of a scroll machine for micro ORC applications by means of a RE/CFD methodology. Applied Thermal Engineering. 2015;80:132-40.
[129] Mendoza LC, Navarro-Esbrí J, Bruno JC, Lemort V, Coronas A. Characterization and modeling of a scroll expander with air and ammonia as working fluid. Applied Thermal Engineering. 2014;70:630-40.
[130] Twomey B, Jacobs PA, Gurgenci H. Dynamic performance estimation of small-scale solar cogeneration with an organic Rankine cycle using a scroll expander. Applied Thermal Engineering. 2013;51:1307-16.
[131] R.Zanelli, D.Favrat. Experimental Inverstigation of a Hermetic Scroll Expander-Generator. International Compressor Engineering ConferencePaper 10211994.
[132] H. Wang RBP, T. Herron. Experimental performance of a compliant scroll expander for an organic Rankine cycle. Proceedings of the Institution of Mechanical Engineers Part A-Journal of Power and Energy. 2003;223:863-73.
[133] Quoilin S, Lemort V, Lebrun J. Experimental study and modeling of an Organic Rankine Cycle using scroll expander. Applied Energy. 2010;87:1260-8.
[134] Declaye S, Quoilin S, Guillaume L, Lemort V. Experimental study on an open-drive scroll expander integrated into an ORC (Organic Rankine Cycle) system with R245fa as working fluid. Energy. 2013;55:173-83.
[135] Chang J-C, Hung T-C, He Y-L, Zhang W. Experimental study on low-temperature organic Rankine cycle utilizing scroll type expander. Applied Energy. 2015;155:150-9.

[136] Song P, Wei M, Shi L, Danish SN, Ma C. A review of scroll expanders for organic Rankine cycle systems. Applied Thermal Engineering. 2014.
[137] T.Yanagisawa, M.Fukuta, Y.Ogi, T.Hikichi. Performance of an oil-free scroll type air expander. in:Proceedings of the IMechE Conference on Compressors and their Systems. 2001:167-74.
[138] Saitoh T, Yamada N, Wakashima S. Solar Rankine cycle system using scroll expander. Journal of Environment and Engineering. 2007;2:708-18.
[139] Lemort V, Quoilin S, Cuevas C, Lebrun J. Testing and modeling a scroll expander integrated into an Organic Rankine Cycle. Applied Thermal Engineering. 2009;29:3094-102.
[140] Bao J, Zhao L. A review of working fluid and expander selections for organic Rankine cycle. Renewable and Sustainable Energy Reviews. 2013;24:325-42.
[141] Yang B, Peng X, He Z, Guo B, Xing Z. Experimental investigation on the internal working process of a CO2 rotary vane expander. Applied Thermal Engineering. 2009;29:2289-96.
[142] Qiu G, Shao Y, Li J, Liu H, Riffat SB. Experimental investigation of a biomass-fired ORC-based micro-CHP for domestic applications. Fuel. 2012;96:374-82.
[143] Aoun B. Micro combined heat and power operating on renewable energy for residential building. Ecole des Mines de Paris2008.
[144] Borgnakke C, Sonntag RE. Thermodynamic and Transport Properties. New York : John Wiley & Sons Inc. 1997.
[145] AG GK. EXPANDABLE GRAPHITE. http://www.graphite.de/englisch/pdf/blaehgraphitprospekt_e.pdf.
[146] S. Grunwald, W. Beagle. Check Valve Movement in a Scroll Compressor (1990). International Compressor Engineering Conference http://docslibpurdueedu/icec/7641990.
[147] Lee SJL, D. S.; Lee, B. C.; and Joo, Y. S. The Development of New Check Valve for Scroll Compressor (1998). International Compressor Engineering Conference http://docslibpurdueedu/icec/12891998.
[148] USA S. SCROLL COMPRESSORS-TR SERIES, http://www.sanden.com/scrollcompressors.html. obtained date 18th Feb 2016.
[149] Liansheng L. Scroll compressor: China Machine Press; 1998.
[150] Li TX, Wang RZ, Kiplagat JK, Chen H. Experimental study and comparison of thermochemical resorption refrigeration cycle and adsorption refrigeration cycle. Chemical Engineering Science. 2010;65:4222-30.
[151] Software F-C. Engineering Equation Solver (EES) software overview.
[152] Bao H, Wang Y, Roskilly AP. Modelling of a chemisorption refrigeration and power cogeneration system. Applied Energy. 2014;119:351-62.
[153] Han JH, Lee K-H, Kim DH, Kim H. Transformation Analysis of Thermochemical Reactor Based on Thermophysical Properties of Graphite−MnCl2 Complex. Industrial & Engineering Chemistry Research. 2000;39:4127-39.
[154] Oliveira RG, Wang RZ. Study of a non-isothermal, non-isobaric consolidated reactive bed for chemisorption icemakers. Chemical Engineering Journal. 2008;138:416-24.
[155] Jiang L, Wang L, Zhang XF, Liu CZ, Wang R. Performance prediction on a resorption cogeneration cycle for power and refrigeration with energy storage. Renewable Energy. 2015;83:1250-9.
[156] Jiang L, Wang LW, Jin ZQ, Wang RZ, Dai YJ. Effective thermal conductivity and permeability of compact compound ammoniated salts in the adsorption/desorption process. International Journal of Thermal Sciences. 2013;71:103-10.

[157] Mendoza LC, Ayou DS, Navarro-Esbrí J, Bruno JC, Coronas A. Small capacity absorption systems for cooling and power with a scroll expander and ammonia based working fluids. Applied Thermal Engineering. 2014;72:258-65.
[158] Wang J, Luo X, Yang L, Shpanin LM, Jia N, Mangan S, et al. Mathematical modeling study of scroll air motors and energy efficiency analysis - Part II. IEEE ASME Trans Mechatron. 2011;16:122-32.

Appendices

Appendix 1 Components of the adsorption performance test rig

No	Name	Quantity	Model	Operational ranges
1	Oil bath	1	Julabo SE-6	20-300 ^{o}C 3kW
2	Cryostat	1	Julabo CF-41	-40-200 ^{o}C 2kW
3	Differential pressure transmitter	1	Rosemount 2051	4-20mA
4	Pressure sensor	2	EFE PET163	40 bar Power supply 5Vdc
5	Thermocouple	2	Omega K type thermocouple SA1-K-72	-60-175 ^{o}C
6	RTD temperature sensor	4	Omega SSLK-M60-18P 4-wire	-30-200 ^{o}C
4	Electric coil	2	Omega Engineering; 5x STH102-080 (5x 1256 W, 240V, 25mm x 2.4m),+Controller CN 7833,+ 5x Timer Relay	20-260 ^{o}C
5	Pressure relief valve	1	RS225-8239, Flowstar Ni/10.2' Right Angle Safety Valve	30 bar 300 ^{o}C
6	Control valve	5	Hedley Hydraulics Ltd Needle Valve 12mm A Lok	414bar

			Stainless Steel	
7	Vacuum pump	1	Pump vacuum 220/240 07061-42	Max temperature 38 ^{o}C Max Pressure 4.14 bar
8	Mesh for the adsorbent	6	120 stainless steel woven wire	n.a
9	PTFE gasket	6	Toughgask gasket 2.1/2 NB 150 2.5mm thick 304 stainless steel insert	n.a

Appendix 2 Components in the scroll expander test bench

No	Name	Quantity	Material	Producer and type
1	Pipe	2*6m	Stainless steel	5/8 inch www.swagelok.com, SS-T10-S-049-6ME, 5/8 inch OD, 0.049inc wall thickness
2	Check valve	1	Stainless steel	Swagelok, SS-58F8, 1/2 inch, Pmax=37Bar
3	Pressure regulating valve	1		Swagelok, KPF1LWA8A8P20000
4	Male connector	2	Stainless steel	SS-1010-1-8, 5/8 in. Tube OD x 1/2 in. Male NPT
5	Male connector	2	Stainless steel	SS-1010-1-12, 5/8 in. Tube OD x 3/4 in. Male NPT
6	Straight fitting	4	Stainless steel	SS-1010-6, 5/8 in. Tube OD
4	Flowmeter	1		Krohne; OPTISWIRL 4070/C
5	Electric coils	5		Omega Engineering; 5x STH102-080 (5x 1256 W, 240V, 25mm x 2.4m),+Controller CN 7833,+ 5x Timer Relay RS225-8239,
6	Temperature sensor	2		Omega Engineering; 2 x SA1-K1-3M, Max Temperature:300 C
7	High pressure sensor		Stainless steel	Omega Engineering; 1x PXM 35MD1-040BARGY (0-40BAR) +
8	Low pressure	1	Stainless steel	Omega Engineering; 1x PXM209-020G10

	sensor		(VACUM-20bar)
9	Electricity generator	1	S15W-85
10	Datataker	1	Grant Instruments (Cambridge) Ltd; Datataker DT80series
11	Scroll compressor	1	TRSA09 compressor
12	Power meter	1	Fluke 435

Appendix 3 Performance curve of TRSA09[148]

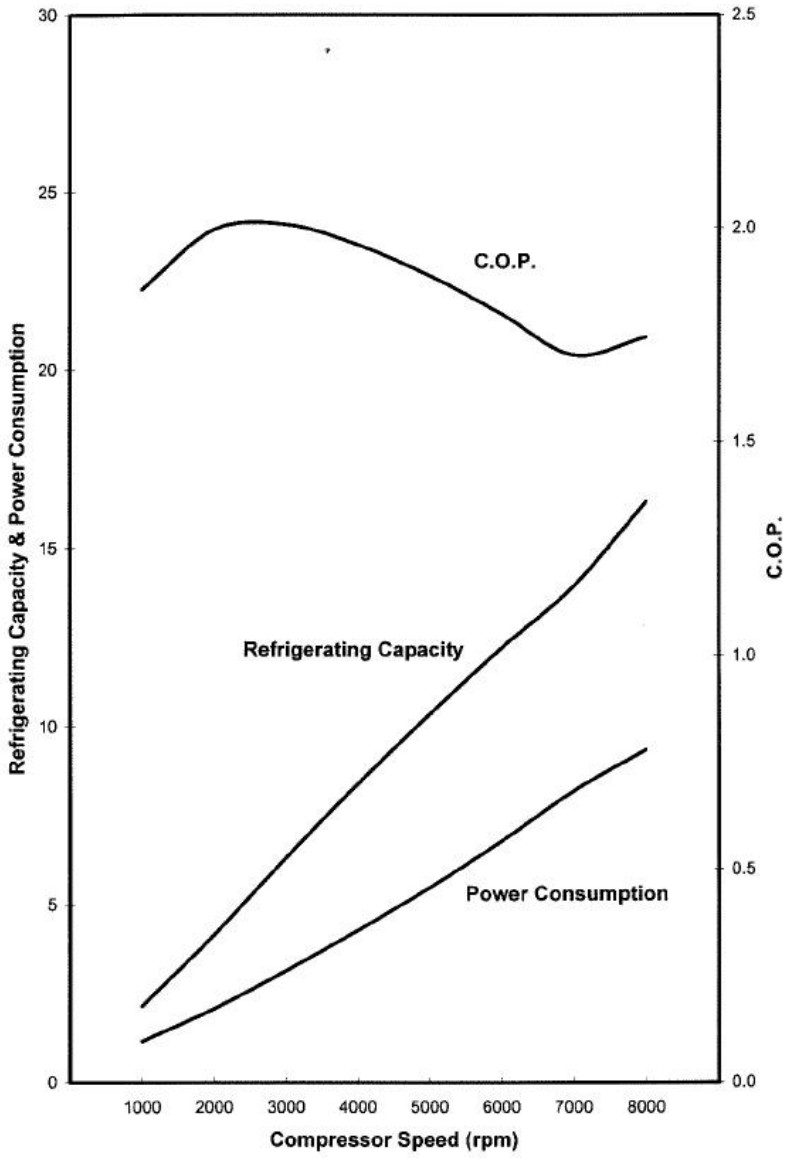

TRSA09 Performance

Pressure Dis /Suc : 1.67(MPa) / 196(kPa) [gage]

Sub Cool / Super Heat : 0 / 10(K)